

# PHYSICAL PROPERTIES OF THE CURRENT CENSUS OF NORTHERN WHITE DWARFS WITHIN 40 pc OF THE SUN

M.-M. Limoges,<sup>1,3</sup> P. Bergeron,<sup>1</sup> and S. Lépine<sup>2,4</sup>

<sup>1</sup>*Département de Physique, Université de Montréal, C.P. 6128, Succ. Centre-Ville, Montréal, Québec H3C 3J7, Canada*

<sup>2</sup>*Department of Physics and Astronomy, Georgia State University, Atlanta, GA 30302-4106*

limoges@astro.umontreal.ca, bergeron@astro.umontreal.ca,  
slepine@chara.gsu.edu

## ABSTRACT

We present a detailed description of the physical properties of our current census of white dwarfs within 40 pc of the Sun, based on an exhaustive spectroscopic survey of northern hemisphere candidates from the SUPERBLINK proper motion database. Our method for selecting white dwarf candidates is based on a combination of theoretical color-magnitude relations and reduced proper motion diagrams. We reported in an earlier publication the discovery of nearly 200 new white dwarfs, and we present here the discovery of an additional 133 new white dwarfs, among which we identify 96 DA, 3 DB, 24 DC, 3 DQ, and 7 DZ stars. We further identify 178 white dwarfs that lie within 40 pc of the Sun, representing a 40% increase of the current census, which now includes 492 objects. We estimate the completeness of our survey at between 66 and 78%, allowing for uncertainties in the distance estimates. We also perform a homogeneous model atmosphere analysis of this 40 pc sample and find a large fraction of massive white dwarfs, indicating that we are successfully recovering the more massive, and less luminous objects often missed in other surveys. We also show that the 40 pc sample is dominated by cool and old white dwarfs, which populate the faint end of the luminosity function, although trigonometric parallaxes will be needed to shape this part of the luminosity function more accurately. Finally, we identify 4 probable members of the 20 pc sample, 4 suspected double degenerate binaries, and we also report the discovery of two new ZZ Ceti pulsators.

---

<sup>3</sup>Visiting Astronomer, Kitt Peak National Observatory, National Optical Astronomy Observatory, which is operated by the Association of Universities for Research in Astronomy (AURA) under cooperative agreement with the National Science Foundation.

<sup>4</sup>Department of Astrophysics, American Museum of Natural History, New York, NY 10024

*Subject headings:* Solar neighborhood – surveys – techniques: spectroscopic – white dwarfs – stars: distances – stars: fundamental parameters – stars: luminosity function, mass function

## 1. INTRODUCTION

The determination of the atmospheric parameters of individual white dwarf stars — effective temperature ( $T_{\text{eff}}$ ), surface gravity ( $\log g$ ), and atmospheric composition — has now reached an unprecedented level of accuracy, thanks to significant progress on both the observational and theoretical fronts. On the observational side, large samples of high signal-to-noise optical spectra can now be routinely obtained and analyzed using the so-called *spectroscopic technique* where observed line profiles are compared to the predictions of model atmospheres (see, e.g., Bergeron et al. 1992), reaching a precision as high as 1.2% in  $T_{\text{eff}}$  measurements and 0.038 dex in  $\log g$  for the DA stars (Liebert et al. 2005). This technique has been applied successfully to large samples of various spectral types including DA stars from the ESO SN Ia Progenitor Survey (Koester et al. 2009), from the Villanova Catalogue of Spectroscopically Identified White Dwarfs (Gianninas et al. 2011), and in particular from the Sloan Digital Sky Survey (SDSS; Kepler et al. 2007, Tremblay et al. 2011). The same spectroscopic technique has also been used for DB stars (Voss et al. 2007; Kepler et al. 2007; Bergeron et al. 2011). Similarly, optical and infrared photometry can be combined and compared with synthetic photometry to measure effective temperatures, as well as stellar radii when trigonometric parallaxes are available. This *photometric technique*, first applied to large photometric data sets by Bergeron et al. (1997, 2001), is particularly useful to study cool white dwarfs that lack the presence of strong absorption lines required by the spectroscopic method. Particularly interesting in this context is the large set of optical *ugriz* photometry available for white dwarfs in the SDSS, combined with independent *JHK* photometry (see, e.g., Kilic et al. 2010; Gianninas et al. 2015). The photometric approach, however, is more sensitive to issues related to the calibration of the synthetic photometry (Holberg & Bergeron 2006), unlike the spectroscopic approach.

Several independent model atmosphere grids have been widely used for the analysis of white dwarf stars (e.g., Bergeron et al. 1992, Vennes 1992, Koester et al. 2001), and the results obtained from these models are reassuringly comparable (see Figure 9 of Liebert et al. 2005). Despite this agreement between models, significant improvements on the theoretical front are still being achieved. For instance, new calculations for the Stark broadening of hydrogen lines that include nonideal effects directly inside the line profile calculations have recently become available (Tremblay & Bergeron 2009). These models yield systematically

higher  $T_{\text{eff}}$  (up to 1000 K) and  $\log g$  (up to 0.1 dex) values, and a mean mass for DA stars shifted by  $+0.034 M_{\odot}$ . Similarly, Kowalski & Saumon (2006) have successfully modeled the opacity from the red wing of  $\text{Ly}\alpha$ , an important absorption process that affects the flux in the ultraviolet region of the energy distribution of cool, hydrogen-atmosphere white dwarfs. More importantly perhaps, Tremblay et al. (2013b, see also Tremblay et al. 2011, 2013a) have produced realistic 3D hydrodynamical model atmospheres of hydrogen-rich white dwarfs and successfully showed that the so-called high- $\log g$  problem — the apparent increase of spectroscopic  $\log g$  values below  $T_{\text{eff}} \sim 13,000$  K (see Tremblay et al. 2010 and references therein) — was related to the limitations of the mixing-length theory used to describe the convective energy transport in previous model atmosphere calculations.

With the availability of large data sets and improved model atmospheres, the statistical properties of white dwarf stars can now be studied in greater detail, including the luminosity function, space density, mass distribution, age distribution, and space kinematics. This can be achieved not only for the local population of white dwarfs, but also for various components of the Galaxy, including open and globular clusters (see, e.g., Tremblay et al. 2012, Woodley et al. 2012). Since white dwarfs represent the endpoint of over 97% of the stars in the Galaxy, they are a powerful tool to study the overall evolutionary history of the Galaxy. However, the determinations of these global properties are always confronted with the problem of defining statistically complete samples, minimally affected by selection biases. For instance, ultraviolet color excess surveys such as the Palomar-Green (PG) survey (Green et al. 1986) or the Kiso Schmidt (KUV) ultraviolet excess survey (Kondo et al. 1984) are restricted to the detection of blue and thus hot white dwarfs. Consequently, the luminosity functions derived from these surveys (Liebert et al. 2005; Limoges et al. 2010; Bergeron et al. 2011) do not sample the faint end of the distribution where the majority of white dwarf stars are located. Even the luminosity function determined by Harris et al. (2006) using the magnitude-limited SDSS sample, which covers the entire range of bolometric magnitudes ( $7 \lesssim M_{\text{bol}} \lesssim 16$ ), includes *several* corrections for completeness and contamination to counterbalance important selection effects, and these corrections critically determine the faint end of the luminosity function. It is however possible, as shown by Kilic et al. (2006), to refine the selection criteria by combining the SDSS photometry and astrometry with the USNO-B plate astrometry to build a reduced proper motion diagram, which helps to identify cool white dwarf candidates in the SDSS imaging area and thus recover the faint end of the luminosity function. White dwarfs identified in proper motion surveys are indeed much better suited to identify cool white dwarfs at the faint end of the luminosity function. For many years, one of the most commonly used observational luminosity function had been that published by Liebert, Dahn, & Monet (1988), and revised by Leggett et al. (1998), based on the Luyten Half-Second Catalog (Luyten 1979), but the major drawback is that

the sample contains only 43 spectroscopically confirmed white dwarfs.

Other types of statistical biases occur in determining the distribution of mass as a function of effective temperature ( $M$  versus  $T_{\text{eff}}$ ), or the cumulative mass distribution ( $N$  versus  $M$ ). For instance, color excess surveys (PG, KUV, and even SDSS) are also magnitude-limited, and as such the samples drawn from these surveys suffer from a bias in mass where low-mass white dwarfs with their large radii and high luminosities are over represented, while high-mass white dwarfs are undersampled (see, e.g., Section 3.2 of Liebert et al. 2005). Another important issue is that, until recently, spectroscopic masses at low effective temperatures could not be trusted due to the high- $\log g$  problem discussed above. Thus, most analyses restricted their determination of the mass distribution of DA stars to temperatures higher than 13,000 K. Alternatively, Giammichele et al. (2012) applied an empirical correction to the  $\log g$  distribution, based on the DA white dwarfs from the Data Release 4 of the SDSS analyzed by Tremblay et al. (2011). More recently, Tremblay et al. (2013b) produced a more accurate set of  $T_{\text{eff}}$  and  $\log g$  corrections to be applied to spectroscopic determinations, based on a comparison of detailed 3D hydrodynamical simulations with 1D model atmospheres calculated within the mixing length theory. Another problem arises at low effective temperatures when spectroscopic lines can no longer be used efficiently. This occurs below  $T_{\text{eff}} \sim 13,000$  K and  $\sim 6500$  K for helium- and hydrogen-atmosphere white dwarfs, respectively, i.e. near the peak of the luminosity function, in which cases one must rely on the photometric technique to measure the atmospheric parameters. With the photometric technique, unfortunately, stellar radii or masses can only be determined for white dwarfs with trigonometric parallax measurements, which are only available for 200 stars or so. This situation will of course change dramatically when the Gaia mission is completed.

Also of interest is the study of the spectral evolution, which describes the various physical mechanisms (gravitational settling, convective mixing, convective dredge-up from the core, accretion from the interstellar medium or circumstellar material, radiative acceleration, stellar winds, etc.) that affect the surface composition of white dwarfs as they evolve along the cooling sequence. Of particular interest is the spectral evolution of white dwarfs at low  $T_{\text{eff}}$ , where convective mixing of a thin superficial hydrogen convective layer with the deeper helium convection zone is believed to occur (see Tremblay & Bergeron 2008 and references therein). Bergeron et al. (1997, 2001) also suggested the presence of a non-DA gap (or deficiency) between  $T_{\text{eff}} \sim 5000$  K and 6000 K where most stars appear to have hydrogen-rich compositions, while helium-atmosphere white dwarfs exist above and below this temperature range. On the other hand, Kowalski & Saumon (2006, see also Giammichele et al. 2012) suggested that most, if not all, cool DC stars probably have hydrogen-rich atmospheres, based on a reanalysis of the Bergeron et al. (1997, 2001) photometry with their improved atmospheric models, which include the previously missing red wing opacity from  $\text{Ly}\alpha$ . Unfortunately,

the white dwarf samples analyzed by Bergeron et al. (1997, 2001) are not complete in any statistical sense. For instance, Kilic et al. (2010) analyzed 126 cool white dwarfs identified in the SDSS and uncovered several helium-atmosphere white dwarfs in the  $T_{\text{eff}}$  range of the gap. To complicate matters, Chen & Hansen (2011, 2012) showed that the evolution of cool white dwarfs cannot be interpreted monotonically as a function of  $T_{\text{eff}}$ , and that upon mixing the  $T_{\text{eff}}$  of a white dwarf can actually *increase*. Hence our understanding of the spectral evolution of cool white dwarfs is at best sketchy, a situation that can only be improved by studying better-defined, large, statistically complete samples.

The best way around the completeness problems discussed above is the use of a volume-limited sample. Efforts to identify white dwarfs in the immediate solar neighborhood, within 20 or 25 pc of the Sun, have been summarized in Limoges et al. (2013, hereafter Paper I). Giammichele et al. (2012) performed a detailed photometric and/or spectroscopic analysis of every white dwarf suspected to lie within 20 parsecs of the Sun. Although Holberg et al. (2008) and Giammichele et al. (2012) have established the completeness of the 20 parsec sample at 80% and 90%, respectively, one is confronted with small number statistics since this sample contains only 130 objects or so. Hence some results reported by Giammichele et al. may not be statistically significant. For example, while the luminosity function shown in their Figure 22 agrees well with previous investigations at low temperatures and luminosities, space densities in the brighter luminosity bins (above  $T_{\text{eff}} \sim 12,000$  K) are larger by a factor of  $\sim 2$ . As mentioned by the authors, one likely explanation for this apparent overdensity is the small number of white dwarfs in the brightest luminosity bins, which contain only a few objects ( $\sim 2$  to 8). The only way out of this situation is to significantly increase the volume sampled by these surveys. For instance, Holberg et al. (2011) are working on defining the sample of white dwarfs to 25 parsecs of the Sun, nearly doubling the number of objects analyzed by Giammichele et al. (2012).

It is with this idea in mind that we embarked in a large effort (see Paper I) to increase the census of white dwarfs to the larger distance range of 40 pc from the Sun (corresponding to a volume *8 times* that of the 20 pc sample). Given the space density of  $4.39 \times 10^{-3}$  pc $^{-3}$  derived by Giammichele et al. (2012), the expected number of white dwarfs within 40 pc is  $\sim 1200$ , or  $\sim 600$  if we restrict our search to the northern hemisphere, a sample size that would markedly improve the statistical significance of previous analyses. The SUPERBLINK survey is an all-sky search for high proper motion stars ( $\mu > 40$  mas yr $^{-1}$ ) based on a re-analysis of the Digitized Sky Surveys, with its 20-45 yr baseline (Lépine & Shara 2005; Lépine & Gaidos 2011). The SUPERBLINK catalog is at least 95% complete for the entire northern sky down to  $V = 19.0$ , with a very low rate of spurious detection. As discussed in Paper I, the SUPERBLINK catalog should contain all white dwarfs down to the luminosity function turnover (which occurs at  $L/L_{\odot} \simeq 10^{-4}$ ) to a distance of 56.7 pc from the Sun.

Our method for selecting white dwarf candidates, described in detail in Paper I, is based on reduced proper motion diagrams of the 1.6 million stars in SUPERBLINK with  $\delta > 0$ , combined with distances estimated from theoretical color-magnitude relations. A list of 1341 candidates with *photometric distance* estimates of  $D < 40$  pc, to within the uncertainties, was established for follow-up spectroscopic observations, excluding the objects with an already known spectral type. We successfully confirmed 193 new white dwarfs, among which 93 had *spectroscopic distances* placing them within 40 pc. Only DA stars with strong enough Balmer lines were analyzed in Paper I, using the spectroscopic method described above.

The specific goal of this work is to obtain a complete sample of white dwarfs within 40 pc of the Sun in the northern hemisphere. We report in this paper the outcome of our survey, and present a detailed photometric and spectroscopic model atmosphere analysis of all the new white dwarfs that were identified. We also provide a comprehensive analysis of the mass distribution and the chemical distribution of white dwarf stars in this volume-limited sample. In particular, since only about a third of the white dwarfs in our sample have trigonometric parallax measurements available, we develop a robust method to derive distances from spectroscopic and photometric data alone.

We first present in Section 2 an update of our census of white dwarfs within 40 pc of the Sun, which includes a summary of our earlier work as well as a detailed description of the follow-up spectroscopic observations of our list of white dwarf candidates. We then perform in Section 3 a detailed photometric and spectroscopic analysis of all objects in our sample with state-of-the-art model atmospheres, where we also include all known white dwarfs in the SUPERBLINK catalog and from the literature, suspected to belong to the 40 pc sample. The resulting distance estimates are then used to build a complete sample of white dwarfs within 40 pc of the Sun, which we analyze in further detail in Section 4. In particular, we discuss several physical properties of this sample, including its completeness, kinematics, mass distribution, spectral evolution, and luminosity function. We then offer some concluding remarks in Section 5.

## 2. UPDATE ON OUR CENSUS OF WHITE DWARFS WITHIN 40 PC OF THE SUN

### 2.1. Selection of the Candidates Based on Reduced Proper Motion Diagrams

Our method for selecting white dwarf candidates from the SUPERBLINK catalog using reduced proper motion diagrams is discussed at length in Paper I. We briefly summarize here, for completeness, the various steps involved.



The white dwarf candidates are identified from the SUPERBLINK catalog of stars with proper motions  $\mu > 40 \text{ mas yr}^{-1}$  (Lépine et al. 2002; Lépine & Shara 2005; Lépine & Gaidos 2011). Our selection method takes advantage of the coordinates and proper motions provided by SUPERBLINK for 1,567,461 stars in the northern hemisphere ( $\delta > 0$ ). White dwarf candidates are selected on the basis of their particular location at the bottom left of reduced proper motion diagrams. Since the construction of such diagrams requires, in addition to proper motion measurements, a set of photometric color indices for each star, we cross-correlate SUPERBLINK with other catalogs to obtain photometric data covering a large portion of the electromagnetic spectrum, and in some cases, we also obtain improved coordinates and proper motion measurements. Our version of SUPERBLINK used in Paper I includes — in the northern hemisphere only — 1,472,666 counterparts in the Two Micron All Sky Survey (2MASS) Point Source Catalog (Skrutskie et al. 2006), 345,958 in the Sloan Digital Sky Survey (SDSS, Adelman-McCarthy et al. 2008), 118,475 in the *Hipparcos* and *Tycho-2* catalogs (Høg et al. 2000), 1,567,461 in the USNO-B1.0 database (Monet et al. 2003), and 143,096 in the sixth data release (GR6) of the *GALEX* database (Gil de Paz et al. 2009). Each object in SUPERBLINK with  $\delta > 0$  is then placed in all corresponding ( $H_m$ , color-index) diagrams, depending on the available photometry, where  $H_m$  represents the reduced proper motion defined as  $H_m = m + 5 \log \mu + 5$ ,  $m$  is the apparent magnitude in some bandpass, and  $\mu$  is the proper motion measured in arcseconds per year. More specifically, we rely on  $(H_g, g - z)$  based on *ugriz* photometry,  $(H_V, NUV - V)$  based on UV *GALEX* photometry,  $(H_V, V - J)$  based on 2MASS *JHK<sub>S</sub>* photometry, and  $(H_V, V - I_N)$  based on USNO-B1 photographic magnitudes. We also restrict our search to stars with  $V < 19$ , since SUPERBLINK has an estimated false detection level of less than 1% down to  $V = 19$ , but the false detection rate increases significantly for fainter sources.

The limit that defines the white dwarf region in each diagram is determined from the location of SUPERBLINK objects with known white dwarf counterparts in the 2008 May electronic version of the Catalogue of Spectroscopically Identified White Dwarfs<sup>1</sup> (McCook & Sion 1999, hereafter WD Catalog). To be selected as a white dwarf candidate, a SUPERBLINK object must be identified in the expected white dwarf region of the diagram with the most accurate photometry. The highest priority is thus given to the reduced proper motion diagram based on SDSS magnitudes. If *ugriz* photometry is not available, the second priority is given to UV *GALEX* photometry, the third priority to 2MASS *JHK<sub>S</sub>* photometry, and if no other photometric system is available, we use USNO-B1 photographic magnitudes. Finally, a criterion in  $V - J$  is applied to the stars identified in  $(H_V, V - J)$  diagrams to exclude bright, red, main sequence contaminants.

---

<sup>1</sup><http://www.astronomy.villanova.edu/WDCatalog/index.html>

Since we want to restrain our survey to a distance less than  $D = 40$  pc from the Sun, and in the absence of trigonometric parallax measurements for most white dwarf candidates in our sample, we must rely on *photometric distances* estimated from the distance modulus,  $m - M = 5 \log D - 5$ , where the absolute magnitude  $M$  of each object is determined from theoretical color-magnitude relations combined with a measured color index in some specified photometric system. These theoretical relations at constant mass values (see Figures 5 to 8 of Paper I) are based on synthetic photometry from white dwarf model atmospheres, following the procedure described in Holberg & Bergeron (2006). Hence, absolute magnitudes for each white dwarf candidate are determined from color-magnitude relations in  $(M_g, g - z)$ ,  $(M_V, NUV - V)$ ,  $(M_V, V - J)$  or  $(M_V, V - I_N)$ , for a  $0.6 M_\odot$  hydrogen-atmosphere sequence, and for a helium-atmosphere sequence at the same mass in order to evaluate the distance uncertainty resulting from the unknown atmospheric composition of our candidates. A comparison of these photometric distances with those obtained from parallax measurements show a  $1\sigma$  dispersion of 8.5 pc (see Figure 9 of Paper I), and we thus adopt in our survey a conservative buffer of 15 pc to include all white dwarfs that could potentially lie within 40 pc of the Sun, that is with  $D_{\text{phot}} < 55$  pc.

The method described above led to the identification of 193 new spectroscopically identified white dwarfs in Paper I. However, even though 14594+3618 (we omit here and below the letters “PM I” from the designation) was identified as a white dwarf in Paper I, a new spectrum at a significantly improved S/N shows that the star is a main sequence F star, hence reducing the total of new white dwarfs identified to 192. We also established that our survey is efficient at identifying nearby white dwarfs distributed uniformly across the northern sky, and estimated the ratio of new to known white dwarfs to be around 77% within 40 pc. More importantly, our survey has identified a large amount of cool white dwarfs that could possibly refine the determination of the faint end of the luminosity function. We describe in the next section the update of our spectroscopic survey.

## 2.2. Spectroscopic Follow-up of White Dwarf Candidates Within 40 pc of the Sun

In Paper I, we compiled a list of 1341 white dwarf candidates within 40 pc of the Sun — but likely extending to 55 pc given the uncertainties — and reported spectroscopic observations for 422 objects from this target list, including 192 new white dwarf identifications. We also reported that our selection criteria recovered 499 known nearby white dwarfs from the literature (see Figure 11 of Paper I). However, a thorough search indicated that while several of these objects have a WD spectral classification in Simbad, they have never been



*confirmed spectroscopically* (and indeed, some of these turned out not to be white dwarfs after all). We also improved the cross-correlation of objects in our target list with known white dwarfs from the literature, and discovered several improper matches. Hence the number of previously known, actual white dwarfs identified from our selection criteria is 416. Finally, we have recently determined that our criterion based on  $V - J$  color used to exclude bright, red, main sequence contaminants (see above) had not in fact been applied to our list of white dwarf candidates. Taking all these changes into account, our list of white dwarf candidates now numbers 1180 objects.

The spectroscopic observing log of our earlier survey is presented in Table 2 of Paper I. Since then, additional optical spectra have been obtained with the Steward Observatory 2.3-m telescope and the NOAO Mayall 4-m and 2.1-m telescopes during 7 different observing campaigns between 2011 January and 2013 October. A few of the brightest candidates were also observed in spectroscopy with the 1.6-m Mont-Mégantic Observatory (OMM), while  $\sim 60$  hours with the Gemini North and South 8-m telescopes were used to observe our faintest candidates ( $V \simeq 17 - 18$ ). The adopted configurations allow a spectral coverage of  $\lambda \sim 3200 - 5300 \text{ \AA}$  and  $\sim 3800 - 6700 \text{ \AA}$ , at an intermediate resolution of  $\sim 6 \text{ \AA}$  FWHM. Spectra were first obtained at low signal-to-noise ratio ( $S/N \sim 25$ ), which is sufficient to identify main sequence objects, but also represents the lower limit required to obtain reliable model fits to the spectral lines. Some stars were however reobserved at higher  $S/N$  and resolution, whenever required. Table 1 summarizes our spectroscopic observation campaigns carried out since Paper I, along with their instrumental setups.

We have now secured spectra for 588 objects from our list of 1180 candidates, thus adding 163 spectra to the list of 422 objects reported in Paper I. The content of our complete spectroscopic data set, described in the next subsection, includes 325 new white dwarf identifications (192 reported in Paper I), and 263 spectra from contaminants, mainly main sequence stars and quasars. We note that 3 of the newly identified white dwarfs are included in the SDSS Data Release 7 but were not classified as such; we rely on the corresponding SDSS spectra for these stars.

The current state of our survey is summarized in Figure 1 (upper panel), which plots the estimated absolute visual magnitudes (from the calculated  $V$  magnitudes and photometric distances — see Paper I) as a function of the photometric distance for the 325 new white dwarfs (filled symbols) and the 416 previously known white dwarfs (open symbols). We note that the subset of new white dwarfs is dominated by objects fainter than  $V = 16$ , and that most of them are found at photometric distances larger than 20 pc. The 592 white dwarf candidates on our list still without spectroscopic confirmation are displayed separately in the lower panel of Figure 1; objects selected on the basis of the less reliable

USNO photographic magnitudes (crosses) are considered second priority targets because of their higher probability of being main-sequence contaminants. If we exclude these second priority targets, we are left with  $\sim 330$  first-priority candidates for the spectroscopic follow-up survey. However, only 4 candidates with  $D < 30$  pc and  $V < 18$  remain to be observed, and every candidate with a high probability of being a white dwarf with an estimated distance less than 20 pc has been observed.

### 2.3. Spectroscopic Content of our Updated Survey

Our spectroscopic follow-up observations from 2011 January to 2013 October (Table 1) have led to the identification of the 133 new white dwarfs listed in Tables 2 and 3 (including the 3 SDSS white dwarfs discussed above). Table 2 provides astrometric data as well as NLTT and SDSS designations, when available, while Table 3 lists the available photometry and adopted spectral types for the same objects. Since Paper I, the SUPERBLINK catalog has been updated with optical magnitudes from the 7th Data Release of the SDSS catalog, and ultraviolet magnitudes from the DR4-5 data release of *GALEX*. In particular, the number of stars with *GALEX* counterparts has increased to 258,076 objects, while the number of stars with SDSS counterparts now reaches 740,826. This improved photometry is essential for the analysis of the energy distribution of the SUPERBLINK white dwarfs, as well as for the estimation of their distances. For this reason, we also include in Table 3 revised photometry for the 192 new white dwarfs identified in Paper I. In summary, the new white dwarfs reported in this paper comprise 96 DA (including 1 DAZ, 3 DA+dM, and 50 magnetics), 3 DB, 24 DC, 3 DQ, and 7 DZ (including 1 DZA) stars.

Our new DA spectra are displayed in Figures 2 and 3; only  $H\alpha$  is displayed in Figure 3 since the bluer portion of the spectrum is either featureless or too noisy to be of any use in the coolest DA stars. We also show at the bottom of the last panel of Figure 2, 3 new spectra of stars already presented in Paper I (see Table 4), that are double degenerate binary candidates and are further analyzed below. Note that 05431+3637 is actually a DAZ star. Two of the DA stars discovered in our survey — 06018+2751 (GD 258) and 18435+2740 (GD 381) — were flagged as WD candidates in Giclas et al. (1980), but to our knowledge these had not been spectroscopically confirmed, suggesting that many of the Giclas objects may still be white dwarfs awaiting spectroscopic confirmation. The magnetic DA white dwarfs, or magnetic candidates, in our updated sample are displayed in Figure 4. The bottom five objects are new identifications, with the Zeeman triplets clearly visible despite their low S/N. The top object, 04523+2519, was initially classified non-magnetic in Paper I, but the flat bottom line cores observed in our spectroscopic fit (see Figure 17 of Paper I) led us

to reobserve this star at  $H\alpha$ , where the weak Zeeman splitting is now just barely detected, making us believe this star is magnetic as well. Finally, our survey also led to the discovery of 3 new DA + M dwarf binary systems, shown separately in Figure 5.

Our subsample of new DZ (DZA), DB (DBZ), and DQ stars are displayed together in Figure 6. The first object in the figure, 00050+4003, is the star GD 1, another WD candidate listed in Giclas et al. (1980). Also shown are 5 DZ stars already identified in Paper I but for which new optical spectra in the blue have been secured: 01216+3440, 03196+3630, 16477+2636, 21420+2252, and 23003+2204. Indeed, the observational setup used with the 2.1-m and 4-m NOAO telescopes does not allow simultaneous coverage of wavelengths shorter than  $\sim 3900$  Å and of  $H\alpha$  in the red. In order to better constrain the metal abundances in these objects, additional spectra covering the blue portion of the spectral energy distribution were thus obtained with the Steward Observatory 2.3-m Bok telescope. The 3 new DB white dwarfs displayed in Figure 6 also include 02236+4816, also known as GD 27, another WD candidate from Giclas et al. (1980) that was also lacking spectroscopic confirmation to this date. Finally, our 3 DQ spectra, some of which are easily recognizable from their strong  $C_2$  Swan bands, are shown in the bottom right section of Figure 6; 16142+1729 is actually one of those peculiar DQ stars with shifted  $C_2$  Swan bands referred to as DQpec white dwarfs, a phenomenon explained by Kowalski (2010) as a result of pressure shifts of the carbon bands that occur in very cool, helium-dominated atmospheres. 05449+2602 has a DC spectral type in the WD Catalog (WD 0541+260), but this spectral classification was erroneously taken from Table 2 of Limoges et al. (2010), where it was confused by McCook & Sion with LSPM J0021+2640. Our spectrum displayed here actually shows a weak unidentified absorption feature near 5200 Å. Since it does not show any of the calcium features usually observed in DZ stars, it was classified as a DQ? star in Table 3, although it could also be magnetic.

Finally, our featureless DC spectra are displayed in Figure 7 in order of right ascension. All spectra cover the  $\lambda \sim 3900 - 6700$  Å range, except for 05462+1115 for which only the blue part of the spectrum ( $\lambda < 5200$  Å) is available, and we notice a few cases where the blue portion of the spectrum is particularly noisy, preventing us from detecting the possible presence of calcium lines. These noisier spectra actually come from Gemini North and South, where the integration times were calculated for the central wavelengths near 5000 Å, but the gratings used with the GMOS-N and -S instruments (B600 G5307), chosen for their spectral coverage, have a quantum efficiency that falls below 43% blueward of 3937 Å, compared with 83% at 4983 Å.

The progress of our spectroscopic survey can also be summarized in the color-color diagram shown in Figure 8, where we display the subset of 151 spectroscopically confirmed white dwarfs in our sample that also have available *ugriz* photometry from SDSS. White

dwarf candidates without spectroscopic confirmation are shown in red, and most of these have estimated distances larger than 30 pc, as can be seen from Figure 1. This figure reveals that our sample of new white dwarfs is composed mainly of DA stars, but also contains a significant number of cool ( $T_{\text{eff}} < 5000$  K) white dwarfs, with objects as cool as  $T_{\text{eff}} \sim 4000$  K.

Finally, the entire white dwarf population detected in SUPERBLINK is presented in Figure 9, where we display its distribution on the sky. In the upper panel, the 325 new identifications are shown with solid dots, while the white dwarfs from the literature are represented with open circles. In the bottom panel, we plot the sky density as a function of right ascension for the ‘old’ white dwarf population (dotted line), and compare it to that of the 325 new identifications (dashed line) and to the sum of the old and new white dwarfs (solid line). In Paper I, Figure 11 showed that the white dwarf candidates in our survey had the potential to fill the void left in the galactic plane by earlier surveys. Here we notice that the density of new identifications, especially near  $\text{RA} = 100$ , suggests we are on our way to identify the missing white dwarfs in this particular region of the sky.

### 3. ATMOSPHERIC PARAMETER DETERMINATION

#### 3.1. Theoretical Framework

Our model atmospheres and synthetic spectra for hydrogen-atmosphere white dwarfs are built from the model atmosphere code originally described in Bergeron et al. (1995) and references therein, with recent improvements discussed in Tremblay & Bergeron (2009). These are pure hydrogen, plane-parallel model atmospheres, with non-local thermodynamic equilibrium effects explicitly taken into account above  $T_{\text{eff}} = 30,000$  K, and energy transport by convection included in cooler models following the  $\text{ML2}/\alpha = 0.7$  prescription of the mixing-length theory. The theoretical spectra are calculated within the occupation formalism of Hummer & Mihalas (1988), which provides a detailed treatment of the level populations as well as a consistent description of bound-bound and bound-free opacities. We also include the improved calculations for the Stark broadening of hydrogen lines from Tremblay & Bergeron (2009), which take into account nonideal perturbations from protons and electrons directly inside the line profile calculations, as well as the opacity from the red wing of  $\text{Ly}\alpha$  calculated by Kowalski & Saumon (2006), which is known to affect the flux in the ultraviolet region of the energy distribution, and in particular the FUV, NUV, and  $u$  magnitudes used in our analysis. Our model grid covers a range of effective temperatures between  $T_{\text{eff}} = 1500$  K and 120,000 K in steps of 250 K for  $T_{\text{eff}} < 5500$  K, 500 K up to  $T_{\text{eff}} = 17,000$  K, and 5000 K above. The  $\log g$  ranges from 6.0 to 9.5 by steps of 0.25 dex. We also calculated cooler models with mixed hydrogen and helium compositions (see Gianninas et al. 2015) for the

analysis of white dwarfs in our sample that show evidence for collision-induced absorptions by molecular hydrogen due to collisions with helium.

Our model atmospheres and synthetic spectra for helium-atmosphere stars are described at length in Bergeron et al. (2011). These include the Stark profiles of neutral helium from Beauchamp et al. (1997) as well as van der Waals broadening. The synthetic spectra are calculated using the occupation probability formalism of Hummer & Mihalas (1988) for helium populations and corresponding bound-bound, bound-free, and pseudo-continuum opacities. Our model grid covers a range of effective temperatures between  $T_{\text{eff}} = 3000$  K and 40,000 K in steps of 1000 K, while the  $\log g$  ranges from 7.0 to 9.0 in steps of 0.5 dex. In addition to pure helium models, we also calculated models above 11,000 K with  $\log \text{H}/\text{He} = -6.5$  to  $-2.0$  by steps of 0.5 dex.

The photometric analyses of DQ and DZ white dwarfs rely on the LTE model atmosphere calculations developed by Dufour et al. (2005, 2007) for the study of DQ and DZ stars, respectively. Both are based on a modified version of the code described in Bergeron et al. (1995). The main addition to the models is the inclusion of metals and molecules in the equation of state and opacity calculations. These heavier elements provide enough free electrons to affect the atmospheric structures and predicted energy distributions of cool, helium-rich white dwarfs.

## 3.2. Photometric Analysis

### 3.2.1. General Procedure

The photometric technique developed by Bergeron et al. (1997) makes use of the apparent magnitudes in any photometric system in order to measure the atmospheric parameters ( $T_{\text{eff}}$  and  $\log g$ ) and the chemical composition. This method is particularly useful for the analysis of cool white dwarfs when spectral features are either too weak or completely absent. The magnitudes in each bandpass are first converted into a set of average fluxes  $f_{\lambda}^m$  following the procedure described in Holberg & Bergeron (2006), which is mainly based on the Vega fluxes from Bohlin & Gilliland (2004), but also includes *ugriz* photometry in the AB magnitude system. In particular here, we make use of the transmission functions described in Morrissey & GALEX Science Team (2004) and available from the *GALEX* Web site<sup>2</sup> for the FUV and NUV filters, while the bandpasses for the *ugriz* system (Fukugita et al. 1996) are

---

<sup>2</sup><http://GALEXgi.gsfc.nasa.gov/docs/GALEX/Documents/PostLaunchResponseCurveData.html>

taken from the SDSS Web site<sup>3</sup>. Similarly, for the 2MASS filters described in Cohen et al. (2003), we use the transmission functions from the 2MASS survey Web site<sup>4</sup>. Finally, the USNO-B1.0  $B_J$ ,  $R_F$ , and  $I_N$  magnitudes are described in Monet et al. (2003), and the transmission functions are taken from the Digitized Sky Survey website<sup>5</sup>.

These observed average fluxes can be compared to the average model fluxes  $H_\lambda^m$  by the relation

$$f_\lambda^m = 4\pi(R/D)^2 H_\lambda^m \quad (1)$$

where  $R/D$  defines the ratio of the radius of the star to its distance from Earth. The model fluxes  $H_\lambda^m$  — which depend on  $T_{\text{eff}}$ ,  $\log g$ , and chemical composition — are obtained from averages over the transmission function of the corresponding bandpass<sup>6</sup>. We then minimize the  $\chi^2$  value defined in terms of the difference between observed and model fluxes over all bandpasses, properly weighted by the photometric uncertainties. Our minimization procedure relies on the nonlinear least-squares method of Levenberg-Marquardt (Press et al. 1986), which is based on a steepest descent method. Only  $T_{\text{eff}}$  and the solid angle  $\pi(R/D)^2$  are considered free parameters (for an assumed chemical composition), while the error of both parameters are obtained directly from the covariance matrix of the fit. For stars with known trigonometric parallax measurements, we first assume a value of  $\log g = 8$  and determine  $T_{\text{eff}}$  and the solid angle, which combined with the distance  $D$  obtained from the trigonometric parallax measurement, yields directly the radius of the star  $R$ . The radius is then converted into mass using evolutionary models similar to those described in Fontaine et al. (2001) but with C/O cores,  $q(\text{He}) \equiv \log M_{\text{He}}/M_\star = 10^{-2}$  and  $q(\text{H}) = 10^{-4}$ , which are representative of hydrogen-atmosphere white dwarfs, and  $q(\text{He}) = 10^{-2}$  and  $q(\text{H}) = 10^{-10}$ , which are representative of helium-atmosphere white dwarfs. In general, the  $\log g$  value obtained from the inferred mass and radius ( $g = GM/R^2$ ) will be different from our initial assumption of  $\log g = 8$ , and the fitting procedure is thus repeated until an internal consistency in  $\log g$  is reached. For white dwarfs with no parallax measurement, we simply assume a value of  $\log g = 8$  and an uncertainty of 0.25 dex, which corresponds approximately to a  $2\sigma$  dispersion of the surface gravity distribution of hot DA stars (Gianninas et al. 2011).

---

<sup>3</sup><http://www.sdss.org/dr6/instruments/imager/#filters>

<sup>4</sup>[http://www.ipac.caltech.edu/2mass/releases/allsky/doc/sec6\\_4a.html](http://www.ipac.caltech.edu/2mass/releases/allsky/doc/sec6_4a.html)

<sup>5</sup><http://www3.cadc-ccda.hia-ihp.nrc-cnrc.gc.ca/dss/>

<sup>6</sup>This synthetic photometry is available at <http://www.astro.umontreal.ca/~bergeron/CoolingModels>



### 3.2.2. Analysis with Hydrogen- and Helium-atmosphere Models

We first perform a photometric analysis of all featureless DC stars in our sample, and of all DA stars for which the Balmer lines are too weak to be analyzed with the spectroscopic method. Sample fits are shown in Figure 10 for a subsample of 5 newly identified white dwarfs. Average observed fluxes are represented by error bars in the left panels (with the photometric bandpasses used in the fitting procedure indicated at the top of each panel), while our best fits with pure hydrogen and pure helium models are shown as filled or open circles, respectively. The corresponding atmospheric parameters are given at the bottom of each panel. The USNO-B1.0 photographic magnitudes have an error of 0.5 mag, which explains the large error bars associated with their photometry. However, since the fit is weighted by the photometric uncertainty, these less accurate magnitudes will have little impact on the solution but they are still useful when no other photometric information is available. Also, some bandpasses had to be removed from the fitting procedure (shown in red in the left panels) either because they are obviously incorrect, or because they are contaminated by the presence of a red companion. In the right panels we compare the spectroscopic observations near  $H\alpha$  with the model predictions *assuming the pure hydrogen solution*; these only serve as an internal check of our photometric solutions and are not used in the fitting procedure. When  $H\alpha$  is observed spectroscopically, we adopt the pure hydrogen solution, as is the case for two objects in Figure 10, and even for magnetic DA stars (one shown in Figure 10). When  $H\alpha$  is predicted by the pure hydrogen solution but is not observed spectroscopically, we adopt the pure helium solution instead (see, e.g., second object from the top in Figure 10). In cases where the star is too cool to show  $H\alpha$  ( $T_{\text{eff}} \leq 5000$  K), one has to rely on the predicted energy distributions to decide which atmospheric composition best fit the photometric data. However, according to Kowalski & Saumon (2006) based on their analysis of cool white dwarfs with models including the  $\text{Ly}\alpha$  opacity, almost all cool DC stars appear to have hydrogen-rich atmospheres, a conclusion also reached by Giammichele et al. (2012, see their Figure 9 and their Section 4.2). We thus assume here the pure hydrogen solution for all cool DC stars in our sample (bottom object in Figure 10 for instance). Based on a close inspection of these photometric fits and predicted  $H\alpha$  features, we adopt the solution shown in red in the left panels.

The photometric fits for all 146 DC and cool DA stars in our sample are displayed in Figure 11. The particular case of the DZ star 12145+7822 will be discussed in Section 3.2.3. Also included here are the photometric fits to 3 DA + M dwarf systems (03031+2317, 04032+2520E, and 08184+6606) hot enough to be analyzed with the spectroscopic method, but for which the optical spectra are so heavily contaminated by the presence of the companion that the spectroscopic technique cannot be used reliably. In those cases, we also had to omit from our photometric fits the  $I_N$  and  $JHK_s$  magnitudes for 03031+2317, the  $R_F$ ,

$I_N$ , and  $JHK_s$  for 04032+2520E, and we kept only the  $B_J$ ,  $R_F$ , and  $ugr$  magnitudes for 08184+6606. Figure 11 also includes the fits to 11 new magnetic white dwarfs identified in our survey. For these, the photometric technique is adopted since the presence of such small magnetic fields are not likely to affect the predicted energy distributions.

A closer inspection of all the photometric fits shown in Figure 11 reveals that most solutions for the DA stars predict an  $H\alpha$  feature that agrees remarkably well with observations (with the glaring exception of 04263+4820, 11337+6243, 11598+0007, and 14278+0532, discussed further in Section 3.4), giving us confidence in our photometric temperature scale, even for non-DA stars. Since we are often forced in our survey to rely on magnitudes with large uncertainties, we need to worry about the overall accuracy of the photometric method. But our results indicate that the lack of accurate photometric measurements for some objects is compensated to some extent by the large number of data points, and also by the fact that the fit is weighted by the error on the photometry.

### 3.2.3. Photometric Analysis of DQ and DZ Stars

The photometric technique used to fit the energy distributions of DQ and DZ stars is similar to that described above for the cool DA and DC stars in our sample, with the exception that the abundance of heavy elements (carbon or metals) is determined from fits to the optical spectra (see also Giammichele et al. 2012). Briefly, the energy distribution is first fitted for an arbitrary abundance of heavy elements to obtain an initial estimate of the effective temperature ( $\log g$  is assumed or constrained from trigonometric parallax measurements). The spectroscopic observations are then used to determine the carbon abundance in the case of DQ stars — fitting the  $C_2$  Swan bands — or the metal abundances in the case of DZ stars — fitting the Ca II H & K doublet — at these initial values of  $T_{\text{eff}}$  and  $\log g$ . This improved determination of heavy element abundances is then used to obtain new estimates of the atmospheric parameters, and this procedure is repeated until a consistent photometric and spectroscopic solution is reached.

Results for the 5 new DQ stars in our sample (3 from Paper I and 2 from this work) are presented in Figure 12, where we display in the left panels the observed and model fluxes, as well as the adopted  $T_{\text{eff}}$ ,  $\log g$ , and carbon abundance, and in the right panels, the observed and model spectra (for the DQ? star 05449+2602, we assumed a pure helium composition and our best fit is shown in Figure 11). The predicted energy distributions and spectra agree well for the two normal DQ stars shown at the top. The three other objects are DQpec white dwarfs, with characteristic pressure-shifted  $C_2$  Swan bands (Kowalski 2010). Since these pressure shifts are not included in our models, the line strengths and shifts are not properly

reproduced. For these DQpec stars, we simply fit/force the carbon abundance to reproduce the overall strength of the  $C_2$  molecular bands, which is sufficient for our purposes. Note also that the effective temperature for 12476+0646 has been forced to  $T_{\text{eff}} = 5000$  K, which corresponds to the coolest temperature in our DQ model grid.

The results for the 13 new DZ stars in our sample (6 from Paper I and 7 from this work) are presented in Figure 13, where the spectroscopic observations used to determine the calcium abundances in the fitting procedure are shown in the right panels. As mentioned above, the calcium abundances are determined from the strength of the Ca II H & K doublet (see also Dufour et al. 2007), while the abundance of other heavy elements, whether or not they are spectroscopically detected, are assumed to have solar ratios. Because hydrogen is often present in some of these DZ stars (DZA stars), we rely on model grids calculated with hydrogen abundances of  $\log H/He = -3, -4, \text{ and } -5$ . The insert in the right panels shows the  $H\alpha$  absorption line used to measure or constrain the hydrogen abundance in these stars. The  $H\alpha$  line is particularly strong in 17574+1021, a new DZA star identified in our survey. For stars without  $H\alpha$  or in the absence of spectroscopic data in this region sample, the fits are performed at a fixed hydrogen abundance, determined from the quality of the fit to the H & K doublet, since the amount of hydrogen present in the atmosphere influences the strength of these lines. The predicted energy distributions and spectra agree well with the observations for all 13 stars, except for 12145+7822, for which it is impossible to reproduce the narrow calcium lines with helium-atmosphere models at the low inferred temperature of  $T_{\text{eff}} \sim 4200$  K. This suggests that this star has a hydrogen-rich atmosphere instead, which should produce much narrower absorption lines due to lower atmospheric pressures. Because we do not have model atmospheres that cover the appropriate range of parameters to fit this star, we adopt a photometric solution based on pure hydrogen models (see Figure 11), since the presence of metals are not expected to affect the atmospheric structures of hydrogen-rich models.

### 3.3. Spectroscopic Analysis

#### 3.3.1. Spectroscopic Analysis of DA Stars

The atmospheric parameters of DA stars with well-defined Balmer lines ( $T_{\text{eff}} \gtrsim 6500$  K) can be accurately determined from the optical spectra using the so-called spectroscopic technique pioneered by Bergeron et al. (1992, see also Liebert et al. 2005). The optical spectrum of each star, as well as all model spectra (convolved with a Gaussian instrumental profile), are first normalized to a continuum set to unity. The calculation of  $\chi^2$  is then carried out in terms of these normalized line profiles only. The atmospheric parameters –

$T_{\text{eff}}$  and  $\log g$  – are considered free parameters in the fitting procedure. Since two solutions exist for a given star, one on each side of the maximum strength of the Balmer lines, we take advantage of our photometry to resolve the ambiguity. Also, since most of our spectra cover  $H\alpha$ , we include this line in our fitting procedure, allowing us to extend our spectroscopic fits down to  $T_{\text{eff}} \sim 6100$  K, when  $H\alpha$  is available. We however find that the internal errors on  $\log g$  increase significantly for stars cooler than  $T_{\text{eff}} < 6300$  K — and in particular for spectra with low signal-to-noise ratios ( $S/N < 40$ ) — reaching a spread of values as large as  $\sigma_{\log g} \sim 0.3$  dex, while for the best spectra  $\sigma_{\log g}$  can be as low as 0.04. In such cases where the internal errors become too large,  $\log g$  is fixed at 8.0 and the uncertainty is set at 0.25 dex, which corresponds to a  $\sim 2\sigma$  dispersion of the surface gravity distribution of hot DA stars (Gianninas et al. 2011).

Spectroscopic fits for 158 new DA stars identified in our survey, which can be analyzed with the spectroscopic technique, are presented in Figure 14. It is worth mentioning that 05025+5401 and 07029+4406 have atmospheric parameters placing them within the ZZ Ceti instability strip, and that periodic light variations are confirmed by observations that are presented along with the dominant pulsation periods in Green et al. (2015). Special care needs to be taken in the case of DA stars with unresolved M dwarf companions, in order to reduce the contamination from the companion. When the contamination affects only  $H\beta$  and/or  $H\gamma$ , we simply exclude these lines from the fit, as indicated in Figure 14 by the green lines. At other times, emission lines from the M dwarf are also observed in the center of some Balmer lines (see, e.g., 13096+6933), in which case we simply exclude the line centers from our fitting procedure. A similar approach is adopted when the contribution from the M dwarf is large enough to fill up the Balmer line cores, resulting in predicted lines that are too deep (see, e.g., 04586+6209). However, as discussed in Section 3.2.2, the white dwarf spectrum is sometimes too contaminated by the M dwarf companion to be fitted with the spectroscopic technique (03031+2317, 04032+2520E, and 08184+6606), and we must therefore rely on the photometric technique alone for these stars. Note that 04389+6351 was classified as a single DA star in Paper I, but we now find from our fits that the predicted  $H\beta$  is too deep, suggesting that a red dwarf companion is filling the line ( $H\beta$  is actually excluded from our fit here). Our photometric fit for this star (not shown here) shows a significant infrared excess at  $I_N$  and  $JHK_S$ , also suggesting the presence of a companion. We thus reclassify this star as a DA + M dwarf binary system.

There are also a few DAZ stars in our sample (including our new DAZ identifications 05431+3637, 14106+0245, and 22276+1753), for which the calcium H line (at 3968 Å) is blended with  $H\epsilon$ . Since the upper Balmer lines are particularly sensitive to surface gravity, it is important to model properly the calcium lines for these stars. To do so, we relied on a small grid of synthetic spectra, based on our grid of pure hydrogen models, where calcium lines

have been included in the calculation of the synthetic spectrum only (see Gianninas et al. 2011 and references therein). This grid covers a range in  $T_{\text{eff}}$  from 6000 to 9000 K in steps of 500 K,  $\log g$  from 7.0 to 9.5 in steps of 0.5 dex, and  $\log \text{Ca}/\text{H}$  from  $-7.0$  to  $-9.5$  in steps of 0.5 dex.

### 3.3.2. Spectroscopic Analysis of DB Stars

For the analysis of the DB and DBA white dwarfs in our sample, we rely on the spectroscopic technique described at length in Bergeron et al. (2011), which is similar to that used for DA stars but modified to fit simultaneously  $T_{\text{eff}}$ ,  $\log g$ , and H/He. The first step is to normalize the flux from individual predefined wavelength segments, in both observed and model spectra, to a continuum set to unity. The comparison with model spectra, which are convolved with the appropriate Gaussian instrumental profile, is then carried out in terms of this normalized spectrum only. However, as for DA stars, two solutions exist for a given DB spectrum, one on each side of the maximum strength of the neutral helium lines. Fortunately, all DB stars in our sample are relatively cool and it is easy to distinguish the cool and hot solutions from an examination of our best fits. Furthermore, the hydrogen abundance in DBA stars is better constrained if spectroscopic data near  $\text{H}\alpha$  are available, which is the case for most of our DB stars.

The spectroscopic fits for the 4 DB white dwarfs identified in our survey, of which 2 are DBA stars, are presented in Figure 15. Note that the hydrogen abundances in 12430+2057 represent only upper limits based on the absence of  $\text{H}\alpha$ .

## 3.4. Unresolved Double Degenerate Binaries

Four objects in Figure 11 — 04263+4820, 11337+6243, 11598+0007, and 14278+0532 — show a predicted  $\text{H}\alpha$  absorption feature significantly deeper than the observed profile; these are plotted separately in Figure 16 for clarity. Note that 14278+0532 (1425+057) was fitted as a helium-rich DC white dwarf in Sayres et al. (2012) based on a noisy SDSS spectrum, but we clearly detect the  $\text{H}\alpha$  feature in our spectrum (see also Limoges et al. 2010). For all stars, we achieve excellent fits of the model spectral energy distributions to the photometry, but the fits to the observed spectra are poor. We experimented with helium-rich models containing traces of hydrogen instead of pure hydrogen models (see, e.g., L745-46A and Ross 640 shown in Figure 14 of Giammichele et al. 2012). For 11337+6243 and 14278+0532, our best fits to these stars (not shown here) predict  $\text{H}\alpha$  profiles that are

much broader than the observed profiles due to van der Waals broadening of hydrogen lines by neutral helium. The sharp features observed here rather suggest that these correspond to DA stars whose H $\alpha$  absorption lines are diluted by the presence of an unresolved DC white dwarf companion. While it was possible to reproduce the H $\alpha$  profile for 04263+4820 using helium-rich models, our best solution predicts a steep Balmer decrement due to the destruction of the high atomic levels of hydrogen, in sharp contrast with the optical spectrum which shows the whole Balmer series all the way to H $\epsilon$ . Here again we suggest that we are rather dealing with an unresolved DA+DC degenerate binary.

For 11598+0007, although the discrepancy observed in Figure 16 is not as extreme as for the other three objects, further evidence that we are also dealing with an unresolved binary is provided by the spectroscopic fit, displayed in Figure 17. Also shown for comparison is our best spectroscopic fit to 04263+4820, discussed above, and SDSS 1257+5428, a double white dwarf binary (DA + DA) discussed in Badenes et al. (2009), Kulkarni & van Kerkwijk (2010), and Marsh et al. (2011), of which the optical spectrum has been kindly provided to us by M. H. van Kerkwijk and S. R. Kulkarni. Not only is the spectroscopic temperature for 11598+0007 ( $T_{\text{eff}} \sim 7900$  K) significantly different from the photometric temperature ( $\sim 9700$  K), but the quality of the fit is poor, not unlike our best fit to SDSS 1257+5428 under the assumption of a single DA star. In addition, the hydrogen lines in 11598+0007 exhibit a strong asymmetry similar to that observed in Figure 1 of Kulkarni & van Kerkwijk (2010) for SDSS 1257+5428, attributed in this case to orbital motion and differences in gravitational redshift from both components of the binary system. Kulkarni & van Kerkwijk obtained  $T_{\text{eff}} = 6250$  K and  $\log g = 6.0$  for the primary, and  $T_{\text{eff}} = 13,000$  K and  $\log g = 8.5$  for the secondary; Marsh et al. obtained slightly different parameters but the basic suggestion of a cool, low-mass primary with a hotter, high-mass secondary remains the same. We thus suggest that 11598+0007 also represents an unresolved DA + DA double degenerate system. As demonstrated by Liebert et al. (1991), it is normally impossible to infer the presence of such DA + DA binary systems using the spectroscopic technique alone since the coaddition of synthetic spectra of two DA stars with different values of  $T_{\text{eff}}$  and  $\log g$  can be reproduced almost perfectly by a single DA spectrum *unless the surface gravities of both components differ significantly*, which is certainly the case for SDSS 1257+5428, and it is thus most probably the case for 11598+0007 as well. Finally, the similarity between our best spectroscopic fits to 11598+0007 and 04263+4820, both displayed in Figure 17, clearly suggests the same interpretation, although in the latter case, there is no obvious asymmetry in the line profiles, either because there is no velocity difference between both components of the system, or perhaps 04263+4820 is composed of a DA + DC system.

We do not attempt here to deconvolve the individual components of these double white dwarf binary candidates, and we simply adopt the effective temperatures from the photo-



metric fits, which are more reliable than those derived from the line profiles. We further assume that both components have identical effective temperatures and surface gravities, and thus that they contribute equally to the total luminosity of the system, resulting in distances that are a factor of  $\sqrt{2}$  larger than the values obtained under the assumption of a single white dwarf. These binaries will also contribute as two objects for the calculations of the luminosity function and the space density. A more detailed analysis of these double degenerate binaries will be presented elsewhere.

### 3.5. Known White Dwarfs within 40 pc of the Sun

In order to get a full picture of the physical properties of white dwarfs within 40 pc of the Sun, we must also include, in addition to the new white dwarfs identified in our survey, all previously known white dwarfs suspected to lie within 40 pc of the Sun. Our selection criteria applied to the SUPERBLINK catalog recovered a total of 416 known white dwarfs with  $D_{\text{phot}} < 55$  pc. We reexamine this subset to exclude from the lot the known white dwarfs with distances well beyond 40 pc. This we do based on (1) a more robust photometric distance estimate described in Section 3.6, and (2) reliable spectroscopic distances found in the literature. We find 116 relatively distant white dwarfs, which leaves 300 white dwarfs that need to be included in our model atmosphere analysis, and for which optical spectra are thus required. Fortunately we already had spectra for 208 objects in this list, acquired over the years for various independent projects. Spectra for another 12 stars were directly available from the SDSS database. Also, optical spectra for 46 additional white dwarfs hot enough to be analyzed with the spectroscopic technique were secured during the spectroscopic observation campaigns listed in Table 1. Among these, GD 338 listed as a WD candidate by Giclas et al. (1980), turned out to be a main sequence star, thus reducing the number of known nearby white dwarfs to 299. Finally, 34 white dwarfs on our list are classified in the literature as DC or very cool DA stars, subtypes that can only be analyzed using the photometric technique, and for which we did not obtain new optical spectra because only a spectral type is sufficient for our present purposes.

We also need to include all known white dwarfs suspected to lie within  $\sim 40$  pc of the Sun but that were missed in our search of the SUPERBLINK catalog, either because they failed our selection criteria or are missing from the SUPERBLINK catalog itself for any reason. As discussed in Paper I, about 20% of the nearby white dwarfs are likely to be missed in our search because of their unusual photometry, in particular Sirius-like systems of white dwarfs companions to main-sequence stars. With this limitation in mind, we searched the following papers for objects with parallaxes larger than  $0''.025 \text{ yr}^{-1}$  or photometric/spectroscopic dis-

tances less than 40 pc of the Sun: the WD Catalog, Bergeron et al. (1997), Bergeron et al. (2001), Kawka & Vennes (2006), Kilic et al. (2006), Gatewood & Coban (2009), Kilic et al. (2010), Kilic et al. (2012), Sayres et al. (2012), Giammichele et al. (2012), Harris et al. (2013), Gianninas et al. (2015), as well as the large spectroscopic samples of Gianninas et al. (2011) and Genest-Beaulieu & Bergeron (2014, SDSS DR7) for DA stars, and Bergeron et al. (2011) for DB stars, and also Holberg et al. (2013) for Sirius-like systems. We also included individual objects such as the ultracool white dwarfs LHS 3250 (Harris et al. 1999; Bergeron & Leggett 2002), WD 0343+247 (Hambly et al. 1999), and SDSS J1102+4113 (Hall et al. 2008). Finally, we also searched nearby DZ stars in the sample of Dufour et al. (2007) and nearby DQ stars in the samples of Dufour et al. (2005) and Koester & Knist (2006), although we did not do a thorough search of the latest data releases of the SDSS. As was the case for the 20 pc sample, identifying all known white dwarfs with 40 pc of the Sun is a major endeavor, and we do not pretend that the above list is complete, in particular given the large number of white dwarfs continuously being identified in the SDSS.

All these *known* white dwarfs suspected to lie within 40 pc of the Sun, within the uncertainties, have been combined with the 325 *new* white dwarfs identified in our survey of SUPERBLINK. We performed a spectroscopic or photometric analysis of each known white dwarf following the same fitting procedures described above. Since most of these stars have already been analyzed elsewhere in the literature, we do not provide here the detailed fits for individual stars, although our atmospheric parameters may reflect improved data sets and/or model spectra. We discuss some specific cases in turn.

As pointed out in Bergeron et al. (2011), several DB stars cooler than  $T_{\text{eff}} \sim 15,000$  K show masses in excess of  $1 M_{\odot}$ , most likely because these cool objects, with their weak and shallow line profiles, lie at the limit of reliability for the spectroscopic technique. Three of these DB stars (KUV 02499+3442, 21003+3426, and 21499+2816) are in our sample of nearby candidates. Since the spectroscopic  $\log g$  values and inferred distances are uncertain, we adopt  $\log g = 8.0$  for these 3 white dwarfs. Doing so, we obtain for 21499+2816 a distance of  $37.7 \pm 1.5$  pc, in better agreement with the value of  $35.3 \pm 3.8$  pc suggested by the trigonometric parallax. As mentioned in Bergeron et al., a value of  $\log g = 8.2$  would actually reconcile both distance estimates perfectly, which suggests that the spectroscopic  $\log g$  values for these stars are likely overestimated.

An interesting object in our sample is 09487+2421 (0945+245, LB 11146), an unresolved binary system composed of a DA star and a magnetic white dwarf (DA + DAXP). We use here the values from Liebert et al. (1993) obtained by the deconvolution of both spectra:  $T_{\text{eff}} = 14,500 \pm 1000$  K,  $\log g = 8.4 \pm 0.1$  for the DA component, and  $T_{\text{eff}} = 16,000 \pm 2000$  K and  $\log g = 8.5 \pm 0.2$  for the magnetic component. Based on their distance estimate of  $40 \pm 5$

pc, this binary system is included in the 40 pc sample, and will count as 2 white dwarfs in the luminosity function.

Another interesting object in our sample is 01489+1902 (GD 16), a helium-rich DAZB star analyzed in detail by Koester et al. (2005). They obtained  $T_{\text{eff}} = 11,500 \pm 300$  K,  $\log \text{H}/\text{He} = -2.89 \pm 0.3$ , and  $\log \text{Ca}/\text{He} = -8.7 \pm 0.2$  under the assumption of  $\log g = 8.0$ . Since this last assumption will affect the spectroscopic distance estimate, we analyzed this star ourselves using the same spectroscopic technique for DB stars outlined in Section 3.3.2, with mixed H/He model atmospheres that also include the opacity from Ca II H & K; the additional lines of Mg and Fe visible in the spectrum are not included in our models. Our best fit is displayed in Figure 18 where we find  $T_{\text{eff}} = 10,420$  K and  $\log g = 7.71$ ; these are the only two free parameters in our fit. The helium abundance is set according to the depth of the HeI 5875 line reported by Koester et al. (2005), while the calcium abundance is fixed at a value that reproduces the observed strength of the calcium lines in our spectrum. The values we obtain for the helium abundance ( $\log \text{H}/\text{He} = -2.70$ ), and for the calcium abundance ( $\log \text{Ca}/\text{He} = -8.5$ ), are in good agreement with the values derived by Koester et al. (2005), while the effective temperature is  $\sim 1100$  K lower, a difference that may be explained by the fact that we do fit  $\log g$  instead of simply assuming a value of 8.0. The corresponding distance of  $D = 63.7 \pm 2.9$  pc is 13.7 pc further away than the distance obtained by Koester et al., and significantly outside our limit of 40 pc. Finally, we notice that our spectrum displayed in Figure 18 shows what appears to be a blue component in the wings of H $\beta$ , H $\gamma$ , and H $\delta$ , which could indicate that this object is in fact an unresolved double degenerate binary.

### 3.6. Adopted Atmospheric Parameters

As discussed in the Introduction, the spectroscopic  $\log g$  values of DA stars show a significant increase at low temperatures ( $T_{\text{eff}} \lesssim 13,000$  K) with respect to the  $\log g$  distribution of hotter DA stars — the so-called high- $\log g$  problem. Hydrodynamical 3D models (Tremblay et al. 2013b, see also Tremblay et al. 2011, 2013a) have now successfully shown that this problem is related to the limitations of the mixing-length theory used to describe the convective energy transport in standard 1D model atmospheres calculations. These spurious  $\log g$  values prevent us from obtaining reliable mass and distance estimates for DA stars in our sample in this particular range of temperature. Indeed, those higher  $\log g$  values will yield underestimated spectroscopic distances, biasing our census of white dwarfs within 40 pc. To overcome this problem, Giammichele et al. (2012) derived an empirical procedure (see their Section 5 and Figure 16) to correct the  $\log g$  values based on the DA stars in the

SDSS (DR4), analyzed by Tremblay et al. (2011); this was also our approach in Paper I. Here we make use of the latest results from Tremblay et al. (2013b) who presented their first complete grid of 3D synthetic spectra for DA white dwarfs based on 3D hydrodynamical model atmospheres. In particular, they provided correction functions to be applied to both  $T_{\text{eff}}$  and  $\log g$  measurements determined using the spectroscopic technique with model spectra calculated within the mixing-length theory — the  $ML2/\alpha = 0.7$  prescription in our case. We thus apply these corrections to our sample of DA stars whose atmospheric parameters have been obtained using the spectroscopic method.

Because the distance to each white dwarf in our sample is a key issue in our study, some care must be taken to reduce the uncertainty on the distance estimates as much as possible. For stars with trigonometric parallax measurements available (167 objects), we adopt the corresponding distances directly. Out of these 167 parallax measurements, 9 have uncertainties larger than 20%, while Feige 4 and HZ 9 have uncertainties of 31% and 30%, respectively. However, even for these last two objects we prefer to use the parallax-based distances because the spectroscopic distance to Feige 4 is largely inconsistent with the parallax value (Bergeron et al. 2011), and because HZ 9 is a DA + M dwarf system whose spectral energy distribution is highly contaminated by the M dwarf, which means we only have a single data point to determine the distance from the photometric fit. For stars without parallaxes and fitted using the photometric method (DC, DQ, DZ, and cool DA stars), the distance is determined from the measured solid angle  $\pi(R/D)^2$  combined with the stellar radius corresponding to  $\log g = 8.0 \pm 0.25$ , as discussed in Section 3.2.1. Finally, for white dwarfs in our sample only fitted with the spectroscopic technique and without parallaxes, we fit all the available photometric data but force the spectroscopic values of  $T_{\text{eff}}$  and  $\log g$  (and the corresponding radius) and derive the distance from the fitted solid angle (see also Limoges et al. 2013). The distance uncertainty in this case is obtained from the combination in quadrature of the error on the spectroscopic  $\log g$  and the solid angle. This approach for measuring spectroscopic distances has the advantage of using all the photometric information rather than relying on the distance modulus from a single bandpass.

Our final results for the 325 white dwarfs identified in our survey are presented in Table 4, while the results for the 492 white dwarfs, or white dwarf systems, identified within 40 pc of the Sun with  $\delta > 0$  are presented in Table 5, which includes 178 new objects from our survey. Note that Table 5 includes several unresolved double degenerate systems (noted in the table). We give for each object the PM I designation if the white dwarf is a SUPERBLINK object, the spectral type, effective temperature ( $T_{\text{eff}}$ ), surface gravity ( $\log g$ ), stellar mass ( $M/M_{\odot}$ ), atmospheric composition (H- or He-dominated), absolute visual magnitude ( $M_V$ ), luminosity ( $L/L_{\odot}$ ), distance ( $D$ ), trigonometric parallax ( $\pi$ ) if available, white dwarf cooling time ( $\log \tau$ ), and the method used to determine the atmospheric parameters. As discussed

above, the spectroscopic solutions for both  $T_{\text{eff}}$  and  $\log g$  for the DA stars have been corrected for the high- $\log g$  problem and these differ from the uncorrected values given in Figure 14.

#### 4. PHYSICAL PROPERTIES OF THE 40 PC SAMPLE

The atmospheric parameters of white dwarfs within 40 pc of the Sun given in Table 5 represent the end result of our large spectroscopic survey undertaken in 2009, and the foundation of the homogeneous study of the local white dwarf population presented below. Although not yet complete, this sample of 492 white dwarfs — or white dwarf systems — should be relatively free of kinematic bias, allowing us to draw a picture of the local white dwarf population (in the northern hemisphere) to a distance twice as large as the 20 pc sample analyzed by Holberg et al. (2008), Giammichele et al. (2012), and their predecessors. We provide in the following a detailed analysis of the physical properties of this sample, but we first attempt to evaluate the completeness of the sample in order to better understand its limitations.

##### 4.1. Completeness of the 40 pc Sample

We compile 492 white dwarfs (501 including the double degenerate binaries) within 40 pc — to within the distance uncertainties — among which 178 are new identifications, marked with a star symbol in Table 5. Only 167 of these stars have trigonometric parallax measurements, however, and additional measurements in the near future (e.g. by the Gaia mission) will most likely add or remove stars from this sample. Until then, we can still evaluate the completeness of the 40 pc sample by calculating the cumulative number of stars as a function of distance. The results are displayed in Figure 19 where the cumulative number of stars in our sample is compared to the expected number of white dwarfs assuming a space density of  $4.8 \times 10^{-3} \text{ pc}^{-3}$ , which corresponds to the value derived from the smaller 13 pc sample, which is however believed to be complete (Holberg et al. 2008). The expected number of stars is also divided by a factor of two since our survey is restricted to the northern hemisphere. Also shown for comparison is the expected number of stars for the whole celestial sphere.

We first notice that within 20 pc, the cumulative number of stars reaches a value of 69, out of an expected number around 80 (or 85%), but the number of white dwarfs in our sample increases to 99 if we take into account the formal uncertainties in our distance measurements, stressing the importance of improving these distance estimates through precise

trigonometric parallax measurements. Out of the 69 stars within 20 pc in our sample, 4 are new identifications (13413+0500, 14456+2527, 16325+0851, 23098+5506E), among which only 2 are actually fitted with the spectroscopic method allowing for more robust distance measurements, while for the other 2 objects, the distances are only estimated from the photometric method under the assumption of  $\log g = 8$ . We also find 4 additional known white dwarfs within 20 pc with respect to the sample of Giammichele et al. (2012) — 00222+4236, 11508+6831, 15350+1247, and 15425+2329. Hence, these results suggest that the 20 pc sample in the northern hemisphere is probably close to completeness, with a density consistent with the 13 pc sample.

Similarly, we find 125 white dwarfs within 25 pc (possibly up to 172 if we consider the distance uncertainties), whereas Sion et al. (2014) report a total of 224 white dwarfs for the same volume but in both hemispheres. Sion et al. estimate the completeness of their sample at 65%, which implies an expected number of white dwarfs around  $\sim 172$  in the northern hemisphere only, precisely the number we are finding if we allow for distance uncertainties. At 30 pc, the cumulative number of stars in Figure 19 becomes significantly less than expected (assuming that the space density of the 13 pc sample is valid everywhere), which suggests that our sample is significantly incomplete beyond this range.

By taking only the subsample of 427 stars with  $D < 40$  pc from Table 5, we derive a space density of  $3.19 \times 10^{-3} \text{ pc}^{-3}$ , with an upper estimate of  $3.74 \times 10^{-3} \text{ pc}^{-3}$  if we take into account the distance uncertainties, which correspond to 66% to 78% of the density of the 13 pc sample ( $4.8 \times 10^{-3} \text{ pc}^{-3}$ ). Our upper estimate is thus consistent with the 77% completeness value estimated in Paper I for the present efficiency of our survey in detecting white dwarfs using reduced proper motion diagrams. However, as mentioned in Section 2.2,  $\sim 330$  high-priority objects still remain to be observed out of our larger list of 1180 white dwarf candidates. Results from Paper I suggested that our discovery rate dropped to 54% when stars that did not meet our best selection criteria (but with distance estimates less than 30 pc) were observed spectroscopically. Therefore, even if only 50% of the remaining 330 high-priority candidates are confirmed as white dwarfs within 40 pc of the Sun, the number of such stars could rise to more than 600, which is the expected number of objects in Figure 19 based on the space density at 13 pc.

We must also consider the various sources of incompleteness in our survey that can prevent the identification of all white dwarfs within 40 pc of the Sun, especially those associated with our use of the SUPERBLINK catalog as the primary source of candidates. First, our selection excludes stars fainter than  $V = 19$  since the rate of spurious detection in SUPERBLINK increases significantly at fainter magnitudes. Stars are also excluded if they have non-standard magnitudes for a white dwarf, a good example of which are Sirius-like



systems, which are completely overlooked in our selected sample. In Sirius-like systems, as opposed to binary systems where the companion is an M dwarf, the flux is completely dominated by the main sequence star. In the 20 pc sample of Giammichele et al. (2012), there are 7 Sirius-like systems, all of which are in the southern hemisphere, with the exception of Procyon B (0736+053), while in Holberg et al. (2013), there are 6 Sirius-like systems with  $D < 40$  pc in the northern hemisphere only. As expected, none of these were recovered by our selection criteria. We note, however, that 5 of these 6 systems were included in our analysis afterward; 0911+023 at 34.8 pc was let aside, however, since it is unresolved with a B star. The Sirius-like systems thus represent 3% of the white dwarf population within 25 pc, and we may expect that  $\sim 13$  of these systems are missed in the 40 pc sample. Five other stars were missed because of their inaccurate colors, or because of a mismatch with SDSS and/or 2MASS magnitudes.

Some white dwarfs were also missed simply because they are not in the SUBERBLINK catalog to begin with. Stars with proper motions  $< 40$  mas yr $^{-1}$  would of course not be part of our selection, but there are other cases where stars might be missing from the catalog. To be included in SUPERBLINK, a star must either be a TYCHO-2 or Hipparcos catalog stars, or it must be detected as a high proper motion star on the digitized POSS I and II plates. As discussed by Lépine & Shara (2005), SUPERBLINK is less efficient at recovering stars with bright saturated cores on those plates, leaving some bright stars out. Thus we note that some WD + M dwarf systems known to be within 40 pc were missed, in particular HZ 9, which is brighter than  $V = 13$  at  $I_N$ . Sixteen very bright white dwarfs could also not be found in the published version of the SUPERBLINK catalog of Lépine & Shara (2005), and are thus also missing from our candidate list.

Finally, some stars can also be overlooked because of missing or inaccurate tabulated photometry in SUPERBLINK, most often due to faulty optical magnitudes from the USNO-B1.0 catalog counterpart. Because our selection criteria and distance estimates are based on empirical  $V$  magnitudes derived from USNO-B1.0 magnitudes, the estimated distances can be severely affected if the  $B_J$ ,  $R_F$ , and  $I_N$  are inaccurate by more than the adopted 0.5 mag value. We actually identified 2 known white dwarfs that were not recovered in the USNO-B1.0 catalog, and 11 white dwarfs were also excluded from our candidate list because we estimated a distance larger than 55 pc. All in all, about 3% of the stars are missed in this manner.

Taking into account all the sources of incompleteness, we estimate that, to the best of our knowledge, some 50 white dwarfs have probably been overlooked by our survey, for a ratio of missed-to-found of 17%, a value consistent with the apparent 77% efficiency of our survey at detecting white dwarfs, as discussed above. With these limitations in mind, we

provide a detailed statistical analysis of our sample knowing that  $\sim 25\%$  of the white dwarfs might still be missing from our sample. Nevertheless, even if our 40 pc sample cannot be analyzed as thoroughly as the 20 pc sample, the small number statistics problem inherent to the 20 pc sample discussed by Giammichele et al. (2012) has been significantly improved.

#### 4.2. Kinematics of the 40 pc Sample

Before interpreting the global properties of the 40 pc sample, we must first verify if the sample is relatively free of kinematic bias, which we do by examining its velocity-space distribution. The velocity components ( $U, V, W$ ) are determined from the photometric distances (or trigonometric parallaxes when available) and proper motions for each star. Since radial velocities are not available for most of the stars in our sample, we assume  $V_{\text{rad}} = 0$ , but in order to obtain an unbiased representation of the motion of the stars in our sample despite this approximation, we use the method described in Lépine et al. (2013). We first evaluate the ( $X, Y, Z$ ) positions of the stars in the Galactic reference frame and then we use the fact that  $U \propto (X/D)V_{\text{rad}}$ ,  $V \propto (Y/D)V_{\text{rad}}$  and  $W \propto (Z/D)V_{\text{rad}}$  to obtain the ( $U, V, W$ ) velocity components. However, if  $|X| > |Y|$  and  $|X| > |Z|$ , then the position vector as well as the radial velocity vector mainly points toward the  $X$  direction, so the radial velocity mainly contributes to the  $U$  component of velocity, but its contribution to the  $V$  and  $W$  components of velocity is small. Then, the  $V_{\text{rad}} = 0$  approximation is valid to obtain *estimates* for the velocity components  $V$  and  $W$ , but not for  $U$ . Likewise, stars with the largest  $\pm Y$  components (or  $\pm Z$  components) are good tracers of the velocity dispersion in  $U$  and  $W$  (or  $U$  and  $V$ ), even if their radial velocities are not known. We can then estimate in this manner at least two velocity components for each star, and the component that depends the most on the radial velocity is excluded from any representation or statistical calculation.

Our results are displayed in Figure 20. For reasons outlined in the previous paragraph, each star appears in a single panel only. The mean values of the velocity components are

$$\begin{aligned} \langle U \rangle &= -9.82, \quad \sigma_U = 41.00 \text{ km s}^{-1} \\ \langle V \rangle &= -26.58, \quad \sigma_V = 29.46 \text{ km s}^{-1} \\ \langle W \rangle &= -8.26, \quad \sigma_W = 17.37 \text{ km s}^{-1} \end{aligned}$$

which happen to be in relative agreement with those reported by Fuchs et al. (2009) for stars in the SDSS belonging to the thin disk:  $\langle U \rangle = -8.6$  and  $\sigma_U = 32.4 \text{ km s}^{-1}$ ,  $\langle V \rangle = -20.0$  and  $\sigma_V = 23.0 \text{ km s}^{-1}$ , and  $\langle W \rangle = -7.1$  and  $\sigma_W = 18.1 \text{ km s}^{-1}$ . If we consider only the new white dwarf identifications (shown as solid circles in Figure 20), the space velocities we derive are of the same order,  $\langle U \rangle = -8.09$  and  $\sigma_U = 34.27 \text{ km s}^{-1}$ ,  $\langle V \rangle = -23.98$  and  $\sigma_V = 27.87$

km s<sup>-1</sup>, and  $\langle W \rangle = -6.85$  and  $\sigma_V = 19.31$  km s<sup>-1</sup>, but we still notice the presence of “holes” in the distribution of new white dwarfs near  $(U, W) = (0, 0)$  and  $(U, V) = (0, 0)$  when compared to the velocity distribution of known white dwarfs. The red circle in each panel of Figure 20 represents the presumed kinematic limit of our survey due to the  $\mu > 0''.04$  yr<sup>-1</sup> proper motion limit and  $D < 40$  pc distance range, which corresponds to a transverse motion  $v_T = 4.74 \mu D = 7.6$  km s<sup>-1</sup>. In *Hipparcos*, 2.3% of the stars fainter than  $V \sim 9$  with  $\delta > 0$  and  $\pi > 0''.25$  yr<sup>-1</sup> ( $D < 40$  pc) have  $\mu > 0''.04$  yr<sup>-1</sup>, implying that we are only missing  $\sim 11$  white dwarfs within 40 pc because of the presumed kinematic limit of our survey. We also notice that the holes are larger than our presumed limit of detection, implying that some low-velocity white dwarfs are probably still hiding in our list of candidates, awaiting spectroscopic confirmation.

We find no white dwarfs in our 40 pc sample that appear reliably old enough to belong to the halo population of old stars. This is consistent with the Sion et al. (2014) study of the 25 pc sample, where no definite halo white dwarf was found either. Our only possible halo candidates are the two DC stars cool enough to be very old, however we cannot be certain of their age because we assumed  $\log g = 8.0$  by default for these stars, and an accurate cooling age can only be obtained when the stellar mass is known. Another possible candidate is the star 19401+8348, seen in the upper right corner of the  $(U, W)$  diagram in Figure 20, which has relatively high velocity components compared to the other stars in the diagram. This object is a DC star with  $T_{\text{eff}} \sim 4800$  K and a distance of  $D = 38.8 \pm 12$  pc, for which we also assumed  $\log g = 8.0$ , which means its cooling age remains uncertain. Even if we extend our search to stars with  $D > 40$  pc (not shown in Figure 20), we do not find any white dwarf that would reliably appear old enough to be a member of the halo population. This is however not inconsistent with the single-point luminosity function of Fontaine et al. (2001) based on the two halo white dwarfs 2316–064 and 1022+009, from which we estimate  $n(L) = 10^{-5.39}$  pc<sup>-3</sup>  $M_{\text{bol}}^{-1}$  at  $\log L/L_{\odot} \sim -4.09$  ( $T_{\text{eff}} \sim 5000$  K), which predicts the existence of only a single halo white dwarf within 40 pc of the Sun in this particular luminosity range. Finally, we note a small asymmetry in the two bottom panels of Figure 20 towards negative  $V$  values, which might suggest a small but non-negligible component of the thick disk population in our sample.

### 4.3. Mass Distribution

The mass distribution for the white dwarfs in Table 5 with  $D \lesssim 40$  pc is displayed in Figure 21 as a function of effective temperature. Only those with a measured mass are shown here (288 out of 492 objects from Table 5); the objects with an assumed value of

$\log g = 8$  are shown at the bottom of the figure. These include the coolest DA stars with weak hydrogen lines analyzed spectroscopically, most of the magnetic white dwarfs, and all non-DA stars analyzed photometrically but without trigonometric parallax measurements. Since most of our new identifications do not have trigonometric parallaxes available yet, the number of cool helium-rich white dwarfs with mass measurements is rather small in this figure, in comparison for instance with the mass distribution displayed in Figure 21 of Bergeron et al. (2001), which includes all cool white dwarfs with trigonometric parallax measurements available at that time. There, 54 out of 150 white dwarfs (or 36%) had helium-rich atmospheres, compared to 39 out 288 (or 13%) in Figure 21. In fact, most cool helium-atmosphere white dwarfs with mass determinations come from the 20 pc sample. The situation will of course change significantly when the Gaia mission is completed.

The cumulative mass distribution for the same subset of white dwarfs, regardless of their effective temperature, is displayed in Figure 22, where the separate contributions of hydrogen- and helium-rich stars are also shown. This distribution can be contrasted with that shown in Figure 21 of Giammichele et al. (2012) for the 20 pc sample. Here again we see that the helium-atmosphere white dwarfs in the 40 pc sample are significantly undersampled in the cumulative mass distribution. The relative number of helium- to hydrogen-rich objects in our sample is small, but we observe that the median masses and mass dispersions of both subsamples are generally comparable. The *mean mass* of the hydrogen-rich sample, however, is about  $0.04 M_{\odot}$  larger than the helium-rich counterpart. This is mostly due to the prominent high-mass tail observed in the distribution of hydrogen-atmosphere white dwarfs. To better illustrate this feature, we contrast in Figure 23 the mass distribution of the 40 pc sample with that of the 20 pc sample from Giammichele et al. (2012), which is based on both spectroscopic and photometric mass measurements, and with the spectroscopic mass distributions of DA stars from the SDSS (Tremblay et al. 2011) and from the WD Catalog (Gianninas et al. 2011). The excess of high mass white dwarfs in the 40 pc sample is quite obvious, a result that strongly suggests we are successfully recovering the high-mass, less luminous white dwarfs, which are often missed in magnitude-limited surveys (see, e.g., Liebert et al. 2005 in the case of the PG survey, and in particular their discussion of Figure 13). A higher fraction of massive white dwarfs has also been identified in the analyses of hot DA stars from ROSAT and EUVE (Vennes et al. 1996, 1997, 1998), since such surveys catalog all sources, regardless of the brightness of the object.

This excess of massive white dwarfs seems to be related to the population of low temperature white dwarfs apparent in Figure 21, between roughly  $T_{\text{eff}} = 6000$  K and 7000 K. These are all DA stars for which the atmospheric parameters — and in particular  $\log g$  and thus  $M$  — have been determined spectroscopically. Note that even though 3D hydrodynamical corrections, which are negligible in this temperature range, have been properly applied to

our spectroscopic results, it is still legitimate to question the validity of the spectroscopic masses in this particular range of temperature. As discussed in Tremblay et al. (2010) — see in particular their Figure 14 (panel b) and Section 5.1 — the strength of the hydrogen lines in this temperature regime is particularly sensitive to the *neutral particle interactions* in the description of the occupation probability formalism, and a slight change in the hard sphere radius in this case may result in significantly lower  $\log g$  values. Indeed, Bergeron et al. (1991) found that a direct implementation of the Hummer-Mihalas occupation probability formalism yields  $\log g$  values that are too low in the regime where non-ideal effects become dominated by neutral interactions ( $T_{\text{eff}} \lesssim 8000$  K), a problem that could be overcome by simply dividing the hydrogen radius by a factor of two to reduce the non-ideal effects for the higher lines of the Balmer series (this is the factor actually used in our models). At the same time, we also notice in Figure 21 that the mass distribution near  $\sim 0.6 M_{\odot}$  in the same temperature range, and below, appears perfectly normal, suggesting that the model spectra are properly calibrated. Hence the high mass tail observed in Figure 22 might be real after all. Clearly, a detailed comparison of mass measurements derived from spectroscopy and *precise* trigonometric parallaxes in this range of temperature should shed some light on this result. Finally, we also note in Figure 21 an abrupt cutoff of massive white dwarfs below  $\sim 6000$  K, but this is certainly due to the fact that cooler objects would appear as DC stars (or weak DA stars) whose masses can only be determined from the photometric method using trigonometric parallax measurements, which are currently unavailable. Hence it is possible that this high mass tail extends to even lower temperatures.

Also superposed on the mass distribution shown in Figure 21 are the theoretical isochrones for our C/O core evolutionary models with thick hydrogen layers, as well as the corresponding isochrones with the main sequence (MS) lifetime taken into account; here we assume for simplicity (see Wood 1992)  $t_{\text{MS}} = 10(M_{\text{MS}}/M_{\odot})^{-2.5}$  Gyr and  $M_{\text{MS}}/M_{\odot} = 8 \ln[(M_{\text{WD}}/M_{\odot})/0.4]$ . In the 20 pc sample of Giammichele et al. (2012), the 5 stars older than 8 Gyr (among which the oldest is 9.5 Gyr old) are all located in the southern hemisphere, and they are thus not included in our sample. The oldest white dwarf in Figure 21 is only  $\sim 8$  Gyr old, although we see that there are plenty of objects without mass determinations that may be significantly older. The isochrones that include the MS lifetime reveal that white dwarfs with  $M \lesssim 0.48 M_{\odot}$  cannot have C/O cores, and yet have been formed from single star evolution within the lifetime of the Galaxy. Some, and probably all, of the low-mass white dwarfs in Figure 21 must be unresolved double degenerate binaries with helium cores, i.e. the result of common envelope evolution. The known double degenerate systems are identified in Figure 21. Three of the low-mass ( $M < 0.45 M_{\odot}$ ) white dwarfs with  $\delta > 0$ , 1345+238, 2048+263, and 2248+293, have already been discussed in Giammichele et al. (2012), while we identify here 01294+1023 (0126+101, DD, Bergeron et al. 2001), 03467+2456 (0343+247), 06026+0904, 09466+4354 (0943+441),

13309+3029 (1328+307, DZ), 13455+4200, 15555+5025 (1554+505), 16540+6253 (1653+630; LHS 3250), 17055+4803W (1704+481.2; Sanduleak B), 18205+1239 (1818+126, DD, Bergeron et al. 2001), 23253+1403 (2322+137), 22225+1221 (2220+121), and 23549+4027 (2352+401, DQ). Not surprisingly, most of these were already known in the literature since these objects, with their large radii and high luminosities, can easily be detected in most surveys.

The mean mass of the 40 pc sample (with mass determinations) is  $\langle M \rangle = 0.699 M_{\odot}$  with a standard deviation of  $\sigma_M = 0.185 M_{\odot}$  (Figure 22). These values are significantly larger than those reported by Giammichele et al. (2012) for the 20 pc sample,  $\langle M \rangle = 0.650 M_{\odot}$  and  $\sigma_M = 0.161 M_{\odot}$ . Our higher mean mass is actually due to the hydrogen-rich white dwarfs in the 40 pc sample, with  $\langle M_{\text{H}} \rangle = 0.705 M_{\odot}$ , while Giammichele et al. obtained  $\langle M_{\text{H}} \rangle = 0.650 M_{\odot}$ . However, the mean masses for the helium-atmosphere white dwarfs are identical,  $\langle M_{\text{He}} \rangle = 0.660 M_{\odot}$ , which also compare really well with the mean mass for DB stars determined spectroscopically by Bergeron et al. (2011),  $\langle M_{\text{H}} \rangle = 0.671 M_{\odot}$ . As mentioned above, the mass distribution of the 40 pc sample also peaks at larger mass values than the 20 pc sample, although it is comparable to the peak value obtained by Gianninas et al. (2011) for the DA stars in the WD catalog of McCook & Sion, also reproduced in Figure 22.

#### 4.4. Evolution of Surface Composition

Since the photometric data set for the 40 pc sample is not as accurate as that of the 20 pc sample, it is not yet possible to study the evolution of the surface composition as a function of temperature in as much detail as in Bergeron et al. (1997, 2001), for instance (see also Bergeron et al. 2013). Also, since trigonometric parallax measurements are not available for most of the new white dwarfs identified in the 40 pc sample, stellar masses cannot be determined for these objects either. It is still possible, however, to examine the spectral evolution of the white dwarfs in our sample by ignoring this second parameter, and by remembering that our temperature scale remains somewhat uncertain for some stars, in particular those that have only USNO-B1.0 photographic magnitudes available.

The distribution of the main spectral types (DA, DC, DQ, DB, and DZ) as a function of effective temperature is displayed in Figure 24; the only 2 white dwarfs missing from this figure are the DXP stars 17481+7052 (1748+708, G240-72) and 18303+5447 (1829+547, G227-35). We can see that, as expected, the local sample is dominated by cool white dwarfs (see also Figure 21), with the typical rise in the number of cool DA and DC stars — the dominant spectral types here — expected at the faint end of the luminosity function. We notice that the sudden drop in the number of DA stars below  $T_{\text{eff}} \sim 5000$  K is largely compensated by the significant increase in the number of DC stars in the same temperature range, which



suggests that several of these DC stars probably have hydrogen-rich atmospheres. Many of them might even reveal the presence of  $H\alpha$  when observed at even larger signal-to-noise ratios using 4 to 10-m class telescopes, as demonstrated for instance by Greenstein (1986) or Bergeron et al. (1997).

While no DB stars were reported in the 20 pc sample studied by Giammichele et al. (2012), the 40 pc sample now includes 7 DB stars — 00051+7313 (0002+729), Feige 4 (0017+136), KUV 05034+1445 (0503+147), GD 325 (1333+487), 16473+3228 (1645+325), 20123+2338 (2010+310) and 21499+2816 (2147+280) — and none of these correspond to new detections. DQ and DZ stars are rather rare in our sample, representing only 5% of all white dwarfs below  $T_{\text{eff}} \sim 12,000$  K, but still 40% of all helium-atmosphere white dwarfs in the 6000 – 12,000 K temperature range (the spectral type alone below 6000 K is not sufficient to infer the chemical composition). While it is difficult to misclassify a DQ star in our sample, in particular at low temperatures where the  $C_2$  Swan bands are usually the strongest, a significant number of DZ stars might still be present among the 118 cool DC stars in our sample due to the lack of appropriate spectral coverage, resolution, or signal-to-noise ratio of our spectroscopic observations.

As discussed in the Introduction, it is now believed that most, if not all, cool DC stars with  $T_{\text{eff}} \lesssim 5000$  K probably have hydrogen-rich atmospheres, a result based on a reanalysis of the existing photometry with model atmospheres that include the red wing opacity from  $Ly\alpha$  (this excludes DQ and strong DZ stars in the same temperature range, which obviously have helium-dominated atmospheres). We have 4 DC white dwarfs below 5000 K in Figure 21 with helium atmospheres, 2 of which are known in the literature and only one with trigonometric parallax, and thus mass measurements. For some of these objects, we do not even have a spectrum near  $H\alpha$ , and in some other cases the photometry is clearly suspicious, in particular at  $JHK$ . Hence for all 4 stars, the pure hydrogen solution would be equally acceptable. We thus reaffirm the conclusion first made by Kowalski & Saumon (2006), and supported by Giammichele et al. (2012), that most cool DC stars probably have hydrogen atmospheres.

One of the most puzzling results of our analysis is displayed in Figure 25 where we show in the left panel the total number of stars as a function of effective temperature per bin size of 2000 K, as well as the individual contribution of the hydrogen-atmosphere white dwarfs, while we show in the right panel the ratio of helium-atmosphere white dwarfs to the total number of stars. As mentioned in the previous paragraph, the results below  $T_{\text{eff}} = 5000$  K should be considered with caution. The results above this temperature, however, are fairly robust since most solutions are constrained by the presence or absence of  $H\alpha$  when the photometric method is used, or in the case of hotter DA stars, the atmospheric parameters

have been obtained from the spectroscopic method. Above 15,000 K, the fraction of helium-atmosphere white dwarfs is around 25%, in good agreement with the fraction of DB stars found in the PG survey, as determined by Bergeron et al. (2011). In the 13,000 – 15,000 K temperature range, this fraction drops to only 5%, although the total number of helium-rich stars in this temperature bin is admittedly small (see left panel). Below 13,000 K, the fraction of helium-atmosphere white dwarfs gradually increases towards lower temperatures, and keeps increasing to a ratio around  $\sim 25\%$  in the 7000 – 9000 K temperature range. Even though this trend is entirely consistent with the results reported by Giammichele et al. (2012, see their Figure 20) for the 20 pc sample, the fraction of helium-atmosphere white dwarfs reaches a much higher value around 40% in the 20 pc sample. To better understand this discrepancy, we show in Figure 26 similar results as those displayed in Figure 25 but only for temperatures in the range  $7000 < T_{\text{eff}} < 9000$  K and this time as *a function of distance*. Below 20 pc, we recover the results of Giammichele et al. (2012) almost perfectly, but beyond this distance, the fraction of helium-atmosphere white dwarfs drops abruptly. By looking at the results shown in the left panel of Figure 26, we can see that the 20 pc sample probably suffers from small number statistics, and that these statistics become more significant at larger distances. Otherwise, we cannot think of a single bias in our survey that would produce such a trend, either in favor of DA stars beyond 20 pc, or against non-DA stars. We thus believe that the peak value near 40% reported by Giammichele et al. was overestimated.

In Giammichele et al. (2012, see also Tremblay & Bergeron 2008), the increase in the fraction of helium-atmosphere white dwarfs at lower temperatures was interpreted as the result of convective mixing, where the thin convective hydrogen atmosphere is mixed with the deeper and more massive helium convection zone. Since the fraction of helium-atmosphere white dwarfs at low temperatures in our sample is now consistent with that of DB stars at higher temperatures (here and in the PG sample), there appears to be little evidence that convective mixing ever occurs in cool DA stars, at least in the temperature range considered here. This in turn implies that DA stars have fairly thick hydrogen layers of the order of  $M_{\text{H}}/M_{\text{tot}} \sim 10^{-6}$  (see Figure 1 of Tremblay & Bergeron 2008). This revised conclusion is a direct consequence of our analysis of a more statistically significant, volume-limited sample.

Finally, as discussed in the Introduction, Bergeron et al. (1997, 2001) suggested the presence of a non-DA gap (or deficiency) between  $T_{\text{eff}} \sim 5000$  K and 6000 K where most stars appear to have hydrogen-rich compositions, while helium-atmosphere white dwarfs exist above and below this temperature range (see also Bergeron et al. 2013). While we have indeed very few ( $\sim 3$ ) helium-atmosphere white dwarfs in Figure 21 with a mass determination in this particular range of temperature, our sample still contains a significant number of such helium-rich stars without mass determinations. However, as mentioned before, the

photometric data for most of these objects are not accurate enough to pinpoint their temperature with sufficient precision, and we will thus refrain from further interpreting the presence or absence of this non-DA gap in our sample at this stage.

#### 4.5. Luminosity Function

As discussed in the Introduction, one of the goals of our spectroscopic survey is to provide an improved determination of the cool end of the white dwarf luminosity function (WDLF), as statistically complete as possible, which can then be compared to those obtained from magnitude-limited surveys, from large photometric and spectroscopic surveys like the SDSS, or from the volume-limited sample of white dwarfs within 20 pc of the Sun. The WDLF is a measure of the number of stars per  $\text{pc}^3$  per unit of bolometric magnitude, which can be obtained in our case using the bolometric magnitude of each white dwarf within 40 pc of the Sun and with  $\delta > 0$  derived from the spectroscopic or photometric results provided in Table 5. The bolometric magnitudes can be obtained from the luminosity of each star given in the table ( $\log L/L_\odot$ ) and the simple relation  $M_{\text{bol}} = -2.5 \log L/L_\odot + M_{\text{bol}}^\odot$ , where  $M_{\text{bol}}^\odot = 4.75$  is the bolometric magnitude of the Sun. We present here an *observed luminosity function*, in the sense that we do not attempt to apply any correction due to the incompleteness of our survey. Each object in the sample is then simply added to the appropriate bolometric magnitude bin, and the overall results are divided by the volume defined by a 40 pc half-sphere. Since the WDLF requires a proper account of the number of individual stars in each magnitude bin, the confirmed and suspected double degenerate binary systems are counted as two stars. Also, in order to obtain the most accurate mass density as possible, we deconvolve the individual masses of each system by using the procedure described in Section 6.4 of Giammichele et al. (2012). Doing so, our luminosity function now includes a total of 501 individual white dwarfs.

The luminosity function for the white dwarfs within 40 pc of the Sun is presented in Figure 27 (the approximate temperature scale for a  $0.6 M_\odot$  evolutionary sequence is shown at the top of the figure). Our results are also compared with those obtained by Giammichele et al. (2012) for the 20 pc sample, by Harris et al. (2006) for white dwarfs in the SDSS, and by Bergeron et al. (2011) for the DA and DB stars in the PG survey. In Figure 28 we reproduce the same luminosity function but in half-magnitude bins together with theoretical luminosity functions from Fontaine et al. (2001) for a total age of 10, 11, and 12 Gyr, normalized to our own observational results between  $M_{\text{bol}} = 12 - 14$ . These were obtained, as explained in Fontaine et al. (2001), with a constant star formation rate (SFR), a classic Salpeter initial mass function (IMF,  $\phi = M^{-2.35}$ ), an initial-to-final mass relation

(IFR) given by  $M_{\text{WD}} = 0.4 e^{0.125M}$ , and a main sequence lifetime law given by  $t_{\text{MS}} = 10 M^{-2.5}$  Gyr ( $M$  and  $M_{\text{WD}}$  are in solar units). The half-magnitude bins have been selected to better match the peak of the theoretical luminosity functions.

If the SFR is constant, we expect a monotonous rise of the luminosity function, as shown by the theoretical curves in Figure 28. Alternatively, bursts in star formation would show up as bumps in the luminosity function (Noh & Scalo 1990). Our WDLF displayed in both Figures 27 and 28 show a definite bump near  $M_{\text{bol}} \sim 10$ . A similar bump was also observed in the WDLF determined by Harris et al. (2006, see their Figures 4 and 8) for the SDSS sample and by Giammichele et al. (2012, see their Figure 22) for the 20 pc sample (both reproduced here in Figure 27), but this peculiar result in Giammichele et al. had been attributed by the authors to small number statistics. Here we have more than tripled the number of stars in the magnitude bins of interest, and the result now appears to be statistically significant. The brightest magnitude bins have error bars that are still large enough to be consistent with the theoretical expectations, but the points at  $M_{\text{bol}} = 10$  and 11 are solid determinations. This particular feature in the WDLF can also be observed *directly* in Figure 21 and in the left panel of Figure 25 and could be explained by a sudden burst of star formation in a recent past. A direct comparison of our results with the simulations shown in Figure 6 of Noh & Scalo (1990) suggests a burst of star formation that occurred about 0.3 Gyr ago, a conclusion also reached by Harris et al. (2006) based on the SDSS data. An alternative, but less likely explanation would be that the luminosity function for  $M_V > 10$  is still very incomplete. Indeed, the drop in the space density near  $M_{\text{bol}} = 11$  is also observed in the luminosity function of the PG sample, precisely in the region where the PG survey becomes incomplete. However, the number of stars missing in our survey would have to be enormous (Figures 27 and 28 use a logarithmic scale), an unlikely possibility given our estimate of the completeness of this survey. In Giammichele et al. (2012), this drop in the number of stars near  $T_{\text{eff}} \sim 14,000$  K was also tentatively explained by the inaccurate treatment of convective energy transport in the models, since this corresponds to the temperature where the atmospheres of DA stars become convective. However, since we applied here the appropriate 3D to 1D hydrodynamical corrections from Tremblay et al. (2013b), this explanation can be ruled out.

As expected, the WDLF displayed in Figure 27 shows that our survey samples the cool end of the luminosity function really well, with a significant number of stars in each magnitude bin, as opposed to the color-excess PG survey for instance. Our derived space density is consistent with that obtained by Harris et al. (2006) for white dwarfs in the SDSS, except near the peak region, but again, our results have not been corrected for incompleteness. At the same time, there are significant corrections applied to the SDSS sample in this particular range of luminosities, all of which remain extremely uncertain. Note also that the number

of stars in the fainter magnitude bins of our WDLF must be considered with caution, since for most cool white dwarfs in our sample, we had to assume a value of  $\log g = 8.0$  due to the lack of trigonometric parallax measurements. Hence a change in  $\log g$  values could shift some stars from one bin to the other. As a matter of fact, the mean mass of our sample is actually closer to  $0.7 M_{\odot}$  rather than the  $0.6 M_{\odot}$  assumed here for those stars. A larger average mass would imply smaller radii and lower luminosities, thus shifting the stars to fainter magnitude bins in both Figures 27 and 28. Precise parallax measurements, like those that will become available from the Gaia mission, will be required to improve the shape of the WDLF at low luminosities, in particular since only the last magnitude bin is sensitive to the age of the galactic disk. Despite these uncertainties, we can still conclude that our results are consistent with an age of the galactic disk around 11 Gyr.

Our WDLF displayed in Figure 28 also fails to reproduce the peak of the theoretical luminosity functions near  $M_{\text{bol}} \sim 15$ , despite the finer resolution used in this plot. This pronounced peak, or bump, in the theoretical luminosity functions has been discussed in detail by Fontaine et al. (2001, see their Figures 5 and 6) who attribute this feature to the combined signatures of both convective coupling and crystallization, although the contribution of the latter process is significantly less than that of the former since the release of latent heat operates over a wide range of luminosities. Consequently, its effects tend to be averaged out over that luminosity interval. Given the size of the error bars of our observed WDLF in this particular region of bolometric magnitudes, it is unlikely that our white dwarf sample misses so many objects. The most likely explanation is that the assumptions built into the construction of these theoretical luminosity functions mentioned above (SFR, IMF, IFR, etc.) should perhaps be reexamined and explored further, and in particular the simplistic initial-to-final mass relation used in these calculations. Another aspect that would need to be explored quantitatively is the effect of an old thick disk component (see Section 4.2) on the predicted luminosity function, with a different scale height appropriate for this population.

Finally, by integrating the WDLF over all magnitude bins, it is possible to obtain a measure of the *total space density* of white dwarfs in our sample, which in turn can be used to evaluate the completeness of our survey. Holberg et al. (2008) obtained for the 13 pc sample, believed to be complete, a space density of  $(4.8 \pm 0.5) \times 10^{-3} \text{ pc}^{-3}$  and a mass density of  $(3.2 \pm 0.3) \times 10^{-3} M_{\odot} \text{ pc}^{-3}$ . Using these numbers as a reference point, Giammichele et al. (2012) concluded that the 20 pc sample was 90% complete. For the 40 pc sample, we derive a space density of  $3.74 \times 10^{-3} \text{ pc}^{-3}$  and a corresponding mass density of  $2.46 \times 10^{-3} M_{\odot} \text{ pc}^{-3}$ , which would imply that the 40 pc sample in the northern hemisphere is 78% complete, in agreement with our other estimates above.

## 5. Concluding Remarks

Our spectroscopic survey of white dwarfs within 40 pc of the Sun is not yet complete and there is still a significant amount of work to be done. First of all, we have a few high-priority targets in our sample, some of which are bright enough to be observed with 2-m class telescopes, while some faint targets around  $V \sim 19$  will require large aperture telescopes, such as Gemini North or South. Among the brightest objects which could not be observed because of uncooperative weather, several candidates with  $D < 30$  pc remain on our target list, as well as 5 Giclas objects: 01309+5321 (GD 278), 02011+1212 (GD 21), 07544+6611 (GD 454), 14065+7418 (GD 492), and 22022+3848 (GD 399). Also, the southern hemisphere should eventually be dealt with, but it is not clear how much effort should be put into this given the work of Sayres et al. (2012) for declinations close to  $\delta = 0$ , as well as the SOAR + SMARTS Southern White Dwarf SURVEY (SSSWDS) of Subasavage et al. (2009), which uncovered 100 new white dwarfs. The current homogeneity of white dwarf surveys within 20 pc of the Sun in both hemispheres is about to be extended to 25 pc in a near future, but eventually to larger distances. The ultimate confirmation of the white dwarfs identified in our survey as members of the 40 pc sample will of course come from precise trigonometric parallaxes from the Gaia mission. In addition to adding or removing stars from the 40 pc sample, these measurements will also help to better define the faint end of the luminosity function revealed by our survey.

We are grateful to the referee, Hugh C. Harris, for his detailed and constructive comments, which have greatly helped improving the content and presentation of our results. We would like to thank the director and staff of Steward Observatory, Kitt Peak National Observatory, and the Observatoire du Mont-Mégantic for the use of their facilities, as well as the Director and staff of Gemini North and South Observatories for the remote observing. We would also like to thank P. Dufour for making his DQ and DZ models available to us, G. Fontaine for the theoretical luminosity functions, and S.R. Kulkarni and M.H. van Kerkwijk for allowing us to use their spectrum of SDSS 1257+5428. This work was supported in part by the NSERC Canada and by the Fund FRQ-NT (Québec). S.L. was supported in this research by NSF grants AST 06-07757 and AST 09-08419. S.L. also acknowledges support from the *GALEX* Guest Investigator program under NASA grant NNX09AF88G. This research made use of the SIMBAD database and the VizieR catalog access tool, operated at CDS, Strasbourg, France, and also made use of data products from the Two Micron All Sky Survey, which is a joint project of the University of Massachusetts and the Infrared Processing and Analysis Center/California Institute of Technology, funded by the National Aeronautics and Space Administration and the National Science Foundation.



## REFERENCES

- Adelman-McCarthy, J. K., Agüeros, M. A., Allam, S. S., et al. 2008, *ApJS*, 175, 297
- Badenes, C., Mullally, F., Thompson, S. E., & Lupton, R. H. 2009, *ApJ*, 707, 971
- Beauchamp, A., Wesemael, F., & Bergeron, P. 1997, *ApJS*, 108, 559
- Bergeron, P., Dufour, P., & Giammichele, N. 2013, in *Astronomical Society of the Pacific Conference Series*, Vol. 469, 18th European White Dwarf Workshop., ed. Krzesiń, J. ski, G. Stachowski, P. Moskalik, & K. Bajan, 127
- Bergeron, P. & Leggett, S. K. 2002, *ApJ*, 580, 1070
- Bergeron, P., Leggett, S. K., & Ruiz, M. T. 2001, *ApJS*, 133, 413
- Bergeron, P., Ruiz, M. T., & Leggett, S. K. 1997, *ApJS*, 108, 339
- Bergeron, P., Saffer, R., & Liebert, J. 1992, *ApJ*, 394, 228
- Bergeron, P., Saumon, D., & Wesemael, F. 1995, *ApJ*, 443, 764
- Bergeron, P., Wesemael, F., Dufour, P., Beauchamp, A., Hunter, C., Saffer, R. A., Gianninas, A., Ruiz, M. T., Limoges, M.-M., Dufour, P., Fontaine, G., & Liebert, J. 2011, *ApJ*, 737, 28
- Bergeron, P., Wesemael, F., & Fontaine, G. 1991, *ApJ*, 367, 253
- Bohlin, R. C. & Gilliland, R. L. 2004, *AJ*, 127, 3508
- Chen, E. Y. & Hansen, B. M. S. 2011, *MNRAS*, 413, 2827
- . 2012, *ApJ*, 753, L16
- Cohen, M., Wheaton, W. A., & Megeath, S. T. 2003, *AJ*, 126, 1090
- Dahn, C. C., Harrington, R. S., Riepe, B. Y., Christy, J. W., Guetter, H. H., Kallarakal, V. V., Miranian, M., Walker, R. L., Vrba, F. J., Hewitt, A. V., Durham, W. S., & Ables, H. D. 1982, *AJ*, 87, 419
- Dufour, P., Bergeron, P., & Fontaine, G. 2005, *ApJ*, 627, 404
- Dufour, P., Bergeron, P., Liebert, J., Harris, H. C., Knapp, G. R., Anderson, S. F., Hall, P. B., Strauss, M. A., Collinge, M. J., & Edwards, M. C. 2007, *ApJ*, 663, 1291

- Fontaine, G., Brassard, P., & Bergeron, P. 2001, *PASP*, 113, 409
- Fuchs, B., Dettbarn, C., Rix, H.-W., Beers, T. C., Bizyaev, D., Brewington, H., Jahreiß, H., Klement, R., Malanushenko, E., Malanushenko, V., Oravetz, D., Pan, K., Simmons, A., & Snedden, S. 2009, *AJ*, 137, 4149
- Fukugita, M., Ichikawa, T., Gunn, J. E., Doi, M., Shimasaku, K., & Schneider, D. P. 1996, *AJ*, 111, 1748
- Gatewood, G. & Coban, L. 2009, *AJ*, 137, 402
- Genest-Beaulieu, C. & Bergeron, P. 2014, *ApJ*, 796, 128
- Giammichele, N., Bergeron, P., & Dufour, P. 2012, *ApJS*, 199, 29
- Gianninas, A., Bergeron, P., & Ruiz, M. T. 2011, *ApJ*, 743, 138
- Gianninas, A., Curd, B., Thorstensen, J. R., Kilic, M., Bergeron, P., Andrews, J. J., Canton, P., & Agüeros, M. A. 2015, *MNRAS*, 449, 3966
- Giclas, H. L., Burnham, Jr., R., & Thomas, N. G. 1980, *Lowell Observatory Bulletin*, 8, 157
- Gil de Paz, A., Boissier, S., Madore, B. F., Seibert, M., Joe, Y. H., Boselli, A., Wyder, T. K., Thilker, D., Bianchi, L., Rey, S.-C., Rich, R. M., Barlow, T. A., Conrow, T., Forster, K., Friedman, P. G., Martin, D. C., Morrissey, P., Neff, S. G., Schiminovich, D., Small, T., Donas, J., Heckman, T. M., Lee, Y.-W., Milliard, B., Szalay, A. S., & Yi, S. 2009, *VizieR Online Data Catalog*, 217, 30185
- Green, E. M., Limoges, M.-M., Gianninas, A., Bergeron, P., Fontaine, G., Dufour, P., O'Malley, C. J., Guvenen, B., Biddle, L. I., Pearson, K., Deyoe, T. W., Bullivant, C. W., Hermes, J. J., Van Grootel, V., & Grosjean, M. 2015, *ArXiv e-prints*
- Green, R., Schmidt, M., & Liebert, J. 1986, *ApJS*, 61, 305
- Greenstein, J. L. 1986, *ApJ*, 304, 334
- Hall, P. B., Kowalski, P. M., Harris, H. C., Awal, A., Leggett, S. K., Kilic, M., Anderson, S. F., & Gates, E. 2008, *AJ*, 136, 76
- Hambly, N. C., Smartt, S. J., Hodgkin, S. T., Jameson, R. F., Kemp, S. N., Rolleston, W. R. J., & Steele, I. A. 1999, *MNRAS*, 309, L33

- Harris, H. C., Dahn, C. C., Dupuy, T. J., Canzian, B., Guetter, H. H., Hartkopf, W. I., Ireland, M. J., Leggett, S. K., Levine, S. E., Liu, M. C., Luginbuhl, C. B., Monet, A. K. B., Stone, R. C., Subasavage, J. P., Tilleman, T., & Walker, R. L. 2013, *ApJ*, 779, 21
- Harris, H. C., Dahn, C. C., Vrba, F. J., Henden, A. A., Liebert, J., Schmidt, G. D., & Reid, I. N. 1999, *ApJ*, 524, 1000
- Harris, H. C., Munn, J. A., Kilic, M., Liebert, J., Williams, K. A., von Hippel, T., Levine, S. E., Monet, D. G., Eisenstein, D. J., Kleinman, S. J., Metcalfe, T. S., Nitta, A., Winget, D. E., Brinkmann, J., Fukugita, M., Knapp, G. R., Lupton, R. H., Smith, J. A., & Schneider, D. P. 2006, *AJ*, 131, 571
- Høg, E., Fabricius, C., Makarov, V. V., Urban, S., Corbin, T., Wycoff, G., Bastian, U., Schwekendiek, P., & Wicenec, A. 2000, *A&A*, 355, L27
- Holberg, J. B. & Bergeron, P. 2006, *AJ*, 132, 1221
- Holberg, J. B., Oswalt, T. D., Sion, E. M., Barstow, M. A., & Burleigh, M. R. 2013, *MNRAS*, 435, 2077
- Holberg, J. B., Sion, E. M., Oswalt, T., McCook, G. P., Foran, S., & Subasavage, J. P. 2008, *AJ*, 135, 1225
- Holberg, J. B., Sion, E. M., & Oswalt, T. D. 2011, in *Bulletin of the American Astronomical Society*, Vol. 43, American Astronomical Society Meeting Abstracts no.217, no.341.02
- Hummer, D. G. & Mihalas, D. 1988, *ApJ*, 331, 794
- Kawka, A. & Vennes, S. 2006, *ApJ*, 643, 402
- Kepler, S. O., Kleinman, S. J., Nitta, A., Koester, D., Castanheira, B. G., Giovannini, O., Costa, A. F. M., & Althaus, L. 2007, *MNRAS*, 375, 1315
- Kilic, M., Leggett, S. K., Tremblay, P.-E., von Hippel, T., Bergeron, P., Harris, H. C., Munn, J. A., Williams, K. A., Gates, E., & Farihi, J. 2010, *ApJS*, 190, 77
- Kilic, M., Munn, J. A., Harris, H. C., Liebert, J., von Hippel, T., Williams, K. A., Metcalfe, T. S., Winget, D. E., & Levine, S. E. 2006, *AJ*, 131, 582
- Kilic, M., Thorstensen, J. R., Kowalski, P. M., & Andrews, J. 2012, *MNRAS*, 423, L132
- Koester, D. & Knist, S. 2006, *A&A*, 454, 951

- Koester, D., Napiwotzki, R., Christlieb, N., Drechsel, H., Hagen, H.-J., Heber, U., Homeier, D., Karl, C., Leibundgut, B., Moehler, S., Nelemans, G., Pauli, E.-M., Reimers, D., Renzini, A., & Yungelson, L. 2001, *A&A*, 378, 556
- Koester, D., Napiwotzki, R., Voss, B., Homeier, D., & Reimers, D. 2005, *A&A*, 439, 317
- Koester, D., Voss, B., Napiwotzki, R., Christlieb, N., Homeier, D., Lisker, T., Reimers, D., & Heber, U. 2009, *A&A*, 505, 441
- Kondo, M., Noguchi, T., & Maehara, H. 1984, *Annals of the Tokyo Astronomical Observatory*, 20, 130
- Kowalski, P. M. 2010, *A&A*, 519, L8
- Kowalski, P. M. & Saumon, D. 2006, *ApJ*, 651, L137
- Kulkarni, S. R. & van Kerkwijk, M. H. 2010, *ApJ*, 719, 1123
- Leggett, S. K., Ruiz, M. T., & Bergeron, P. 1998, *ApJ*, 497, 294
- Lépine, S. & Gaidos, E. 2011, *AJ*, 142, 138
- Lépine, S., Hilton, E. J., Mann, A. W., Wilde, M., Rojas-Ayala, B., Cruz, K. L., & Gaidos, E. 2013, *AJ*, 145, 102
- Lépine, S. & Shara, M. M. 2005, *AJ*, 129, 1483
- Lépine, S., Shara, M. M., & Rich, R. M. 2002, *AJ*, 124, 1190
- Liebert, J., Bergeron, P., & Holberg, J. 2005, *ApJS*, 156, 47
- Liebert, J., Bergeron, P., & Saffer, R. A. 1991, in *NATO ASIC Proc. 336: White Dwarfs*, ed. G. Vauclair & E. Sion, 409
- Liebert, J., Bergeron, P., Schmidt, G. D., & Saffer, R. A. 1993, *ApJ*, 418, 426
- Limoges, M.-M., Bergeron, P., & Lépine, S. 2010, in *American Institute of Physics Conference Series*, Vol. 1273, *American Institute of Physics Conference Series*, ed. K. Werner & T. Rauch, 193–196
- Limoges, M.-M., Lépine, S., & Bergeron, P. 2013, *AJ*, 145, 136
- Marsh, T. R., Gänsicke, B. T., Steeghs, D., Southworth, J., Koester, D., Harris, V., & Merry, L. 2011, *ApJ*, 736, 95

- McCook, G. P. & Sion, E. M. 1999, *ApJS*, 121, 1
- Monet, D. G., Levine, S. E., Canzian, B., Ables, H. D., Bird, A. R., Dahn, C. C., Guetter, H. H., Harris, H. C., Henden, A. A., Leggett, S. K., Levison, H. F., Luginbuhl, C. B., Martini, J., Monet, A. K. B., Munn, J. A., Pier, J. R., Rhodes, A. R., Riepe, B., Sell, S., Stone, R. C., Vrba, F. J., Walker, R. L., Westerhout, G., Brucato, R. J., Reid, I. N., Schoening, W., Hartley, M., Read, M. A., & Tritton, S. B. 2003, *AJ*, 125, 984
- Morrissey, P. & GALEX Science Team. 2004, in *Bulletin of the American Astronomical Society*, Vol. 36, American Astronomical Society Meeting Abstracts, 1385
- Noh, H.-R. & Scalo, J. 1990, *ApJ*, 352, 605
- Press, W. H., Flannery, B. P., & Teukolsky, S. A. 1986, *Numerical recipes. The art of scientific computing*, ed. Press, W. H., Flannery, B. P., & Teukolsky, S. A.
- Rebassa-Mansergas, A., Gänsicke, B. T., Schreiber, M. R., Koester, D., & Rodríguez-Gil, P. 2010, *MNRAS*, 402, 620
- Sayres, C., Subasavage, J. P., Bergeron, P., Dufour, P., Davenport, J. R. A., AlSayyad, Y., & Tofflemire, B. M. 2012, *AJ*, 143, 103
- Schilbach, E. & Röser, S. 2012, *A&A*, 537, A129
- Sion, E. M., Holberg, J. B., Oswalt, T. D., McCook, G. P., Wasatonic, R., & Myszka, J. 2014, *AJ*, 147, 129
- Skrutskie, M. F., Cutri, R. M., Stiening, R., Weinberg, M. D., Schneider, S., Carpenter, J. M., Beichman, C., Capps, R., Chester, T., Elias, J., Huchra, J., Liebert, J., Lonsdale, C., Monet, D. G., Price, S., Seitzer, P., Jarrett, T., Kirkpatrick, J. D., Gizis, J. E., Howard, E., Evans, T., Fowler, J., Fullmer, L., Hurt, R., Light, R., Kopan, E. L., Marsh, K. A., McCallon, H. L., Tam, R., Van Dyk, S., & Wheelock, S. 2006, *AJ*, 131, 1163
- Subasavage, J. P., Jao, W.-C., Henry, T. J., Bergeron, P., Dufour, P., Ianna, P. A., Costa, E., & Méndez, R. A. 2009, *AJ*, 137, 4547
- Tonry, J. L., Stubbs, C. W., Kilic, M., Flewelling, H. A., Deacon, N. R., Chornock, R., Berger, E., Burgett, W. S., Chambers, K. C., Kaiser, N., Kudritzki, R.-P., Hodapp, K. W., Magnier, E. A., Morgan, J. S., Price, P. A., & Wainscoat, R. J. 2012, *ApJ*, 745, 42
- Tremblay, P.-E. & Bergeron, P. 2008, *ApJ*, 672, 1144

- . 2009, *ApJ*, 696, 1755
- Tremblay, P.-E., Bergeron, P., & Gianninas, A. 2011, *ApJ*, 730, 128
- Tremblay, P.-E., Bergeron, P., Kalirai, J. S., & Gianninas, A. 2010, *ApJ*, 712, 1345
- Tremblay, P.-E., Ludwig, H.-G., Steffen, M., & Freytag, B. 2013a, *A&A*, 552, A13
- . 2013b, *A&A*, 559, A104
- Tremblay, P.-E., Schilbach, E., Röser, S., Jordan, S., Ludwig, H.-G., & Goldman, B. 2012, *A&A*, 547, A99
- Vennes, S. 1992, *ApJ*, 390, 590
- Vennes, S., Christian, D. J., & Thorstensen, J. R. 1998, *ApJ*, 502, 763
- Vennes, S. & Kawka, A. 2012, *ApJ*, 745, L12
- Vennes, S., Kawka, A., & Németh, P. 2011, *MNRAS*, 410, 2095
- Vennes, S., Thejll, P. A., Génova Galvan, R., & Dupuis, J. 1997, *ApJ*, 480, 714
- Vennes, S., Thejll, P. A., Wickramasinghe, D. T., & Bessell, M. S. 1996, *ApJ*, 467, 782
- Voss, B., Koester, D., Napiwotzki, R., Christlieb, N., & Reimers, D. 2007, *A&A*, 470, 1079
- Wood, M. A. 1992, *ApJ*, 386, 539
- Woodley, K. A., Goldsbury, R., Kalirai, J. S., Richer, H. B., Tremblay, P.-E., Anderson, J., Bergeron, P., Dotter, A., Esteves, L., Fahlman, G. G., Hansen, B. M. S., Heyl, J., Hurley, J., Rich, R. M., Shara, M. M., & Stetson, P. B. 2012, *AJ*, 143, 50



Table 1. Spectroscopic Observing Runs

Date	Telescope	Spectrograph	Grating ( $1 \text{ mm}^{-1}$ )	Blaze ( $\text{\AA}$ )	Coverage ( $\text{\AA}$ )	Slit ( $''$ )
2011 Jan	NOAO 2.1 m	Goldcam	500	5500	3800–6700	2
2011 Mar	NOAO Mayall 4 m	RC	316	5500	3900–6700	2
2011 Apr	Steward Observatory Bok 2.3 m	B&C	600	3568	3800–5600	4.5
2011 Apr	NOAO 2.1 m	Goldcam	500	5500	3800–6700	2
2012 Sep	NOAO Mayall 4 m	RC	316	5500	3900–6700	2
2011B	Gemini North	GMOS-N	600	4610	3800–6700	1
2011B	Gemini South	GMOS-S	600	4610	3800–6700	1
2012B	Gemini North	GMOS-N	600	4610	3800–6700	1
2013 Jan	Observatoire du Mont-Mégantic 1.6 m	B&C	600	4000	3800–6700	4.3
2013 Jun	Steward Observatory Bok 2.3 m	B&C	600	3568	3800–5600	4.5
2013 Oct	Steward Observatory Bok 2.3 m	B&C	600	3568	3800–5600	4.5

Table 2. Spectroscopically Confirmed White Dwarfs from SUPERBLINK – Astrometry

PM I	NLTT	SDSS	RA ( $J_{2000}$ )	DEC ( $J_{2000}$ )	$\mu_{\text{tot}}$ ( $''\text{yr}^{-1}$ )	$\mu_{\text{RA}}$ ( $''\text{yr}^{-1}$ )	$\mu_{\text{DE}}$ ( $''\text{yr}^{-1}$ )
00050+4003	133		00:05:01.08	+40:03:34.6	0.229	0.206	0.101
00056+4825			00:05:40.41	+48:25:05.9	0.153	0.152	-0.013
00074+3403	301		00:07:28.87	+34:03:39.9	0.199	0.021	0.197
01088+7600			01:08:49.61	+76:00:18.4	0.242	0.237	0.050
01278+7328	4799		01:27:49.09	+73:28:47.7	0.177	-0.160	0.076
01327+4604	5100		01:32:46.67	+46:04:58.8	0.211	-0.211	-0.002
01327+6635			01:32:42.90	+66:35:46.0	0.051	0.039	-0.033
01390+2402		J013900.25+24025	01:39:00.18	+24:02:58.8	0.096	0.094	-0.021
01534+3557			01:53:28.98	+35:57:29.2	0.175	0.174	-0.020
02199+3520			02:19:59.83	+35:20:18.0	0.135	0.133	0.024
02236+4816			02:23:40.36	+48:16:47.5	0.116	0.112	-0.028
02241+2325		J022411.67+23251	02:24:11.70	+23:25:18.8	0.111	-0.086	-0.070
02321+5211			02:32:10.24	+52:11:51.0	0.113	0.085	-0.075
03009+5432			03:00:59.53	+54:32:37.5	0.232	0.162	-0.166
03031+2317			03:03:07.50	+23:17:40.7	0.059	0.058	-0.012
03053+2603	9826		03:05:21.02	+26:03:12.2	0.194	-0.176	-0.081
03471+0520W			03:47:06.63	+05:20:14.5	0.167	0.161	-0.045
04037+1459		J040342.15+14592	04:03:42.08	+14:59:28.7	0.140	0.139	-0.015
04180+4211	12934		04:18:05.53	+42:11:02.2	0.214	-0.046	-0.209
04201+3233			04:20:06.31	+32:33:05.2	0.083	0.046	-0.069
04214+4607			04:21:29.34	+46:07:57.7	0.120	0.059	-0.104
04294+4945			04:29:26.36	+49:45:54.0	0.190	0.021	-0.188
04308+1611			04:30:49.87	+16:11:06.5	0.150	0.045	-0.143
04372+4524			04:37:15.48	+45:24:33.1	0.113	-0.113	-0.001
04588+6410			04:58:53.28	+64:10:44.0	0.074	-0.018	-0.072
05332+0925			05:33:14.80	+09:25:59.8	0.090	-0.067	-0.061
05353+5715	15285		05:35:23.06	+57:15:56.1	0.275	0.173	-0.214
05372+6759			05:37:14.89	+67:59:50.4	0.065	-0.029	-0.058
05383+4436			05:38:18.31	+44:36:47.8	0.080	0.011	-0.078
05410+3959			05:41:03.85	+39:59:45.4	0.566	0.335	-0.448
05431+3637			05:43:07.37	+36:37:01.2	0.163	-0.155	-0.050
05449+2602			05:44:57.66	+26:02:59.9	1.702	0.993	-1.382
05462+1115			05:46:15.59	+11:15:58.7	0.198	-0.127	-0.152
06018+2751			06:01:53.51	+27:51:35.7	0.064	0.012	-0.062
06206+3443		J062038.90+34430	06:20:38.85	+34:43:05.6	0.077	-0.023	-0.073

Table 2—Continued

PM I	NLTT	SDSS	RA ( $J_{2000}$ )	DEC ( $J_{2000}$ )	$\mu_{\text{tot}}$ ( $''\text{yr}^{-1}$ )	$\mu\text{RA}$ ( $''\text{yr}^{-1}$ )	$\mu\text{DE}$ ( $''\text{yr}^{-1}$ )
06445+2731		J064430.09+27311	06:44:30.18	+27:31:11.4	0.153	−0.146	−0.046
06494+7521	16943		06:49:26.50	+75:21:24.9	0.089	0.088	−0.013
06577+4007			06:57:45.12	+40:07:25.7	0.109	0.093	−0.054
07087+2044			07:08:45.79	+20:44:51.6	0.122	0.082	−0.090
07300+2716W		J072959.99+27164	07:30:00.01	+27:16:41.2	0.162	−0.136	−0.089
07504+1740		J075026.30+17402	07:50:26.28	+17:40:30.1	0.127	0.059	−0.112
08015+4852		J080131.82+48525	08:01:31.88	+48:52:52.3	0.117	−0.116	0.014
08054+0735	18922		08:05:27.55	+07:35:35.6	0.378	−0.075	−0.370
08068+2215		J080648.04+22155	08:06:48.05	+22:15:51.6	0.169	−0.008	−0.169
08082+1854	18981		08:08:12.78	+18:54:21.6	0.202	−0.143	−0.143
08184+6606		J081825.96+66064	08:18:26.02	+66:06:45.2	0.074	−0.016	−0.073
08212+7120			08:21:12.39	+71:20:09.3	0.069	−0.068	−0.015
08314+1641			08:31:24.90	+16:41:59.2	0.164	0.072	−0.148
08429+2409		J084257.57+24093	08:42:57.59	+24:09:30.8	0.110	−0.100	−0.046
08490+4439	20277	J084901.61+44393	08:49:01.65	+44:39:35.6	0.223	−0.194	−0.110
09112+1515		J091112.15+15154	09:11:12.21	+15:15:49.2	0.144	0.063	−0.129
09122+2538		J091216.43+25382	09:12:16.40	+25:38:22.3	0.115	0.049	−0.104
09127+2251	21205	J091247.92+22515	09:12:47.95	+22:51:55.3	0.169	−0.097	−0.138
09192+7723			09:19:14.81	+77:23:50.9	0.109	−0.040	−0.101
09222+0504	21580		09:22:13.54	+05:04:37.4	0.251	−0.248	−0.043
09234+0559		J092326.91+05590	09:23:26.92	+05:59:06.3	0.146	0.066	−0.130
09249+3613		J092455.63+36130	09:24:55.42	+36:13:09.7	0.080	−0.061	−0.052
09395+4951		J093931.66+49514	09:39:31.74	+49:51:48.3	0.379	−0.379	−0.010
09422+0942		J094213.02+09424	09:42:13.07	+09:42:45.4	0.142	−0.141	−0.018
09488+1319		J094850.12+13192	09:48:50.08	+13:19:27.4	0.144	0.082	−0.118
09513+1900	22762	J095120.16+19001	09:51:20.08	+19:00:11.9	0.274	0.173	−0.213
10042+2438		J100412.46+24384	10:04:12.44	+24:38:50.2	0.054	0.005	−0.054
10118+2647			10:11:50.99	+26:47:45.3	0.142	0.133	0.049
10170+7619	23808		10:17:04.19	+76:19:02.9	0.212	0.190	−0.094
10228+3904	24170	J102251.63+39041	10:22:51.75	+39:04:14.8	0.464	−0.428	−0.180
10347+2245	24727		10:34:43.40	+22:45:48.3	0.223	−0.221	−0.025
10355+2126	24770	J103532.53+21260	10:35:32.62	+21:26:04.5	0.164	−0.077	−0.145
10471+3453		J104709.16+34534	10:47:09.20	+34:53:46.3	0.063	−0.056	−0.029
10502+3226		J105016.31+32260	10:50:16.32	+32:26:02.1	0.140	0.040	−0.134
10538+2425	25646	J105349.49+24253	10:53:49.64	+24:25:32.6	0.361	−0.355	−0.063

Table 2—Continued

PM I	NLTT	SDSS	RA ( $J_{2000}$ )	DEC ( $J_{2000}$ )	$\mu_{\text{tot}}$ ( $''\text{yr}^{-1}$ )	$\mu_{\text{RA}}$ ( $''\text{yr}^{-1}$ )	$\mu_{\text{DE}}$ ( $''\text{yr}^{-1}$ )
10557+2111		J105544.90+211110	10:55:44.95	+21:11:05.6	0.191	−0.153	−0.114
11111+3848			11:11:09.14	+38:48:57.3	0.128	0.120	−0.044
11132+2859	26653		11:13:16.58	+28:59:07.8	0.381	−0.187	−0.332
11144+3341	26706	J111424.65+33412	11:14:24.67	+33:41:24.3	0.152	−0.031	−0.149
11210+3756		J112105.79+37561	11:21:05.81	+37:56:15.3	0.077	−0.050	−0.059
11222+2839	27173	J112215.84+28394	11:22:15.93	+28:39:42.6	0.265	−0.257	−0.065
11364+0802S			11:36:24.33	+08:02:15.7	0.214	−0.179	−0.118
11364+0838			11:36:27.59	+08:38:37.9	0.084	−0.057	−0.062
11460+0514		J114604.36+05140	11:46:04.39	+05:14:01.7	0.092	−0.090	0.017
11495+2353	28667	J114935.69+23532	11:49:35.72	+23:53:21.0	0.184	−0.183	−0.017
11506+0343	28735	J115038.73+03430	11:50:38.74	+03:43:01.6	0.258	−0.143	−0.215
12019+3400		J120154.69+34005	12:01:54.70	+34:00:55.5	0.130	−0.027	0.127
12033+2439		J120319.77+24395	12:03:19.80	+24:39:54.0	0.110	−0.109	0.012
12145+7822	30084		12:14:31.79	+78:22:56.1	0.290	0.135	−0.256
12429+6542		J124258.39+65421	12:42:58.41	+65:42:20.2	0.161	−0.106	−0.121
12430+2057		J124306.04+20570	12:43:05.99	+20:57:10.6	0.088	0.076	−0.044
13032+7510			13:03:14.16	+75:10:04.1	0.117	0.061	0.100
13096+6933			13:09:38.03	+69:33:15.6	0.084	−0.079	0.029
13108+7236			13:10:50.73	+72:36:33.8	0.088	−0.061	0.064
13291+2450		J132906.08+24502	13:29:06.19	+24:50:25.7	0.405	−0.404	−0.024
13346+0943E			13:34:38.82	+09:43:18.5	0.201	−0.200	0.021
13413+0500			13:41:21.80	+05:00:45.8	0.429	−0.428	0.020
13537+1656		J135342.38+16565	13:53:42.35	+16:56:51.7	0.103	0.072	−0.074
14037+0644		J140346.10+06444	14:03:46.08	+06:44:43.0	0.127	0.057	−0.114
14064+1608		J140625.56+16082	14:06:25.59	+16:08:27.7	0.121	−0.112	−0.045
14456+2527		J144539.44+25271	14:45:39.46	+25:27:15.9	0.155	−0.033	−0.152
15010+6138		J150105.31+61385	15:01:05.31	+61:38:54.6	0.100	−0.050	−0.087
15167+2910		J151644.70+29102	15:16:44.73	+29:10:21.4	0.086	−0.036	0.078
16142+1729	42302	J161414.12+17290	16:14:14.23	+17:29:00.3	0.260	−0.194	−0.173
16144+0906		J161424.60+09060	16:14:24.60	+09:06:04.0	0.380	0.021	−0.379
16222+0532	42621	J162216.16+05325	16:22:16.19	+05:32:52.2	0.135	−0.130	−0.038
16265+1355		J162632.08+13555	16:26:32.04	+13:55:54.5	0.167	0.132	0.103
16286+7053	42988		16:28:38.60	+70:53:21.6	0.462	−0.002	−0.462
16514+6635			16:51:26.02	+66:35:06.3	0.109	−0.059	0.092
17328+0213			17:32:48.41	+02:13:08.8	0.089	0.072	−0.053

Table 2—Continued

PM I	NLTT	SDSS	RA ( $J_{2000}$ )	DEC ( $J_{2000}$ )	$\mu_{\text{tot}}$ ( $''\text{yr}^{-1}$ )	$\mu_{\text{RA}}$ ( $''\text{yr}^{-1}$ )	$\mu_{\text{DE}}$ ( $''\text{yr}^{-1}$ )
17344+4236			17:34:26.42	+42:36:40.5	0.126	−0.079	−0.098
17368+3635			17:36:52.13	+36:35:44.6	0.103	−0.096	−0.038
17376+0138			17:37:41.38	+01:38:49.8	0.093	−0.037	−0.085
17430+1701	45332		17:43:00.76	+17:01:45.9	0.364	−0.248	−0.266
17574+1021			17:57:25.79	+10:21:24.9	0.091	−0.020	−0.088
17579+5441		J175759.50+54412	17:57:59.45	+54:41:21.8	0.074	−0.061	−0.041
18018+0846			18:01:51.35	+08:46:06.9	0.190	0.115	0.151
18154+3158	46186		18:15:27.40	+31:58:49.2	0.210	0.124	0.170
18435+2740			18:43:35.47	+27:40:26.8	0.095	0.043	−0.085
18510+7738	47202	J185106.01+77383	18:51:05.66	+77:38:37.2	0.270	0.261	−0.069
19005+0020			19:00:34.98	+00:20:17.4	0.270	−0.143	−0.229
19033+6035			19:03:19.56	+60:35:52.7	0.194	0.174	0.088
19167+8044			19:16:47.18	+80:44:30.1	0.183	0.073	0.167
19401+8348			19:40:08.67	+83:48:57.7	0.936	−0.838	−0.417
19455+4650N			19:45:30.37	+46:50:15.5	0.612	−0.455	−0.409
20279+0523			20:27:58.78	+05:23:53.8	0.120	0.072	−0.096
20300+0729	49350		20:30:04.10	+07:29:43.7	0.250	0.171	−0.182
21474+1127			21:47:25.20	+11:27:55.3	0.273	0.103	−0.252
22133+0349	53229		22:13:21.32	+03:49:11.1	0.465	0.322	−0.334
22198+4805			22:19:53.89	+48:05:34.3	0.271	0.188	0.196
22230+2201N			22:23:01.60	+22:01:31.8	0.082	0.054	−0.062
22230+2201S			22:23:01.69	+22:01:25.3	0.082	0.054	−0.062
22340+5543			22:34:02.03	+55:43:26.1	0.218	0.202	0.080
22410+3646			22:41:04.63	+36:46:38.8	0.169	0.162	0.047
23162+1720	56301	J231612.68+17204	23:16:12.53	+17:20:45.6	0.287	0.286	−0.014
23186+5458		J231838.29+54581	23:18:38.33	+54:58:16.8	0.099	0.019	−0.097
23300+0120	57056		23:30:05.52	+01:20:46.1	0.247	0.209	−0.132
23489+4300	58060	J234857.96+43003	23:48:57.89	+43:00:39.7	0.295	0.162	−0.247

Table 3. Spectroscopically Confirmed White Dwarfs from SUPERBLINK – Photometry

PM I	FUV	NUV	$B_F$	$R_I$	$I_N$	$J$	$H$	$K_S$	$u$	$g$	$r$	$i$	$z$	ST	Notes
00023+6357	–	–	17.8	16.2	17.3	15.80	15.57	15.51	–	–	–	–	–	DC	
00050+4003	–	18.14	16.3	16.2	16.5	–	–	–	–	–	–	–	–	DZA:	
00056+4825	–	19.38	17.1	16.9	16.5	16.25	15.60	15.89	–	–	–	–	–	DA	
00074+3403	–	21.07	17.7	17.3	16.8	16.39	16.25	15.83	–	–	–	–	–	DC:	
00079+3947	–	–	17.4	16.2	15.8	15.18	14.85	14.65	–	–	–	–	–	DC	
00217+2640	–	–	17.9	17.2	16.9	16.18	15.91	15.81	–	–	–	–	–	DC	
00276+0542	–	–	17.2	15.6	15.4	14.97	14.67	14.57	–	–	–	–	–	DA	
00331+4742S	14.55	14.63	14.9	14.9	–	15.16	15.02	15.14	–	–	–	–	–	DA	
00334+2506	–	20.36	16.6	16.6	16.1	15.96	15.70	15.45	17.88	17.12	16.79	16.69	16.68	DA	
00532+3927	–	18.45	17.9	16.4	16.8	16.03	15.84	15.40	–	–	–	–	–	DA	
00559+5948	–	–	15.2	16.0	15.8	15.44	15.21	15.03	–	–	–	–	–	DC:	
01043+3816	14.70	14.80	15.6	15.4	–	15.29	15.32	15.14	–	–	–	–	–	DA	
01088+7600	–	20.76	17.9	17.4	16.9	16.60	16.40	16.84	–	–	–	–	–	DA	
01216+3440	–	19.64	17.9	16.3	15.9	16.13	16.15	15.88	17.27	16.76	16.64	16.64	16.74	DZ	
01278+7328	–	–	16.2	14.9	14.5	14.76	10.17	9.79	–	–	–	–	–	DA	
01327+4604	18.19	15.94	16.0	15.2	14.3	14.90	15.09	15.23	15.42	14.97	15.08	15.23	15.45	DA	1
01327+6635	16.67	16.56	17.1	16.1	16.4	–	–	–	–	–	–	–	–	DA	
01382+4442	15.79	15.84	15.5	16.0	15.2	15.62	15.61	15.71	–	–	–	–	–	DA	
01390+2402	–	19.66	17.6	16.7	16.7	–	–	–	18.69	17.92	17.84	17.84	17.90	DA	
01457+2918	–	–	18.4	18.0	17.7	16.56	16.09	15.51	–	–	–	–	–	DC	
01486+3615	–	20.64	17.6	16.5	16.3	15.85	15.48	15.42	–	–	–	–	–	DA	
01534+3557	–	19.30	17.1	16.7	16.4	16.53	16.01	15.74	–	–	–	–	–	DA	
01565+2955	14.56	14.68	14.7	14.9	–	14.96	15.04	15.18	–	–	–	–	–	DA	
02062+1836	–	–	19.2	17.8	17.1	16.50	16.38	15.63	–	–	–	–	–	DC	
02118+7119	–	–	17.8	16.4	16.6	15.78	15.42	15.32	19.04	17.57	16.94	16.67	16.57	DC	
02149+7746	–	–	19.2	18.0	18.1	16.48	17.50	15.89	–	–	–	–	–	DC	
02199+3520	–	–	17.9	17.3	16.7	16.53	15.87	16.02	–	–	–	–	–	DA	
02230+5544	–	–	17.2	16.6	16.8	16.07	15.77	15.68	–	–	–	–	–	DA	
02236+4816	–	–	15.1	15.4	14.5	15.42	15.67	15.34	–	–	–	–	–	DB	
02238+2055	–	–	19.6	17.9	17.4	16.77	16.72	17.15	21.30	19.10	18.11	17.77	17.57	DC	



Table 3—Continued

PM I	FUV	NUV	$B_F$	$R_I$	$I_N$	$J$	$H$	$K_S$	$u$	$g$	$r$	$i$	$z$	ST	Notes
02241+2325	—	—	19.4	18.5	18.4	—	—	—	21.02	19.36	18.64	18.39	18.24	DA	
02321+5211	21.78	18.16	16.9	16.9	16.5	—	—	—	—	—	—	—	—	DA	
02334+2125	—	—	18.2	16.5	—	15.95	15.39	15.74	19.85	18.04	17.14	16.88	16.73	DC	
02379+1638	—	—	17.6	16.8	16.7	15.97	15.83	14.88	—	—	—	—	—	DC	
02478+4138	16.81	16.41	15.1	16.3	16.4	16.95	17.86	17.19	—	—	—	—	—	DB	
02497+3307	—	21.05	18.0	16.7	16.4	16.01	15.49	15.39	18.47	17.43	16.97	16.79	16.73	DA	
02557+2106S	—	—	17.7	17.1	16.5	16.48	16.04	16.06	18.47	17.68	17.36	17.25	17.20	DA	
02562+4954	—	—	17.5	17.1	16.4	16.17	15.79	15.45	—	—	—	—	—	DA	
03009+5432	—	18.55	17.2	16.5	16.0	16.07	15.92	15.75	—	—	—	—	—	DA	
03031+2317	15.11	15.73	15.8	15.4	14.1	13.00	12.32	12.07	—	—	—	—	—	DA+dM	
03053+2603	—	—	18.5	17.6	17.3	16.76	16.30	15.77	—	—	—	—	—	DA	
03109+6634	—	—	18.8	17.7	17.4	16.55	16.30	15.31	—	—	—	—	—	DC	
03127+2218	—	19.86	17.8	16.4	16.8	16.13	15.85	15.88	—	—	—	—	—	DA	
03196+3630	—	20.74	17.3	16.2	16.1	15.84	15.84	15.38	—	—	—	—	—	DZ	
03203+2333	—	—	18.9	17.0	17.0	16.21	15.65	15.76	—	—	—	—	—	DC	
03433+1958	—	—	16.6	15.2	15.2	14.95	14.96	15.04	—	—	—	—	—	DA	
03471+0520W	—	21.07	18.8	17.3	17.2	—	—	—	18.63	18.20	18.04	18.06	18.12	DC	
03473+4358	—	—	14.3	14.3	14.3	14.23	14.30	14.36	—	—	—	—	—	DA	
04010+5131W	—	—	17.5	16.8	16.4	15.93	15.74	15.20	19.34	17.78	17.08	16.83	16.72	DC	
04032+2520E	14.42	14.91	15.4	14.6	13.0	12.36	11.77	11.51	—	—	—	—	—	DA+dM	
04032+2520W	14.42	14.91	15.4	14.6	13.0	12.36	11.77	11.51	—	—	—	—	—	DA	
04037+1459	15.07	15.07	15.0	15.2	15.0	15.42	15.70	15.33	15.18	14.88	15.14	15.39	15.65	DA	2
04180+4211	—	—	17.5	16.9	16.4	15.70	15.36	15.61	—	—	—	—	—	DA	
04201+3233	15.68	15.86	16.0	16.1	—	16.38	16.01	16.36	—	—	—	—	—	DA	
04214+4607	—	—	15.5	15.2	15.3	14.72	14.51	14.44	—	—	—	—	—	DA	
04259+4614	—	—	19.0	17.2	17.0	16.46	16.00	16.08	—	—	—	—	—	DC	
04263+4820	16.95	17.00	16.0	15.9	15.9	15.64	15.65	15.30	—	—	—	—	—	DA+DC	
04294+4945	—	17.91	16.5	16.3	16.4	15.97	15.75	15.98	—	—	—	—	—	DA	
04308+1611	—	—	17.0	16.2	16.2	16.16	16.07	14.98	—	—	—	—	—	DA	
04334+0414	—	—	17.4	16.3	16.1	15.55	15.26	15.18	—	—	—	—	—	DA	

Table 3—Continued

PM I	FUV	NUV	$B_F$	$R_I$	$I_N$	$J$	$H$	$K_S$	$u$	$g$	$r$	$i$	$z$	ST	Notes
04339+2827	—	—	16.0	15.8	—	15.48	14.79	14.56	—	—	—	—	—	DA	
04343+3054	—	—	18.8	17.6	17.5	16.49	16.35	15.83	—	—	—	—	—	DC:	
04372+4524	—	—	17.2	17.0	16.6	16.00	15.85	15.52	—	—	—	—	—	DA	
04389+6351	—	—	17.2	16.8	16.1	15.39	14.72	14.24	—	—	—	—	—	DA+dM	
04523+2519	—	—	15.2	14.8	14.6	15.08	15.15	15.17	—	—	—	—	—	DAH	3
04558+3840	—	—	18.1	16.9	16.8	16.14	15.85	15.32	—	—	—	—	—	DA	
04586+6209	15.68	15.77	15.5	14.1	—	11.31	10.76	10.55	—	—	—	—	—	DA+dM	
04588+6410	—	—	17.4	16.8	16.7	—	—	—	—	—	—	—	—	DC	
05025+5401	—	—	15.3	15.4	15.3	15.27	15.30	15.08	—	—	—	—	—	DA	
05158+2839	—	19.58	16.5	16.0	15.9	15.66	15.31	15.27	—	—	—	—	—	DAH	
05269+4435	—	—	18.8	17.4	17.5	16.50	16.42	15.85	—	—	—	—	—	DC	
05280+4850	18.42	17.63	17.2	15.0	13.1	12.60	12.00	11.73	—	—	—	—	—	DA+dM	
05327+0624	—	—	16.5	16.1	16.1	—	—	—	—	—	—	—	—	DA	
05332+0925	—	—	15.8	15.3	15.5	15.55	15.60	15.61	—	—	—	—	—	DA	
05353+5715	—	—	18.3	17.2	17.0	16.46	16.18	16.29	—	—	—	—	—	DC	
05372+6759	21.23	18.08	16.3	16.2	15.7	15.89	15.89	15.55	—	—	—	—	—	DAH:	
05383+4436	—	21.13	17.3	16.8	16.8	16.21	15.77	15.85	—	—	—	—	—	DA	
05410+3959	—	—	17.6	17.3	18.2	16.35	16.20	15.73	—	—	—	—	—	DA	
05431+3637	—	—	16.0	15.5	15.3	14.78	14.60	14.51	—	—	—	—	—	DAZ	
05449+2602	—	—	18.1	16.1	15.4	15.82	15.29	15.14	—	—	—	—	—	DQ?	
05462+1115	—	—	18.9	17.4	16.8	16.33	16.08	15.63	—	—	—	—	—	DC:	
05492+5747	16.16	16.18	15.8	14.7	13.6	12.76	12.21	12.00	—	—	—	—	—	DA+dM	
06018+2751	—	—	15.6	15.4	—	15.42	15.35	15.28	—	—	—	—	—	DA	1
06019+3726	—	—	16.4	17.0	16.3	—	—	—	—	—	—	—	—	DAH	
06026+0904	—	—	17.4	16.5	16.0	15.95	15.54	15.25	—	—	—	—	—	DA	
06206+3443	20.50	17.48	16.5	16.6	16.4	—	—	—	16.91	16.51	16.59	16.69	16.86	DA	
06324+2230	—	—	—	17.1	16.5	16.12	15.81	15.76	—	—	—	—	—	DA	
06445+2731	—	19.60	18.2	17.2	16.5	16.23	16.75	16.38	17.72	17.15	16.95	16.91	16.97	DA	
06492+1519	—	—	18.1	17.3	16.6	—	—	—	—	—	—	—	—	DC	
06494+7521	—	20.00	17.1	16.6	—	16.13	15.80	15.46	—	—	—	—	—	DA	

Table 3—Continued

PM I	FUV	NUV	$B_F$	$R_I$	$I_N$	$J$	$H$	$K_S$	$u$	$g$	$r$	$i$	$z$	ST	Notes
06506+1657	—	—	17.9	16.9	16.6	16.14	15.73	15.31	—	—	—	—	—	DA	
06513+6242	—	20.38	17.5	17.6	16.8	—	—	—	—	—	—	—	—	DAH	
06538+6355	—	—	16.7	15.8	—	15.28	15.10	14.91	—	—	—	—	—	DA	
06556+5920	17.37	16.60	15.9	14.7	13.2	12.05	11.41	11.17	—	—	—	—	—	DA+dM	
06577+4007	—	19.78	17.2	16.8	16.4	16.36	15.90	17.11	—	—	—	—	—	DA	
07029+4406	18.08	16.04	15.2	15.4	15.3	15.30	15.31	15.48	—	—	—	—	—	DA	
07087+2044	—	22.99	17.3	16.4	16.3	15.92	15.73	15.39	—	—	—	—	—	DA	
07241+0431	—	—	19.1	17.5	17.2	—	—	—	—	—	—	—	—	DA	
07270+1434	—	—	17.2	16.2	16.2	15.71	15.27	15.18	18.20	17.13	16.69	16.51	16.45	DA	
07300+2716W	20.64	17.36	16.4	15.9	16.0	15.97	15.90	15.97	16.71	16.24	16.28	16.37	16.53	DA	
07419+0136	—	21.57	18.6	18.4	17.3	—	—	—	—	—	—	—	—	DC	
07419+1511	15.75	15.88	15.2	15.5	—	16.06	16.12	15.91	16.02	15.76	15.97	16.22	16.51	DA	
07451+2627	—	—	20.1	18.6	17.9	—	—	—	22.06	19.98	18.74	18.18	17.98	DC	
07475+1107	—	—	16.6	16.4	16.5	16.10	15.77	15.64	17.13	16.74	16.68	16.69	16.78	DA	
07504+1740	—	19.55	17.1	16.8	—	16.84	16.32	15.74	17.77	17.26	17.08	17.04	17.11	DA	4
08015+4852	—	22.57	18.4	16.9	16.9	16.31	15.78	15.68	19.47	17.99	17.37	17.12	17.03	DA	
08054+0735	—	22.27	17.8	17.0	16.7	16.24	15.95	15.59	19.21	17.89	17.34	17.11	17.02	DA:	
08068+2215	—	—	18.5	17.5	17.2	16.73	16.56	16.85	19.23	18.25	17.78	17.64	17.58	DA	
08082+1854	—	23.18	18.3	17.3	17.0	16.82	16.36	16.24	19.28	18.22	17.76	17.57	17.50	DA	
08126+1737	13.48	13.76	13.5	13.8	—	13.76	13.84	13.94	14.01	14.55	15.20	14.23	14.26	DA	3
08152+1633	—	—	18.9	17.9	17.7	16.78	16.14	15.67	20.83	18.98	18.16	17.88	17.68	DC:	
08184+6606	16.82	17.06	16.6	15.3	14.1	12.96	12.37	12.13	17.20	16.54	15.80	15.11	14.31	DA+dM	
08212+7120	21.28	18.05	16.5	16.2	16.0	15.94	15.56	15.18	—	—	—	—	—	DA	
08223+2023	—	18.42	16.4	15.6	—	15.62	15.48	15.39	16.73	16.27	16.14	16.14	16.20	DC	
08281+0942	—	—	19.0	17.8	17.7	—	—	—	—	—	—	—	—	DC	
08293+2539	—	—	20.1	18.4	17.9	16.83	16.93	17.10	21.45	19.14	18.29	17.96	17.76	DC	
08314+1641	—	—	17.7	17.2	—	—	—	—	—	—	—	—	—	DA	
08429+2409	23.91	20.87	17.4	16.9	16.5	15.99	15.92	15.60	18.36	17.43	17.03	16.86	16.83	DA	5
08490+4439	—	21.83	18.7	17.5	17.7	16.28	16.03	16.18	18.76	17.98	17.64	17.51	17.47	DC	
08516+1624	—	21.99	16.9	16.4	16.0	15.75	15.69	15.70	17.92	16.97	16.58	16.46	16.47	DC	

Table 3—Continued

PM I	FUV	NUV	$B_F$	$R_I$	$I_N$	$J$	$H$	$K_S$	$u$	$g$	$r$	$i$	$z$	ST	Notes
08558+3700	—	—	17.9	17.1	16.5	16.51	16.17	15.85	19.06	17.98	17.48	17.29	17.25	DA	6
09021+2010	—	21.46	18.9	17.4	17.3	—	—	—	18.94	18.86	17.79	17.25	17.29	DQ	
09026+1535	—	—	18.6	17.4	—	16.23	16.08	15.20	20.37	18.51	17.66	17.34	17.19	DC	
09027+3120	—	—	14.9	14.9	—	15.05	14.90	15.07	15.62	15.28	15.30	15.39	15.56	DA	
09033+2012	—	19.26	17.5	16.8	16.7	16.27	16.19	15.86	17.59	17.07	16.91	16.88	16.96	DA	
09106+2156	—	21.64	17.7	17.1	16.6	16.31	16.11	16.03	18.65	17.66	17.22	17.06	17.00	DA	5
09112+1515	—	—	19.6	18.3	—	—	—	—	21.24	19.37	18.59	18.32	18.16	DC	
09122+2538	—	19.60	16.8	16.8	16.2	15.90	15.44	15.08	17.53	16.88	16.63	16.55	16.56	DA	
09127+2251	—	—	18.2	18.1	17.4	16.75	16.55	15.99	20.44	18.81	18.09	17.83	17.69	DC	
09192+7723	19.62	16.30	15.7	14.9	14.4	14.91	14.91	14.92	—	—	—	—	—	DA	
09222+0504	—	22.66	18.1	17.4	16.5	—	—	—	19.37	18.39	17.95	17.79	17.73	DAH	
09234+0559	—	22.21	17.8	16.8	—	16.53	16.04	16.43	18.91	17.92	17.50	17.30	17.27	DA	
09245+3120	—	—	18.1	17.4	17.5	16.47	15.97	16.91	20.56	18.75	17.95	17.64	17.55	DC	5
09249+3613	20.20	19.16	16.3	17.5	—	—	—	—	—	—	—	—	—	DAH	
09286+1841	—	18.28	16.9	16.4	—	15.99	16.27	15.68	17.09	16.70	16.58	16.57	16.68	DA	
09395+4951	—	—	17.5	16.7	16.8	16.20	16.28	15.53	18.45	17.59	17.24	17.10	17.09	DA	
09422+0942	—	—	18.1	17.5	—	16.76	16.14	15.44	19.92	18.52	17.89	17.69	17.61	DA	
09432+5134	—	—	19.1	17.5	17.5	16.68	16.60	16.07	20.77	18.89	18.14	17.83	17.72	DC	6
09481+2023	—	—	18.7	17.3	17.3	16.62	16.26	15.74	20.32	18.53	17.76	17.46	17.34	DC	
09488+1319	—	19.95	17.3	17.0	—	16.47	16.09	16.51	18.06	17.47	17.28	17.21	17.25	DA	
09503+1509	—	—	18.5	17.2	—	16.16	15.95	15.36	19.14	17.94	17.39	17.17	17.10	DC	
09513+1900	—	—	17.6	17.2	17.3	16.70	16.36	17.33	18.94	18.10	17.68	17.55	17.54	DC	5
10042+2438	18.37	17.10	17.4	16.4	16.1	—	—	—	16.85	16.43	16.55	16.74	16.94	DA	
10118+2647	—	—	18.3	17.5	—	16.61	16.19	15.62	19.57	18.26	17.72	17.51	17.42	DA	4
10155+1850	—	—	19.2	18.4	—	16.73	16.97	16.50	21.32	19.40	18.44	18.14	18.01	DC	
10170+7619	—	19.04	16.8	16.2	16.2	16.09	15.65	15.47	—	—	—	—	—	DA	
10228+3904	—	23.76	17.5	17.5	17.1	16.69	16.28	16.45	18.81	17.59	17.28	17.22	17.24	DZ	
10289+1105	15.75	15.68	15.3	15.4	—	15.99	15.95	15.40	15.86	15.49	15.77	16.01	16.26	DA	
10347+2245	—	19.96	16.6	16.1	16.4	16.24	16.41	15.75	—	—	—	—	—	DZ	5
10355+2126	—	19.56	17.7	16.2	16.7	16.50	16.83	15.60	—	—	—	—	—	DAH	

Table 3—Continued

PM I	FUV	NUV	$B_F$	$R_I$	$I_N$	$J$	$H$	$K_S$	$u$	$g$	$r$	$i$	$z$	ST	Notes
10403+1004	—	21.12	17.7	16.7	—	16.01	16.33	16.10	18.19	17.42	17.07	16.96	16.95	DC	
10471+3453	—	—	16.7	16.4	16.2	16.01	15.96	15.73	16.98	16.48	16.45	16.49	16.58	DA	
10502+3226	—	—	17.9	16.9	17.1	16.55	16.49	16.09	19.14	18.00	17.53	17.36	17.31	DA:	
10521+4050	—	20.29	17.7	16.6	16.5	16.11	15.53	15.21	17.68	17.00	16.68	16.60	16.63	DC	
10538+2425	—	—	18.7	17.3	17.4	16.76	16.34	16.12	18.93	18.02	17.62	17.47	17.41	DA	
10557+2111	—	21.26	18.3	17.5	—	16.62	17.09	15.80	18.73	17.81	17.49	17.40	17.38	DAH	
10565+2336	—	—	19.0	17.6	17.5	16.52	16.57	16.25	19.83	18.41	17.77	17.55	17.41	DA	5
11036+1555	—	—	15.6	13.8	—	11.57	11.16	10.76	18.60	15.88	14.72	17.14	12.86	DA+dM	
11071+1446	—	19.38	17.4	16.6	15.9	15.75	15.47	15.42	17.37	16.75	16.52	16.45	16.49	DA	5
11111+3848	—	—	18.6	17.8	18.0	—	—	—	20.12	18.81	18.17	17.87	17.75	DC	4
11132+2859	—	—	18.8	17.4	17.2	16.33	15.81	15.87	20.21	18.51	17.73	17.44	17.29	DA	5
11144+3341	—	—	17.8	17.8	17.7	16.27	15.65	15.20	18.25	17.87	17.82	17.76	17.63	DA	7
11210+3756	—	—	15.8	15.4	15.5	15.33	15.15	15.14	15.88	15.45	15.53	15.65	15.81	DA	
11222+2839	—	—	18.3	17.2	17.3	16.52	16.99	16.18	19.38	18.27	17.81	17.64	17.56	DA	5
11253+2111	—	19.83	16.8	16.7	16.6	16.24	16.18	15.65	17.88	17.18	16.90	16.79	16.79	DC	
11337+6243	—	19.55	16.5	15.9	15.4	15.57	15.39	15.56	17.09	16.50	16.27	16.20	16.23	DA+DC	
11364+0802S	—	—	18.4	17.4	—	—	—	—	19.46	18.29	17.80	17.60	17.48	DA	
11364+0838	—	20.79	18.1	17.3	—	—	—	—	18.41	17.80	17.52	17.43	17.43	DA	
11401+0112W	19.48	16.73	15.2	14.2	13.5	—	—	—	16.19	15.77	15.83	15.89	16.08	DA	
11460+0514	—	—	16.9	16.5	16.1	16.02	5 1	0.215	17.68	17.0	04	0.00	730	DA	5
11495+2353	—	—	18.3	17.2	17.7	16.42	15.99	17.03	20.35	18.67	17.95	17.70	17.61	DC	
11506+0343	—	21.64	17.7	17.3	17.4	16.50	17.18	16.51	18.81	17.95	17.55	17.37	17.39	DA	
11545+2422	21.23	16.95	15.6	15.2	15.4	15.24	15.11	15.40	15.94	15.60	15.61	15.66	15.80	DA	5
11582+0004	—	—	18.7	18.1	17.5	16.72	15.99	17.20	20.93	18.90	17.87	17.51	17.33	DC	6
11592+4842	—	21.91	18.5	17.5	16.9	16.47	15.96	16.08	18.65	17.74	17.34	17.17	17.15	DA	
11598+0007	23.40	17.32	15.5	16.0	—	15.62	15.37	15.54	16.00	15.75	15.81	15.87	16.01	DA	
12019+3400	—	20.68	17.2	16.4	16.5	16.76	15.95	15.53	18.24	17.74	17.26	17.18	17.23	DQ	
12033+2439	17.45	16.76	21.0	16.9	16.9	—	—	—	16.50	16.54	16.83	17.05	17.31	DB	
12113+0724	—	—	17.2	16.1	16.4	15.37	15.09	15.10	18.51	17.14	16.52	16.30	16.20	DA	5
12145+7822	—	—	18.0	17.2	16.8	16.18	15.65	15.64	—	—	—	—	—	DZ	

Table 3—Continued

PM I	FUV	NUV	$B_F$	$R_I$	$I_N$	$J$	$H$	$K_S$	$u$	$g$	$r$	$i$	$z$	ST	Notes
12155+4630	—	19.83	17.1	16.7	16.4	16.18	16.07	15.74	17.85	17.24	17.01	16.95	16.98	DA	8
12274+3150	—	19.59	16.5	16.3	15.8	15.89	15.50	15.49	17.47	16.82	16.56	16.49	16.51	DA	5, 9
12280+3300	—	—	18.6	17.7	17.3	16.70	16.16	16.01	20.71	18.88	17.97	17.61	17.46	DC	
12370+1814	19.82	17.79	17.8	16.8	16.6	—	—	—	16.96	16.79	16.88	17.03	17.17	DC	
12377+6023	—	—	18.4	17.5	17.6	16.65	15.99	15.60	19.81	18.48	17.87	17.67	17.57	DA	
12405+1807W	—	—	19.1	17.3	16.9	16.59	15.93	15.79	19.20	17.99	17.42	17.19	17.11	DA	
12425+1311W	—	—	19.5	18.0	17.6	—	—	—	20.42	18.74	18.05	17.80	17.69	DC	
12429+6542	—	20.46	17.5	16.8	—	16.55	17.14	16.10	18.29	17.66	17.43	17.34	17.35	DA	
12430+2057	17.62	16.95	18.0	17.0	16.1	—	—	—	16.72	16.74	17.02	17.25	17.43	DB	
12476+0646	—	—	20.2	18.5	18.0	—	—	—	20.93	20.03	18.67	18.37	18.22	DQpec	
12541+3620	—	—	18.1	16.7	16.1	15.90	15.72	15.40	19.74	17.93	17.15	16.83	16.66	DC	
13032+7510	—	18.36	16.9	16.2	16.2	16.16	15.79	15.27	—	—	—	—	—	DC	
13096+6933	—	18.94	17.5	16.1	14.2	13.14	12.55	12.26	—	—	—	—	—	DA+dM	
13103+1404	21.82	17.71	16.2	16.3	—	15.84	15.89	15.67	16.79	16.33	16.34	16.40	16.51	DA	5
13108+7236	—	—	17.4	16.6	17.1	16.03	16.00	15.24	—	—	—	—	—	DA	
13176+0621	—	—	19.3	17.5	16.1	—	—	—	19.98	18.62	17.97	17.74	17.67	DA	6
13246+0857	—	18.10	17.4	16.3	15.1	16.17	16.17	15.81	17.08	16.63	16.60	16.62	16.73	DA	5
13291+2450	—	—	20.6	19.0	18.1	—	—	—	22.35	19.93	18.76	18.26	18.13	DC	
13333+2450	—	—	20.2	19.0	18.0	—	—	—	—	—	—	—	—	DC	
13346+0943E	—	—	18.4	18.1	18.3	—	—	—	19.19	18.43	17.38	18.42	16.90	DA	
13349+6945	15.61	15.76	15.9	15.6	15.2	15.93	16.23	15.58	—	—	—	—	—	DA	
13413+0500	—	—	17.5	16.0	15.5	14.70	14.59	14.48	19.67	17.41	16.29	15.85	15.68	DC	5
13455+4200	—	—	17.9	16.4	16.3	15.61	15.43	14.99	19.76	17.86	17.01	16.71	16.55	DC	
13521+1053	—	20.76	17.1	16.0	16.0	15.74	15.59	15.06	17.92	17.10	16.74	16.57	16.55	DA	
13537+1656	—	17.91	16.5	16.2	16.0	16.39	15.84	15.76	17.11	16.60	16.64	16.70	16.81	DA	
14037+0644	—	20.44	17.3	17.0	17.0	16.58	16.62	16.36	18.02	17.44	17.27	17.25	17.33	DC	5
14064+1608	—	20.45	17.2	16.8	16.6	16.60	16.31	17.28	18.23	17.61	17.37	17.31	17.34	DA	5
14067+3130	—	—	19.4	17.3	17.3	16.61	15.88	16.12	20.54	18.72	17.92	17.64	17.52	DC	
14106+0245	—	—	16.9	16.2	16.0	15.48	15.14	15.02	18.05	17.00	16.50	16.33	16.27	DAZ	5
14149+4336	—	20.65	18.2	17.3	16.8	16.46	15.76	15.67	18.22	17.54	17.25	17.19	17.16	DA	



Table 3—Continued

PM I	FUV	NUV	$B_F$	$R_I$	$I_N$	$J$	$H$	$K_S$	$u$	$g$	$r$	$i$	$z$	ST	Notes
14236+3037	—	—	18.8	17.3	16.8	16.44	16.18	15.67	19.51	18.15	17.56	17.36	17.28	DA	
14244+6246	—	—	19.4	17.8	17.7	—	—	—	20.35	18.83	18.14	17.86	17.70	DA	
14278+0532	23.10	19.25	17.6	16.7	16.6	16.30	16.03	15.93	17.61	17.02	16.86	16.82	16.86	DA+DC	5
14339+1907	—	—	19.1	18.1	17.5	16.88	16.07	15.33	20.43	18.76	18.10	17.82	17.75	DA	
14407+0807	—	—	19.3	17.6	17.0	16.54	15.94	16.30	19.20	18.01	17.48	17.30	17.20	DA	
14456+2527	—	21.63	16.8	15.5	15.3	14.68	14.13	14.21	17.97	16.66	16.00	15.73	15.56	DA	
14553+5655	14.87	14.85	15.4	14.7	14.1	15.13	15.15	15.40	14.96	14.67	14.98	15.24	15.52	DA	
14588+1146	—	—	18.9	17.5	17.6	—	—	—	20.67	18.86	18.02	17.71	17.66	DC	5, 6
15010+6138	—	21.56	18.0	17.1	16.7	16.29	16.05	16.13	18.83	17.84	17.40	17.22	17.18	DA	
15164+2803	—	18.25	17.6	16.3	—	15.98	16.27	15.70	17.02	16.59	16.52	16.53	16.62	DAH	
15167+2910	17.33	17.24	17.6	17.0	—	—	—	—	17.25	16.85	17.07	17.29	17.56	DA	
15206+3903	22.29	18.32	16.9	16.9	16.7	16.35	16.52	15.83	17.44	16.95	17.00	16.82	16.79	DA	
15263+2936	—	—	18.4	16.1	15.8	15.30	14.97	14.80	18.64	17.12	16.46	16.20	16.11	DA	
15342+0218	21.86	17.73	16.5	16.7	—	15.78	15.79	15.56	16.68	16.32	16.27	16.30	16.42	DA	5
15359+2125	—	20.46	17.4	16.6	16.7	16.29	16.08	16.98	18.28	17.53	17.22	17.12	17.12	DA	
15494+4802	—	19.92	17.0	16.9	16.8	16.63	15.85	16.75	18.03	17.41	17.16	17.09	17.11	DC	5
15589+0417	—	18.78	16.6	—	15.8	15.46	15.27	14.82	16.86	16.26	15.97	15.97	16.09	DC	
16053+5556	—	19.99	17.5	17.4	16.6	15.98	15.53	15.57	18.28	17.68	17.49	18.74	17.29	DA	
16096+4735	—	—	16.3	16.3	16.1	—	—	—	16.74	16.38	16.63	16.86	17.17	DA	
16142+1729	—	22.44	19.0	17.9	18.0	—	—	—	19.22	18.67	17.86	17.74	17.84	DQpec	
16144+0906	—	—	18.4	17.0	16.3	15.87	15.77	15.40	19.69	17.96	17.14	16.84	16.69	DC	
16171+0530	15.07	15.01	15.1	14.6	13.6	11.53	10.96	10.67	15.12	14.63	14.61	14.09	13.06	DA+dM	
16222+0532	—	18.52	16.9	16.4	16.7	15.92	15.85	15.22	17.31	16.82	16.73	16.71	16.80	DA	
16264+1938	—	20.48	17.0	16.2	15.8	15.64	15.33	15.41	17.61	16.83	16.48	16.35	16.36	DA	
16265+1355	—	—	18.4	17.1	16.9	16.49	16.16	15.85	18.08	17.48	17.26	17.21	17.24	DA	
16286+7053	—	—	18.8	17.6	16.9	16.10	15.85	15.63	—	—	—	—	—	DA	
16325+0851	—	20.16	15.7	14.6	14.4	13.85	13.61	13.49	16.44	15.34	14.88	14.69	14.64	DA	5
16335+5231	—	—	18.1	17.5	16.8	16.37	16.19	15.70	18.11	17.50	17.24	17.14	17.14	DA	
16477+2636	—	19.22	17.4	17.0	16.7	16.10	17.33	14.33	17.51	17.02	16.90	16.95	17.09	DZ	
16514+6635	20.55	18.04	16.6	16.1	16.3	16.33	15.93	14.81	—	—	—	—	—	DZ	

Table 3—Continued

PM I	FUV	NUV	$B_F$	$R_I$	$I_N$	$J$	$H$	$K_S$	$u$	$g$	$r$	$i$	$z$	ST	Notes
16546+5742	—	—	16.0	16.0	15.3	15.65	15.95	15.20	—	—	—	—	—	DA	
17027+1022	—	—	18.4	17.3	16.8	16.41	16.05	17.04	19.81	18.27	17.61	17.38	17.26	DA	
17052+0423	—	17.49	16.2	16.0	15.5	15.70	15.65	15.40	—	—	—	—	—	DA	
17238+0458	—	18.29	17.0	16.7	16.4	16.40	16.05	15.86	—	—	—	—	—	DA	
17283+0211	—	17.77	16.1	15.6	15.7	15.67	15.95	15.94	—	—	—	—	—	DA	
17328+0213	—	19.09	17.3	16.3	—	16.14	16.15	15.51	—	—	—	—	—	DA	
17335+7949	—	22.64	18.0	16.0	15.8	16.06	16.05	15.48	—	—	—	—	—	DC	
17344+4236	22.32	18.66	16.2	16.3	16.6	15.95	15.91	15.39	—	—	—	—	—	DA	
17368+3635	—	20.09	17.1	17.4	17.3	—	—	—	—	—	—	—	—	DA	
17376+0138	—	18.86	17.2	16.3	—	16.18	15.76	15.07	—	—	—	—	—	DA	
17417+2401	—	—	16.8	16.5	15.9	15.99	15.57	15.70	—	—	—	—	—	DA	
17433+1434S	17.41	15.74	14.9	14.2	13.7	14.89	14.83	15.05	—	—	—	—	—	DC	
17430+1701	—	—	18.8	17.6	17.3	16.34	15.70	15.78	—	—	—	—	—	DC	
17471+2859	—	—	18.1	17.1	16.8	16.23	16.17	16.16	—	—	—	—	—	DC	
17574+1021	21.60	18.36	16.8	16.0	—	15.92	15.97	15.35	—	—	—	—	—	DZA	
17579+5441	—	19.04	17.1	16.7	—	—	—	—	17.71	17.25	17.14	17.15	17.24	DA	
18014+5049	—	—	18.2	17.1	16.5	16.00	16.20	15.94	19.87	18.15	17.33	17.05	16.91	DC	
18018+0846	—	—	18.1	16.8	16.8	16.38	16.01	15.53	—	—	—	—	—	DA	
18073+0357	—	—	15.6	14.8	14.4	14.57	14.51	14.46	—	—	—	—	—	DA	
18138+2119	—	—	15.9	15.8	—	15.70	15.63	15.55	—	—	—	—	—	DA	
18154+3158	—	—	19.1	17.6	17.5	16.70	16.31	16.07	—	—	—	—	—	DA	
18199+1739	—	—	18.4	17.5	17.3	16.39	16.02	15.96	—	—	—	—	—	DC	
18435+2740	17.39	15.67	14.9	15.0	—	13.98	13.34	13.14	—	—	—	—	—	DA	1
18510+7738	—	22.70	18.3	16.4	15.7	15.93	15.80	14.93	19.07	17.60	16.97	16.72	16.64	DC:	
18572+2026	—	—	16.3	16.5	16.3	15.87	15.61	16.11	—	—	—	—	—	DA	
19005+0020	—	—	17.8	17.2	17.2	15.85	14.60	13.99	—	—	—	—	—	DA	
19033+6035	16.84	15.78	14.8	14.8	14.3	15.10	15.16	14.84	—	—	—	—	—	DA	
19128+5343	—	—	13.2	13.2	12.9	13.62	13.73	13.82	—	—	—	—	—	DA	
19132+2949	—	—	17.4	17.0	15.9	16.12	15.67	15.48	—	—	—	—	—	DA	
19146+1428	—	—	16.5	15.1	15.6	15.26	14.92	14.78	—	—	—	—	—	DA	

Table 3—Continued

PM I	FUV	NUV	$B_F$	$R_I$	$I_N$	$J$	$H$	$K_S$	$u$	$g$	$r$	$i$	$z$	ST	Notes
19167+8044	—	—	18.3	17.1	16.6	16.28	16.07	15.21	—	—	—	—	—	DA	
19401+8348	—	—	18.7	17.6	17.3	16.65	16.24	16.96	—	—	—	—	—	DC	
19493+0747	—	—	15.1	15.6	15.2	15.21	15.27	15.17	—	—	—	—	—	DA	
19455+4650N	—	—	18.0	16.9	16.4	15.88	15.56	15.48	—	—	—	—	—	DA	
20062+5902	15.58	15.61	16.2	16.3	15.8	15.70	15.87	15.10	15.76	15.36	15.65	15.88	16.16	DA	
20069+6143	—	22.08	17.5	16.2	16.0	15.17	14.90	14.68	18.16	16.91	16.34	16.13	16.06	DA	
20223+8333	—	—	17.5	16.8	16.7	16.17	16.40	15.99	—	—	—	—	—	DC	
20235+7001	—	20.94	19.1	17.9	17.4	—	—	—	—	—	—	—	—	DA	
20279+0523	—	19.57	17.1	17.0	—	16.31	15.90	15.46	—	—	—	—	—	DA	
20300+0729	—	17.77	16.3	15.8	15.6	15.66	16.08	15.60	—	—	—	—	—	DC	
20597+5517	—	—	18.7	17.0	16.4	15.66	15.45	15.49	19.97	17.97	17.02	16.67	16.49	DC	
21077+0740	—	18.63	16.3	15.8	—	15.77	15.79	15.14	—	—	—	—	—	DA	
21117+0120	15.01	15.12	15.2	15.1	—	15.52	15.69	15.32	—	—	—	—	—	DA	
21134+0727	—	19.30	16.0	15.6	15.8	15.21	14.95	14.81	—	—	—	—	—	DA	
21222+0413	—	—	17.5	16.2	15.7	15.24	15.01	14.88	18.86	17.20	16.49	16.23	16.12	DA	5
21384+1856	—	—	17.5	16.7	16.3	15.96	15.38	15.45	17.55	17.16	17.32	17.54	17.76	DA	
21420+2252	19.81	17.17	15.9	16.1	15.6	15.98	15.74	15.54	—	—	—	—	—	DZ	
21429+0805	—	—	18.0	15.6	15.5	15.77	15.27	15.18	—	—	—	—	—	DA	
21474+1127	—	—	19.5	16.6	17.4	—	—	—	20.86	19.18	18.42	18.14	18.01	DA	6
21492+0415	—	22.32	17.4	15.5	15.3	15.38	15.21	15.10	—	—	—	—	—	DA	
21551+4103	—	—	17.9	16.4	16.3	16.18	15.80	15.80	—	—	—	—	—	DZA	
21597+2936	13.47	13.94	14.7	15.5	—	15.83	15.90	15.36	—	—	—	—	—	DA	3
22105+4532	—	—	18.1	17.1	16.5	16.20	15.97	15.74	—	—	—	—	—	DC	
22118+5649	—	—	13.9	13.6	13.4	13.19	12.99	12.86	—	—	—	—	—	DA	
22133+0349	—	—	18.9	15.9	16.2	16.56	16.38	16.55	—	—	—	—	—	DC	
22198+4805	—	—	18.6	17.5	16.7	—	—	—	—	—	—	—	—	DA	
22230+2201N	14.78	14.90	14.7	14.8	—	16.05	16.19	15.66	15.64	15.58	15.91	16.22	16.50	DA	
22230+2201S	—	—	15.3	15.0	—	16.42	15.71	16.10	16.36	15.99	16.20	16.45	16.69	DA	
22276+1753	—	19.41	16.8	16.0	15.2	15.85	15.57	15.47	—	—	—	—	—	DAZ	
22299+3024	18.61	17.02	16.1	16.0	—	15.55	15.22	15.02	—	—	—	—	—	DA	

Table 3—Continued

PM I	FUV	NUV	$B_F$	$R_I$	$I_N$	$J$	$H$	$K_S$	$u$	$g$	$r$	$i$	$z$	ST	Notes
22331+2610	15.63	15.72	15.6	15.3	—	15.94	15.65	16.01	—	—	—	—	—	DA	
22340+5543	—	—	17.7	17.1	16.6	16.57	15.70	15.99	—	—	—	—	—	DA	
22410+3646	—	19.14	17.6	16.9	16.5	16.38	16.17	16.98	—	—	—	—	—	DA	
22418+0432	—	21.07	18.7	17.6	17.2	—	—	—	—	—	—	—	—	DQ <sub>pec</sub>	
22447+1513W	—	22.83	19.0	17.8	17.3	—	—	—	—	—	—	—	—	DA	
22497+3623	—	—	19.1	17.7	16.9	16.58	16.22	17.12	—	—	—	—	—	DA	
22595+5717	—	—	19.1	17.2	16.0	16.18	15.93	15.20	—	—	—	—	—	DA	
23003+2204	—	20.55	17.8	17.0	16.6	—	—	—	—	—	—	—	—	DZ	
23027+4312	—	—	17.7	16.2	16.4	15.96	15.97	17.03	—	—	—	—	—	DA	
23056+4334	—	—	19.4	18.1	17.5	16.76	16.04	16.47	—	—	—	—	—	DC	
23098+5506E	—	—	16.0	14.3	11.4	14.27	13.94	13.93	—	—	—	—	—	DA	
23160+0559	16.71	16.85	17.1	17.1	16.5	—	—	—	16.95	16.64	16.92	17.15	17.40	DA	
23162+1720	—	—	18.4	17.3	17.1	16.51	16.57	15.57	20.30	18.54	17.76	17.44	17.31	DC	
23186+5458	—	—	17.0	16.9	16.6	—	—	—	16.76	16.73	16.92	17.12	17.30	DZ	
23229+3358	16.84	16.84	16.2	15.4	13.2	13.14	12.59	12.28	—	—	—	—	—	DA+dM	
23234+7255	—	18.33	16.8	16.0	16.1	15.83	15.77	16.16	—	—	—	—	—	DA	
23243+2835	—	18.53	16.3	15.9	—	15.60	15.24	15.41	—	—	—	—	—	DA	
23283+3319	15.81	15.89	15.1	14.9	—	12.14	11.62	11.42	—	—	—	—	—	DA+dM	
23300+0120	—	20.73	17.7	17.5	16.5	—	—	—	—	—	—	—	—	DC	
23389+2101E	—	—	18.2	16.8	17.2	16.32	16.18	15.14	—	—	—	—	—	DA	
23390+5316	—	—	17.0	16.9	16.2	16.10	15.48	15.63	—	—	—	—	—	DA	
23462+1158	—	21.93	18.1	17.0	16.6	16.33	15.93	15.62	—	—	—	—	—	DC	
23475+0304	—	—	17.8	16.2	15.5	15.61	15.60	15.87	19.14	17.25	16.52	16.25	16.16	DC	
23478+0223	—	—	18.8	17.5	16.5	16.44	16.28	16.30	20.00	18.56	17.91	17.65	17.60	DA	
23489+4300	—	—	18.6	17.5	17.1	16.67	15.95	15.74	20.32	18.64	17.81	17.50	17.36	DC:	

Note. — (1) WD in McCook and Sion. (2) Also in Schilbach & Röser (2012). (3) Also in Vennes et al. (2011). (4) SDSS spectrum. (5) Also in Sayres et al. (2012). (6) Also in Kilic et al. (2010). (7) DA+dM in Rebassa-Mansergas et al. (2010). (8) Also in Tonry et al. (2012). (9) LSPM J1227+3150 wrongly identified as PM I12273+3150 in Limoges et al. (2013).

Table 4. Atmospheric Parameters of New White Dwarfs from SUPERBLINK

PM I	ST	$T_{\text{eff}}$ (K)	$\log g$	$M/M_{\odot}$	Comp.	$M_V$	$\log L/L_{\odot}$	$D$ (pc)	$\log \tau$	Fit <sup>a</sup>	Other name <sup>b</sup>
00023+6357	DC	4630 (563)	8.00 (0.25)	0.58 (0.15)	H	14.77	-4.18	26.7 (5.2)	9.85	2	
00050+4003	DZA:	8150 (549)	8.00 (0.25)	0.58 (0.15)	He	12.50	-3.20	52.2 (9.4)	9.05	2	GD 1
00056+4825	DA	6970 (105)	7.95 (0.09)	0.56 (0.05)	H	13.47	-3.43	48.4 (1.3)	9.15	1	
00074+3403	DC:	5830 (113)	8.00 (0.25)	0.57 (0.15)	He	14.23	-3.79	42.0 (5.2)	9.46	2	
00079+3947	DC	4890 (453)	8.00 (0.25)	0.58 (0.15)	H	15.16	-4.09	20.2 (3.0)	9.79	2	
00217+2640	DC	5160 (645)	8.00 (0.25)	0.58 (0.15)	H	14.67	-3.99	35.2 (6.1)	9.69	2	
00276+0542	DA	5520 (855)	8.00 (0.25)	0.58 (0.15)	H	14.65	-3.87	21.5 (3.7)	9.49	2	
00331+4742S	DA	16580 (265)	8.02 (0.05)	0.63 (0.03)	H	11.13	-1.95	55.0 (1.6)	8.17	1	
00334+2506	DA	6310 (107)	7.89 (0.16)	0.52 (0.09)	H	13.81	-3.58	42.1 (0.8)	9.22	1	
00532+3927	DA	7530 (113)	7.96 (0.08)	0.57 (0.05)	H	13.19	-3.31	55.3 (1.9)	9.08	1	
00559+5948	DC:	5840 (1061)	8.00 (0.25)	0.57 (0.15)	He	13.32	-3.78	26.2 (4.7)	9.45	2	
01043+3816	DA	16280 (257)	8.05 (0.05)	0.64 (0.03)	H	11.20	-2.00	57.7 (1.6)	8.22	1	
01088+7600	DA	6430 (128)	8.52 (0.22)	0.93 (0.14)	H	14.66	-3.93	38.0 (1.3)	9.66	1	
01216+3440	DZ	6890 (116)	8.00 (0.25)	0.58 (0.15)	He	13.66	-3.49	41.7 (0.9)	9.23	2	
01278+7328	DA	7400 (117)	8.20 (0.10)	0.72 (0.07)	H	13.61	-3.48	25.1 (1.4)	9.26	1	
01327+6635	DA	11940 (288)	8.09 (0.11)	0.66 (0.07)	H	11.80	-2.57	75.2 (2.5)	8.63	1	
01327+4604	DA	10680 (163)	7.97 (0.06)	0.59 (0.04)	H	11.91	-2.70	41.7 (0.8)	8.69	1	
01382+4442	DA	11200 (170)	8.12 (0.06)	0.68 (0.04)	H	11.99	-2.70	49.5 (1.5)	8.72	1	
01390+2402	DA	8710 (166)	6.88 (0.27)	0.19 (0.06)	H	11.14	-2.46	234.5 (5.3)	8.33	1	
01457+2918	DC	4740 (879)	8.00 (0.25)	0.58 (0.15)	H	15.04	-4.14	39.6 (14.2)	9.83	2	
01486+3615	DA	6480 (119)	8.68 (0.19)	1.03 (0.11)	H	14.91	-4.03	24.0 (0.8)	9.68	1	
01534+3557	DA	7330 (114)	8.32 (0.09)	0.80 (0.06)	H	13.82	-3.57	43.7 (1.4)	9.41	1	
01565+2955	DA	15270 (238)	7.99 (0.05)	0.61 (0.03)	H	11.23	-2.08	49.5 (1.4)	8.27	1	
02062+1836	DC	4230 (530)	8.00 (0.25)	0.58 (0.15)	H	15.92	-4.34	31.0 (7.8)	9.92	2	
02118+7119	DC	5150 ( 52)	8.00 (0.25)	0.58 (0.15)	H	14.75	-4.00	28.0 (3.2)	9.69	2	

Table 4—Continued

PM I	ST	$T_{\text{eff}}$ (K)	$\log g$	$M/M_{\odot}$	Comp.	$M_V$	$\log L/L_{\odot}$	$D$ (pc)	$\log \tau$	Fit <sup>a</sup>	Other name <sup>b</sup>
02149+7746	DC	5480 (598)	8.00 (0.25)	0.57 (0.15)	He	14.32	-3.89	67.4 (10.1)	9.61	2	
02199+3520	DA	5580 (791)	8.00 (0.25)	0.58 (0.15)	H	14.28	-3.85	43.1 (8.3)	9.47	2	
02230+5544	DA	6980 (110)	8.40 (0.10)	0.85 (0.07)	H	14.14	-3.70	35.3 (1.3)	9.54	1	
02236+4816	DB	16590 (295)	8.25 (0.07)	0.75 (0.04)	He	11.44	-2.11	54.1 (2.2)	8.35	1	GD 27
02238+2055	DC	4300 ( 91)	8.00 (0.25)	0.58 (0.15)	H	16.02	-4.31	33.5 (3.9)	9.91	2	
02241+2325	DA	4980 (130)	8.00 (0.25)	0.58 (0.15)	H	14.97	-4.06	58.3 (7.3)	9.76	2	
02321+5211	DA	9330 (157)	8.00 (0.13)	0.60 (0.08)	H	12.43	-2.95	84.6 (2.6)	8.86	1	
02334+2125	DC	4730 ( 52)	8.00 (0.25)	0.58 (0.15)	H	15.15	-4.15	26.3 (3.0)	9.83	2	
02379+1638	DC	5150 (607)	8.00 (0.25)	0.57 (0.15)	He	14.63	-4.00	30.7 (5.0)	9.74	2	
02478+4138	DB	16960 (294)	8.18 (0.10)	0.70 (0.06)	He	11.27	-2.02	128.1 (3.8)	8.27	1	
02497+3307	DA	5890 (119)	8.31 (0.26)	0.79 (0.17)	H	14.72	-3.94	31.6 (0.7)	9.67	1	
02557+2106S	DA	6320 (105)	8.16 (0.15)	0.69 (0.10)	H	14.17	-3.72	46.3 (1.0)	9.45	1	
02562+4954	DA	6050 (101)	8.00 (0.25)	0.59 (0.15)	H	14.14	-3.71	41.0 (1.3)	9.34	1	
03009+5432	DA	7780 (125)	8.23 (0.10)	0.74 (0.07)	H	13.46	-3.41	43.7 (1.3)	9.23	1	
03031+2317	DA+dM	23330 (6829)	8.00 (0.25)	0.63 (0.14)	H	9.47	-1.34	43.7 (1.3)	7.50	2	
03053+2603	DA	5190 (686)	8.00 (0.25)	0.58 (0.15)	H	14.64	-3.98	45.0 (9.0)	9.67	2	
03109+6634	DC	4620 (662)	8.00 (0.25)	0.58 (0.15)	H	15.31	-4.19	36.4 (9.1)	9.86	2	
03127+2218	DA	6670 (114)	7.70 (0.16)	0.43 (0.08)	H	13.34	-3.38	55.1 (1.6)	9.06	1	
03196+3630	DZ	5770 (234)	8.00 (0.25)	0.57 (0.15)	He	14.26	-3.80	29.9 (1.5)	9.48	2	
03203+2333	DC	4510 (447)	8.00 (0.25)	0.58 (0.15)	H	15.52	-4.23	29.3 (5.4)	9.88	2	
03433+1958	DA	7150 (107)	8.47 (0.08)	0.89 (0.05)	H	14.16	-3.71	22.8 (0.9)	9.55	1	
03471+0520W	DC	7010 ( 81)	8.00 (0.25)	0.58 (0.15)	He	13.37	-3.46	82.0 (9.2)	9.22	2	
03473+4358	DA	13650 (316)	7.99 (0.05)	0.60 (0.03)	H	11.42	-2.27	33.9 (1.3)	8.41	1	
04010+5131W	DC	5220 (342)	8.00 (0.25)	0.58 (0.15)	H	14.57	-3.97	30.8 (4.2)	9.66	2	
04032+2520E	DA+dM	21580 (3633)	8.00 (0.25)	0.63 (0.14)	H	9.95	-1.47	97.1 (29.5)	7.68	2	

Table 4—Continued

PM I	ST	$T_{\text{eff}}$ (K)	$\log g$	$M/M_{\odot}$	Comp.	$M_V$	$\log L/L_{\odot}$	$D$ (pc)	$\log \tau$	Fit <sup>a</sup>	Other name <sup>b</sup>
04032+2520W	DA	22770 (441)	8.06 (0.06)	0.67 (0.04)	H	10.63	-1.42	101.9 (3.3)	7.64	1	
04037+1459	DA	14710 (344)	8.41 (0.05)	0.87 (0.03)	H	11.95	-2.41	40.7 (1.0)	8.61	1	
04180+4211	DA	4580 (374)	8.00 (0.25)	0.58 (0.15)	H	15.17	-4.20	23.8 (3.6)	9.86	2	
04201+3233	DA	11280 (250)	8.05 (0.12)	0.63 (0.07)	H	11.86	-2.64	73.3 (2.4)	8.67	1	
04214+4607	DA	7790 (123)	7.87 (0.11)	0.52 (0.06)	H	12.94	-3.19	30.5 (1.2)	8.98	1	
04259+4614	DC	4520 (504)	8.00 (0.25)	0.58 (0.15)	H	15.44	-4.22	32.5 (7.0)	9.88	2	
04263+4820	DA+DC	4240 (325)	8.00 (0.25)	0.58 (0.15)	H	14.23	-4.34	29.0 (4.6)	9.92	2	
04294+4945	DA	8380 (153)	8.09 (0.15)	0.65 (0.09)	H	12.98	-3.19	49.4 (1.6)	9.04	1	
04308+1611	DA	8710 (134)	8.05 (0.09)	0.63 (0.05)	H	12.76	-3.10	57.8 (2.4)	8.97	1	
04334+0414	DA	5220 (596)	8.00 (0.25)	0.58 (0.15)	H	14.62	-3.97	26.5 (4.2)	9.66	2	
04339+2827	DA	13930 (331)	8.05 (0.05)	0.64 (0.03)	H	11.47	-2.27	69.0 (4.1)	8.42	1	
04343+3054	DC:	4670 (577)	8.00 (0.25)	0.58 (0.15)	H	15.28	-4.17	36.2 (7.5)	9.85	2	
04372+4524	DA	6570 (112)	8.12 (0.15)	0.66 (0.10)	H	13.96	-3.63	40.4 (1.4)	9.36	1	
04389+6351	DA+dM	13190 (640)	7.78 (0.10)	0.49 (0.05)	H	11.20	-2.22	146.0 (8.1)	8.33	1	
04523+2519	DAH	11500 (2655)	8.00 (0.25)	0.60 (0.14)	H	11.66	-2.58	43.7 (6.5)	8.62	2	
04558+3840	DA	5020 (613)	8.00 (0.25)	0.58 (0.15)	H	14.82	-4.04	32.5 (5.9)	9.75	2	
04586+6209	DA+dM	10960 (704)	8.88 (0.13)	1.14 (0.07)	H	13.40	-3.27	21.6 (0.9)	9.30	1	
04588+6410	DC	6860 (913)	8.00 (0.25)	0.58 (0.15)	He	13.37	-3.50	52.1 (11.4)	9.24	2	
05025+5401	DA	11290 (169)	8.09 (0.05)	0.65 (0.03)	H	11.92	-2.67	44.2 (1.4)	8.69	1	
05158+2839	DAH	6640 (104)	8.00 (0.25)	0.59 (0.15)	H	13.39	-3.55	35.0 (4.1)	9.24	2	
05269+4435	DC	4700 (632)	8.00 (0.25)	0.58 (0.15)	H	15.14	-4.16	37.0 (8.7)	9.84	2	
05280+4850	DA+dM	11100 (393)	8.72 (0.12)	1.05 (0.07)	H	13.04	-3.12	57.9 (2.2)	9.22	1	
05327+0624	DA	9110 (134)	8.10 (0.06)	0.66 (0.04)	H	12.67	-3.05	54.3 (3.6)	8.95	1	
05332+0925	DA	13900 (393)	8.09 (0.05)	0.66 (0.03)	H	11.53	-2.30	57.9 (2.2)	8.45	1	
05353+5715	DC	5210 (462)	8.00 (0.25)	0.57 (0.15)	He	14.66	-3.98	39.1 (5.1)	9.72	2	



Table 4—Continued

PM I	ST	$T_{\text{eff}}$ (K)	$\log g$	$M/M_{\odot}$	Comp.	$M_V$	$\log L/L_{\odot}$	$D$ (pc)	$\log \tau$	Fit <sup>a</sup>	Other name <sup>b</sup>
05372+6759	DAH:	8710 (1615)	8.00 (0.25)	0.60 (0.15)	H	12.55	-3.07	51.2 (9.3)	8.93	2	
05383+4436	DA	6200 (134)	7.99 (0.25)	0.58 (0.15)	H	14.02	-3.66	43.0 (1.2)	9.31	1	
05410+3959	DA	5970 (147)	8.00 (0.25)	0.59 (0.15)	H	14.20	-3.73	44.7 (1.6)	9.36	1	
05431+3637	DAZ	6540 (101)	7.84 (0.11)	0.50 (0.06)	H	13.59	-3.48	27.2 (1.1)	9.16	1	
05449+2602	DQ?	4460 (393)	8.00 (0.25)	0.57 (0.15)	He	15.27	-4.26	22.4 (3.2)	9.86	2	
05462+1115	DC:	4290 (137)	8.00 (0.25)	0.57 (0.15)	He	15.84	-4.32	27.5 (3.3)	9.88	2	
05492+5747	DA+dM	16810 (416)	8.20 (0.07)	0.74 (0.04)	H	11.37	-2.04	106.9 (3.5)	8.28	1	
06018+2751	DA	13950 (718)	8.06 (0.08)	0.65 (0.05)	H	11.49	-2.28	54.8 (2.3)	8.43	1	GD 258
06019+3726	DAH	15750 (8579)	8.00 (0.25)	0.61 (0.14)	H	11.06	-2.03	122.8 (90.4)	8.23	2	
06026+0904	DA	5920 (132)	7.75 (0.29)	0.45 (0.14)	H	13.91	-3.61	40.4 (1.4)	9.21	1	
06206+3443	DA	9910 (148)	8.21 (0.07)	0.73 (0.04)	H	12.52	-2.97	62.7 (1.4)	8.92	1	
06324+2230	DA	5620 (1471)	8.00 (0.25)	0.58 (0.15)	H	14.72	-3.84	37.4 (10.3)	9.45	2	
06445+2731	DA	7020 (119)	8.69 (0.13)	1.04 (0.08)	H	14.63	-3.90	30.7 (0.8)	9.63	1	
06492+1519	DC	5050 (392)	8.00 (0.25)	0.57 (0.15)	He	14.85	-4.04	34.9 (6.3)	9.76	2	
06494+7521	DA	5450 (1044)	8.00 (0.25)	0.58 (0.15)	H	14.02	-3.89	34.4 (7.4)	9.53	2	
06506+1657	DA	5240 (661)	8.00 (0.25)	0.58 (0.15)	H	14.60	-3.96	34.2 (6.4)	9.65	2	
06513+6242	DAH	6900 (289)	8.00 (0.25)	0.59 (0.15)	H	13.30	-3.48	65.3 (12.4)	9.20	2	
06538+6355	DA	6220 (137)	8.44 (0.23)	0.87 (0.15)	H	14.67	-3.93	20.8 (0.7)	9.67	1	
06556+5920	DA+dM	12050 (490)	8.48 (0.10)	0.91 (0.06)	H	12.39	-2.80	53.1 (1.8)	8.89	1	
06577+4007	DA	6900 (118)	8.21 (0.16)	0.73 (0.10)	H	13.89	-3.60	50.3 (1.7)	9.37	1	
07029+4406	DA	10920 (161)	8.09 (0.05)	0.65 (0.03)	H	12.02	-2.72	47.4 (1.3)	8.73	1	
07087+2044	DA	5810 (117)	8.00 (0.25)	0.59 (0.15)	H	14.33	-3.78	35.2 (1.3)	9.39	1	
07241+0431	DA	5670 (120)	8.00 (0.25)	0.59 (0.15)	H	14.45	-3.83	64.2 (4.5)	9.44	1	
07270+1434	DA	5680 ( 89)	8.00 (0.25)	0.59 (0.15)	H	14.44	-3.82	30.5 (0.6)	9.43	1	
07300+2716W	DA	9600 (161)	8.44 (0.11)	0.88 (0.07)	H	13.02	-3.17	44.2 (1.1)	9.15	1	

Table 4—Continued

PM I	ST	$T_{\text{eff}}$ (K)	$\log g$	$M/M_{\odot}$	Comp.	$M_V$	$\log L/L_{\odot}$	$D$ (pc)	$\log \tau$	Fit <sup>a</sup>	Other name <sup>b</sup>
07419+0136	DC	6270 (432)	8.00 (0.25)	0.57 (0.15)	He	13.79	−3.66	80.7 (18.0)	9.34	2	
07419+1511	DA	14400 (262)	8.01 (0.05)	0.62 (0.03)	H	11.36	−2.20	76.6 (1.7)	8.36	1	
07451+2627	DC	3620 (144)	8.00 (0.25)	0.58 (0.15)	H	16.68	−4.61	32.3 (3.8)	10.00	2	
07475+1107	DA	8060 (126)	8.82 (0.08)	1.11 (0.05)	H	14.35	−3.75	29.3 (0.8)	9.53	1	
07504+1740	DA	6900 (103)	8.01 (0.08)	0.60 (0.05)	H	13.60	−3.48	51.2 (1.1)	9.20	1	075026.30+174029
08015+4852	DA	5280 (365)	8.00 (0.25)	0.58 (0.15)	H	14.76	−3.95	36.1 (5.3)	9.63	2	
08054+0735	DA:	5370 ( 45)	8.00 (0.25)	0.58 (0.15)	H	14.42	−3.92	37.0 (4.2)	9.58	2	
08068+2215	DA	5920 (116)	8.97 (0.19)	1.18 (0.08)	H	15.88	−4.41	26.2 (0.8)	9.73	1	
08082+1854	DA	5690 (126)	8.21 (0.28)	0.72 (0.18)	H	14.73	−3.94	43.8 (1.0)	9.65	1	
08126+1737	DA	16400 (241)	8.09 (0.04)	0.67 (0.03)	H	11.25	−2.02	32.7 (1.0)	8.24	1	
08152+1633	DC:	4710 ( 80)	8.00 (0.25)	0.58 (0.15)	H	15.23	−4.15	40.4 (4.6)	9.84	2	
08184+6606	DA+dM	12990 (1078)	8.00 (0.25)	0.61 (0.14)	H	10.57	−3.52	113.8 (51.2)	8.48	2	
08212+7120	DA	8690 (171)	7.93 (0.19)	0.56 (0.10)	H	12.60	−3.04	56.8 (1.6)	8.90	1	
08223+2023	DC	7240 (150)	8.00 (0.25)	0.58 (0.15)	He	13.12	−3.41	35.6 (4.1)	9.18	2	
08281+0942	DC	5190 (372)	8.00 (0.25)	0.57 (0.15)	He	14.59	−3.99	54.5 (9.1)	9.72	2	
08293+2539	DC	4010 ( 95)	8.00 (0.25)	0.58 (0.15)	H	16.58	−4.43	32.4 (3.6)	9.95	2	
08314+1641	DA	7190 (164)	8.32 (0.23)	0.80 (0.15)	H	13.90	−3.60	53.1 (4.3)	9.44	1	
08429+2409	DA	5900 (120)	8.00 (0.25)	0.59 (0.15)	H	14.26	−3.76	38.7 (0.8)	9.37	1	
08490+4439	DC	5990 ( 56)	8.00 (0.25)	0.57 (0.15)	He	14.43	−3.74	51.1 (5.7)	9.41	2	
08516+1624	DC	5580 ( 78)	8.00 (0.25)	0.57 (0.15)	He	14.19	−3.86	29.0 (3.3)	9.56	2	
08558+3700	DA	5620 ( 59)	8.00 (0.25)	0.58 (0.15)	H	14.17	−3.84	43.4 (5.0)	9.45	2	
09021+2010	DQ	5010 ( 34)	8.00 (0.25)	0.57 (0.15)	He	15.98	−4.05	37.6 (0.6)	9.78	2	
09026+1535	DC	4670 ( 36)	8.00 (0.25)	0.58 (0.15)	H	15.38	−4.17	31.6 (3.5)	9.85	2	
09027+3120	DA	9930 (143)	8.23 (0.05)	0.75 (0.03)	H	12.56	−2.98	34.1 (0.8)	8.94	1	
09033+2012	DA	7170 (113)	8.01 (0.11)	0.60 (0.06)	H	13.45	−3.42	50.8 (1.1)	9.16	1	

Table 4—Continued

PM I	ST	$T_{\text{eff}}$ (K)	$\log g$	$M/M_{\odot}$	Comp.	$M_V$	$\log L/L_{\odot}$	$D$ (pc)	$\log \tau$	Fit <sup>a</sup>	Other name <sup>b</sup>
09106+2156	DA	5640 ( 90)	8.00 (0.25)	0.59 (0.15)	H	14.47	-3.83	37.5 (0.7)	9.44	1	
09112+1515	DC	4740 (124)	8.00 (0.25)	0.58 (0.15)	H	15.30	-4.14	50.4 (6.2)	9.83	2	
09122+2538	DA	6720 (105)	8.32 (0.11)	0.80 (0.07)	H	14.17	-3.72	32.5 (0.8)	9.52	1	
09127+2251	DC	4960 ( 69)	8.00 (0.25)	0.58 (0.15)	H	14.76	-4.06	43.9 (5.0)	9.77	2	
09192+7723	DA	9290 (164)	7.72 (0.16)	0.45 (0.08)	H	12.06	-2.81	41.6 (1.1)	8.72	1	
09222+0504	DAH	5910 ( 77)	8.00 (0.25)	0.59 (0.15)	H	13.74	-3.75	59.3 (7.1)	9.37	2	
09234+0559	DA	6040 (111)	8.00 (0.25)	0.59 (0.15)	H	14.15	-3.71	51.8 (1.2)	9.34	1	
09245+3120	DC	4800 ( 71)	8.00 (0.25)	0.58 (0.15)	H	14.66	-4.12	38.8 (4.3)	9.82	2	
09249+3613	DAH	11690 (306)	8.00 (0.25)	0.61 (0.14)	H	9.80	-2.56	237.1 (35.2)	8.60	2	
09286+1841	DA	7730 (116)	8.45 (0.07)	0.88 (0.05)	H	13.83	-3.56	35.9 (0.9)	9.45	1	
09395+4951	DA	5990 ( 69)	8.00 (0.25)	0.59 (0.15)	H	13.79	-3.73	43.3 (5.1)	9.35	2	
09422+0942	DA	5250 ( 60)	8.00 (0.25)	0.58 (0.15)	H	14.32	-3.96	46.2 (5.3)	9.64	2	
09432+5134	DC	4800 ( 75)	8.00 (0.25)	0.58 (0.15)	H	15.08	-4.12	41.9 (4.7)	9.82	2	
09481+2023	DC	4820 ( 60)	8.00 (0.25)	0.58 (0.15)	H	15.11	-4.11	35.8 (4.1)	9.81	2	
09488+1319	DA	6800 (110)	7.69 (0.13)	0.42 (0.06)	H	13.24	-3.34	66.3 (1.3)	9.04	1	
09503+1509	DC	5440 ( 54)	8.00 (0.25)	0.58 (0.15)	H	14.78	-3.90	38.8 (4.5)	9.53	2	
09513+1900	DC	5870 ( 73)	8.00 (0.25)	0.57 (0.15)	He	13.70	-3.78	51.2 (5.8)	9.45	2	
10042+2438	DA	11540 (177)	8.04 (0.05)	0.63 (0.03)	H	11.81	-2.60	85.0 (1.8)	8.64	1	
10118+2647	DA	5280 (121)	8.00 (0.25)	0.58 (0.15)	H	14.66	-3.95	41.6 (5.0)	9.63	2	101151.05+264745
10155+1850	DC	4600 ( 89)	8.00 (0.25)	0.58 (0.15)	H	15.38	-4.19	45.0 (5.1)	9.86	2	
10170+7619	DA	7170 (115)	8.00 (0.12)	0.59 (0.07)	H	13.43	-3.41	44.7 (1.2)	9.16	1	
10228+3904	DZ	5300 ( 50)	8.00 (0.25)	0.57 (0.15)	He	14.74	-3.95	37.1 (0.5)	9.68	2	
10289+1105	DA	13970 (348)	8.11 (0.05)	0.68 (0.03)	H	11.56	-2.31	63.6 (1.4)	8.46	1	
10347+2245	DZ	6510 ( 96)	8.00 (0.25)	0.57 (0.15)	He	13.40	-3.59	36.5 (0.7)	9.30	2	
10355+2126	DAH	7110 (144)	8.00 (0.25)	0.59 (0.15)	H	13.18	-3.43	54.2 (6.8)	9.16	2	

Table 4—Continued

PM I	ST	$T_{\text{eff}}$ (K)	$\log g$	$M/M_{\odot}$	Comp.	$M_V$	$\log L/L_{\odot}$	$D$ (pc)	$\log \tau$	Fit <sup>a</sup>	Other name <sup>b</sup>
10403+1004	DC	5920 ( 94)	8.00 (0.25)	0.57 (0.15)	He	14.11	-3.76	39.1 (4.5)	9.43	2	
10471+3453	DA	8690 (129)	7.57 (0.08)	0.38 (0.04)	H	12.12	-2.85	73.4 (1.5)	8.73	1	
10502+3226	DA:	5610 ( 57)	8.00 (0.25)	0.58 (0.15)	H	14.02	-3.84	44.6 (5.1)	9.46	2	
10521+4050	DC	6180 (116)	8.00 (0.25)	0.57 (0.15)	He	14.26	-3.68	35.7 (4.1)	9.36	2	
10538+2425	DA	5900 ( 55)	8.00 (0.25)	0.59 (0.15)	H	14.36	-3.76	50.7 (5.9)	9.37	2	
10557+2111	DAH	6490 ( 82)	8.00 (0.25)	0.59 (0.15)	H	13.76	-3.59	63.1 (7.4)	9.26	2	
10565+2336	DA	5190 ( 58)	8.00 (0.25)	0.58 (0.15)	H	15.06	-3.98	42.1 (4.8)	9.67	2	
11036+1555	DA+dM	9800 (368)	7.72 (0.29)	0.45 (0.14)	H	11.85	-2.71	171.1 (6.3)	8.66	1	
11071+1446	DA	6700 (110)	8.32 (0.12)	0.80 (0.08)	H	14.18	-3.73	30.5 (0.7)	9.53	1	
11111+3848	DC	5080 (145)	8.00 (0.25)	0.57 (0.15)	He	14.64	-4.03	48.1 (6.0)	9.76	2	111109.10+384856
11132+2859	DA	4830 ( 62)	8.00 (0.25)	0.58 (0.15)	H	15.27	-4.11	34.9 (4.0)	9.81	2	
11144+3341	DA	8270 (133)	8.03 (0.11)	0.62 (0.07)	H	12.94	-3.18	92.5 (2.3)	9.01	1	
11210+3756	DA	9810 (145)	8.26 (0.06)	0.76 (0.04)	H	12.65	-3.02	36.5 (0.8)	8.97	1	
11222+2839	DA	5690 ( 56)	8.00 (0.25)	0.59 (0.15)	H	14.01	-3.82	52.7 (6.1)	9.43	2	
11253+2111	DC	6390 (117)	8.00 (0.25)	0.57 (0.15)	He	13.51	-3.63	41.2 (4.8)	9.32	2	
11337+6243	DA+DC	6660 ( 81)	8.00 (0.25)	0.59 (0.15)	H	13.41	-3.54	48.1 (5.6)	9.24	2	
11364+0802S	DA	5500 ( 45)	8.00 (0.25)	0.58 (0.15)	H	14.39	-3.88	47.3 (5.4)	9.50	2	
11364+0838	DA	6600 (101)	8.26 (0.10)	0.75 (0.07)	H	14.14	-3.71	49.5 (1.1)	9.49	1	
11401+0112W	DA	9800 (144)	8.12 (0.06)	0.67 (0.04)	H	12.43	-2.93	46.2 (1.0)	8.88	1	
11460+0514	DA	6770 (111)	7.68 (0.14)	0.42 (0.07)	H	13.25	-3.34	54.4 (1.1)	9.04	1	
11495+2353	DC	4960 ( 54)	8.00 (0.25)	0.58 (0.15)	H	14.51	-4.06	42.0 (4.7)	9.77	2	
11506+0343	DA	6120 ( 44)	8.00 (0.25)	0.59 (0.15)	H	13.66	-3.69	54.5 (6.2)	9.33	2	
11545+2422	DA	8790 (141)	8.57 (0.09)	0.96 (0.06)	H	13.57	-3.42	25.2 (0.7)	9.38	1	
11582+0004	DC	4400 ( 81)	7.82 (0.12)	0.47 (0.06)	H	15.55	-4.18	34.5 (1.8)	9.77	2	
11592+4842	DA	6080 ( 92)	8.60 (0.09)	0.98 (0.06)	H	15.04	-4.08	31.6 (0.8)	9.73	1	

Table 4—Continued

PM I	ST	$T_{\text{eff}}$ (K)	$\log g$	$M/M_{\odot}$	Comp.	$M_V$	$\log L/L_{\odot}$	$D$ (pc)	$\log \tau$	Fit <sup>a</sup>	Other name <sup>b</sup>
11598+0007	DA	9640 (805)	8.00 (0.25)	0.60 (0.15)	H	12.20	-2.89	66.9 (9.5)	8.82	2	
12019+3400	DQ	6110 ( 84)	8.00 (0.25)	0.57 (0.15)	He	14.41	-3.70	46.4 (0.8)	9.38	2	
12033+2439	DB	13810 (255)	8.08 (0.14)	0.64 (0.09)	He	11.62	-2.33	104.4 (2.7)	8.49	1	
12113+0724	DA	5270 ( 41)	8.00 (0.25)	0.58 (0.15)	H	14.57	-3.95	24.7 (2.8)	9.63	2	
12145+7822	DZ	5000 (656)	8.00 (0.25)	0.58 (0.15)	H	14.88	-4.05	32.9 (6.4)	9.75	2	
12155+4630	DA	6720 (109)	8.17 (0.12)	0.70 (0.08)	H	13.94	-3.63	42.6 (1.0)	9.37	1	
12274+3150	DA	6580 (106)	7.99 (0.13)	0.58 (0.08)	H	13.77	-3.56	37.9 (0.8)	9.24	1	
12280+3300	DC	4630 ( 75)	8.00 (0.25)	0.58 (0.15)	H	15.24	-4.18	35.7 (4.1)	9.85	2	
12370+1814	DC	9860 (256)	8.00 (0.25)	0.58 (0.15)	He	12.66	-2.87	80.0 (9.4)	8.84	2	
12377+6023	DA	5300 ( 75)	8.00 (0.25)	0.58 (0.15)	H	14.48	-3.94	46.5 (5.4)	9.61	2	
12405+1807W	DA	5420 ( 46)	8.00 (0.25)	0.58 (0.15)	H	15.14	-3.90	39.0 (4.5)	9.54	2	
12425+1311W	DC	4970 (135)	8.00 (0.25)	0.58 (0.15)	H	15.38	-4.06	44.7 (5.6)	9.77	2	
12429+6542	DA	6960 (121)	8.85 (0.14)	1.12 (0.07)	H	14.95	-4.03	33.0 (1.0)	9.63	1	
12430+2057	DB	14470 (273)	7.97 (0.20)	0.57 (0.11)	He	11.34	-2.18	136.5 (3.3)	8.35	1	
12476+0646	DQpec	5000 (—)	8.00 (0.25)	0.57 (0.15)	He	15.90	-4.06	66.8 (0.6)	9.78	2	
12541+3620	DC	4790 ( 52)	8.00 (0.25)	0.58 (0.15)	H	15.15	-4.12	26.8 (3.0)	9.82	2	
13032+7510	DC	7550 (264)	8.00 (0.25)	0.58 (0.15)	He	13.25	-3.33	42.9 (5.4)	9.14	2	
13096+6933	DA+dM	8810 (202)	8.45 (0.17)	0.88 (0.11)	H	13.36	-3.33	70.8 (2.8)	9.28	1	
13103+1404	DA	8560 (126)	8.07 (0.07)	0.64 (0.04)	H	12.86	-3.14	49.4 (1.1)	9.00	1	
13108+7236	DA	7960 (129)	8.06 (0.11)	0.63 (0.07)	H	13.12	-3.26	59.4 (2.7)	9.07	1	
13176+0621	DA	5250 ( 60)	8.00 (0.25)	0.58 (0.15)	H	14.91	-3.96	47.6 (5.4)	9.65	2	
13246+0857	DA	8170 (128)	8.02 (0.10)	0.61 (0.06)	H	12.96	-3.19	53.7 (1.2)	9.02	1	
13291+2450	DC	3990 ( 72)	8.00 (0.25)	0.58 (0.15)	H	16.72	-4.44	38.9 (4.3)	9.96	2	
13333+2450	DC	4110 (850)	8.00 (0.25)	0.58 (0.15)	H	15.96	-4.39	50.1 (28.7)	9.94	2	
13346+0943E	DA	5140 (585)	8.00 (0.25)	0.58 (0.15)	H	15.03	-4.00	40.7 (13.9)	9.70	2	

Table 4—Continued

PM I	ST	$T_{\text{eff}}$ (K)	$\log g$	$M/M_{\odot}$	Comp.	$M_V$	$\log L/L_{\odot}$	$D$ (pc)	$\log \tau$	Fit <sup>a</sup>	Other name <sup>b</sup>
13349+6945	DA	14420 (258)	7.98 (0.05)	0.60 (0.03)	H	11.31	-2.17	73.2 (2.1)	8.33	1	
13413+0500	DC	4180 ( 46)	8.00 (0.25)	0.58 (0.15)	H	16.05	-4.36	13.2 (1.5)	9.93	2	
13455+4200	DC	4600 ( 48)	7.09 (0.09)	0.19 (0.02)	H	14.20	-3.77	37.0 (1.0)	9.30	2	
13521+1053	DA	6070 (111)	8.12 (0.21)	0.67 (0.13)	H	14.30	-3.78	32.6 (0.7)	9.47	1	
13537+1656	DA	8720 (130)	7.68 (0.08)	0.43 (0.04)	H	12.24	-2.89	74.7 (1.5)	8.77	1	
14037+0644	DC	6470 (102)	8.00 (0.25)	0.57 (0.15)	He	13.45	-3.60	51.0 (5.8)	9.30	2	
14064+1608	DA	6950 (132)	8.79 (0.18)	1.09 (0.10)	H	14.85	-3.99	33.8 (0.9)	9.64	1	
14067+3130	DC	4750 ( 83)	8.00 (0.25)	0.58 (0.15)	H	15.41	-4.14	37.2 (4.3)	9.83	2	
14106+0245	DAZ	5840 ( 90)	8.00 (0.25)	0.59 (0.15)	H	14.31	-3.77	30.6 (0.6)	9.38	1	
14149+4336	DA	6670 (121)	8.65 (0.16)	1.01 (0.10)	H	14.74	-3.95	33.8 (0.9)	9.66	1	
14236+3037	DA	5300 ( 52)	8.00 (0.25)	0.58 (0.15)	H	14.92	-3.95	40.1 (4.6)	9.62	2	
14244+6246	DA	5000 ( 65)	8.00 (0.25)	0.58 (0.15)	H	15.22	-4.05	45.0 (5.1)	9.75	2	
14278+0532	DA+DC	7030 (218)	8.00 (0.25)	0.59 (0.15)	H	13.57	-3.45	69.3 (8.4)	9.18	2	
14339+1907	DA	5020 ( 62)	8.00 (0.25)	0.58 (0.15)	H	15.16	-4.04	45.8 (5.2)	9.75	2	
14407+0807	DA	5670 (100)	8.00 (0.25)	0.59 (0.15)	H	14.45	-3.83	45.4 (1.1)	9.44	1	
14456+2527	DA	5190 ( 52)	8.00 (0.25)	0.58 (0.15)	H	14.84	-3.98	17.5 (2.0)	9.67	2	
14553+5655	DA	15140 (238)	8.09 (0.05)	0.67 (0.03)	H	11.38	-2.15	48.5 (1.1)	8.34	1	
14588+1146	DC	4810 ( 71)	8.00 (0.25)	0.58 (0.15)	H	15.02	-4.12	40.9 (4.6)	9.82	2	
15010+6138	DA	5820 (173)	8.04 (0.39)	0.61 (0.23)	H	14.38	-3.80	43.8 (0.9)	9.43	1	
15164+2803	DAH	7930 (197)	8.00 (0.25)	0.59 (0.15)	H	13.32	-3.23	50.5 (6.1)	9.04	2	
15167+2910	DA	13670 (435)	7.96 (0.06)	0.59 (0.03)	H	11.38	-2.26	127.7 (2.7)	8.39	1	
15206+3903	DA	8710 (129)	8.05 (0.07)	0.62 (0.04)	H	12.75	-3.10	68.0 (1.4)	8.96	1	
15263+2936	DA	5110 (109)	8.00 (0.25)	0.58 (0.15)	H	15.43	-4.01	22.4 (2.6)	9.71	2	
15342+0218	DA	8260 (126)	8.62 (0.08)	1.00 (0.05)	H	13.89	-3.57	29.8 (0.8)	9.47	1	
15359+2125	DA	6500 (112)	8.47 (0.16)	0.89 (0.10)	H	14.54	-3.88	37.6 (0.9)	9.64	1	

Table 4—Continued

PM I	ST	$T_{\text{eff}}$ (K)	$\log g$	$M/M_{\odot}$	Comp.	$M_V$	$\log L/L_{\odot}$	$D$ (pc)	$\log \tau$	Fit <sup>a</sup>	Other name <sup>b</sup>
15494+4802	DC	6730 (125)	8.00 (0.25)	0.57 (0.15)	He	13.20	-3.54	52.0 (5.9)	9.26	2	
15589+0417	DC	6680 (117)	8.00 (0.25)	0.57 (0.15)	He	51.52	-3.55	30.3 (3.5)	9.27	2	
16053+5556	DA	6840 (113)	7.57 (0.14)	0.37 (0.06)	H	13.06	-3.27	64.8 (2.6)	8.98	1	
16096+4735	DA	13270 (264)	8.17 (0.06)	0.71 (0.04)	H	11.74	-2.44	87.4 (2.0)	8.56	1	
16142+1729	DQ <sub>pec</sub>	5230 (182)	8.00 (0.25)	0.57 (0.15)	He	15.24	-3.98	48.5 (2.9)	9.71	2	
16144+0906	DC	4810 ( 43)	8.00 (0.25)	0.58 (0.15)	H	15.44	-4.12	26.8 (3.0)	9.81	2	
16171+0530	DA+dM	15000 (345)	7.92 (0.06)	0.56 (0.03)	H	11.15	-2.07	56.1 (1.3)	8.24	1	
16222+0532	DA	7690 (179)	8.20 (0.23)	0.72 (0.15)	H	13.46	-3.41	45.5 (1.0)	9.22	1	
16264+1938	DA	6300 (102)	8.32 (0.14)	0.79 (0.09)	H	14.43	-3.83	27.6 (0.6)	9.59	1	
16265+1355	DA	6820 (101)	7.97 (0.09)	0.57 (0.05)	H	13.60	-3.48	56.9 (1.2)	9.19	1	
16286+7053	DA	4790 (918)	8.00 (0.25)	0.58 (0.15)	H	15.57	-4.12	31.7 (11.1)	9.82	2	
16325+0851	DA	5730 ( 90)	8.00 (0.25)	0.59 (0.15)	H	14.40	-3.81	13.8 (0.3)	9.42	1	
16335+5231	DA	6700 (111)	8.08 (0.14)	0.64 (0.09)	H	13.82	-3.58	51.1 (1.1)	9.29	1	
16477+2636	DZ	7230 (135)	8.00 (0.25)	0.58 (0.15)	He	13.44	-3.41	52.1 (1.2)	9.18	2	
16514+6635	DZ	7920 (142)	8.00 (0.25)	0.58 (0.15)	He	12.81	-3.25	47.8 (2.1)	9.08	2	
16546+5742	DA	9340 (141)	7.82 (0.08)	0.50 (0.05)	H	12.18	-2.85	56.9 (2.3)	8.76	1	
17027+1022	DA	5080 ( 57)	8.00 (0.25)	0.58 (0.15)	H	14.86	-4.02	37.3 (4.2)	9.72	2	
17052+0423	DA	8450 (137)	8.37 (0.10)	0.83 (0.07)	H	13.37	-3.35	34.9 (1.1)	9.25	1	
17238+0458	DA	8480 (130)	8.16 (0.09)	0.69 (0.05)	H	13.03	-3.21	56.0 (1.6)	9.07	1	
17283+0211	DA	8050 (121)	8.17 (0.08)	0.70 (0.05)	H	13.23	-3.31	40.2 (1.3)	9.13	1	
17328+0213	DA	7230 (118)	7.97 (0.12)	0.57 (0.07)	H	13.36	-3.38	49.2 (1.5)	9.13	1	
17335+7949	DC	4970 (231)	8.00 (0.25)	0.57 (0.15)	He	14.57	-4.07	29.5 (3.6)	9.78	2	
17344+4236	DA	7370 (114)	7.47 (0.12)	0.33 (0.04)	H	12.64	-3.09	61.7 (1.8)	8.87	1	
17368+3635	DA	6820 (139)	7.46 (0.26)	0.32 (0.10)	H	12.94	-3.22	82.6 (3.0)	8.95	1	
17376+0138	DA	7450 (119)	8.11 (0.11)	0.66 (0.07)	H	13.45	-3.41	45.3 (1.3)	9.18	1	



Table 4—Continued

PM I	ST	$T_{\text{eff}}$ (K)	$\log g$	$M/M_{\odot}$	Comp.	$M_V$	$\log L/L_{\odot}$	$D$ (pc)	$\log \tau$	Fit <sup>a</sup>	Other name <sup>b</sup>
17417+2401	DA	7150 (111)	8.38 (0.09)	0.84 (0.06)	H	14.02	-3.65	32.6 (1.2)	9.50	1	
17430+1701	DC	4720 (433)	8.00 (0.25)	0.58 (0.15)	H	15.54	-4.15	32.1 (5.5)	9.84	2	
17433+1434S	DC	10440 (234)	8.00 (0.25)	0.58 (0.15)	He	11.67	-2.77	35.7 (4.3)	8.77	2	
17471+2859	DC	5350 (495)	8.00 (0.25)	0.57 (0.15)	He	14.58	-3.94	37.9 (5.1)	9.66	2	
17574+1021	DZA	7880 (243)	8.00 (0.25)	0.58 (0.15)	He	13.05	-3.26	44.1 (3.3)	9.09	2	
17579+5441	DA	7680 (120)	7.97 (0.10)	0.58 (0.06)	H	13.13	-3.28	64.3 (1.3)	9.06	1	
18014+5049	DC	4990 (103)	8.00 (0.25)	0.58 (0.15)	H	14.87	-4.05	34.0 (4.0)	9.76	2	
18018+0846	DA	5930 (100)	8.00 (0.25)	0.59 (0.15)	H	14.23	-3.74	44.3 (1.7)	9.36	1	
18073+0357	DA	10410 (150)	8.09 (0.05)	0.65 (0.03)	H	12.17	-2.81	34.7 (1.5)	8.79	1	
18138+2119	DA	18200 (279)	7.95 (0.05)	0.59 (0.03)	H	10.87	-1.75	80.3 (3.1)	7.97	1	
18154+3158	DA	5020 (949)	8.00 (0.25)	0.58 (0.15)	H	15.17	-4.04	41.0 (10.8)	9.75	2	
18199+1739	DC	4820 (677)	8.00 (0.25)	0.58 (0.15)	H	15.08	-4.11	35.1 (8.0)	9.81	2	
18435+2740	DA	11060 (163)	8.10 (0.05)	0.66 (0.03)	H	12.00	-2.71	39.7 (1.3)	8.73	1	GD 381
18510+7738	DC:	5230 ( 49)	8.00 (0.25)	0.58 (0.15)	H	14.86	-3.97	30.3 (3.5)	9.65	2	
18572+2026	DA	5350 (1009)	8.00 (0.25)	0.58 (0.15)	H	13.72	-3.93	31.7 (7.9)	9.59	2	
19005+0020	DA	9580 (154)	8.14 (0.09)	0.68 (0.06)	H	12.54	-2.99	99.1 (6.7)	8.92	1	
19033+6035	DA	11550 (178)	8.07 (0.05)	0.65 (0.03)	H	11.84	-2.62	44.1 (1.3)	8.66	1	
19128+5343	DA	17870 (273)	8.32 (0.05)	0.81 (0.03)	H	11.45	-2.01	22.1 (0.9)	8.29	1	
19132+2949	DA	6110 (114)	8.00 (0.25)	0.59 (0.15)	H	14.09	-3.69	39.9 (1.2)	9.33	1	
19146+1428	DA	7050 (126)	8.68 (0.14)	1.03 (0.09)	H	14.59	-3.89	35.0 (4.7)	9.62	1	
19167+8044	DA	5040 (632)	8.00 (0.25)	0.58 (0.15)	H	14.83	-4.03	35.4 (7.2)	9.74	2	
19401+8348	DC	4840 (672)	8.00 (0.25)	0.58 (0.15)	H	15.08	-4.11	38.8 (8.9)	9.81	2	
19455+4650N	DA	4800 (398)	8.00 (0.25)	0.58 (0.15)	H	15.13	-4.12	27.5 (4.1)	9.82	2	
19493+0747	DA	9310 (134)	8.19 (0.06)	0.71 (0.04)	H	12.72	-3.07	36.2 (1.2)	8.98	1	
20062+5902	DA	13750 (263)	7.79 (0.05)	0.50 (0.03)	H	11.13	-2.15	73.8 (1.6)	8.28	1	

Table 4—Continued

PM I	ST	$T_{\text{eff}}$ (K)	$\log g$	$M/M_{\odot}$	Comp.	$M_V$	$\log L/L_{\odot}$	$D$ (pc)	$\log \tau$	Fit <sup>a</sup>	Other name <sup>b</sup>
20069+6143	DA	5540 ( 91)	8.00 (0.25)	0.58 (0.15)	H	14.57	-3.87	26.2 (0.5)	9.49	1	
20223+8333	DC	5880 (713)	8.00 (0.25)	0.57 (0.15)	He	14.04	-3.77	39.3 (5.8)	9.44	2	
20235+7001	DA	7250 (134)	8.15 (0.16)	0.69 (0.10)	H	13.61	-3.48	100.4 (5.5)	9.24	1	
20279+0523	DA	7170 (115)	7.91 (0.12)	0.54 (0.06)	H	13.31	-3.36	56.8 (1.7)	9.10	1	
20300+0729	DC	8180 (285)	8.00 (0.25)	0.58 (0.15)	He	12.79	-3.19	42.2 (5.1)	9.05	2	
20597+5517	DC	4530 ( 59)	8.00 (0.25)	0.58 (0.15)	H	15.98	-4.22	22.6 (2.5)	9.87	2	
21077+0740	DA	7080 (116)	8.06 (0.12)	0.63 (0.08)	H	13.57	-3.47	35.8 (1.2)	9.20	1	
21117+0120	DA	16390 (266)	8.10 (0.05)	0.67 (0.03)	H	11.26	-2.02	63.1 (1.8)	8.24	1	
21134+0727	DA	6510 (112)	8.26 (0.15)	0.76 (0.10)	H	14.20	-3.74	24.3 (1.6)	9.51	1	
21222+0413	DA	4970 ( 36)	8.00 (0.25)	0.58 (0.15)	H	15.07	-4.06	21.6 (2.4)	9.77	2	
21384+1856	DA	12600 (258)	7.74 (0.08)	0.47 (0.04)	H	11.22	-2.27	153.2 (3.0)	8.36	1	
21420+2252	DZ	8170 (150)	8.00 (0.25)	0.58 (0.15)	He	12.88	-3.20	38.9 (0.7)	9.05	2	
21429+0805	DA	4830 (515)	8.00 (0.25)	0.58 (0.15)	H	14.74	-4.11	25.1 (4.4)	9.81	2	
21474+1127	DA	4870 (130)	8.00 (0.25)	0.58 (0.15)	H	14.54	-4.10	49.1 (6.2)	9.80	2	
21492+0415	DA	5440 (187)	8.00 (0.25)	0.58 (0.15)	H	14.28	-3.90	26.2 (3.1)	9.53	2	
21551+4103	DZA	5950 (703)	8.00 (0.25)	0.57 (0.15)	He	14.21	-3.75	37.0 (5.8)	9.42	2	
21597+2936	DA	52250 (1135)	7.65 (0.08)	0.55 (0.03)	H	8.50	+0.36	266.8 (8.8)	6.28	1	
22105+4532	DC	5110 (597)	8.00 (0.25)	0.58 (0.15)	H	14.78	-4.01	34.4 (5.8)	9.71	2	
22118+5649	DA	16880 (287)	8.11 (0.05)	0.68 (0.03)	H	11.23	-1.97	22.3 (1.0)	8.21	1	
22133+0349	DC	4190 (323)	8.00 (0.25)	0.58 (0.15)	H	14.95	-4.36	30.4 (6.5)	9.93	2	
22198+4805	DA	6400 (101)	8.23 (0.12)	0.74 (0.08)	H	14.23	-3.75	59.5 (4.2)	9.50	1	
22230+2201N	DA	19440 (387)	8.46 (0.06)	0.91 (0.04)	H	11.55	-1.96	67.3 (1.7)	8.30	1	
22230+2201S	DA	17730 (336)	8.46 (0.06)	0.91 (0.04)	H	11.71	-2.12	74.7 (2.1)	8.42	1	
22276+1753	DAZ	6750 (151)	8.28 (0.23)	0.77 (0.15)	H	14.08	-3.68	30.5 (1.0)	9.48	1	
22299+3024	DA	10630 (155)	7.72 (0.05)	0.46 (0.03)	H	11.58	-2.57	75.6 (2.1)	8.57	1	

Table 4—Continued

PM I	ST	$T_{\text{eff}}$ (K)	$\log g$	$M/M_{\odot}$	Comp.	$M_V$	$\log L/L_{\odot}$	$D$ (pc)	$\log \tau$	Fit <sup>a</sup>	Other name <sup>b</sup>
22331+2610	DA	11810 (180)	8.05 (0.05)	0.64 (0.03)	H	11.76	-2.57	54.9 (1.7)	8.62	1	
22340+5543	DA	6830 (120)	7.55 (0.17)	0.36 (0.07)	H	13.05	-3.26	69.9 (2.6)	8.98	1	
22410+3646	DA	7350 (113)	8.20 (0.09)	0.72 (0.06)	H	13.63	-3.49	53.2 (1.7)	9.27	1	
22418+0432	DQpec	5000 (—)	8.00 (0.25)	0.57 (0.15)	He	14.83	-4.06	43.4 (4.3)	9.78	2	
22447+1513W	DA	5860 (104)	8.00 (0.25)	0.59 (0.15)	H	14.29	-3.77	66.3 (3.8)	9.38	1	
22497+3623	DA	5430 (826)	8.00 (0.25)	0.58 (0.15)	H	15.08	-3.90	43.7 (7.9)	9.54	2	
22595+5717	DA	5170 (1286)	8.00 (0.25)	0.58 (0.15)	H	15.34	-3.99	34.9 (14.3)	9.68	2	
23003+2204	DZ	6110 (177)	8.00 (0.25)	0.57 (0.15)	He	14.00	-3.70	44.9 (3.0)	9.38	2	
23027+4312	DA	8060 (119)	8.12 (0.07)	0.67 (0.05)	H	13.16	-3.28	57.0 (2.5)	9.10	1	
23056+4334	DC	4220 (1039)	8.00 (0.25)	0.58 (0.15)	H	15.86	-4.35	35.7 (39.3)	9.93	2	
23098+5506E	DA	5700 ( 86)	8.00 (0.25)	0.59 (0.15)	H	14.42	-3.82	16.2 (0.7)	9.42	1	
23160+0559	DA	15300 (256)	7.98 (0.05)	0.60 (0.03)	H	11.21	-2.07	127.9 (2.8)	8.26	1	
23162+1720	DC	4810 ( 61)	8.00 (0.25)	0.58 (0.15)	H	14.99	-4.12	35.2 (4.0)	9.81	2	
23186+5458	DZ	11720 (459)	8.00 (0.25)	0.59 (0.15)	He	11.78	-2.56	97.7 (3.2)	8.64	2	
23229+3358	DA+dM	14090 (574)	8.20 (0.06)	0.73 (0.04)	H	11.68	-2.35	100.6 (3.3)	8.51	1	
23234+7255	DA	7600 (117)	7.99 (0.09)	0.59 (0.05)	H	13.20	-3.31	46.6 (1.5)	9.08	1	
23243+2835	DA	7060 (118)	7.83 (0.13)	0.50 (0.07)	H	13.27	-3.35	38.6 (1.1)	9.07	1	
23283+3319	DA+dM	15040 (738)	8.72 (0.07)	1.06 (0.04)	H	12.45	-2.60	49.3 (1.8)	8.81	1	
23300+0120	DC	6230 (254)	8.00 (0.25)	0.57 (0.15)	He	13.82	-3.67	52.9 (10.5)	9.35	2	
23389+2101E	DA	5300 (636)	8.00 (0.25)	0.58 (0.15)	H	14.36	-3.94	40.4 (6.8)	9.61	2	
23390+5316	DA	6290 (105)	7.66 (0.16)	0.41 (0.08)	H	13.54	-3.46	48.8 (1.9)	9.11	1	
23462+1158	DC	5220 (285)	8.00 (0.25)	0.57 (0.15)	He	14.77	-3.98	34.0 (4.3)	9.71	2	
23475+0304	DC	4900 ( 47)	8.00 (0.25)	0.58 (0.15)	H	15.12	-4.08	22.7 (2.6)	9.79	2	
23478+0223	DA	5120 ( 48)	8.00 (0.25)	0.58 (0.15)	H	14.87	-4.01	42.7 (4.9)	9.71	2	
23489+4300	DC:	4810 ( 63)	8.00 (0.25)	0.58 (0.15)	H	15.12	-4.11	36.2 (4.1)	9.81	2	

<sup>a</sup>Fit: (1) spectroscopic, (2) photometric.<sup>b</sup>SDSS name unless noted otherwise.

Table 5. Atmospheric Parameters of Northern White Dwarfs within 40 pc of the Sun

PM I	ST	$T_{\text{eff}}$ (K)	$\log g$	$M/M_{\odot}$	Comp.	$M_V$	$\log L/L_{\odot}$	$D$ (pc)	$\pi$ (mas)	$\log \tau$	Fit <sup>a</sup>	WDname	Notes
00023+6357*	DC	4630 (563)	8.00 (0.25)	0.58 (0.15)	H	14.77	-4.18	26.7 (7.2)		9.85	2		
00051+7313	DB	14490 (236)	8.34 (0.12)	0.80 (0.08)	He	11.90	-2.40	34.7 (5.8)	28.8 ( 4.7)	8.59	1	0002+729	
00073+1230	DC	5090 ( 65)	8.00 (0.25)	0.57 (0.15)	He	14.62	-4.02	21.0 (3.4)		9.76	2	0004+122	
00074+3403*	DC:	5830 (113)	8.00 (0.25)	0.57 (0.15)	He	14.23	-3.79	42.0 (7.3)		9.46	2		
00079+3947*	DC	4890 (453)	8.00 (0.25)	0.58 (0.15)	H	15.16	-4.09	20.2 (4.2)		9.79	2		
00113+4240	DA	7140 (106)	8.24 (0.07)	0.75 (0.05)	H	13.80	-3.56	19.3 (0.8)		9.35	1	0008+424	
00122+5025	DAP	6420 ( 99)	8.15 (0.10)	0.68 (0.06)	H	14.09	-3.69	11.0 (0.4)	90.6 ( 3.7)	9.42	1	0009+501	
00136+0019	DA	9520 (137)	7.97 (0.05)	0.58 (0.03)	H	12.31	-2.90	30.4 (4.5)	32.9 ( 4.8)	8.82	1	0011+000	
	DB	18110 (288)	8.09 (0.06)	0.65 (0.04)	He	10.99	-1.86	33.3 (11.6)	30.0 ( 9.4)	8.12	1	0017+136	
00217+2640*	DC	5160 (645)	8.00 (0.25)	0.58 (0.15)	H	14.67	-3.99	35.2 (8.5)		9.69	2		
00222+4236	DA	5590 (782)	8.00 (0.25)	0.58 (0.15)	H	14.00	-3.85	12.9 (3.0)		9.46	2	0019+423	
00276+0542*	DA	5520 (855)	8.00 (0.25)	0.58 (0.15)	H	14.65	-3.87	21.5 (5.1)		9.49	2		
00355+0153	DA	10830 (157)	8.71 (0.05)	1.05 (0.03)	H	13.10	-3.16	32.9 (4.4)	30.4 ( 4.0)	9.24	1	0033+016	
	DA	8850 (130)	8.45 (0.06)	0.89 (0.04)	H	13.35	-3.33	33.9 (2.0)		9.28	1	0033+771	
00413+5550E	DC	8860 (2029)	8.00 (0.25)	0.58 (0.15)	He	12.34	-3.05	20.9 (5.4)		8.96	2	0038+555	
00491+0523	DZ	6110 (144)	8.16 (0.01)	0.67 (0.01)	He	13.88	-3.80	4.3 (0.0)	232.5 ( 1.9)	9.55	2	0046+051	
00547+2256	DA	9540 (142)	8.55 (0.06)	0.95 (0.04)	H	13.25	-3.26	37.1 (1.6)		9.28	1	0052+226	
00559+5948*	DC:	5840 (1061)	8.00 (0.25)	0.57 (0.15)	He	13.32	-3.78	26.2 (6.5)		9.45	2		
01038+0504	DA	8480 (122)	8.17 (0.05)	0.70 (0.04)	H	13.04	-3.22	21.3 (1.8)	46.9 ( 3.8)	9.08	1	0101+048	1
01049+2119	DA	4960 (600)	8.00 (0.25)	0.58 (0.15)	H	15.04	-4.06	40.0 (10.2)		9.77	2	0102+210A	
01049+2120	DC	4890 (497)	8.00 (0.25)	0.58 (0.15)	H	15.27	-4.09	38.8 (9.1)		9.79	2	0102+210B	
01088+7600*	DA	6430 (128)	8.52 (0.22)	0.93 (0.14)	H	14.66	-3.93	38.0 (1.9)		9.66	1		
01107+2758	DA	6260 ( 72)	8.00 (0.25)	0.59 (0.15)	H	13.06	-3.65	26.6 (4.4)		9.30	2	0108+277	
01180+1610	DQ	9050 (250)	8.16 (0.07)	0.68 (0.04)	He	12.91	-3.11	15.4 (0.8)	64.9 ( 3.0)	9.02	2	0115+159	
01243+4023	DA	5300 (112)	7.91 (0.28)	0.53 (0.16)	H	14.92	-3.90	31.2 (5.6)	32.1 ( 5.5)	9.50	2	0121+401	

Table 5—Continued

PM I	ST	$T_{\text{eff}}$ (K)	$\log g$	$M/M_{\odot}$	Comp.	$M_V$	$\log L/L_{\odot}$	$D$ (pc)	$\pi$ (mas)	$\log \tau$	Fit <sup>a</sup>	WDname	Notes
01278+7328*	DA	7400 (117)	8.20 (0.10)	0.72 (0.07)	H	13.61	-3.48	25.1 (1.9)		9.26	1		
01294+1023	DA	8550 (122)	7.61 (0.05)	0.39 (0.02)	H	12.22	-2.89	35.2 (3.9)	28.4 ( 3.1)	8.76	1	0126+101	1
	DA	7970 (114)	8.19 (0.05)	0.72 (0.03)	H	13.31	-3.34	21.2 (0.8)		9.17	1	0136+152	
01414+8334	DA	19420 (300)	8.07 (0.05)	0.66 (0.03)	H	10.93	-1.70	27.8 (1.3)		7.97	1	0134+833	
01451+3132	DA	9270 (133)	8.12 (0.05)	0.67 (0.03)	H	12.63	-3.03	35.5 (5.5)	28.2 ( 4.3)	8.94	1	0142+312	
01457+2918*	DC	4740 (879)	8.00 (0.25)	0.58 (0.15)	H	15.04	-4.14	39.6 (18.5)		9.83	2		
01466+2154	DA	9210 (132)	8.32 (0.05)	0.80 (0.03)	H	12.97	-3.17	26.1 (1.2)		9.08	1	0143+216	
	DA	12910 (219)	8.11 (0.05)	0.67 (0.03)	H	11.69	-2.45	34.3 (1.6)		8.55	1	0145+234	
01486+3615*	DA	6480 (119)	8.68 (0.19)	1.03 (0.11)	H	14.91	-4.03	24.0 (1.2)		9.68	1		
01518+6425	DA	8880 (126)	8.20 (0.05)	0.72 (0.03)	H	12.92	-3.16	16.2 (0.9)		9.04	1	0148+641	
	DA	13910 (279)	8.05 (0.05)	0.64 (0.03)	H	11.48	-2.28	15.9 (0.9)	63.0 ( 3.7)	8.43	1	0148+467	
01528+2553	DA	7530 (124)	7.98 (0.12)	0.58 (0.07)	H	13.22	-3.32	30.4 (1.3)		9.09	1	0150+256	
01596+1548	DC	7760 (117)	8.00 (0.25)	0.58 (0.15)	He	12.87	-3.29	38.3 (6.3)		9.11	2	0156+155	
02062+1836*	DC	4230 (530)	8.00 (0.25)	0.58 (0.15)	H	15.92	-4.34	31.0 (10.6)		9.92	2		
02087+2514	DA	21120 (316)	7.91 (0.05)	0.58 (0.02)	H	10.54	-1.46	33.3 (2.8)	30.0 ( 2.5)	7.63	1	0205+250	
02113+3955	DAZ	7250 (107)	7.82 (0.08)	0.49 (0.04)	H	13.16	-3.30	16.7 (1.0)	59.8 ( 3.5)	9.04	1	0208+396	
02118+7119*	DC	5150 ( 52)	8.00 (0.25)	0.58 (0.15)	H	14.75	-4.00	28.0 (4.6)		9.69	2		
02162+3951	DA	9230 (133)	8.38 (0.05)	0.84 (0.03)	H	13.06	-3.20	19.6 (0.9)		9.14	1	0213+396	
02169+4258	DA	5410 (127)	8.03 (0.13)	0.60 (0.08)	H	14.80	-3.92	19.9 (1.8)	50.2 ( 4.1)	9.58	2	0213+427	
02199+3520*	DA	5580 (791)	8.00 (0.25)	0.58 (0.15)	H	14.28	-3.85	43.1 (11.6)		9.47	2		
02230+5544*	DA	6980 (110)	8.40 (0.10)	0.85 (0.07)	H	14.14	-3.70	35.3 (1.8)		9.54	1		
02238+2055*	DC	4300 ( 91)	8.00 (0.25)	0.58 (0.15)	H	16.02	-4.31	33.5 (5.4)		9.91	2		
02258+4228W	DA	5410 (177)	8.00 (0.25)	0.58 (0.15)	H	14.70	-3.91	38.1 (1.7)		9.55	1	0222+422.2	
02265+6459	DC	4530 (264)	8.00 (0.04)	0.58 (0.03)	H	15.78	-4.22	31.8 (4.4)	31.4 ( 0.8)	9.87	2	0222+648	
02302+0515	DA	19640 (296)	7.90 (0.05)	0.57 (0.03)	H	10.65	-1.58	26.9 (1.1)		7.75	1	0227+050	

Table 5—Continued

PM I	ST	$T_{\text{eff}}$ (K)	$\log g$	$M/M_{\odot}$	Comp.	$M_V$	$\log L/L_{\odot}$	$D$ (pc)	$\pi$ (mas)	$\log \tau$	Fit <sup>a</sup>	WDname	Notes
02316+2709	DA	4850 (107)	8.00 (0.25)	0.58 (0.15)	H	14.92	-4.10	26.2 (4.4)		9.80	2	0228+269	
02334+2125*	DC	4730 ( 52)	8.00 (0.25)	0.58 (0.15)	H	15.15	-4.15	26.3 (4.2)		9.83	2		
02355+5715	DA	13790 (314)	8.03 (0.05)	0.63 (0.03)	H	11.47	-2.28	28.4 (1.7)		8.43	1	0231+570	
02363+5244	DA	17760 (275)	8.38 (0.05)	0.85 (0.03)	H	11.57	-2.06	30.5 (1.5)		8.35	1	0232+525	
02379+1638*	DC	5150 (607)	8.00 (0.25)	0.57 (0.15)	He	14.63	-4.00	30.7 (7.1)		9.74	2		
02393+2609	DA	5590 ( 60)	8.00 (0.25)	0.58 (0.15)	H	14.48	-3.85	21.1 (3.4)		9.47	2	0236+259	
02421+1112	DAH	8510 (196)	8.00 (0.25)	0.60 (0.15)	H	12.68	-3.11	45.9 (8.0)		8.96	2	0239+109	
02486+5423	DAZ	5040 (100)	8.16 (0.05)	0.68 (0.03)	H	15.28	-4.12	10.4 (1.8)	96.6 ( 3.1)	9.85	2	0245+541	
02497+3307*	DA	5890 (119)	8.31 (0.26)	0.79 (0.17)	H	14.72	-3.94	31.6 (1.0)		9.67	1		
02562+4954*	DA	6050 (101)	8.00 (0.25)	0.59 (0.15)	H	14.14	-3.71	41.0 (1.9)		9.34	1		
02599+0811	DAP	6740 (480)	7.96 (0.15)	0.57 (0.09)	H	13.25	-3.50	27.9 (2.9)	35.9 ( 3.5)	9.20	2	0257+080	
03053+2603*	DA	5190 (686)	8.00 (0.25)	0.58 (0.15)	H	14.64	-3.98	45.0 (12.5)		9.67	2		
03062+6222	DA	10990 (162)	8.11 (0.05)	0.67 (0.03)	H	12.03	-2.73	38.8 (1.8)		8.74	1	0302+621	
03109+6634*	DC	4620 (662)	8.00 (0.25)	0.58 (0.15)	H	15.31	-4.19	36.4 (12.4)		9.86	2		
03196+3630*	DZ	5770 (234)	8.00 (0.25)	0.57 (0.15)	He	14.26	-3.80	29.9 (2.1)		9.48	2		
03203+2333*	DC	4510 (447)	8.00 (0.25)	0.58 (0.15)	H	15.52	-4.23	29.3 (7.5)		9.88	2		
03302+7401	DC	5170 (381)	7.89 (0.26)	0.51 (0.14)	He	14.79	-3.94	40.0 (7.5)	25.0 ( 3.8)	9.63	2	0324+738	
03433+1958*	DA	7150 (107)	8.47 (0.08)	0.89 (0.05)	H	14.16	-3.71	22.8 (1.2)		9.55	1		
03445+1826	DQ	6420 (108)	7.93 (0.09)	0.53 (0.05)	He	13.80	-3.58	19.0 (1.1)	52.6 ( 3.0)	9.26	2	0341+182	
03467+2456	DC	2970 ( 37)	7.66 (0.26)	0.39 (0.12)	H	16.84	-4.79	27.8 (4.0)	36.0 ( 5.0)	9.96	2	0343+247	
03471+0138	DQ	4850 ( 76)	8.00 (0.25)	0.57 (0.15)	He	15.25	-4.11	17.9 (0.4)		9.80	2	0344+014	
03473+4358*	DA	13650 (316)	7.99 (0.05)	0.60 (0.03)	H	11.42	-2.27	33.9 (1.9)		8.41	1		
03553+0947	DA	14550 (379)	8.31 (0.05)	0.81 (0.03)	H	11.80	-2.36	35.2 (1.3)		8.55	1	0352+096	
03582+4628	DA+dM	8230 (171)	7.75 (0.11)	0.46 (0.05)	H	12.57	-3.04	38.4 (1.5)		8.87	1	0354+463	2
04004+0814	DA	5450 ( 62)	8.03 (0.10)	0.60 (0.06)	H	14.58	-3.91	17.8 (1.4)	56.1 ( 3.7)	9.56	2	0357+081	

Table 5—Continued

PM I	ST	$T_{\text{eff}}$ (K)	$\log g$	$M/M_{\odot}$	Comp.	$M_V$	$\log L/L_{\odot}$	$D$ (pc)	$\pi$ (mas)	$\log \tau$	Fit <sup>a</sup>	WDname	Notes
04010+5131W*	DC	5220 (342)	8.00 (0.25)	0.58 (0.15)	H	14.57	-3.97	30.8 (5.9)		9.66	2		
04037+1459*	DA	14710 (344)	8.41 (0.05)	0.87 (0.03)	H	11.95	-2.41	40.7 (1.4)		8.61	1		
04045+2508	DA	12610 (203)	8.03 (0.05)	0.63 (0.03)	H	11.61	-2.44	27.0 (1.6)	37.0 ( 2.2)	8.53	1	0401+250	
04101+1802	DA	14260 (246)	7.92 (0.05)	0.57 (0.03)	H	11.25	-2.16	38.2 (9.8)	26.2 ( 6.3)	8.31	1	0407+179	
04102+1954	DC	4910 (760)	8.00 (0.25)	0.58 (0.15)	H	14.89	-4.08	33.2 (10.5)		9.79	2	0407+197	
04180+4211*	DA	4580 (374)	8.00 (0.25)	0.58 (0.15)	H	15.17	-4.20	23.8 (5.1)		9.86	2		
04214+4607*	DA	7790 (123)	7.87 (0.11)	0.52 (0.06)	H	12.94	-3.19	30.5 (1.7)		8.98	1		
04258+1211	DC	5900 ( 77)	8.00 (0.07)	0.57 (0.04)	He	14.70	-3.77	17.4 (4.5)	57.6 ( 2.5)	9.43	2	0423+120	
04259+4614*	DC	4520 (504)	8.00 (0.25)	0.58 (0.15)	H	15.44	-4.22	32.5 (9.6)		9.88	2		
04263+0432	DA	4760 (552)	8.15 (0.12)	0.67 (0.08)	H	15.33	-4.22	20.7 (4.7)	48.2 ( 3.9)	9.91	2	0423+044	
04263+4820*	DA+DC	4240 (325)	8.00 (0.25)	0.58 (0.15)	H	14.23	-4.34	29.0 (6.5)		9.92	2		1
04312+5858	DC	7130 (182)	8.15 (0.01)	0.67 (0.00)	He	13.71	-3.52	5.5 (1.9)	180.7 ( 0.8)	9.29	2	0426+588	1
	DA+dM	17620 (427)	8.02 (0.06)	0.63 (0.03)	H	11.02	-1.84	50.0 (16.5)	20.0 ( 6.0)	8.08	1	0429+176	2
04334+0414*	DA	5220 (596)	8.00 (0.25)	0.58 (0.15)	H	14.62	-3.97	26.5 (6.0)		9.66	2		
04343+3054*	DC:	4670 (577)	8.00 (0.25)	0.58 (0.15)	H	15.28	-4.17	36.2 (10.4)		9.85	2		
04367+2709	DA	5920 (112)	8.87 (0.19)	1.13 (0.10)	H	15.68	-4.34	16.6 (0.8)	60.2 ( 2.9)	9.75	1	0433+270	
04372+4524*	DA	6570 (112)	8.12 (0.15)	0.66 (0.10)	H	13.96	-3.63	40.4 (2.0)		9.36	1		
04404+0923	DA	6310 ( 97)	8.46 (0.11)	0.89 (0.07)	H	14.65	-3.92	29.2 (1.3)		9.66	1	0437+093	
04439+5106	DA	8630 (125)	8.13 (0.06)	0.68 (0.04)	H	12.92	-3.16	46.3 (11.9)	21.6 ( 5.2)	9.03	1	0440+510	
04523+2519*	DAH	11500 (2655)	8.00 (0.25)	0.60 (0.14)	H	11.66	-2.58	43.7 (9.2)		8.62	2		
04558+3840*	DA	5020 (613)	8.00 (0.25)	0.58 (0.15)	H	14.82	-4.04	32.5 (8.2)		9.75	2		
04573+4155	DA	14290 (255)	7.82 (0.05)	0.51 (0.03)	H	11.10	-2.10	43.5 (5.0)	23.0 ( 2.6)	8.24	1	0453+418	
04586+6209*	DA+dM	10960 (704)	8.88 (0.13)	1.14 (0.07)	H	13.40	-3.27	21.6 (1.2)		9.30	1		
05062+1448	DBA	15640 (258)	8.09 (0.07)	0.64 (0.04)	He	11.33	-2.11	28.5 (1.4)		8.33	1	0503+147	
05140+0800	DA	6620 (106)	8.33 (0.12)	0.80 (0.08)	H	14.23	-3.75	20.3 (0.6)	49.3 ( 1.5)	9.54	1	0511+079	



Table 5—Continued

PM I	ST	$T_{\text{eff}}$ (K)	$\log g$	$M/M_{\odot}$	Comp.	$M_V$	$\log L/L_{\odot}$	$D$ (pc)	$\pi$ (mas)	$\log \tau$	Fit <sup>a</sup>	WDname	Notes
05158+2839*	DAH	6640 (104)	8.00 (0.25)	0.59 (0.15)	H	13.39	-3.55	35.0 (5.8)		9.24	2		
05269+4435*	DC	4700 (632)	8.00 (0.25)	0.58 (0.15)	H	15.14	-4.16	37.0 (11.8)		9.84	2		
05298+5239	DA	22550 (343)	9.16 (0.05)	1.26 (0.01)	H	12.67	-2.26	40.2 (2.3)		8.70	1	0525+526	
05353+5715*	DC	5210 (462)	8.00 (0.25)	0.57 (0.15)	He	14.66	-3.98	39.1 (7.2)		9.72	2		
05363+4129	DA	7600 (109)	7.97 (0.05)	0.57 (0.03)	H	13.16	-3.29	20.6 (0.9)		9.07	1	0532+414	
05431+3637*	DAZ	6540 (101)	7.84 (0.11)	0.50 (0.06)	H	13.59	-3.48	27.2 (1.5)		9.16	1		
05449+2602*	DQ?	4460 (393)	8.00 (0.25)	0.57 (0.15)	He	15.27	-4.26	22.4 (4.5)		9.86	2		
05462+1115*	DC:	4290 (137)	8.00 (0.25)	0.57 (0.15)	He	15.84	-4.32	27.5 (4.6)		9.88	2		
05557+4650S	DA	5260 (302)	8.00 (0.25)	0.58 (0.15)	H	14.68	-3.96	30.0 (5.6)		9.64	2	0551+468	
05564+0521	DAH	5790 (134)	8.22 (0.04)	0.73 (0.03)	H	14.78	-3.92	8.0 (2.0)	125.1 ( 3.6)	9.63	2	0553+053	
06025+1553	DA	7110 (115)	8.48 (0.11)	0.90 (0.07)	H	14.20	-3.72	33.1 (1.6)		9.56	1	0559+158	
06026+0904*	DA	5920 (132)	7.75 (0.29)	0.45 (0.14)	H	13.91	-3.61	40.4 (2.0)		9.21	1		
06072+7332	DA	7480 (259)	8.67 (0.07)	1.02 (0.04)	H	14.41	-3.77	31.4 (4.7)	31.8 ( 1.9)	9.57	2	0600+735	
06137+2050*	DA+DQ	5950 (668)	8.00 (0.25)	0.59 (0.15)	H	13.81	-3.74	40.0 (6.0)		9.36	2	GD 73	1, 3
06153+1743	DA	26100 (389)	7.98 (0.05)	0.63 (0.03)	H	10.25	-1.13	36.1 (2.9)	27.7 ( 2.2)	7.23	1	0612+177	
06207+0645	DA	5990 (126)	8.52 (0.27)	0.93 (0.17)	H	14.98	-4.05	22.6 (2.1)	44.2 ( 4.2)	9.73	1	0618+067	
06324+2230*	DA	5620 (1471)	8.00 (0.25)	0.58 (0.15)	H	14.72	-3.84	37.4 (13.9)		9.45	2		
06364+4054	DA	7860 (120)	8.73 (0.08)	1.06 (0.04)	H	14.27	-3.73	29.7 (1.4)		9.54	1	0632+409	
06412+4744	DAP	14060 (3216)	8.00 (0.25)	0.61 (0.14)	H	11.39	-2.23	48.1 (10.4)		8.38	2	0637+477	
06445+2731*	DA	7020 (119)	8.69 (0.13)	1.04 (0.08)	H	14.63	-3.90	30.7 (1.1)		9.63	1		
06473+0231	DA	7080 (103)	8.53 (0.06)	0.94 (0.04)	H	14.31	-3.77	18.5 (1.9)	54.2 ( 5.5)	9.58	1	0644+025	
06476+3730	DA	22140 (337)	8.09 (0.05)	0.68 (0.03)	H	10.73	-1.49	15.1 (0.5)	66.3 ( 2.1)	7.74	1	0644+375	
06492+1519*	DC	5050 (392)	8.00 (0.25)	0.57 (0.15)	He	14.85	-4.04	34.9 (8.8)		9.76	2		
06494+7521*	DA	5450 (1044)	8.00 (0.25)	0.58 (0.15)	H	14.02	-3.89	34.4 (10.2)		9.53	2		
06506+1657*	DA	5240 (661)	8.00 (0.25)	0.58 (0.15)	H	14.60	-3.96	34.2 (8.9)		9.65	2		

Table 5—Continued

PM I	ST	$T_{\text{eff}}$ (K)	$\log g$	$M/M_{\odot}$	Comp.	$M_V$	$\log L/L_{\odot}$	$D$ (pc)	$\pi$ (mas)	$\log \tau$	Fit <sup>a</sup>	WDname	Notes
06534+6403	DA	6050 ( 98)	8.60 (0.15)	0.98 (0.09)	H	15.07	-4.09	33.3 (5.9)	30.0 ( 5.2)	9.73	1	0648+641	
06538+6355*	DA	6220 (137)	8.44 (0.23)	0.87 (0.15)	H	14.67	-3.93	20.8 (1.1)		9.67	1		
06573+0241	DC	8100 (893)	8.22 (0.21)	0.72 (0.13)	He	13.24	-3.34	38.5 (7.1)	26.0 ( 3.7)	9.18	2	0654+027	
07008+3157	DA	4880 ( 96)	8.02 (0.03)	0.59 (0.02)	H	14.67	-4.10	18.7 (2.0)	53.5 ( 0.9)	9.81	2	0657+320	
07087+2044*	DA	5810 (117)	8.00 (0.25)	0.59 (0.15)	H	14.33	-3.78	35.2 (1.8)		9.39	1		
07102+3740N	DQ	6060 (562)	7.82 (0.10)	0.47 (0.05)	He	13.43	-3.63	24.3 (1.4)	41.2 ( 2.4)	9.26	2	0706+377	
07180+4547	DC	8890 (158)	8.00 (0.25)	0.58 (0.15)	He	12.17	-3.05	34.1 (5.7)		8.95	2	0714+458	
07181+1229	DA	7130 (111)	7.98 (0.10)	0.58 (0.06)	H	13.43	-3.41	33.0 (1.4)		9.15	1	0715+125	
07270+1434*	DA	5680 ( 89)	8.00 (0.25)	0.59 (0.15)	H	14.44	-3.82	30.5 (0.9)		9.43	1		
07307+4810A	DA	4910 (105)	7.86 (0.02)	0.50 (0.01)	H	14.51	-4.01	11.1 (1.7)	90.0 ( 1.0)	9.66	2	0727+482A	
07307+4810B	DA	4940 ( 85)	8.12 (0.02)	0.65 (0.01)	H	15.33	-4.13	11.1 (1.7)	90.0 ( 1.0)	9.86	2	0727+482B	
07335+6409	DAP	5170 (141)	8.00 (0.25)	0.58 (0.15)	H	14.53	-3.99	18.6 (3.0)		9.68	2	0728+642	
07344+4841	DA	14870 (330)	8.58 (0.05)	0.98 (0.03)	H	12.21	-2.51	35.0 (1.8)		8.72	1	0730+487	
	DQZ	7870 (433)	8.08 (0.00)	0.63 (0.00)	He	13.21	-3.31	3.5 (0.0)	285.0 ( 0.8)	9.13	2	0736+053	
07451+2627*	DC	3620 (144)	8.00 (0.25)	0.58 (0.15)	H	16.68	-4.61	32.3 (5.4)		10.00	2		
07474+4408W	DA	15120 (336)	8.47 (0.05)	0.91 (0.03)	H	12.00	-2.40	37.5 (1.3)		8.62	1	0743+442	
07475+1107*	DA	8060 (126)	8.82 (0.08)	1.11 (0.05)	H	14.35	-3.75	29.3 (1.2)		9.53	1		
07502+0711N	DC	4370 ( 92)	7.83 (0.02)	0.48 (0.01)	H	15.65	-4.20	18.3 (1.7)	54.7 ( 0.7)	9.80	2	0747+073.1	
07502+0711S	DC	4390 ( 92)	7.84 (0.02)	0.48 (0.01)	H	15.44	-4.19	18.3 (1.7)	54.7 ( 0.7)	9.80	2	0747+073.2	
07532+4230	DC	4620 (110)	7.87 (0.05)	0.50 (0.03)	H	15.06	-4.12	27.8 (1.8)	36.0 ( 1.0)	9.76	2	0749+426	
07534+5229	DC	6950 (148)	8.00 (0.25)	0.58 (0.15)	He	13.00	-3.48	27.5 (4.5)		9.22	2	0749+526	
07554+3621	DA	7780 (115)	8.03 (0.07)	0.61 (0.04)	H	13.17	-3.29	33.9 (5.1)	29.5 ( 4.3)	9.08	1	0752+365	
07560+5741	DC	9290 (171)	7.90 (0.22)	0.52 (0.12)	He	12.23	-2.92	35.2 (5.1)	28.4 ( 3.8)	8.83	2	0751+578	
07565+4139	DA	6750 (117)	8.05 (0.15)	0.62 (0.09)	H	13.74	-3.55	39.9 (1.2)		9.26	1	0753+417	
07599+4335	DC	6910 (307)	8.00 (0.25)	0.58 (0.15)	He	13.44	-3.49	32.5 (5.6)		9.23	2	0756+437	

Table 5—Continued

PM I	ST	$T_{\text{eff}}$ (K)	$\log g$	$M/M_{\odot}$	Comp.	$M_V$	$\log L/L_{\odot}$	$D$ (pc)	$\pi$ (mas)	$\log \tau$	Fit <sup>a</sup>	WDname	Notes
08015+4852*	DA	5280 (365)	8.00 (0.25)	0.58 (0.15)	H	14.76	-3.95	36.1 (7.4)		9.63	2		
08054+0735*	DA:	5370 ( 45)	8.00 (0.25)	0.58 (0.15)	H	14.42	-3.92	37.0 (6.0)		9.58	2		
08056+3832	DZ	10200 (206)	8.14 (0.19)	0.67 (0.12)	He	12.46	-2.89	41.7 (6.8)	24.0 ( 3.0)	8.87	2	0802+386	
08059+3833	DA	5160 ( 69)	8.23 (0.03)	0.73 (0.02)	H	14.98	-4.13	20.8 (1.8)	48.0 ( 1.0)	9.86	2	0802+387	
08068+2215*	DA	5920 (116)	8.97 (0.19)	1.18 (0.08)	H	15.88	-4.41	26.2 (1.1)		9.73	1		
08091+3527	DA	8950 (128)	8.37 (0.05)	0.83 (0.03)	H	13.15	-3.25	24.5 (0.8)		9.17	1	0805+356	
08097+2920	DA	6900 ( 99)	8.00 (0.05)	0.59 (0.03)	H	13.58	-3.48	32.7 (1.0)		9.19	1	0806+294	
08126+1737*	DA	16400 (241)	8.09 (0.04)	0.67 (0.03)	H	11.25	-2.02	32.7 (1.4)		8.24	1		
08141+4845	DC	6640 (142)	8.00 (0.25)	0.57 (0.15)	He	13.66	-3.56	18.0 (2.9)		9.28	2	0810+489	
08152+1633*	DC:	4710 ( 80)	8.00 (0.25)	0.58 (0.15)	H	15.23	-4.15	40.4 (6.5)		9.84	2		
08167+2137	DA	6250 (116)	8.10 (0.22)	0.65 (0.14)	H	14.13	-3.71	37.0 (1.1)		9.40	1	0813+217	
08200+3834W	DA	7750 (154)	8.27 (0.14)	0.77 (0.09)	H	7.00	-3.44	39.7 (5.8)	25.2 ( 2.5)	9.28	2	0816+387	
08223+2023*	DC	7240 (150)	8.00 (0.25)	0.58 (0.15)	He	13.12	-3.41	35.6 (5.8)		9.18	2		
08293+2539*	DC	4010 ( 95)	8.00 (0.25)	0.58 (0.15)	H	16.58	-4.43	32.4 (5.2)		9.95	2		
08306+3241	DA	7270 (106)	8.38 (0.06)	0.83 (0.04)	H	13.94	-3.62	22.3 (1.9)	44.9 ( 3.8)	9.47	1	0827+328	
08429+2409*	DA	5900 (120)	8.00 (0.25)	0.59 (0.15)	H	14.26	-3.76	38.7 (1.1)		9.37	1	0840+243	
08454+3801	DA	7940 (114)	8.00 (0.05)	0.59 (0.03)	H	13.04	-3.23	38.8 (1.1)		9.04	1	0842+382	
08467+3538	DZ	8580 (126)	8.00 (0.25)	0.58 (0.15)	He	12.73	-3.11	25.5 (0.5)		8.99	2	0843+358	
08491+3429	DA	7530 (111)	8.08 (0.07)	0.64 (0.04)	H	13.36	-3.37	28.7 (0.9)		9.15	1	0846+346	
08516+1624*	DC	5580 ( 78)	8.00 (0.25)	0.57 (0.15)	He	14.19	-3.86	29.0 (4.6)		9.56	2		
08558+3700*	DA	5620 ( 59)	8.00 (0.25)	0.58 (0.15)	H	14.17	-3.84	43.4 (7.1)		9.45	2		
	DA+dM	8150 (169)	7.76 (0.10)	0.47 (0.05)	H	12.62	-3.06	42.1 (2.2)		8.88	1	0852+630	2
08592+3257	DQ	10650 (166)	8.82 (0.08)	1.10 (0.04)	He	13.52	-3.28	20.5 (1.4)	48.8 ( 3.4)	9.29	2	0856+331	
09018+3607	DA	12080 (179)	8.16 (0.05)	0.70 (0.03)	H	11.87	-2.59	33.6 (1.1)		8.66	1	0858+363	
09021+2010*	DQ	5010 ( 34)	8.00 (0.25)	0.57 (0.15)	He	15.98	-4.05	37.6 (0.9)		9.78	2		

Table 5—Continued

PM I	ST	$T_{\text{eff}}$ (K)	$\log g$	$M/M_{\odot}$	Comp.	$M_V$	$\log L/L_{\odot}$	$D$ (pc)	$\pi$ (mas)	$\log \tau$	Fit <sup>a</sup>	WDname	Notes
09026+1535*	DC	4670 ( 36)	8.00 (0.25)	0.58 (0.15)	H	15.38	-4.17	31.6 (5.0)		9.85	2		
09027+3120*	DA	9930 (143)	8.23 (0.05)	0.75 (0.03)	H	12.56	-2.98	34.1 (1.1)		8.94	1		
09055+7314	DC	5120 (609)	8.00 (0.25)	0.58 (0.15)	H	14.76	-4.01	25.9 (6.0)		9.71	2	0900+734	
09106+2156*	DA	5640 ( 90)	8.00 (0.25)	0.59 (0.15)	H	14.47	-3.83	37.5 (1.0)		9.44	1	0907+221	
09122+2538*	DA	6720 (105)	8.32 (0.11)	0.80 (0.07)	H	14.17	-3.72	32.5 (1.1)		9.52	1		
09127+1951	DA	5040 ( 45)	8.00 (0.25)	0.58 (0.15)	H	14.75	-4.03	34.0 (5.4)		9.74	2	0909+200	
09127+2251*	DC	4960 ( 69)	8.00 (0.25)	0.58 (0.15)	H	14.76	-4.06	43.9 (7.0)		9.77	2		
09159+5325	DCP	7370 (120)	8.42 (0.03)	0.85 (0.02)	He	14.05	-3.63	10.3 (0.8)	97.0 ( 1.9)	9.48	2	0912+536	
09160+1011	DQ	7930 (180)	8.00 (0.25)	0.58 (0.15)	He	13.05	-3.25	35.0 (0.9)		9.08	2	0913+103	
09166+4359	DA	8590 (123)	8.03 (0.05)	0.62 (0.03)	H	12.80	-3.12	28.9 (3.4)	34.6 ( 4.0)	8.97	1	0913+442	
09229+0103	DAZ	6010 (111)	8.00 (0.25)	0.59 (0.15)	H	14.17	-3.72	31.2 (1.0)		9.35	1	0920+012	
09245+3120*	DC	4800 ( 71)	8.00 (0.25)	0.58 (0.15)	H	14.66	-4.12	38.8 (6.1)		9.82	2		
09251+0509	DA	10780 (155)	8.16 (0.05)	0.70 (0.03)	H	12.16	-2.79	40.8 (1.2)		8.79	1	0922+053	
09286+1841*	DA	7730 (116)	8.45 (0.07)	0.88 (0.05)	H	13.83	-3.56	35.9 (1.2)		9.45	1		
09336+2911	DA	8290 (121)	8.52 (0.06)	0.93 (0.04)	H	13.70	-3.49	32.1 (4.8)	31.2 ( 4.6)	9.42	1	0930+294	
09395+4951*	DA	5990 ( 69)	8.00 (0.25)	0.59 (0.15)	H	13.79	-3.73	43.3 (7.1)		9.35	2		
09402+0907W	DC	5120 (115)	8.00 (0.25)	0.58 (0.15)	H	14.74	-4.01	43.1 (7.2)		9.71	2	0937+093	
09422+0942*	DA	5250 ( 60)	8.00 (0.25)	0.58 (0.15)	H	14.32	-3.96	46.2 (7.5)		9.64	2		
09432+5134*	DC	4800 ( 75)	8.00 (0.25)	0.58 (0.15)	H	15.08	-4.12	41.9 (6.7)		9.82	2		
09463+3251N	DA	6860 (119)	8.56 (0.14)	0.96 (0.09)	H	14.48	-3.85	34.2 (1.2)		9.62	1	0943+330	
09466+4354	DA	13240 (285)	7.69 (0.05)	0.45 (0.02)	H	11.07	-2.16	34.2 (3.4)	29.2 ( 2.9)	8.27	1	0943+441	
09481+2023*	DC	4820 ( 60)	8.00 (0.25)	0.58 (0.15)	H	15.11	-4.11	35.8 (5.8)		9.81	2		
09487+2421	DAXP+DA	14530 (1021)	8.40 (0.11)	0.86 (0.07)	H	12.16	-2.42	40.0 (5.0)		8.61	1	0945+245	1, 4
09502+5315	DC	8790 (253)	8.43 (0.11)	0.86 (0.07)	He	13.47	-3.33	23.0 (2.1)	43.5 ( 3.5)	9.27	2	0946+534	
09503+1509*	DC	5440 ( 54)	8.00 (0.25)	0.58 (0.15)	H	14.78	-3.90	38.8 (6.3)		9.53	2		

Table 5—Continued

PM I	ST	$T_{\text{eff}}$ (K)	$\log g$	$M/M_{\odot}$	Comp.	$M_V$	$\log L/L_{\odot}$	$D$ (pc)	$\pi$ (mas)	$\log \tau$	Fit <sup>a</sup>	WDname	Notes
09578+2432	DA	8530 (122)	8.18 (0.05)	0.70 (0.03)	H	13.03	-3.21	24.4 (2.8)	40.9 ( 4.5)	9.07	1	0955+247	
10013+4656	DC	4440 (119)	8.00 (0.25)	0.58 (0.15)	H	15.81	-4.26	39.0 (6.8)		9.89	2	0958+471	
10024+6108	DC	4240 (119)	8.00 (0.25)	0.58 (0.15)	H	16.08	-4.34	37.6 (6.5)		9.92	2	0958+613	
10116+2845	DQpecP	4020 ( 46)	7.93 (0.01)	0.52 (0.01)	He	15.95	-4.40	14.8 (0.5)	67.4 ( 0.4)	9.87	2	1008+290	
10118+2647*	DA	5280 (121)	8.00 (0.25)	0.58 (0.15)	H	14.66	-3.95	41.6 (7.0)		9.63	2		
10140+0305N	DA	5190 (143)	8.00 (0.25)	0.58 (0.15)	H	15.07	-3.98	47.8 (8.5)		9.67	2	1011+033	
10145+4226	DA	7490 (109)	8.28 (0.06)	0.77 (0.04)	H	13.68	-3.51	33.1 (1.1)		9.34	1	1011+426	
10150+0806S	DC	4630 (102)	7.95 (0.19)	0.55 (0.11)	H	15.01	-4.16	29.0 (3.4)	34.5 ( 3.9)	9.83	2	1012+083.2	
10150+0806N	DA	6530 (105)	7.89 (0.12)	0.53 (0.07)	H	13.67	-3.52	29.0 (3.4)	34.5 ( 3.9)	9.19	1	1012+083.1	
10155+1850*	DC	4600 ( 89)	8.00 (0.25)	0.58 (0.15)	H	15.38	-4.19	45.0 (7.2)		9.86	2		
10221+4612	DA	7000 (101)	8.24 (0.06)	0.75 (0.04)	H	13.88	-3.60	30.6 (0.9)		9.38	1	1022+461	
10225+4600	DA	6510 (121)	8.52 (0.17)	0.93 (0.11)	H	14.62	-3.91	27.3 (1.1)		9.65	1	1019+462	
10228+3904*	DZ	5300 ( 50)	8.00 (0.25)	0.57 (0.15)	He	14.74	-3.95	37.1 (0.8)		9.68	2		
10231+6327	DA	6780 (100)	7.90 (0.08)	0.54 (0.05)	H	13.53	-3.46	16.3 (1.0)	61.2 ( 3.6)	9.16	1	1019+637	
10291+1127	DAP	6940 (116)	8.00 (0.25)	0.59 (0.15)	H	13.30	-3.47	40.0 (6.7)		9.19	2	1026+117	
10291+0205	DA	14610 (229)	7.99 (0.05)	0.61 (0.03)	H	11.31	-2.16	38.1 (1.1)		8.32	1	1026+023	
10347+2245*	DZ	6510 ( 96)	8.00 (0.25)	0.57 (0.15)	He	13.40	-3.59	36.5 (1.0)		9.30	2	1032+230	
10370+7110	DC	4730 ( 95)	8.00 (0.25)	0.58 (0.15)	H	15.11	-4.14	19.7 (3.2)		9.83	2	1033+714	
10403+1004*	DC	5920 ( 94)	8.00 (0.25)	0.57 (0.15)	He	14.11	-3.76	39.1 (6.3)		9.43	2		
10418+1415	DQ	7340 ( 98)	7.90 (0.26)	0.52 (0.14)	He	13.65	-3.33	45.0 (8.4)	22.2 ( 3.5)	9.09	2	1039+145	
10480+6334	DA	5080 ( 57)	8.00 (0.25)	0.58 (0.15)	H	14.93	-4.02	32.3 (5.2)		9.72	2	1044+638	
10502+3226*	DA:	5610 ( 57)	8.00 (0.25)	0.58 (0.15)	H	14.02	-3.84	44.6 (7.2)		9.46	2		
10521+4050*	DC	6180 (116)	8.00 (0.25)	0.57 (0.15)	He	14.26	-3.68	35.7 (5.7)		9.36	2		
10547+2706	DA	23930 (366)	8.41 (0.05)	0.88 (0.03)	H	11.10	-1.56	40.1 (1.4)		7.96	1	1052+273	
10565+2336*	DA	5190 ( 58)	8.00 (0.25)	0.58 (0.15)	H	15.06	-3.98	42.1 (6.8)		9.67	2		

Table 5—Continued

PM I	ST	$T_{\text{eff}}$ (K)	$\log g$	$M/M_{\odot}$	Comp.	$M_V$	$\log L/L_{\odot}$	$D$ (pc)	$\pi$ (mas)	$\log \tau$	Fit <sup>a</sup>	WDname	Notes
11062+4518	DC	3860 ( 31)	8.00 (0.25)	0.58 (0.15)	H	16.00	-4.50	36.3 (5.6)		9.97	2	1059+415	
11071+1446*	DA	7310 (112)	8.38 (0.08)	0.84 (0.05)	H	13.93	-3.61	39.5 (1.3)		9.47	1	1103+455	
11075+4855	DC	6700 (110)	8.32 (0.12)	0.80 (0.08)	H	14.18	-3.73	30.5 (1.1)		9.53	1		
11077+5958	DC	4460 (139)	8.00 (0.25)	0.58 (0.15)	H	16.27	-4.25	47.3 (8.5)		9.89	2	1104+491	
11087+0801	DA	18780 (283)	8.08 (0.05)	0.67 (0.03)	H	11.01	-1.77	35.6 (1.6)		8.03	1	1104+602	
11109+2026	DA	7520 (108)	8.03 (0.05)	0.61 (0.03)	H	13.30	-3.35	36.4 (1.1)		9.12	1	1106+082	
11111+3848*	DA	6980 (110)	8.41 (0.09)	0.85 (0.06)	H	14.15	-3.71	40.2 (1.3)		9.54	1	1106+554	
11132+2859*	DC	4730 (109)	8.09 (0.11)	0.64 (0.07)	H	15.38	-4.20	26.1 (2.0)	38.3 ( 2.7)	9.89	2	1108+207	
11156+0033	DC	5080 (145)	8.00 (0.25)	0.57 (0.15)	He	14.64	-4.03	48.1 (8.5)		9.76	2		
11166+0627	DA	4830 ( 62)	8.00 (0.25)	0.58 (0.15)	H	15.27	-4.11	34.9 (5.6)		9.81	2	1110+292	
11192+0220	DA	5210 ( 71)	8.00 (0.25)	0.58 (0.15)	H	14.74	-3.97	32.8 (5.4)		9.66	2	1113+008	
11210+3756*	DA	6410 (124)	8.11 (0.20)	0.66 (0.12)	H	14.05	-3.67	34.7 (1.1)		9.38	1	1114+067	
11235+0701	DA	12400 (186)	8.08 (0.05)	0.65 (0.03)	H	11.71	-2.50	37.7 (1.1)		8.58	1	1116+026	
11242+2121	DA	9810 (145)	8.26 (0.06)	0.76 (0.04)	H	12.65	-3.02	36.5 (1.2)		8.97	1		
11253+2111*	DC	4460 (106)	8.00 (0.25)	0.58 (0.15)	H	15.84	-4.25	24.9 (4.2)		9.89	2	1120+073	
11268+5919	DA	7330 (105)	8.09 (0.06)	0.65 (0.04)	H	13.47	-3.42	13.4 (0.5)	74.5 ( 2.8)	9.18	1	1121+216	
11324+1517	DC	6390 (117)	8.00 (0.25)	0.57 (0.15)	He	13.51	-3.63	41.2 (6.8)		9.32	2		
11354+2717	DA	10360 (160)	8.69 (0.07)	1.04 (0.04)	H	13.21	-3.22	24.0 (0.9)		9.28	1	1124+595	
11364+0802S*	DA	17990 (277)	8.24 (0.05)	0.77 (0.03)	H	11.33	-1.95	35.8 (1.6)		8.23	1	1129+155	
11370+2947	DC	4250 (359)	8.00 (0.25)	0.58 (0.15)	H	15.69	-4.33	39.7 (9.6)		9.92	2	1132+275	
11457+6305	DA	5500 ( 45)	8.00 (0.25)	0.58 (0.15)	H	14.39	-3.88	47.3 (7.6)		9.50	2		
11459+3149W	DA	22310 (339)	8.56 (0.05)	0.98 (0.03)	H	11.50	-1.79	14.2 (2.2)	70.6 ( 10.9)	8.20	1	1134+300	
11495+2353*	DC	5270 ( 58)	8.00 (0.25)	0.58 (0.15)	H	14.74	-3.95	21.3 (3.4)		9.63	2	1143+633	
	DA	15890 (265)	8.05 (0.05)	0.64 (0.03)	H	11.24	-2.04	31.6 (2.3)	31.6 ( 2.3)	8.25	1	1143+321	
	DC	4960 ( 54)	8.00 (0.25)	0.58 (0.15)	H	14.51	-4.06	42.0 (6.6)		9.77	2		

Table 5—Continued

PM I	ST	$T_{\text{eff}}$ (K)	$\log g$	$M/M_{\odot}$	Comp.	$M_V$	$\log L/L_{\odot}$	$D$ (pc)	$\pi$ (mas)	$\log \tau$	Fit <sup>a</sup>	WDname	Notes
11508+6831	DA	6650 ( 95)	8.17 (0.05)	0.69 (0.04)	H	13.98	-3.64	18.0 (0.6)		9.38	1	1148+687	
11519+0528	DA	11100 (160)	8.07 (0.05)	0.64 (0.03)	H	11.94	-2.69	40.2 (1.2)		8.70	1	1149+057	
11545+2422*	DA	8790 (141)	8.57 (0.09)	0.96 (0.06)	H	13.57	-3.42	25.2 (1.0)		9.38	1	1151+246	
11562+1315	DC	4730 (115)	8.00 (0.25)	0.58 (0.15)	H	15.66	-4.15	28.0 (4.7)		9.83	2	1153+135	
11567+1822	DC	7710 (221)	8.07 (0.16)	0.62 (0.10)	He	13.39	-3.34	29.9 (3.5)	33.5 ( 3.5)	9.15	2	1154+186	
11582+0004*	DC	4400 ( 81)	7.82 (0.12)	0.47 (0.06)	H	15.55	-4.18	34.5 (2.6)	29.0 ( 2.0)	9.77	2		
11592+4842*	DA	6080 ( 92)	8.60 (0.09)	0.98 (0.06)	H	15.04	-4.08	31.6 (1.1)		9.73	1		
12000+4335	DA	7730 (111)	7.82 (0.06)	0.49 (0.03)	H	12.90	-3.18	37.5 (1.1)		8.96	1	1157+438	
12113+0724*	DA	5270 ( 41)	8.00 (0.25)	0.58 (0.15)	H	14.57	-3.95	24.7 (4.0)		9.63	2	1208+076	
12114+5724	DA	5870 (106)	7.79 (0.25)	0.47 (0.13)	H	14.01	-3.65	20.4 (1.9)	48.9 ( 4.6)	9.25	1	1208+576	
12145+7822*	DZ	5000 (656)	8.00 (0.25)	0.58 (0.15)	H	14.88	-4.05	32.9 (8.9)		9.75	2		
12157+5231	DA+dM	18840 (446)	8.30 (0.07)	0.80 (0.05)	H	11.33	-1.90	37.3 (4.0)	26.8 ( 2.8)	8.21	1	1213+528	2
12168+0258S	DA	6900 (104)	7.91 (0.08)	0.54 (0.05)	H	13.47	-3.43	21.6 (1.4)	46.3 ( 3.0)	9.14	1	1214+032	
12175+3205N	DC	8530 (998)	9.02 (0.12)	1.20 (0.05)	He	14.54	-3.83	31.1 (5.5)	32.2 ( 3.6)	9.45	2	1215+323	
12263+1836	DC	7600 (110)	8.00 (0.25)	0.58 (0.15)	He	13.16	-3.32	40.4 (6.5)		9.13	2	1223+188	
12265+3513	DA	5100 ( 56)	8.00 (0.25)	0.58 (0.15)	H	14.59	-4.01	31.2 (5.1)		9.72	2	1224+354	
12274+3150*	DA	6580 (106)	7.99 (0.13)	0.58 (0.08)	H	13.77	-3.56	37.9 (1.1)		9.24	1	1224+321	
12280+3300*	DC	4630 ( 75)	8.00 (0.25)	0.58 (0.15)	H	15.24	-4.18	35.7 (5.7)		9.85	2		
12281+0022	DA	9390 (134)	7.97 (0.05)	0.58 (0.03)	H	12.36	-2.92	33.1 (1.0)		8.83	1	1225+006	
12377+6023*	DA	5300 ( 75)	8.00 (0.25)	0.58 (0.15)	H	14.48	-3.94	46.5 (7.7)		9.61	2		
12378+4156	DQ	6350 (244)	8.00 (0.25)	0.57 (0.15)	He	13.64	-3.64	46.2 (7.9)		9.33	2	1235+422	
12392+4525	DA	6810 (118)	8.66 (0.15)	1.02 (0.09)	H	14.68	-3.93	23.5 (0.9)		9.65	1	1236+457	
12405+1807W*	DA	5420 ( 46)	8.00 (0.25)	0.58 (0.15)	H	15.14	-3.90	39.0 (6.3)		9.54	2		
12425+1311W*	DC	4970 (135)	8.00 (0.25)	0.58 (0.15)	H	15.38	-4.06	44.7 (7.9)		9.77	2		
12429+6542*	DA	6960 (121)	8.85 (0.14)	1.12 (0.07)	H	14.95	-4.03	33.0 (1.3)		9.63	1		



Table 5—Continued

PM I	ST	$T_{\text{eff}}$ (K)	$\log g$	$M/M_{\odot}$	Comp.	$M_V$	$\log L/L_{\odot}$	$D$ (pc)	$\pi$ (mas)	$\log \tau$	Fit <sup>a</sup>	WDname	Notes
12501+5447	DC	4530 (608)	7.96 (0.03)	0.56 (0.02)	H	15.56	-4.20	25.3 (3.1)	39.5 ( 0.7)	9.85	2	1247+550	
12541+3620*	DC	4790 ( 52)	8.00 (0.25)	0.58 (0.15)	H	15.15	-4.12	26.8 (4.3)		9.82	2		
	DC	4600 ( 66)	8.00 (0.25)	0.58 (0.15)	H	15.96	-4.19	44.5 (7.1)		9.86	2	1252+471	
12597+2734	DAZ	8570 (123)	8.11 (0.05)	0.66 (0.03)	H	12.91	-3.16	34.6 (5.0)	28.9 ( 4.1)	9.02	1	1257+278	
13001+0328	DA	5710 ( 94)	8.00 (0.25)	0.59 (0.15)	H	14.41	-3.81	16.6 (1.1)	60.3 ( 3.8)	9.42	1	1257+037	
13003+0130	DA	5450 ( 68)	8.00 (0.25)	0.58 (0.15)	H	14.65	-3.90	37.4 (6.2)		9.53	2	1257+017	
13013+6713	DA	6600 (109)	8.09 (0.13)	0.64 (0.08)	H	13.89	-3.61	33.8 (1.0)		9.32	1	1259+674	
13032+7510*	DC	7550 (264)	8.00 (0.25)	0.58 (0.15)	He	13.25	-3.33	42.9 (7.6)		9.14	2		
13032+2603	DC	4620 (551)	8.33 (0.16)	0.80 (0.11)	H	16.04	-4.38	35.2 (6.0)	28.4 ( 3.3)	9.97	2	1300+263	
13086+8502	DAP	5430 (135)	8.19 (0.02)	0.71 (0.02)	H	14.93	-4.01	16.5 (0.9)	60.7 ( 1.0)	9.74	2	1309+853	
13129+5805	DA	10470 (152)	8.15 (0.05)	0.69 (0.03)	H	12.25	-2.84	23.2 (0.8)		8.82	1	1310+583	
13132+0226	DC	4230 ( 74)	8.00 (0.25)	0.58 (0.15)	H	16.46	-4.34	30.7 (4.9)		9.93	2	1310+027	
13178+2157	DC	6830 (254)	8.00 (0.25)	0.59 (0.15)	H	13.68	-3.50	44.5 (7.6)		9.21	2	1315+222	
13212+4623	DA	14380 (338)	8.31 (0.05)	0.80 (0.03)	H	11.81	-2.38	33.8 (1.1)		8.56	1	1319+466	
13277+5755	DA	6790 (114)	8.03 (0.14)	0.61 (0.09)	H	13.70	-3.53	37.0 (7.9)	27.0 ( 5.5)	9.24	1	1325+581	
13291+2450*	DC	3990 ( 72)	8.00 (0.25)	0.58 (0.15)	H	16.72	-4.44	38.9 (6.1)		9.96	2		
13309+3029	DZ	5950 ( 47)	7.75 (0.28)	0.43 (0.14)	He	13.92	-3.62	29.9 (4.9)	33.4 ( 5.3)	9.24	2	1328+307	
13333+2450*	DC	4110 (850)	8.00 (0.25)	0.58 (0.15)	H	15.96	-4.39	50.1 (35.1)		9.94	2		
13346+0943E*	DA	5140 (585)	8.00 (0.25)	0.58 (0.15)	H	15.03	-4.00	40.7 (18.2)		9.70	2		
13360+4828	DB+dM	15330 (293)	7.95 (0.17)	0.56 (0.10)	He	11.17	-2.07	35.0 (4.0)	28.6 ( 3.2)	8.26	1	1333+487	
13365+0340	DA	4940 ( 74)	7.91 (0.05)	0.53 (0.03)	H	15.04	-4.02	8.2 (3.0)	121.4 ( 3.4)	9.69	2	1334+039	
13388+7017	DA	21150 (320)	7.95 (0.05)	0.60 (0.03)	H	10.59	-1.48	32.8 (6.6)	30.5 ( 5.9)	7.66	1	1337+705	
13413+0500*	DC	4180 ( 46)	8.00 (0.25)	0.58 (0.15)	H	16.05	-4.36	13.2 (2.1)		9.93	2	1338+052	
13455+4200*	DC	4600 ( 48)	7.09 (0.09)	0.19 (0.02)	H	14.20	-3.77	37.0 (1.4)	27.0 ( 1.0)	9.30	2		
13460+5700	DA	13900 (300)	8.06 (0.05)	0.65 (0.03)	H	11.49	-2.29	25.8 (0.8)		8.43	1	1344+572	

Table 5—Continued

PM I	ST	$T_{\text{eff}}$ (K)	$\log g$	$M/M_{\odot}$	Comp.	$M_V$	$\log L/L_{\odot}$	$D$ (pc)	$\pi$ (mas)	$\log \tau$	Fit <sup>a</sup>	WDname	Notes
13474+1021W	DA	6940 (102)	7.91 (0.07)	0.54 (0.04)	H	13.44	-3.42	20.0 (1.4)	49.9 ( 3.6)	9.13	1	1344+106	
13480+2334	DA	4580 ( 85)	7.77 (0.05)	0.45 (0.02)	H	15.56	-4.09	12.1 (1.0)	82.9 ( 2.2)	9.68	2	1345+238	
13490+1155	DC	4640 (108)	8.22 (0.08)	0.72 (0.06)	H	15.59	-4.30	28.6 (3.5)	35.0 ( 2.0)	9.95	2	1346+121	
13497+2755	DA	7260 (120)	8.41 (0.12)	0.86 (0.08)	H	14.01	-3.64	29.6 (1.0)		9.50	1	1347+281	
13521+1053*	DA	6070 (111)	8.12 (0.21)	0.67 (0.13)	H	14.30	-3.78	32.6 (1.0)		9.47	1		
14037+5206	DA	7490 (118)	8.37 (0.09)	0.83 (0.06)	H	13.82	-3.56	33.7 (1.2)		9.43	1	1401+523	
14059+6648	DC	3890 (218)	8.00 (0.25)	0.57 (0.15)	He	16.43	-4.49	29.8 (7.4)		9.93	2	1404+670	
14064+1608*	DA	6950 (132)	8.79 (0.18)	1.09 (0.10)	H	14.85	-3.99	33.8 (1.2)		9.64	1	1404+163	
14067+3130*	DC	4750 ( 83)	8.00 (0.25)	0.58 (0.15)	H	15.41	-4.14	37.2 (6.1)		9.83	2		
	DA	9910 (142)	8.03 (0.05)	0.62 (0.03)	H	12.25	-2.86	36.5 (1.1)		8.81	1	1407+425	
14104+3208	DA	19010 (286)	8.00 (0.05)	0.62 (0.03)	H	10.85	-1.70	39.5 (4.4)	25.3 ( 2.8)	7.93	1	1408+323	
14106+0245*	DAZ	5840 ( 90)	8.00 (0.25)	0.59 (0.15)	H	14.31	-3.77	30.6 (0.9)		9.38	1	1408+029	
14149+4336*	DA	6670 (121)	8.65 (0.16)	1.01 (0.10)	H	14.74	-3.95	33.8 (1.3)		9.66	1		
14201+5322	DA	7600 (114)	8.56 (0.07)	0.96 (0.05)	H	14.09	-3.67	36.7 (1.3)		9.53	1	1418+536	
14236+3037*	DA	5300 ( 52)	8.00 (0.25)	0.58 (0.15)	H	14.92	-3.95	40.1 (6.5)		9.62	2		
14244+6246*	DA	5000 ( 65)	8.00 (0.25)	0.58 (0.15)	H	15.22	-4.05	45.0 (7.2)		9.75	2		
14246+0917	DA	12760 (197)	8.05 (0.05)	0.64 (0.03)	H	11.62	-2.43	38.6 (1.2)		8.53	1	1422+095	
14339+1907*	DA	5020 ( 62)	8.00 (0.25)	0.58 (0.15)	H	15.16	-4.04	45.8 (7.3)		9.75	2		
14367+4332	DC	4710 (110)	7.97 (0.04)	0.56 (0.03)	H	15.36	-4.14	27.0 (5.8)	37.0 ( 1.0)	9.81	2	1434+437	
14454+2921N	DA	13050 (222)	8.00 (0.05)	0.61 (0.03)	H	11.51	-2.36	39.3 (1.1)		8.47	1	1443+295	
14456+2527*	DA	5190 ( 52)	8.00 (0.25)	0.58 (0.15)	H	14.84	-3.98	17.5 (2.8)		9.67	2		
14581+2937	DA	7290 (105)	7.90 (0.06)	0.54 (0.03)	H	13.24	-3.33	34.6 (5.0)	28.9 ( 4.1)	9.08	1	1455+298	
14588+1146*	DC	4810 ( 71)	8.00 (0.25)	0.58 (0.15)	H	15.02	-4.12	40.9 (6.5)		9.82	2		
15096+6332	DA	10380 (148)	7.96 (0.05)	0.58 (0.03)	H	11.99	-2.74	35.5 (1.3)		8.72	1	1508+637	
15111+4048	DA	8650 (126)	8.19 (0.06)	0.71 (0.04)	H	13.00	-3.19	34.7 (1.1)		9.06	1	1509+409	

Table 5—Continued

PM I	ST	$T_{\text{eff}}$ (K)	$\log g$	$M/M_{\odot}$	Comp.	$M_V$	$\log L/L_{\odot}$	$D$ (pc)	$\pi$ (mas)	$\log \tau$	Fit <sup>a</sup>	WDname	Notes
15114+3204	DA	14550 (272)	8.11 (0.05)	0.68 (0.03)	H	11.49	-2.23	47.8 (10.1)	20.9 ( 4.2)	8.41	1	1509+322	
15257+5629	DC	5520 ( 71)	8.00 (0.25)	0.58 (0.15)	H	14.32	-3.87	28.8 (4.8)		9.49	2	1524+566	
15263+2936*	DA	5110 (109)	8.00 (0.25)	0.58 (0.15)	H	15.43	-4.01	22.4 (3.7)		9.71	2		
15342+0218*	DA	8260 (126)	8.62 (0.08)	1.00 (0.05)	H	13.89	-3.57	29.8 (1.1)		9.47	1	1531+024	
15348+4649	DC	4400 (106)	7.97 (0.10)	0.56 (0.06)	H	15.97	-4.26	30.3 (2.1)	33.0 ( 2.0)	9.88	2	1533+469	
15350+1247	DZ	5180 ( 19)	8.00 (0.25)	0.57 (0.15)	He	14.85	-3.99	16.9 (0.2)		9.73	2	1532+129	
15359+2125*	DA	6500 (112)	8.47 (0.16)	0.89 (0.10)	H	14.54	-3.88	37.6 (1.2)		9.64	1		
15377+6501	DA	9660 (141)	7.98 (0.06)	0.59 (0.03)	H	12.27	-2.88	31.1 (0.9)		8.81	1	1537+651	
15405+3308N	DA	8780 (125)	8.15 (0.05)	0.69 (0.03)	H	12.89	-3.15	27.5 (0.8)		9.03	1	1538+333	
15425+2329	DA	6250 (113)	8.82 (0.18)	1.11 (0.10)	H	15.33	-4.20	19.6 (0.8)		9.70	1	1540+236	
15460+3751	DA	13450 (274)	8.06 (0.06)	0.64 (0.04)	H	11.55	-2.34	38.0 (1.1)		8.47	1	1544+380	
15524+1810	DA	14810 (295)	8.37 (0.05)	0.84 (0.03)	H	11.86	-2.37	40.5 (1.6)		8.57	1	1550+183	
15555+5025	DA	6190 (105)	7.62 (0.19)	0.39 (0.08)	H	13.56	-3.47	40.2 (1.1)		9.10	1	1554+505	
15589+0417*	DC	6680 (117)	8.00 (0.25)	0.57 (0.15)	He	51.52	-3.55	30.3 (4.9)		9.27	2		
16012+5316	DA	6680 (102)	8.04 (0.09)	0.61 (0.05)	H	13.77	-3.56	36.1 (1.0)		9.26	1	1559+534	
16013+3648	DA	11240 (162)	8.00 (0.05)	0.60 (0.03)	H	11.81	-2.62	33.1 (3.7)	30.2 ( 3.3)	8.65	1	1559+369	
16048+0055	DC	4810 (115)	8.00 (0.25)	0.58 (0.15)	H	15.56	-4.11	30.8 (5.1)		9.81	2	1602+010	
16072+3423	DA	5790 ( 70)	8.00 (0.25)	0.59 (0.15)	H	13.91	-3.79	36.4 (6.0)		9.40	2	1605+345	
16083+4205	DA	13070 (214)	7.87 (0.05)	0.53 (0.03)	H	11.33	-2.28	45.0 (7.3)	22.2 ( 3.5)	8.39	1	1606+422	
16114+1322	DA	9230 (132)	8.48 (0.05)	0.90 (0.03)	H	13.23	-3.27	18.3 (1.6)	54.5 ( 4.7)	9.25	1	1609+135	
16144+0906*	DC	4810 ( 43)	8.00 (0.25)	0.58 (0.15)	H	15.44	-4.12	26.8 (4.3)		9.81	2		
16264+1938*	DA	6300 (102)	8.32 (0.14)	0.79 (0.09)	H	14.43	-3.83	27.6 (0.9)		9.59	1		
16278+0912	DA	7130 (134)	8.60 (0.16)	0.98 (0.10)	H	14.40	-3.81	23.4 (2.1)	42.8 ( 3.7)	9.60	1	1625+093	
16284+3646	DZA	8020 (156)	7.98 (0.05)	0.56 (0.03)	He	13.01	-3.22	15.9 (0.5)	62.7 ( 2.0)	9.05	2	1626+368	
16286+7053*	DA	4790 (918)	8.00 (0.25)	0.58 (0.15)	H	15.57	-4.12	31.7 (14.4)		9.82	2		

Table 5—Continued

PM I	ST	$T_{\text{eff}}$ (K)	$\log g$	$M/M_{\odot}$	Comp.	$M_V$	$\log L/L_{\odot}$	$D$ (pc)	$\pi$ (mas)	$\log \tau$	Fit <sup>a</sup>	WDname	Notes
16325+0851*	DA	5730 ( 90)	8.00 (0.25)	0.59 (0.15)	H	14.40	-3.81	13.8 (0.4)		9.42	1	1630+089	
16343+5710	DQpec	6200 (105)	8.12 (0.05)	0.65 (0.03)	He	14.19	-3.74	14.4 (0.6)	69.2 ( 2.5)	9.48	2	1633+572	
	DA	10030 (142)	7.79 (0.05)	0.48 (0.02)	H	11.86	-2.70	19.0 (0.9)		8.66	1	1632+177	
16350+4317	DAZ	6560 (112)	7.93 (0.15)	0.55 (0.08)	H	13.69	-3.53	15.1 (0.7)	66.2 ( 3.0)	9.20	1	1633+433	
16376+1340	DA	6570 ( 70)	8.13 (0.26)	0.67 (0.16)	H	13.98	-3.64	38.3 (8.2)	26.1 ( 4.6)	9.37	2	1635+137	
16394+3325	DA	10180 (146)	8.03 (0.05)	0.62 (0.03)	H	12.15	-2.81	28.6 (2.6)	35.0 ( 3.2)	8.78	1	1637+335	
16409+5341	DAH	7410 ( 99)	8.06 (0.11)	0.62 (0.07)	He	13.81	-3.40	21.1 (2.1)	47.4 ( 3.5)	9.19	2	1639+537	
16416+1512	DA	7450 (110)	8.49 (0.07)	0.91 (0.04)	H	14.04	-3.65	30.9 (0.2)	32.4 ( 0.3)	9.51	1	1639+153	1
16473+3228	DB	25250 (370)	7.92 (0.05)	0.57 (0.03)	He	10.33	-1.17	36.6 (4.5)	27.3 ( 3.3)	7.33	1	1645+325	
16484+5903	DA	12570 (197)	8.31 (0.05)	0.80 (0.03)	H	12.02	-2.61	12.2 (0.6)	81.9 ( 4.6)	8.72	1	1647+591	
16540+6253	DC	3080 ( 95)	7.24 (0.03)	0.22 (0.01)	He	15.66	-4.55	30.3 (0.5)	33.0 ( 0.5)	9.70	2	1653+630	
16547+3829	DAZ	5940 (101)	8.00 (0.25)	0.59 (0.15)	H	14.23	-3.74	32.3 (0.9)		9.36	1	1653+385	
16556+2533	DA	10900 (165)	9.18 (0.05)	1.26 (0.02)	H	14.06	-3.53	37.8 (1.7)		9.31	1	1653+256	
16571+2126	DA	9240 (132)	8.02 (0.05)	0.61 (0.03)	H	12.50	-2.98	23.3 (1.7)	43.0 ( 3.1)	8.88	1	1655+215	
16595+4425	DA	5690 (123)	8.09 (0.33)	0.64 (0.20)	H	14.55	-3.87	28.0 (0.8)		9.52	1	1658+445	
17027+1022*	DA	5080 ( 57)	8.00 (0.25)	0.58 (0.15)	H	14.86	-4.02	37.3 (6.0)		9.72	2		
17052+0423*	DA	8450 (137)	8.37 (0.10)	0.83 (0.07)	H	13.37	-3.35	34.9 (1.5)		9.25	1		
17055+4803W	DA	9230 (133)	7.67 (0.05)	0.43 (0.03)	H	12.01	-2.79	30.4 (0.8)		8.70	1	1704+481.2	
17055+4803E	DA	14120 (292)	8.09 (0.05)	0.66 (0.03)	H	11.51	-2.28	39.5 (1.2)		8.43	1	1704+481.1	
17081+0257	DZ	6650 (153)	8.21 (0.14)	0.70 (0.09)	He	13.89	-3.68	17.5 (1.7)	57.0 ( 5.4)	9.45	2	1705+030	
17131+6931	DA	15880 (239)	7.99 (0.05)	0.61 (0.03)	H	11.16	-2.01	27.7 (3.2)	36.1 ( 4.0)	8.21	1	1713+695	
17148+3918	DAP	7010 (123)	8.00 (0.25)	0.59 (0.15)	H	13.75	-3.45	38.2 (6.4)		9.18	2	1713+393	
17185+0156N	DA	13550 (345)	7.91 (0.05)	0.56 (0.03)	H	11.33	-2.24	35.6 (3.3)	28.1 ( 2.6)	8.37	1	1716+020	
17283+0211*	DA	8050 (121)	8.17 (0.08)	0.70 (0.05)	H	13.23	-3.31	40.2 (1.8)		9.13	1		
17335+7949*	DC	4970 (231)	8.00 (0.25)	0.57 (0.15)	He	14.57	-4.07	29.5 (5.1)		9.78	2		

Table 5—Continued

PM I	ST	$T_{\text{eff}}$ (K)	$\log g$	$M/M_{\odot}$	Comp.	$M_V$	$\log L/L_{\odot}$	$D$ (pc)	$\pi$ (mas)	$\log \tau$	Fit <sup>a</sup>	WDname	Notes
17386+0516	DA	9300 (1777)	8.17 (0.24)	0.70 (0.15)	H	12.27	-3.06	42.7 (8.5)	23.4 ( 3.9)	8.97	2	1736+052	
17417+2401*	DA	7150 (111)	8.38 (0.09)	0.84 (0.06)	H	14.02	-3.65	32.6 (1.6)		9.50	1		
17428+4338	DA	5480 (118)	8.00 (0.25)	0.58 (0.15)	H	14.15	-3.88	31.8 (5.3)		9.51	2	1741+436	
17430+1701*	DC	4720 (433)	8.00 (0.25)	0.58 (0.15)	H	15.54	-4.15	32.1 (7.7)		9.84	2		
17433+1434S*	DC	10440 (234)	8.00 (0.25)	0.58 (0.15)	He	11.67	-2.77	35.7 (6.1)		8.77	2		
17471+2859*	DC	5350 (495)	8.00 (0.25)	0.57 (0.15)	He	14.58	-3.94	37.9 (7.1)		9.66	2		
17481+7052	DXP	5260 ( 64)	8.20 (0.02)	0.70 (0.01)	He	15.20	-4.08	6.1 (1.5)	164.7 ( 2.4)	9.79	2	1748+708	
17484+4503	DC	8750 (284)	8.00 (0.25)	0.58 (0.15)	He	12.64	-3.08	37.4 (6.3)		8.97	2	1747+450	
17498+8246	DA	7230 (106)	7.89 (0.07)	0.53 (0.04)	H	13.26	-3.34	15.6 (0.7)	63.9 ( 2.9)	9.08	1	1756+827	
17570+4052	DC	5920 ( 67)	8.00 (0.25)	0.59 (0.15)	H	13.91	-3.75	38.7 (6.4)		9.37	2	1755+408	
17583+1417	DA	5400 (238)	8.00 (0.25)	0.58 (0.15)	H	14.88	-3.91	22.8 (4.1)		9.55	2	1756+143	
18014+5049*	DC	4990 (103)	8.00 (0.25)	0.58 (0.15)	H	14.87	-4.05	34.0 (5.6)		9.76	2		
18073+0357*	DA	10410 (150)	8.09 (0.05)	0.65 (0.03)	H	12.17	-2.81	34.7 (2.1)		8.79	1		
18154+3158*	DA	5020 (949)	8.00 (0.25)	0.58 (0.15)	H	15.17	-4.04	41.0 (14.6)		9.75	2		
18161+2454	DAP	6920 (115)	8.00 (0.25)	0.59 (0.15)	H	13.60	-3.48	46.7 (8.0)		9.19	2	1814+248	
18171+1328	DA	5190 (203)	8.12 (0.03)	0.66 (0.02)	H	15.13	-4.05	14.2 (2.3)	70.3 ( 1.2)	9.79	2	1814+134	
18199+1739*	DC	4820 (677)	8.00 (0.25)	0.58 (0.15)	H	15.08	-4.11	35.1 (11.0)		9.81	2		
18205+1239	DAH	7590 (998)	7.52 (0.38)	0.35 (0.14)	H	12.37	-3.06	40.8 (0.0)	24.5 ( 5.5)	8.86	2	1818+126	1
18213+6101	DA	4880 ( 49)	7.93 (0.09)	0.54 (0.05)	H	15.07	-4.05	12.8 (2.3)	78.2 ( 4.1)	9.74	2	1820+609	
18303+5447	DXP	6210 (101)	8.44 (0.11)	0.86 (0.07)	He	14.25	-3.94	15.0 (2.6)	66.8 ( 5.6)	9.68	2	1829+547	
18434+0420	DA	8900 (127)	8.21 (0.05)	0.73 (0.03)	H	12.92	-3.15	25.0 (2.1)	40.0 ( 3.4)	9.04	1	1840+042	
18435+2740*	DA	11060 (163)	8.10 (0.05)	0.66 (0.03)	H	12.00	-2.71	39.7 (1.8)		8.73	1	GD 381	
18510+7738*	DC:	5230 ( 49)	8.00 (0.25)	0.58 (0.15)	H	14.86	-3.97	30.3 (5.0)		9.65	2		
18572+2026*	DA	5350 (1009)	8.00 (0.25)	0.58 (0.15)	H	13.72	-3.93	31.7 (10.6)		9.59	2		
18575+3357	DA	12300 (186)	8.31 (0.05)	0.80 (0.03)	H	12.07	-2.65	32.8 (4.8)	30.5 ( 4.4)	8.74	1	1855+338	

Table 5—Continued

PM I	ST	$T_{\text{eff}}$ (K)	$\log g$	$M/M_{\odot}$	Comp.	$M_V$	$\log L/L_{\odot}$	$D$ (pc)	$\pi$ (mas)	$\log \tau$	Fit <sup>a</sup>	WDname	Notes
18576+5330	DC	5570 (546)	8.00 (0.25)	0.58 (0.15)	H	14.37	-3.86	31.8 (6.3)		9.47	2	1856+534	
19001+7039	DAP	11880 (744)	8.54 (0.04)	0.93 (0.02)	He	12.69	-2.88	13.0 (2.3)	77.0 ( 2.3)	8.96	2	1900+705	
19128+5343*	DA	17870 (273)	8.32 (0.05)	0.81 (0.03)	H	11.45	-2.01	22.1 (1.3)		8.29	1		
19132+2949*	DA	6110 (114)	8.00 (0.25)	0.59 (0.15)	H	14.09	-3.69	39.9 (1.8)		9.33	1		
19136+1336	DA	13770 (337)	7.98 (0.05)	0.60 (0.03)	H	11.39	-2.26	34.4 (1.5)		8.39	1	1911+135	
19146+1428*	DA	7050 (126)	8.68 (0.14)	1.03 (0.09)	H	14.59	-3.89	35.0 (6.6)	28.6 ( 5.2)	9.62	1		5
19167+8044*	DA	5040 (632)	8.00 (0.25)	0.58 (0.15)	H	14.83	-4.03	35.4 (0.0)		9.74	2		
19189+3843	DC	6410 (163)	8.25 (0.06)	0.73 (0.04)	He	14.27	-3.77	11.7 (2.3)	85.5 ( 3.4)	9.54	2	1917+386	
19216+1440	DA	15340 (245)	8.23 (0.05)	0.75 (0.03)	H	11.58	-2.22	19.8 (2.2)	50.5 ( 5.5)	8.43	1	1919+145	
19372+2743	DA	12490 (187)	8.03 (0.05)	0.62 (0.03)	H	11.63	-2.45	18.0 (0.9)	55.7 ( 2.9)	8.54	1	1935+276	
19384+3253	DA	22120 (341)	7.93 (0.05)	0.59 (0.03)	H	10.49	-1.39	34.8 (2.9)	28.7 ( 2.4)	7.55	1	1936+327	
19401+8348*	DC	4840 (672)	8.00 (0.25)	0.58 (0.15)	H	15.08	-4.11	38.8 (12.1)		9.81	2		
19455+4650N*	DA	4800 (398)	8.00 (0.25)	0.58 (0.15)	H	15.13	-4.12	27.5 (5.8)		9.82	2		
19455+1627	DA	20370 (310)	7.94 (0.05)	0.59 (0.03)	H	10.65	-1.54	42.2 (4.8)	23.7 ( 2.7)	7.74	1	1943+163	
19493+0747*	DA	9310 (134)	8.19 (0.06)	0.71 (0.04)	H	12.72	-3.07	36.2 (1.8)		8.98	1		
19524+2509	DA	11920 (182)	8.04 (0.05)	0.63 (0.03)	H	11.73	-2.54	38.0 (4.4)	26.3 ( 3.0)	8.60	1	1950+250	
20069+6143*	DA	5540 ( 91)	8.00 (0.25)	0.58 (0.15)	H	14.57	-3.87	26.2 (0.8)		9.49	1		
20123+3113	DBP	15900 (2465)	8.77 (0.09)	1.07 (0.05)	He	12.59	-2.54	28.8 (3.2)	34.7 ( 2.7)	8.79	2	2010+310	
20139+0642	DC	6620 (133)	8.19 (0.06)	0.70 (0.04)	He	13.32	-3.68	22.4 (2.4)	44.7 ( 1.9)	9.45	2	2011+065	
20223+8333*	DC	5880 (713)	8.00 (0.25)	0.57 (0.15)	He	14.04	-3.77	39.3 (8.2)		9.44	2		
20299+3913E	DA	24970 (380)	8.04 (0.05)	0.65 (0.03)	H	10.42	-1.24	41.0 (1.5)		7.39	1	2028+390	
20300+0729*	DC	8180 (285)	8.00 (0.25)	0.58 (0.15)	He	12.79	-3.19	42.2 (7.2)		9.05	2		
20343+2503	DA	20500 (307)	8.03 (0.05)	0.64 (0.03)	H	10.77	-1.58	14.3 (0.5)	69.9 ( 2.7)	7.82	1	2032+248	
20491+3728	DA	14600 (282)	8.32 (0.05)	0.81 (0.03)	H	11.81	-2.36	17.3 (0.2)	57.8 ( 0.7)	8.55	1	2047+372	
20503+2630	DC	4940 ( 69)	7.11 (0.15)	0.20 (0.04)	H	13.31	-3.64	20.1 (2.6)	49.8 ( 3.4)	9.21	2	2048+263	1

Table 5—Continued

PM I	ST	$T_{\text{eff}}$ (K)	$\log g$	$M/M_{\odot}$	Comp.	$M_V$	$\log L/L_{\odot}$	$D$ (pc)	$\pi$ (mas)	$\log \tau$	Fit <sup>a</sup>	WDname	Notes
20597+5517*	DC	4530 ( 59)	8.00 (0.25)	0.58 (0.15)	H	15.98	-4.22	22.6 (3.6)		9.87	2		
21005+5051	DA	9680 (139)	8.05 (0.05)	0.63 (0.03)	H	12.37	-2.91	37.5 (1.7)		8.85	1	2058+506	
21017+3148	DQ	9800 (4381)	8.01 (0.19)	0.59 (0.11)	He	7.30	-2.88	34.5 (6.0)	29.0 ( 3.5)	8.85	2	2059+316	
21020+1912	DA	6920 (108)	8.45 (0.10)	0.88 (0.06)	H	14.25	-3.75	38.3 (6.6)	26.1 ( 4.4)	9.57	1	2059+190	
21022+2457	DA	6290 (107)	8.56 (0.16)	0.95 (0.10)	H	14.82	-3.99	27.7 (3.2)	36.1 ( 4.2)	9.69	1	2059+247	
21077+0740*	DA	7080 (116)	8.06 (0.12)	0.63 (0.08)	H	13.57	-3.47	35.8 (1.6)		9.20	1		
21134+0727*	DA	6510 (112)	8.26 (0.15)	0.76 (0.10)	H	14.20	-3.74	24.3 (2.2)	41.1 ( 3.8)	9.51	1		5
21137+2621	DA	8530 (123)	8.15 (0.06)	0.69 (0.04)	H	13.00	-3.20	31.8 (3.8)	31.4 ( 3.7)	9.06	1	2111+261	
21189+5412	DA	14590 (238)	7.92 (0.05)	0.57 (0.03)	H	11.21	-2.12	19.7 (2.9)	50.7 ( 7.4)	8.28	1	2117+539	
21207+5819	DA	8090 (119)	8.03 (0.06)	0.61 (0.04)	H	13.01	-3.22	39.5 (1.8)		9.04	1	2119+581	
21222+0413*	DA	4970 ( 36)	8.00 (0.25)	0.58 (0.15)	H	15.07	-4.06	21.6 (3.4)		9.77	2	2119+040	
21264+5513	DA	13920 (271)	8.53 (0.05)	0.94 (0.03)	H	12.22	-2.59	36.0 (3.9)	27.8 ( 3.0)	8.76	1	2124+550	
21269+7338	DA	15950 (234)	7.97 (0.04)	0.60 (0.03)	H	11.13	-1.99	21.2 (1.1)	47.1 ( 2.4)	8.19	1	2126+734	
21337+8303	DA	17780 (264)	7.99 (0.05)	0.61 (0.03)	H	10.96	-1.81	26.0 (3.1)	38.4 ( 4.5)	8.03	1	2136+828	
21344+3655	DA	7370 (119)	8.17 (0.11)	0.70 (0.07)	H	13.57	-3.46	35.6 (1.8)		9.23	1	2132+367	
21387+2309	DA	10130 (147)	7.93 (0.05)	0.56 (0.03)	H	12.03	-2.77	42.0 (5.5)	23.8 ( 3.1)	8.73	1	2136+229	
21420+2252*	DZ	8170 (150)	8.00 (0.25)	0.58 (0.15)	He	12.88	-3.20	38.9 (1.0)		9.05	2		
21426+2059	DQ	8220 (198)	7.82 (0.06)	0.47 (0.04)	He	12.75	-3.09	12.5 (0.5)	79.9 ( 3.2)	8.91	2	2140+207	
21429+0805*	DA	4830 (515)	8.00 (0.25)	0.58 (0.15)	H	14.74	-4.11	25.1 (6.2)		9.81	2		
21492+0415*	DA	5440 (187)	8.00 (0.25)	0.58 (0.15)	H	14.28	-3.90	26.2 (4.4)		9.53	2		
21499+2816	DB	11920 (237)	8.00 (0.14)	0.59 (0.09)	He	11.85	-2.54	35.3 (3.8)	28.3 ( 3.0)	8.62	1	2147+280	
21524+0223	DA	18200 (265)	8.01 (0.04)	0.63 (0.03)	H	10.95	-1.78	24.5 (1.5)	40.8 ( 2.5)	8.02	1	2149+021	
21551+4103*	DZA	5950 (703)	8.00 (0.25)	0.57 (0.15)	He	14.21	-3.75	37.0 (7.9)		9.42	2		
22097+1429	DA	7570 (110)	8.19 (0.06)	0.71 (0.04)	H	13.50	-3.43	25.5 (2.9)	39.2 ( 4.4)	9.22	1	2207+142	
22105+4532*	DC	5110 (597)	8.00 (0.25)	0.58 (0.15)	H	14.78	-4.01	34.4 (8.1)		9.71	2		

Table 5—Continued

PM I	ST	$T_{\text{eff}}$ (K)	$\log g$	$M/M_{\odot}$	Comp.	$M_V$	$\log L/L_{\odot}$	$D$ (pc)	$\pi$ (mas)	$\log \tau$	Fit <sup>a</sup>	WDname	Notes
22118+5649*	DA	16880 (287)	8.11 (0.05)	0.68 (0.03)	H	11.23	-1.97	22.3 (1.4)		8.21	1		
22133+0349*	DC	4190 (323)	8.00 (0.25)	0.58 (0.15)	H	14.95	-4.36	30.4 (8.9)		9.93	2		
22141+3727	DC	6220 (115)	8.00 (0.25)	0.57 (0.15)	He	13.70	-3.67	39.0 (6.4)		9.35	2	2211+372	
22177+3707	DC	4990 (226)	8.00 (0.25)	0.58 (0.15)	H	14.99	-4.05	23.6 (4.4)		9.76	2	2215+368	
22188+4839	DA	5650 ( 85)	8.00 (0.25)	0.59 (0.15)	H	14.47	-3.83	26.2 (1.2)		9.44	1	2216+484	
22194+2122	DC	4600 (355)	8.00 (0.25)	0.58 (0.15)	H	15.62	-4.19	32.0 (7.3)		9.86	2	2217+211	
22225+1221	DC	4250 (128)	7.74 (0.08)	0.43 (0.04)	H	15.18	-4.20	41.7 (3.4)	24.0 ( 1.0)	9.76	2	2220+121	
22276+1753*	DAZ	6750 (151)	8.28 (0.23)	0.77 (0.15)	H	14.08	-3.68	30.5 (1.3)		9.48	1		
22280+1207	DZ	6950 (126)	8.00 (0.25)	0.58 (0.15)	He	13.54	-3.48	36.4 (1.1)		9.22	2	2225+118	
22309+1523	DA	4820 (478)	8.00 (0.25)	0.58 (0.15)	H	15.30	-4.11	32.8 (7.8)		9.81	2	2228+151	
22418+0432*	DQpec	5000 (—)	8.00 (0.25)	0.57 (0.15)	He	14.83	-4.06	43.4 (6.0)		9.78	2		
22419+1332	DA	6050 ( 73)	8.00 (0.25)	0.59 (0.15)	H	14.14	-3.71	42.3 (7.0)		9.34	2	2239+132	
22490+2236	DA	10470 (151)	8.66 (0.05)	1.02 (0.03)	H	13.13	-3.18	19.0 (1.5)	52.5 ( 4.1)	9.25	1	2246+223	
22497+3623*	DA	5430 (826)	8.00 (0.25)	0.58 (0.15)	H	15.08	-3.90	43.7 (11.0)		9.54	2		
22513+2939	DA	5640 (127)	7.58 (0.16)	0.37 (0.07)	H	13.67	-3.62	20.9 (2.4)	47.8 ( 4.2)	9.18	2	2248+293	1
22536+8130	DC:	5200 (652)	8.00 (0.25)	0.58 (0.15)	H	14.49	-3.98	27.7 (7.4)		9.67	2	2253+812	
22541+1323	DC	4330 (117)	7.98 (0.14)	0.56 (0.08)	H	15.68	-4.29	41.7 (5.7)	24.0 ( 2.0)	9.90	2	2251+131	
22559+0545W	DA	6100 ( 49)	8.14 (0.11)	0.68 (0.07)	H	13.78	-3.78	24.3 (4.6)	41.1 ( 3.0)	9.48	2	2253+054	
22595+5717*	DA	5170 (1286)	8.00 (0.25)	0.58 (0.15)	H	15.34	-3.99	34.9 (18.2)		9.68	2		
23010+4056	DA	9880 (145)	8.17 (0.06)	0.70 (0.04)	H	12.48	-2.95	36.7 (2.1)		8.90	1	2258+406	
23056+4334*	DC	4220 (1039)	8.00 (0.25)	0.58 (0.15)	H	15.86	-4.35	35.7 (44.5)		9.93	2		
23082+2414	DC	4760 (105)	8.00 (0.25)	0.58 (0.15)	H	15.15	-4.14	35.1 (5.8)		9.83	2	2305+239	
23098+5506E*	DA	5700 ( 86)	8.00 (0.25)	0.59 (0.15)	H	14.42	-3.82	16.2 (1.0)		9.42	1		
23121+1310	DA	5110 (113)	8.00 (0.25)	0.58 (0.15)	H	14.65	-4.01	29.8 (5.0)		9.71	2	2309+129	
23162+1720*	DC	4810 ( 61)	8.00 (0.25)	0.58 (0.15)	H	14.99	-4.12	35.2 (5.6)		9.81	2		



Table 5—Continued

PM I	ST	$T_{\text{eff}}$ (K)	$\log g$	$M/M_{\odot}$	Comp.	$M_V$	$\log L/L_{\odot}$	$D$ (pc)	$\pi$ (mas)	$\log \tau$	Fit <sup>a</sup>	WDname	Notes
23220+0946E	DC:	4490 (356)	8.00 (0.25)	0.58 (0.15)	H	15.47	-4.24	46.7 (11.6)		9.88	2	2319+095	
23243+2835*	DA	7060 (118)	7.83 (0.13)	0.50 (0.07)	H	13.27	-3.35	38.6 (1.6)		9.07	1		
23253+1403	DA	5080 ( 58)	7.49 (0.08)	0.32 (0.03)	H	13.95	-3.77	22.3 (1.8)	44.9 ( 2.0)	9.30	2	2322+137	
23259+2552	DA	5940 (111)	8.00 (0.25)	0.59 (0.15)	H	14.23	-3.74	35.8 (1.6)		9.36	1	2323+256	
23261+1600	DC	9980 (356)	8.00 (0.25)	0.58 (0.15)	He	11.90	-2.85	35.5 (6.0)		8.82	2	2323+157.1	
23287+0514	DA	12020 (183)	8.13 (0.05)	0.69 (0.03)	H	11.84	-2.58	13.6 (0.8)	73.4 ( 4.0)	8.65	1	2326+049	
23315+4101	DA	16560 (257)	8.02 (0.05)	0.63 (0.03)	H	11.13	-1.95	34.1 (8.2)	29.3 ( 6.7)	8.17	1	2329+407	
23320+2658	DAH	9540 (896)	8.03 (0.28)	0.62 (0.16)	H	12.17	-2.93	38.6 (7.5)	25.9 ( 4.7)	8.85	2	2329+267	
23389+2101E*	DA	5300 (636)	8.00 (0.25)	0.58 (0.15)	H	14.36	-3.94	40.4 (9.5)		9.61	2		
23438+3232	DA	13030 (199)	8.01 (0.05)	0.62 (0.03)	H	11.54	-2.37	17.6 (0.6)	56.8 ( 1.8)	8.48	1	2341+322	
23462+1158*	DC	5220 (285)	8.00 (0.25)	0.57 (0.15)	He	14.77	-3.98	34.0 (6.0)		9.71	2		
23475+0304*	DC	4900 ( 47)	8.00 (0.25)	0.58 (0.15)	H	15.12	-4.08	22.7 (3.6)		9.79	2		
23478+0223*	DA	5120 ( 48)	8.00 (0.25)	0.58 (0.15)	H	14.87	-4.01	42.7 (6.9)		9.71	2		
23489+4300*	DC:	4810 ( 63)	8.00 (0.25)	0.58 (0.15)	H	15.12	-4.11	36.2 (5.9)		9.81	2		
23499+2934	DA	5850 (143)	7.86 (0.14)	0.51 (0.08)	H	14.19	-3.69	21.5 (2.6)	46.5 ( 4.1)	9.29	2	2347+292	
23532+2051	DA	7390 (152)	8.00 (0.25)	0.59 (0.15)	H	13.10	-3.36	44.9 (7.7)		9.12	2	2350+205	
23549+4027	DQ	7200 (723)	7.65 (0.25)	0.39 (0.11)	He	12.84	-3.24	25.8 (3.8)	38.7 ( 5.6)	8.98	2	2352+401	

Note. — (1) Double degenerate binary (or candidate). (2) Gianninas et al. (2011). (3)  $D$  from Vennes & Kawka (2012). (4) DXP+DA:  $T_{\text{eff}}$ ,  $\log g$  and  $D$  come from Liebert et al. (1993) and belong to the DA component; the values given for the companion are  $T_{\text{eff}} = (16,000 \pm 2000)$  K and  $\log g = 8.5 \pm 0.2$ . (5) Trigonometric parallax from Dahn et al. (1982).

<sup>a</sup>Fit: (1) spectroscopic, (2) photometric.

\*New WD identified in this survey.

Fig. 1.— Absolute visual magnitude as a function of photometric distance for spectroscopically confirmed white dwarfs (top) and our remaining candidates (bottom). In the upper panel, the filled circles represent the 325 new white dwarfs identified in our survey, while the open circles correspond to the 416 white dwarfs already known in the literature. Dashed lines in the figure are lines of constant apparent  $V$  magnitudes. The 592 remaining white dwarf candidates in our survey, still awaiting spectroscopic confirmation, are shown in the lower panel. Lower-priority candidates (those identified on the basis USNO photographic magnitudes and those with  $V > 18$ ) are shown with cross symbols.

Fig. 2.— Optical spectra for our new, spectroscopically confirmed DA white dwarfs, displayed in order of decreasing effective temperature (upper left to bottom right) and shifted vertically for clarity; 05431+3637 is a DAZ star. The  $H\alpha$  line is also shown when available, and normalized to a continuum set to unity. The last 3 spectra at the bottom of the right panel are new observations of stars already presented in Paper I that are double degenerate binary candidates.

Fig. 3.—  $H\alpha$  line for our new, spectroscopically confirmed DA stars, too cool to exhibit the rest of the Balmer series. Spectra are displayed in order of right ascension, normalized to a continuum set to unity, and shifted vertically for clarity.

Fig. 4.— Spectra of our newly identified, magnetic DA white dwarfs, shifted vertically for clarity. 04523 + 2519 was classified as non-magnetic in Paper I. All others are new white dwarf discoveries.

Fig. 5.— Spectra of our newly identified binary systems composed of a DA white dwarf and an M dwarf companion. Spectra are shifted vertically for clarity. The hydrogen line cores are often contaminated by line emission from the chromospherically active M dwarf.

Fig. 6.— New spectra of DZ (DZA), DB (DBZ), and DQ stars. Spectra for the DZ stars 01216+3440, 03196+3630, 16477+2636, 21420+2252, and 23003+2204 represent new higher S/N observations of stars reported in Paper I, used to better constrain the metal abundances.

Fig. 7.— Optical spectra for our new, spectroscopically confirmed DC stars. All spectra are normalized to a continuum set to unity and are offset from each other by a factor of 0.9.

Fig. 8.—  $(u - g, g - r)$  color-color diagram showing all stars in our survey for which *ugriz* photometry is available. The 151 spectroscopically confirmed white dwarfs are shown with various black symbols explained in the legend, while the 125 white dwarf candidates still lacking spectroscopic data are shown with red dots. The solid curves represent pure hydrogen model atmospheres at  $\log g = 7.0, 8.0,$  and  $9.0$  (from bottom to top); effective temperatures

are indicated in units of  $10^3$  K. The dashed curve corresponds to pure helium atmospheres at  $\log g = 8.0$ , and the dotted lines represent DQ models for 5 different compositions, from  $\log C/He = -9.0$  to  $-5.0$ .

Fig. 9.— Upper panel: Equal cylindrical projection of the equatorial coordinates for the sample of white dwarfs identified from SUPERBLINK. The 416 previously known stars from the WD Catalog recovered by our selection criteria (open circles) are compared to the 325 new WD identifications (solid circles). Also shown by the bold solid line is the region of the galactic plane. Lower panel: Sky density as a function of right ascension, normalized to the total number of white dwarf stars (all lines are thus on a comparable scale). The dotted line represents the 416 stars from the WD Catalog recovered by our selection criteria, while the dashed line corresponds to the 325 new identifications only. Finally, the solid line represents the sum of the contributions of the new and known white dwarfs.

Fig. 10.— Sample fits to the photometric energy distributions (represented by error bars) of 5 new white dwarf identifications with pure hydrogen models (filled circles) and with pure helium models (open circles). The adopted solution is indicated in red. In the right panels are shown the observed normalized spectra together with the synthetic line profiles calculated with the atmospheric parameters corresponding to the pure hydrogen solutions.

Fig. 11.— Same as Figure 10 but for all DC and cool DA stars in our sample.

Fig. 12.— Fits to the observed energy distributions for the new DQ identifications. The filled circles correspond to our best fit to the photometry, and the atmospheric parameters and carbon abundances are given in each panel. In the right panels are shown the observed spectra together with the predicted model fit (in red).

Fig. 13.— Fits to the energy distributions for the new DZ identifications. The filled circles correspond to our best fit with the atmospheric parameters given in each panel. In the right panels are shown the observed spectra together with the predicted model fit (in red); the insert shows our fit to  $H\alpha$ , when detected.

Fig. 14.— Fits to the optical spectra of the DA stars in our sample. The lines range from either  $H\alpha$  (when available) or  $H\beta$  (bottom) to  $H8$  (top), each offset vertically by a factor of 0.2. Theoretical line profiles shown in green are not used in the fitting procedure.

Fig. 15.— Fits to the optical spectra for the 4 new DB stars in our sample; the atmospheric parameters ( $T_{\text{eff}}$ ,  $\log g$ , and  $\log H/He$ ) of each object are given in the figure. When available, the region near  $H\alpha$  is used to measure the hydrogen abundance.

Fig. 16.— Same as Figure 10 but for 4 double degenerate binary candidates in our sample.

Fig. 17.— Spectroscopic fits to 2 of our double degenerate binary candidates (04263+4820 and 11598+0007) and to the DA + DA white dwarf binary SDSS 1257+5428 (see text).

Fig. 18.— Our best spectroscopic fit to the helium-rich DAZB white dwarf 01489+1902 (GD 16); the insert shows the region covering the  $H\alpha$  line profile.

Fig. 19.— Cumulative number of stars as a function of distance, for our northern hemisphere census. The solid curve shows the expected number of white dwarfs in one hemisphere, assuming an average space density of  $4.8 \times 10^{-3} \text{ pc}^{-3}$ , while the dotted curve represents the expected number of white dwarfs on the whole celestial sphere.

Fig. 20.— Velocity-space projections for the white dwarfs within 40 pc of the Sun. Velocities are calculated assuming  $V_{\text{rad}} = 0$ , and using only the projections having the smallest contribution to  $V_{\text{rad}}$ . Each star is thus displayed in one panel only. The new white dwarf identifications are plotted with solid circles, while those already known in the literature are shown by open circles; the red circles at  $(0, 0)$  indicate our limit of detection.

Fig. 21.— Mass as a function of effective temperature for the 288 white dwarfs in the 40 pc sample with mass determinations; the 204 white dwarfs fitted with an assumed  $\log g = 8.0$  value are displayed at the bottom the figure. Also shown are theoretical isochrones for our C/O core evolutionary models with thick hydrogen layers labeled in Gyr; solid lines correspond to white dwarf cooling ages only, while the dotted lines also include the main sequence lifetime. The dashed line represents a  $0.661 M_{\odot}$  sequence, which corresponds to the median mass of our sample.

Fig. 22.— Mass distribution for the white dwarfs in our sample that have mass determinations. The thick solid line histogram shows the distribution for the 288 stars with  $D < 40$  pc, while the red and blue shaded histograms correspond, respectively, to the subsamples of 248 hydrogen- and 40 helium-atmosphere white dwarfs. The corresponding mean values and standard deviations are given in the figure.

Fig. 23.— Mass distribution for the white dwarfs in the 40 pc sample with mass determinations, compared with the mass distribution for the 20 pc sample (Giammichele et al. 2012), for the DA stars in the SDSS DR4 (Tremblay et al. 2011), and for the DA stars in the WD Catalog (Gianninas et al. 2011). Note that the peaks of the WD Catalog and 40 pc sample distributions are superposed.

Fig. 24.— Distribution of the various spectral types for the white dwarfs in the 40 pc sample as a function of effective temperature. The number of stars of each spectral type is indicated in the panels.

Fig. 25.— Left panel: total number of white dwarfs (solid-line histogram) and hydrogen-atmosphere white dwarfs (hatched histogram) as a function of effective temperature. Right panel: ratio of helium-atmosphere white dwarfs to the total number of stars as a function of effective temperature.

Fig. 26.— Left panel: total number of white dwarfs in the 7000 – 9000 K temperature bin (solid-line histogram) and hydrogen-atmosphere white dwarfs (hatched histogram) as a function distance. Right panel: ratio of helium-atmosphere white dwarfs to the total number of stars in the same temperature bin as a function of distance.

Fig. 27.— Luminosity function for our sample of white dwarfs within 40 pc of the Sun as a function of  $M_{\text{bol}}$  (red line), compared to the luminosity functions obtained by Giammichele et al. (2012) for the 20 pc sample, by Harris et al. (2006) for white dwarfs in the SDSS, and by Bergeron et al. (2011) for the DA and DB stars in the PG survey; the number of stars in each magnitude bin is given for the 40 pc sample only. The approximate temperature scale for a  $M = 0.6 M_{\odot}$  sequence is shown at the top of the figure.

Fig. 28.— Luminosity function for our sample of white dwarfs within 40 pc of the Sun as a function of  $M_{\text{bol}}$  (red line), given in half-magnitude bins, compared with theoretical luminosity functions from Fontaine et al. (2001) for a total age of 10, 11, and 12 Gyr. The approximate temperature scale for a  $M = 0.6 M_{\odot}$  sequence is shown at the top of the figure.

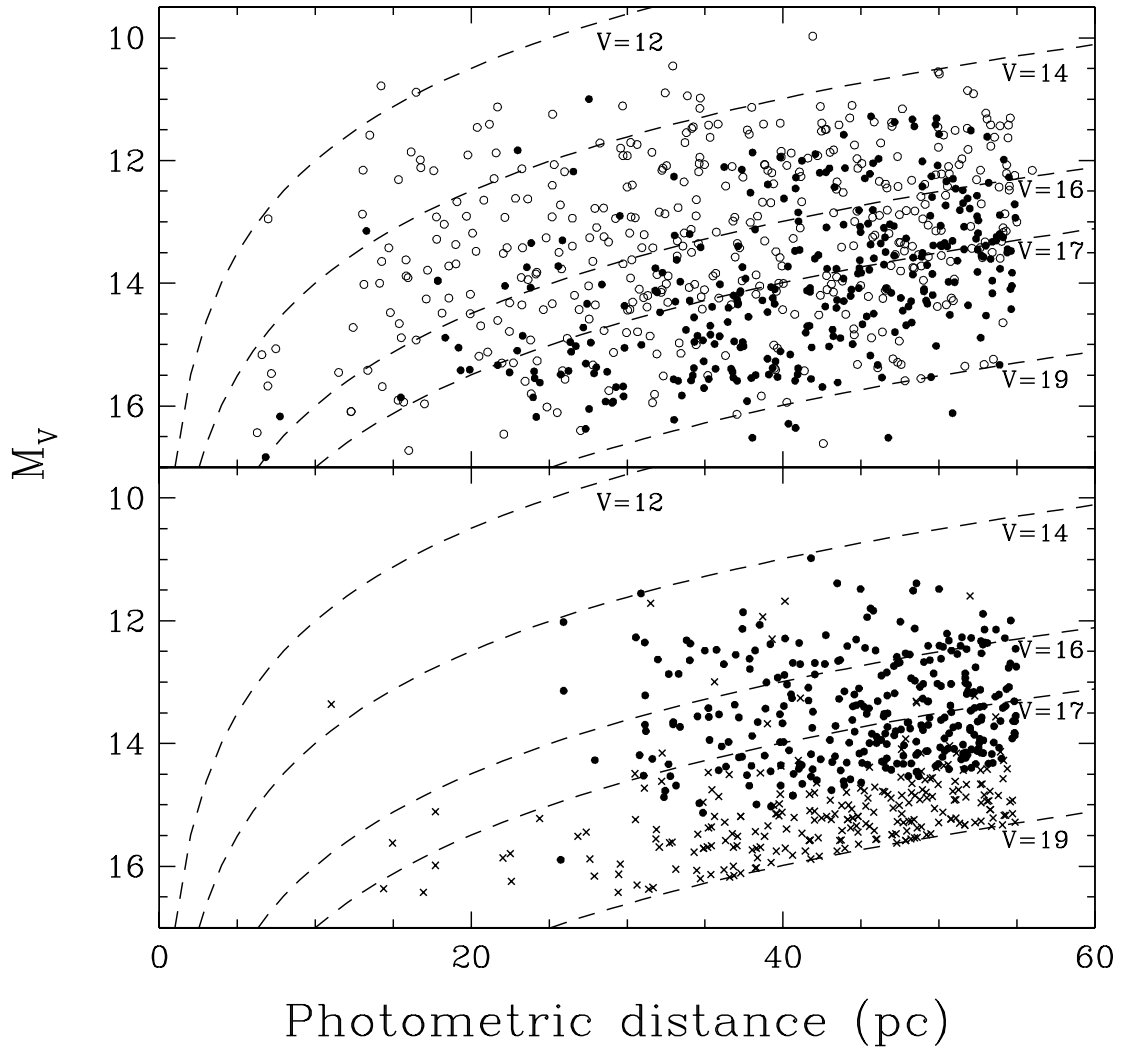


Figure 1

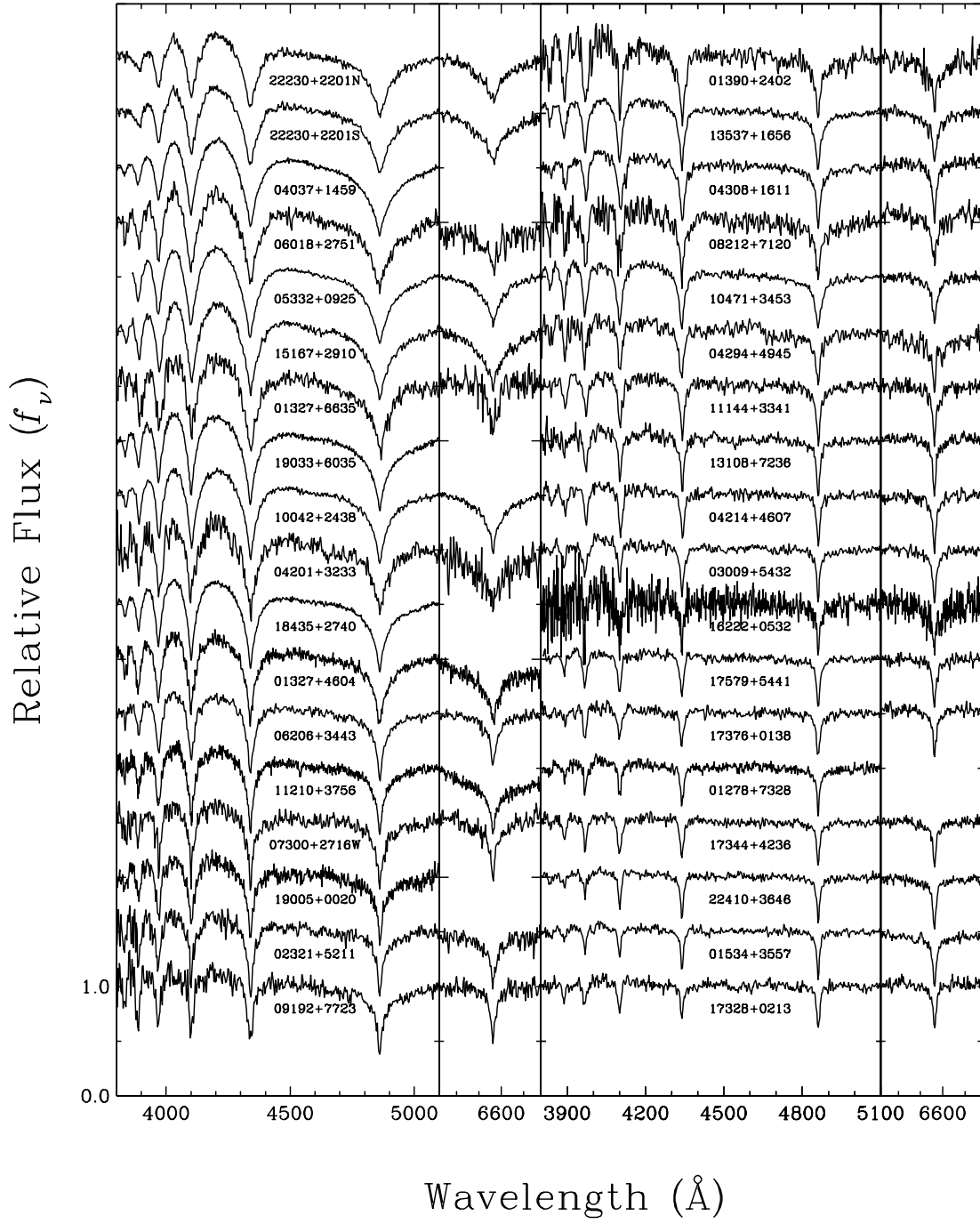


Figure 2a

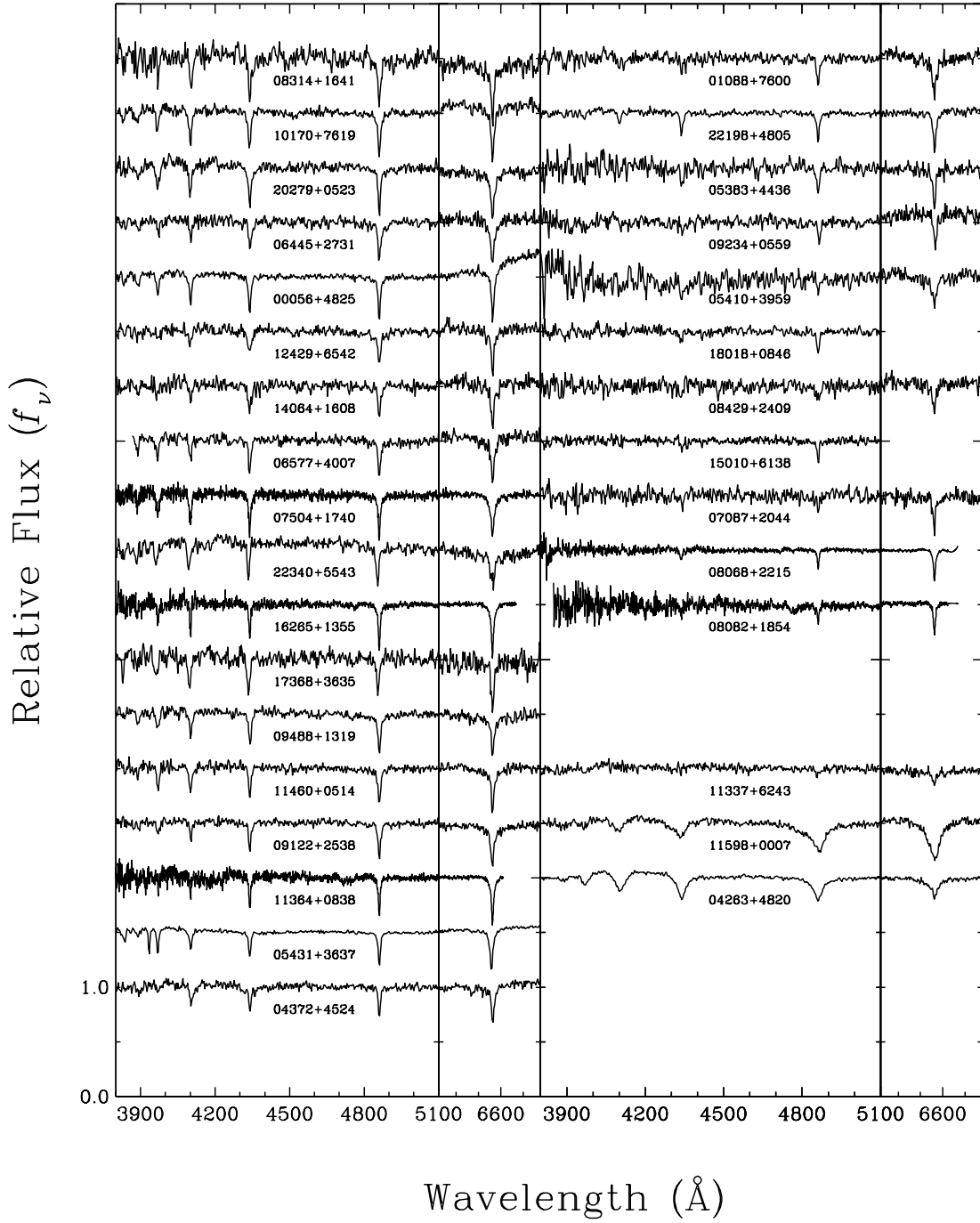


Figure 2b



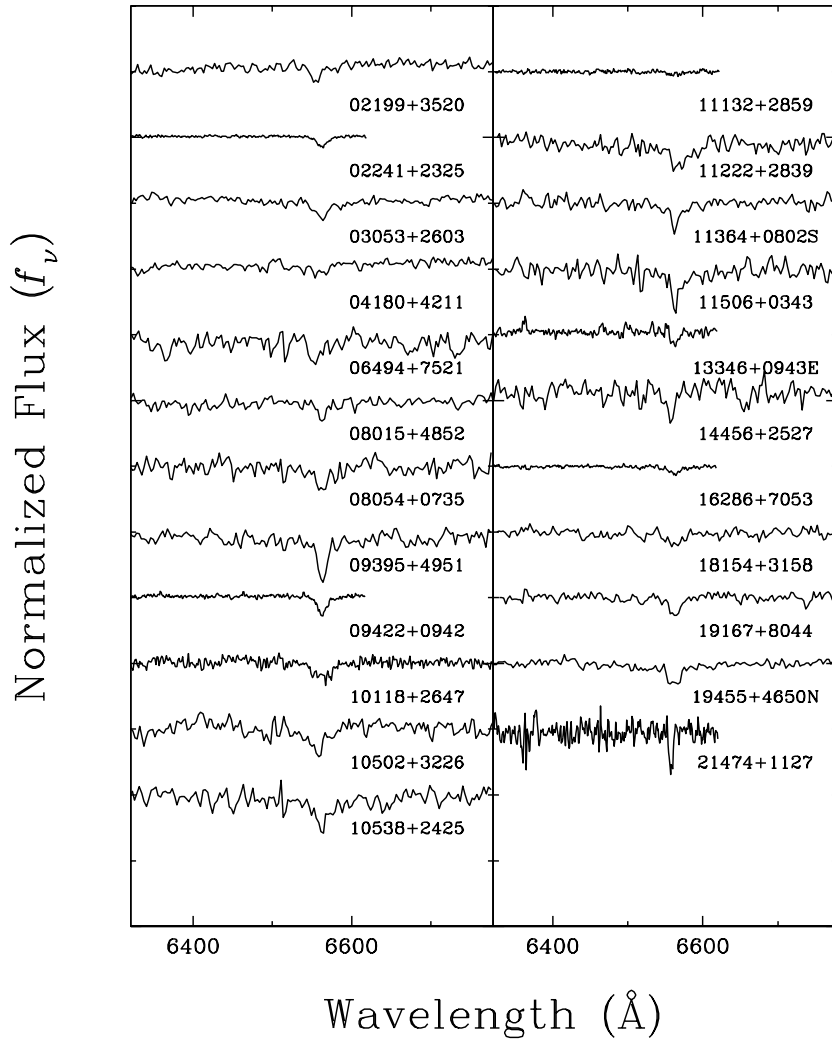


Figure 3

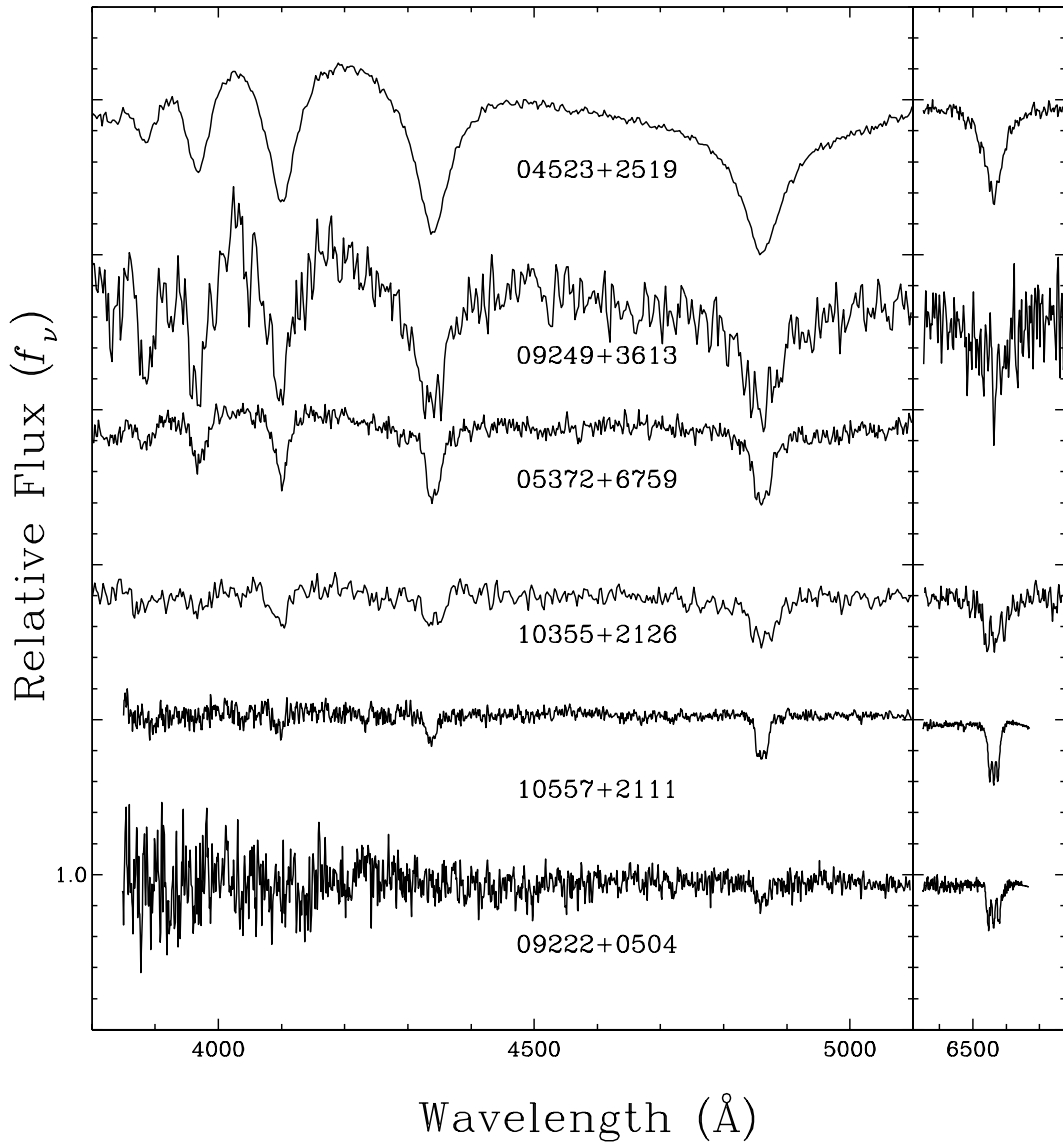


Figure 4

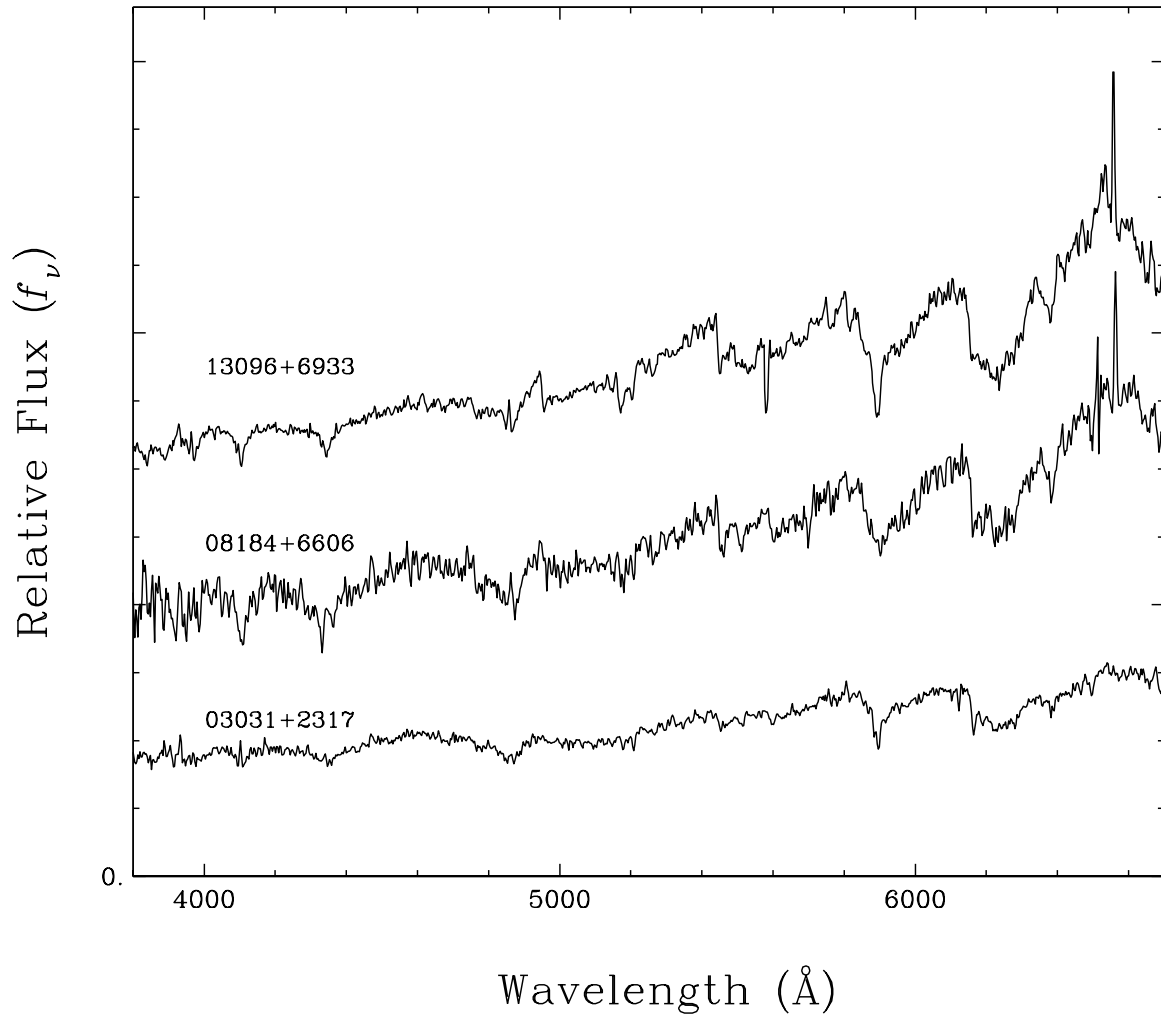


Figure 5

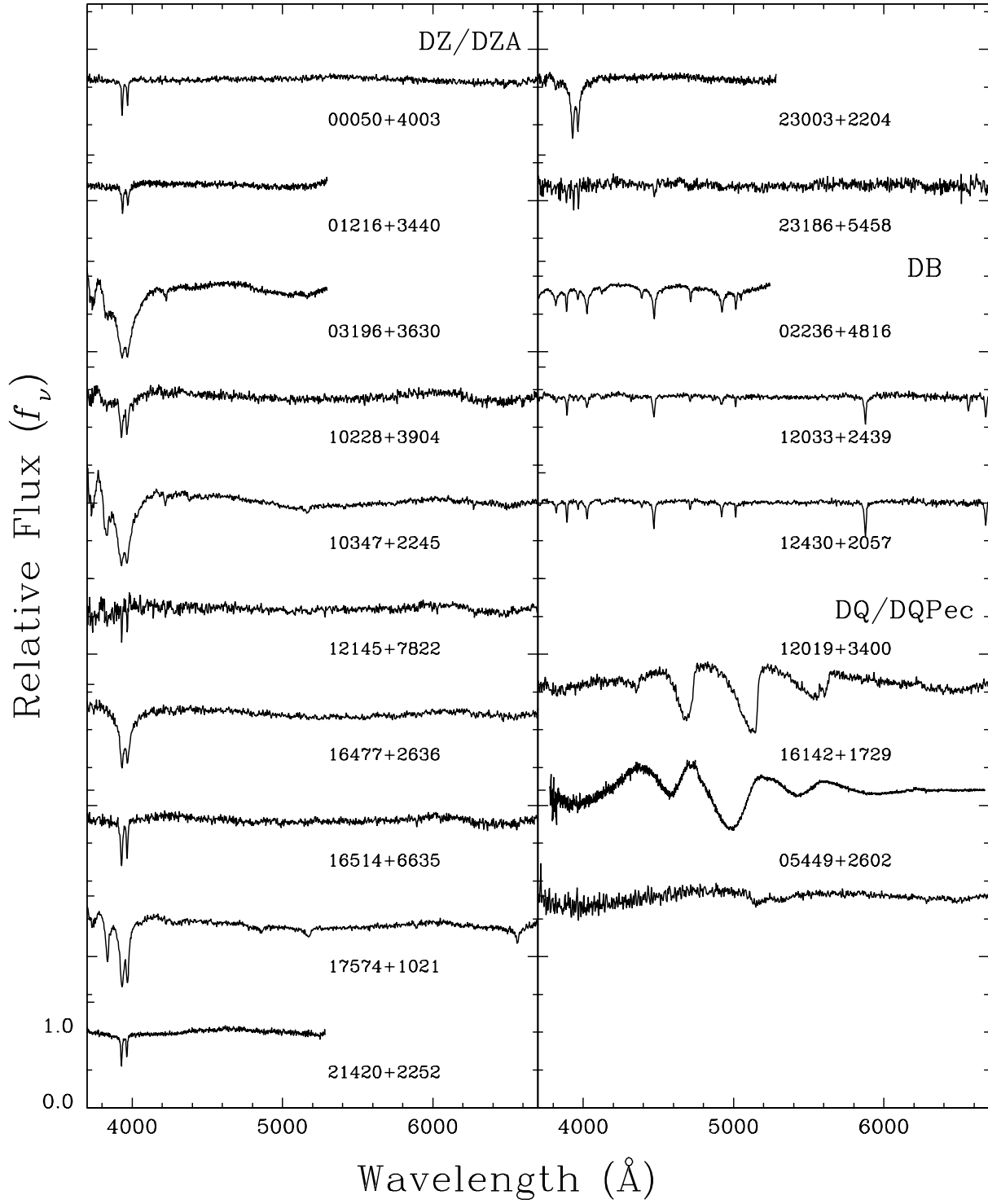


Figure 6

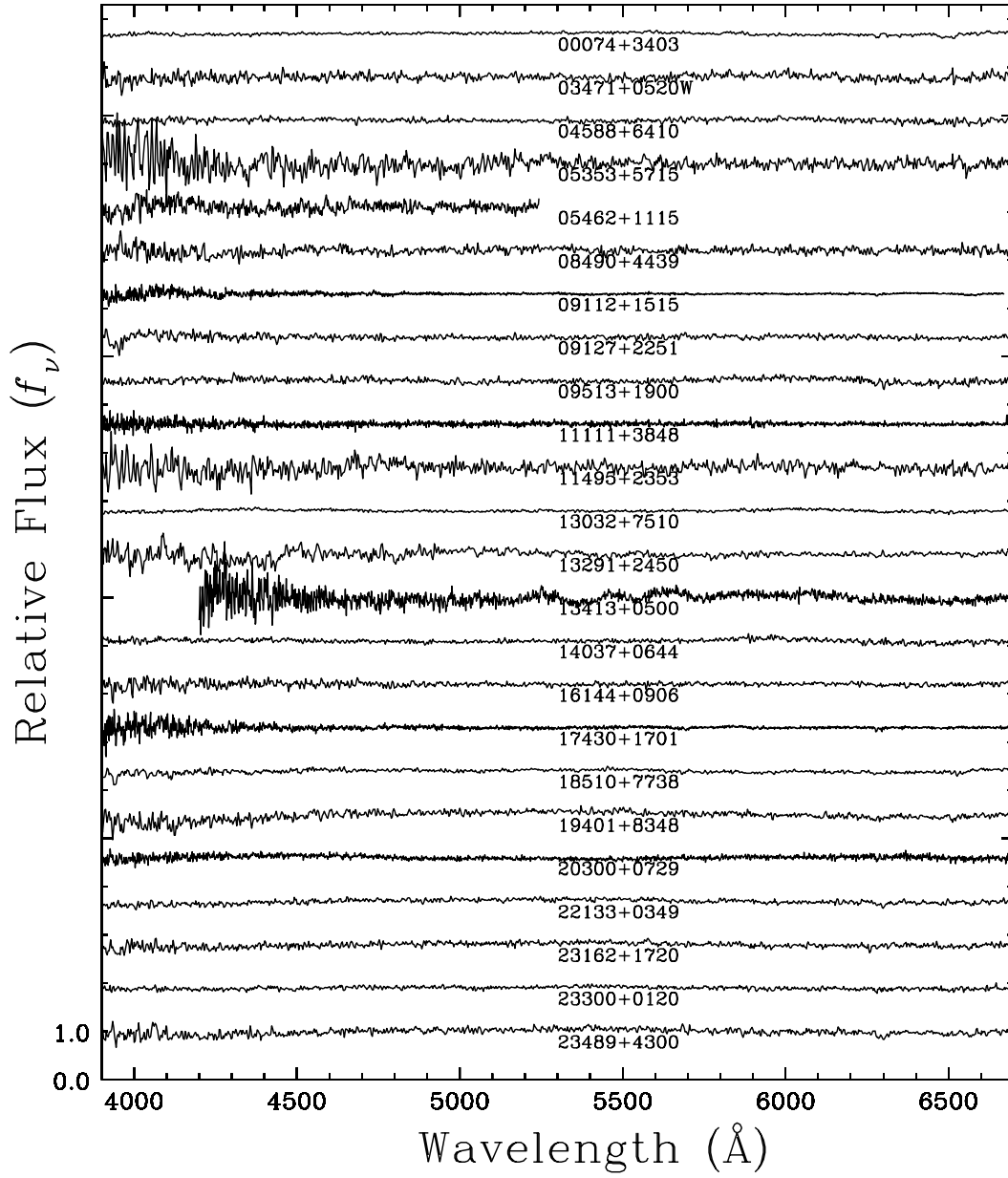


Figure 7

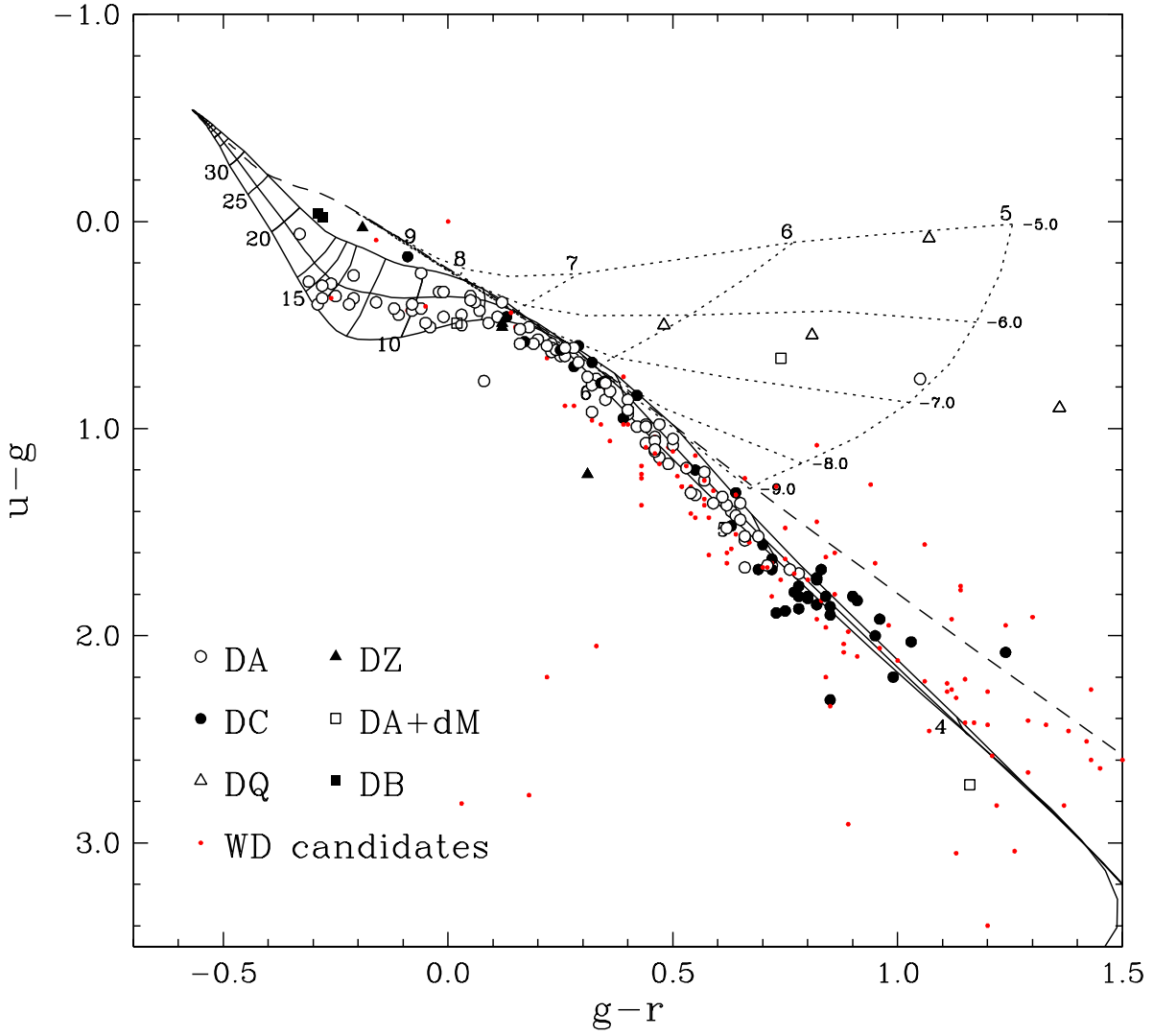


Figure 8

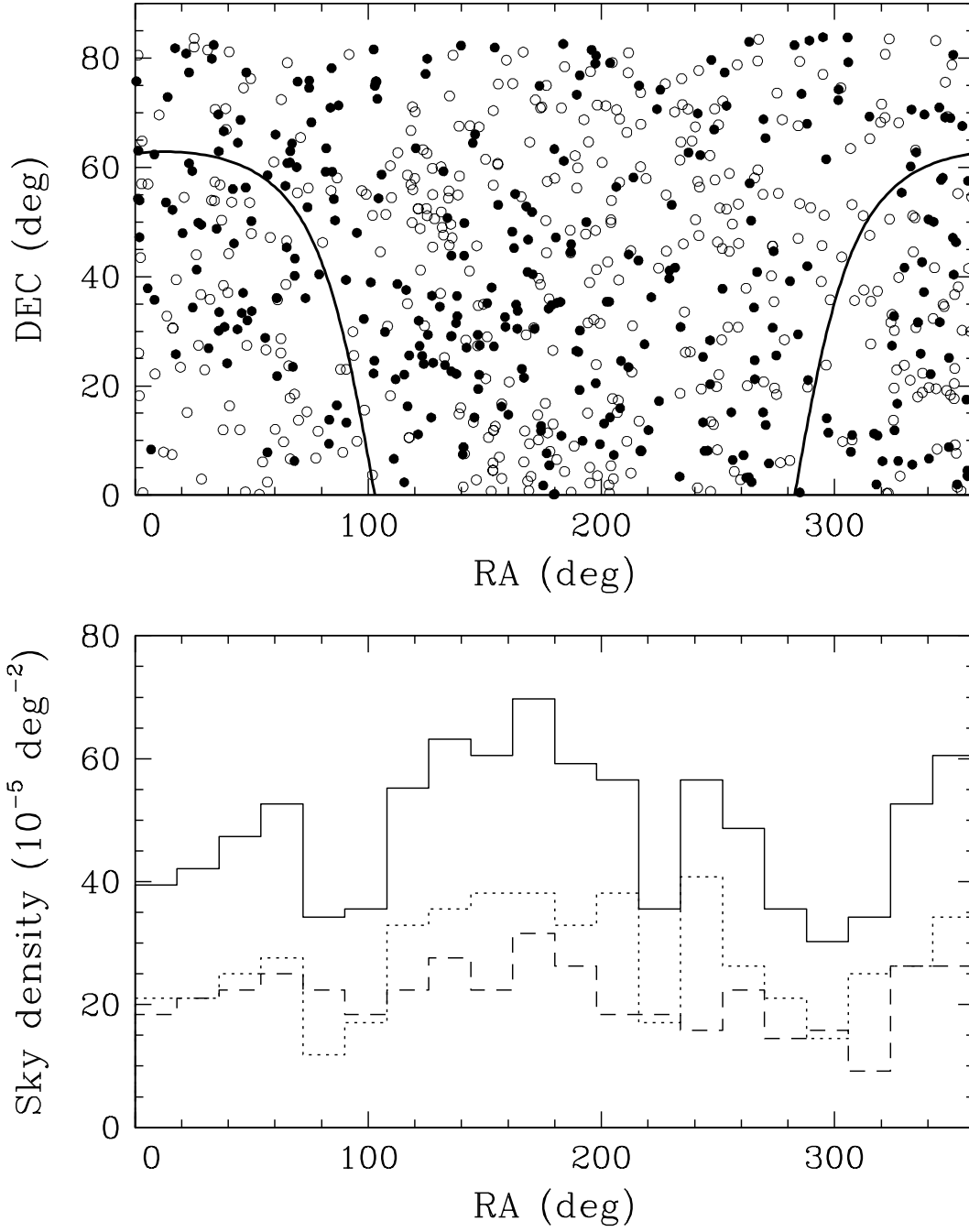


Figure 9

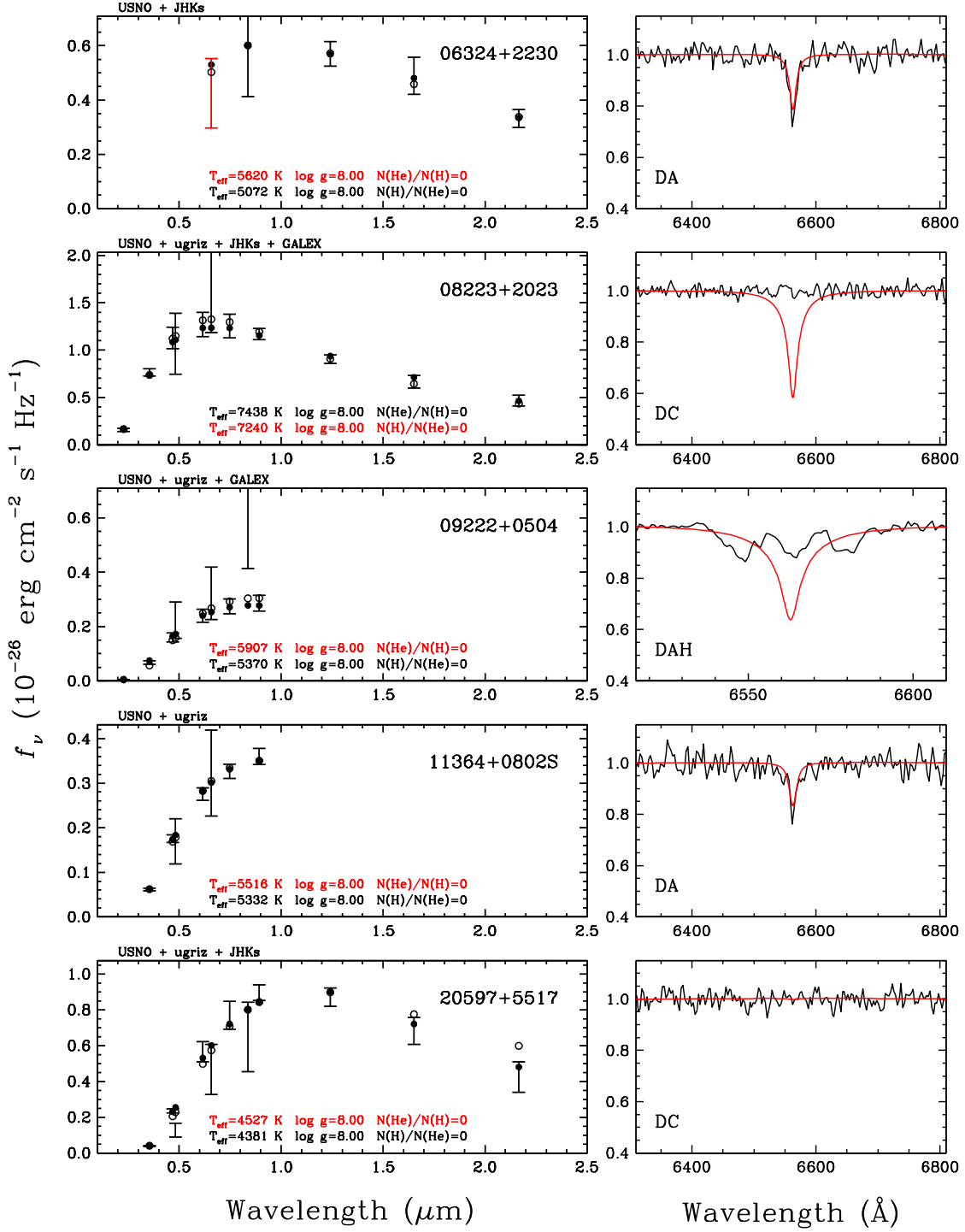


Figure 10



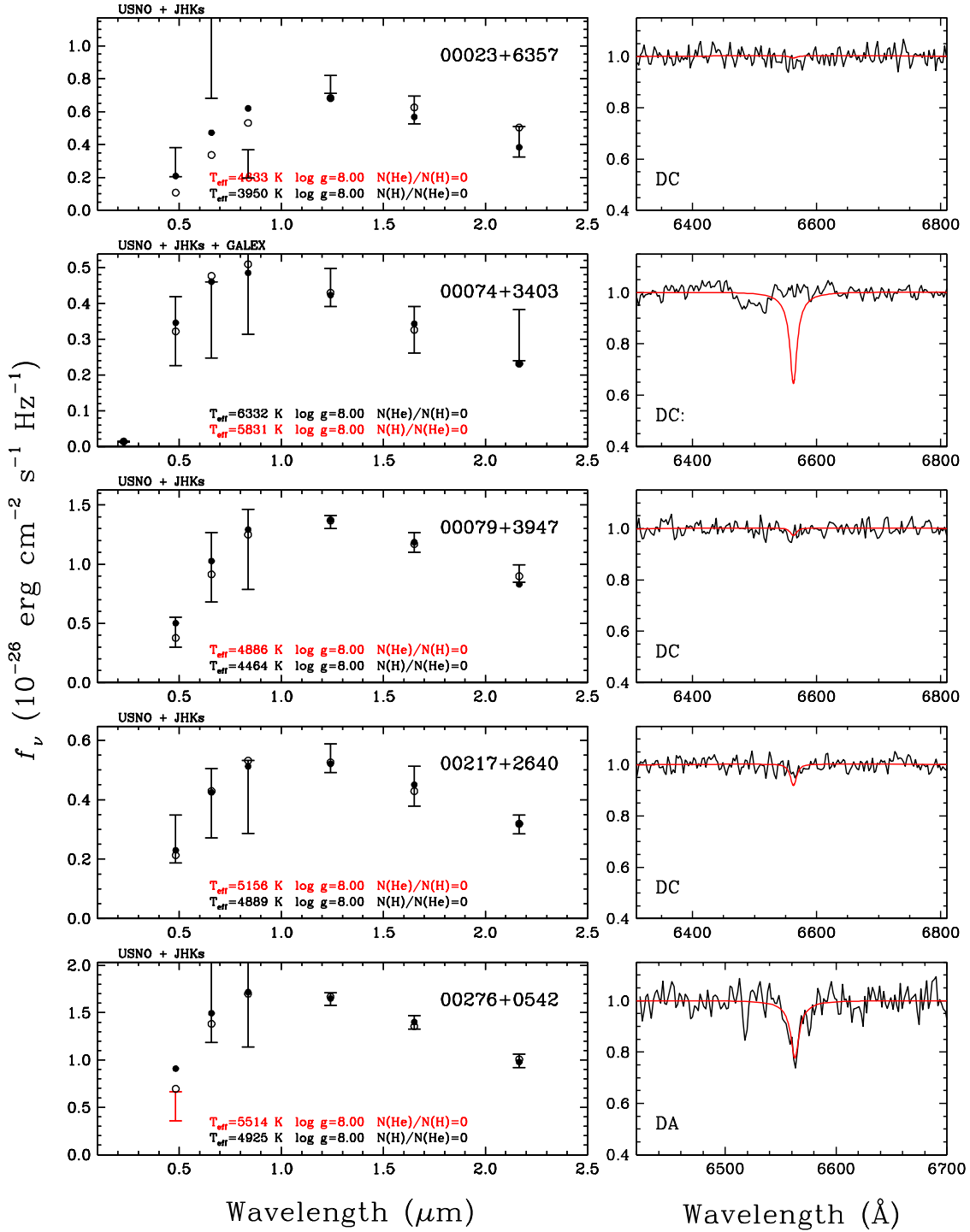


Figure 11a

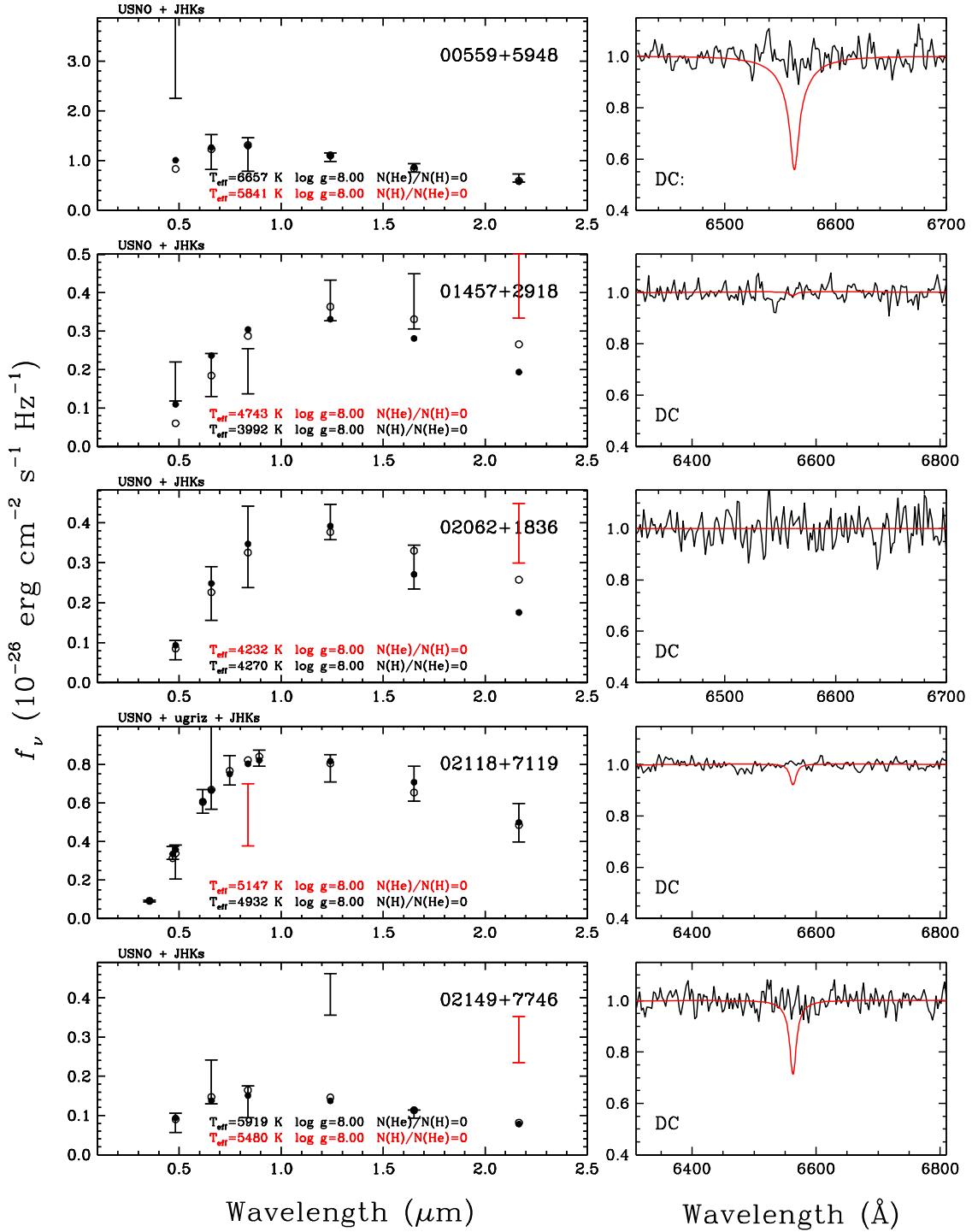


Figure 11b

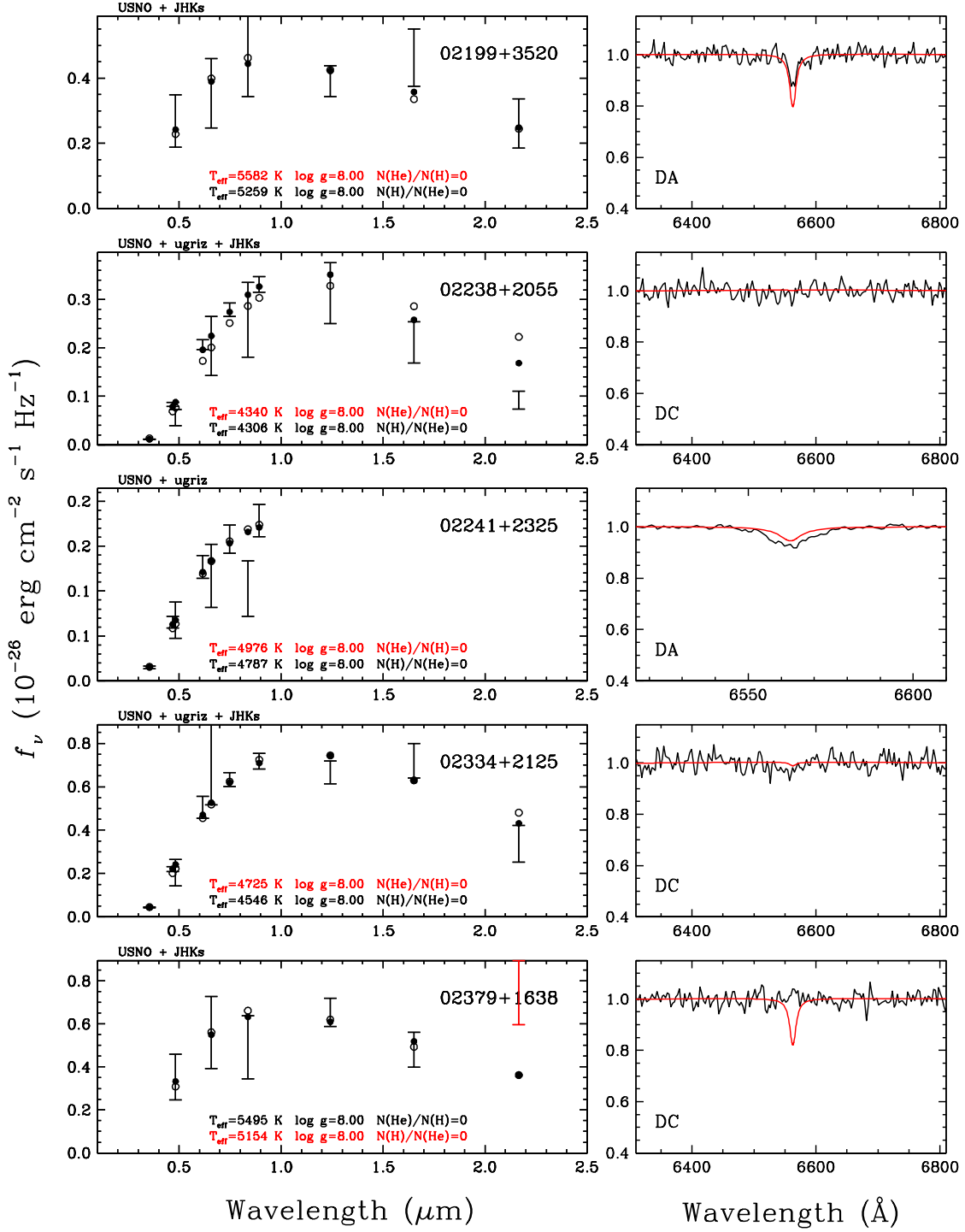


Figure 11c

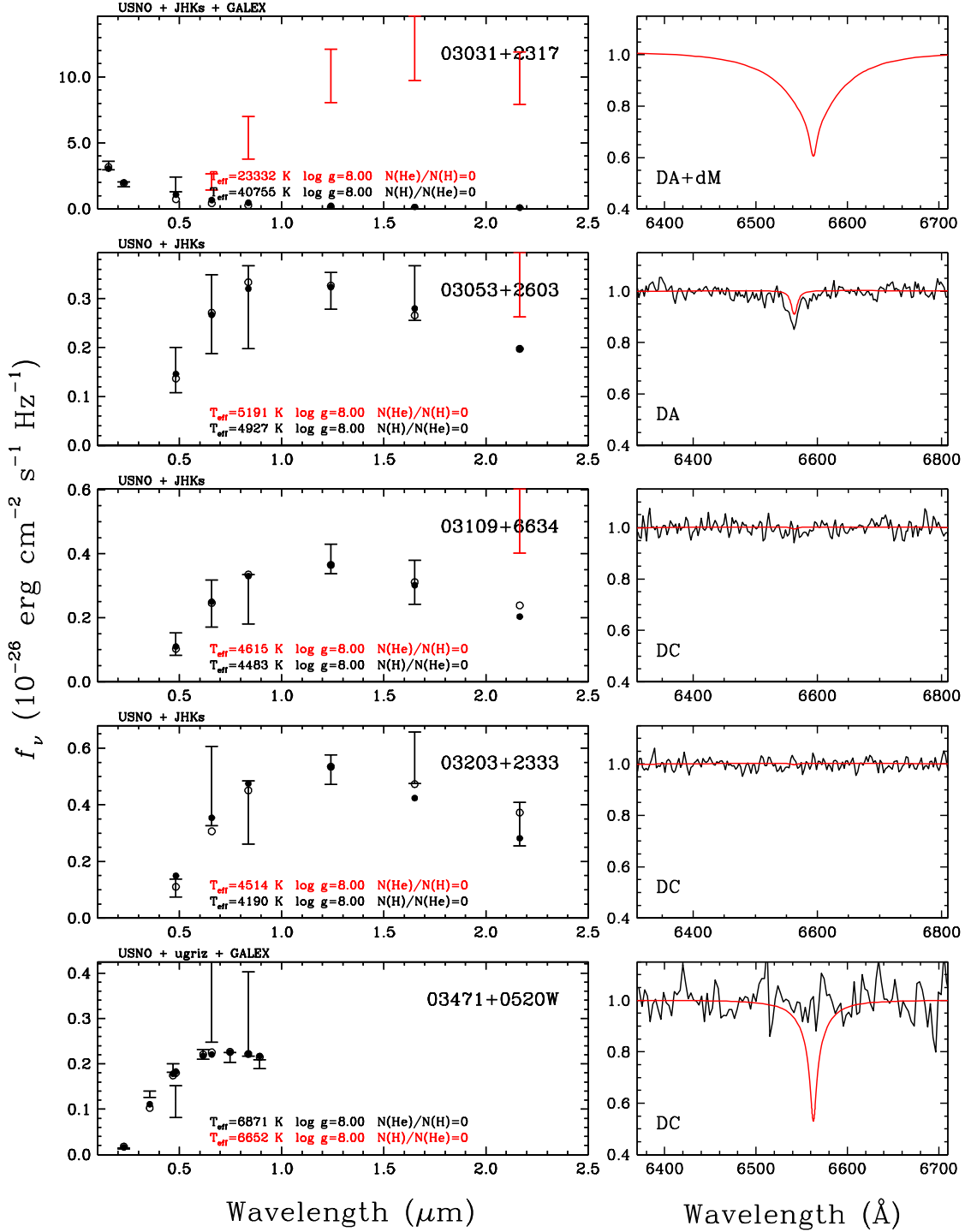


Figure 11d

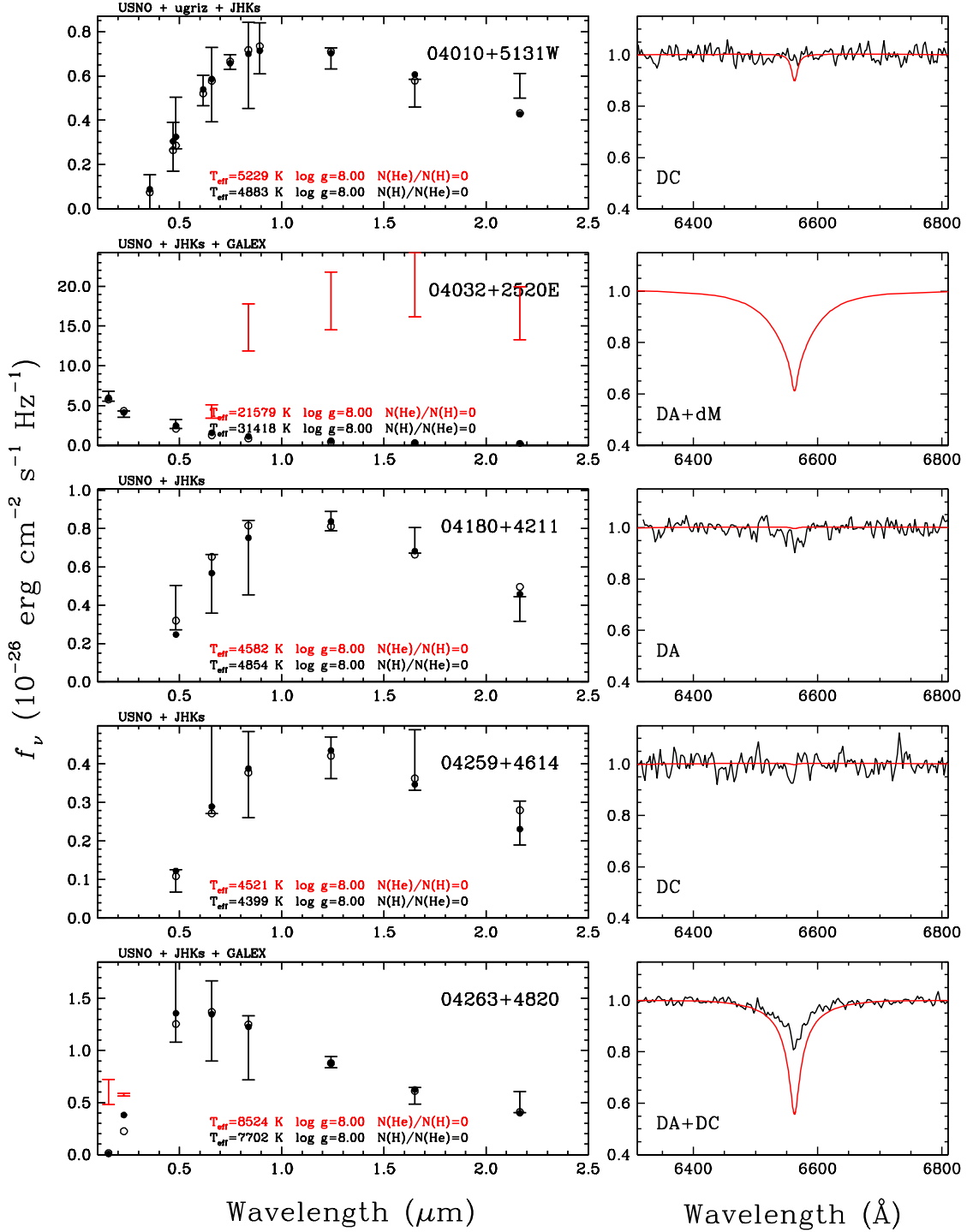


Figure 11e

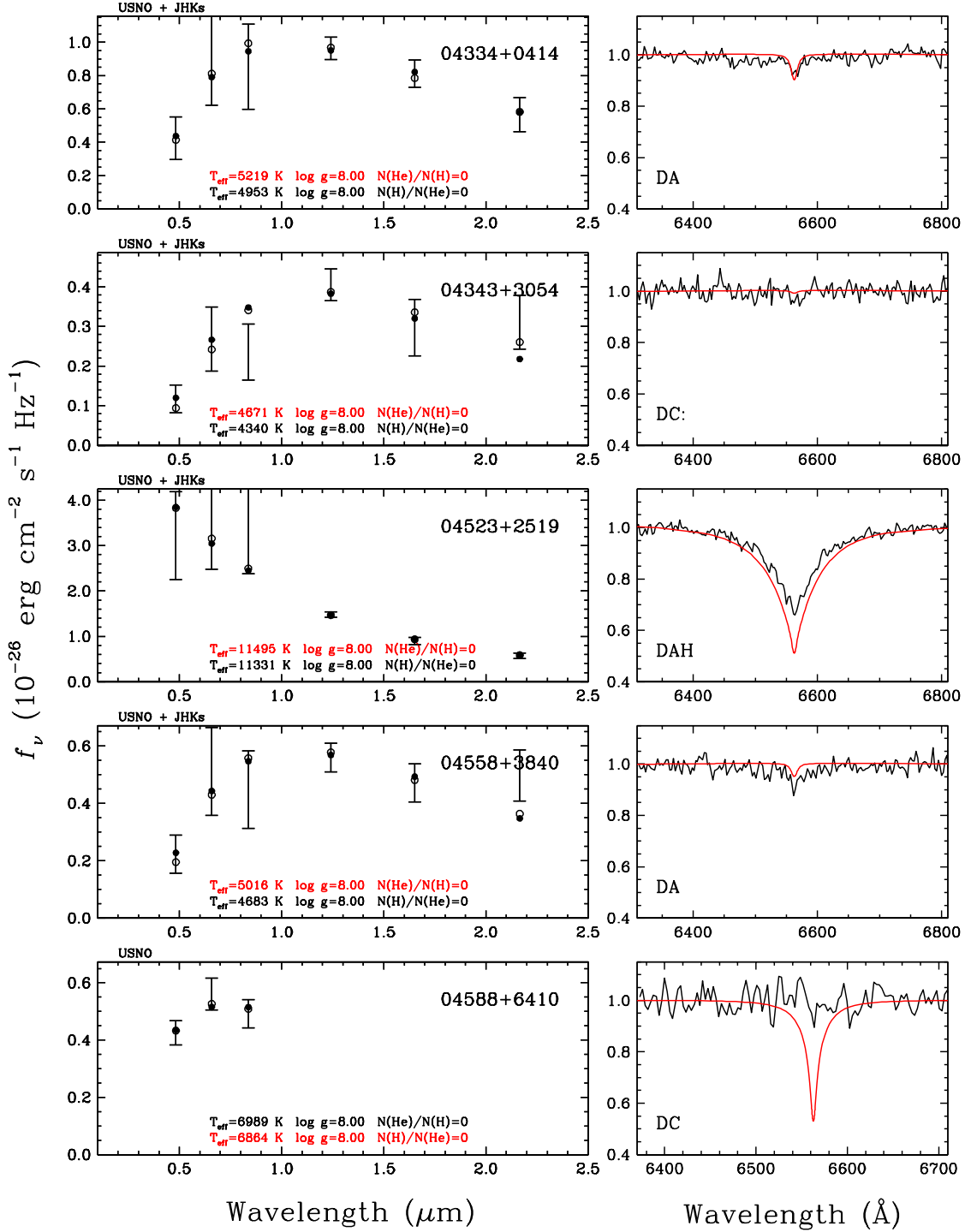


Figure 11f

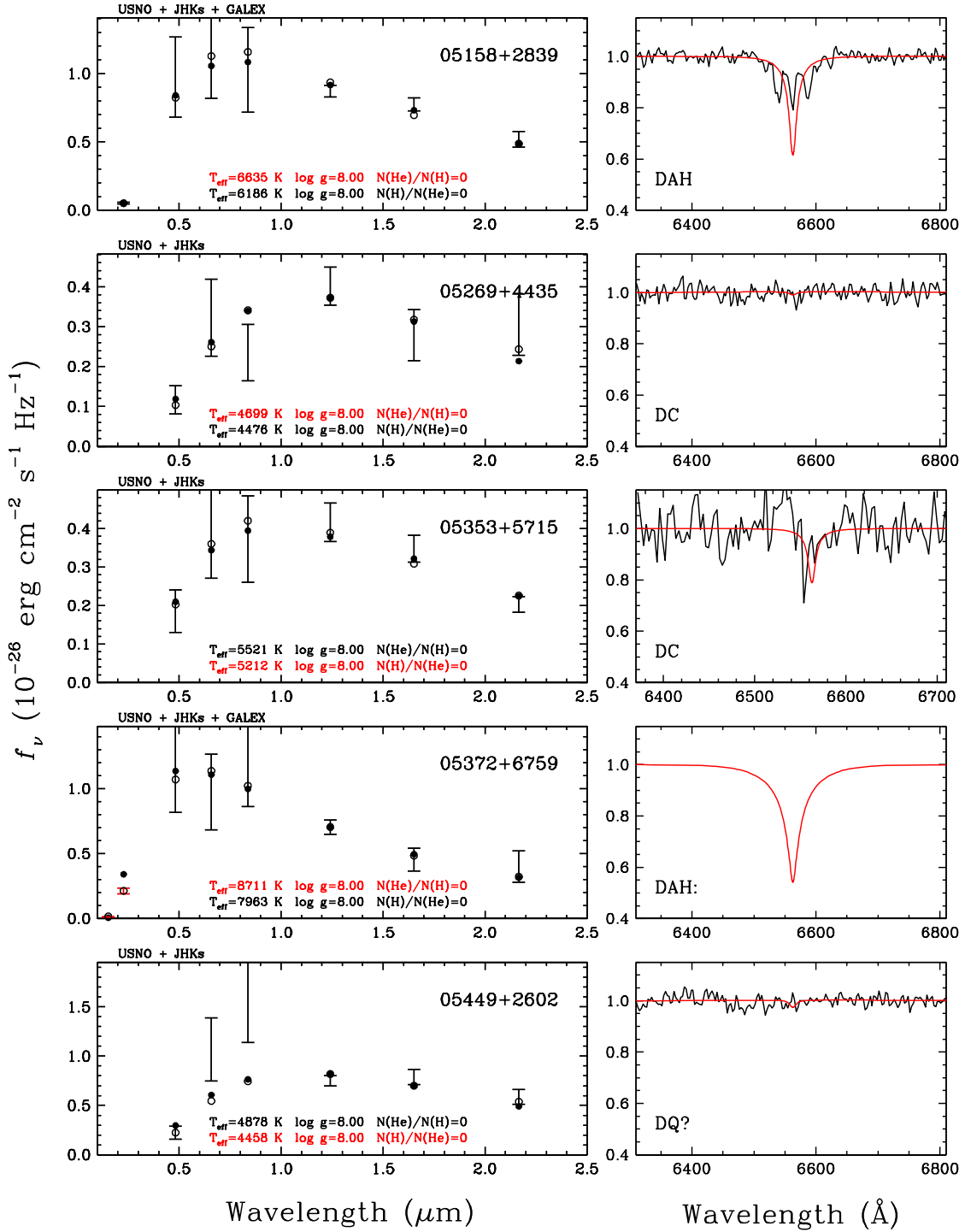


Figure 11g

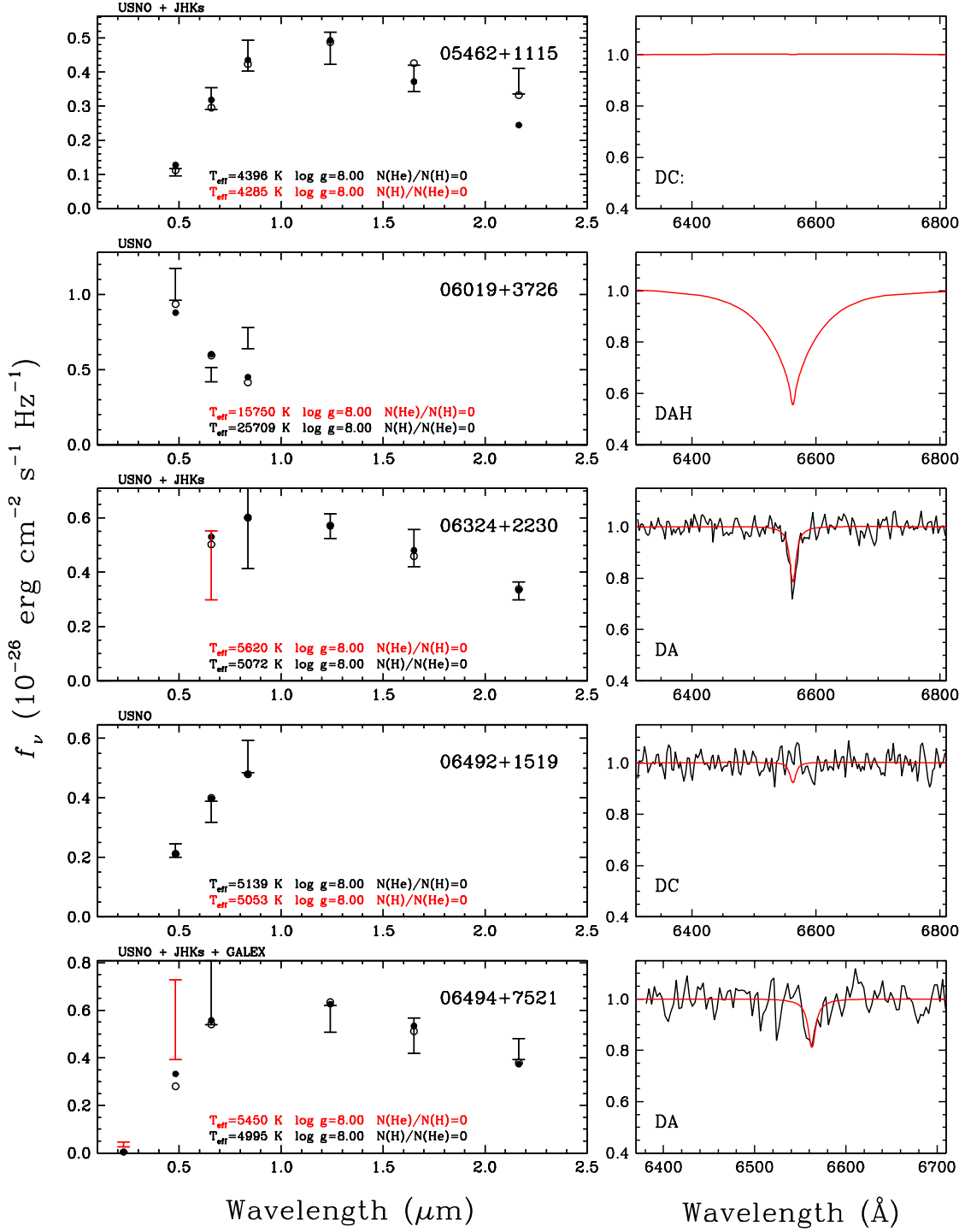


Figure 11h



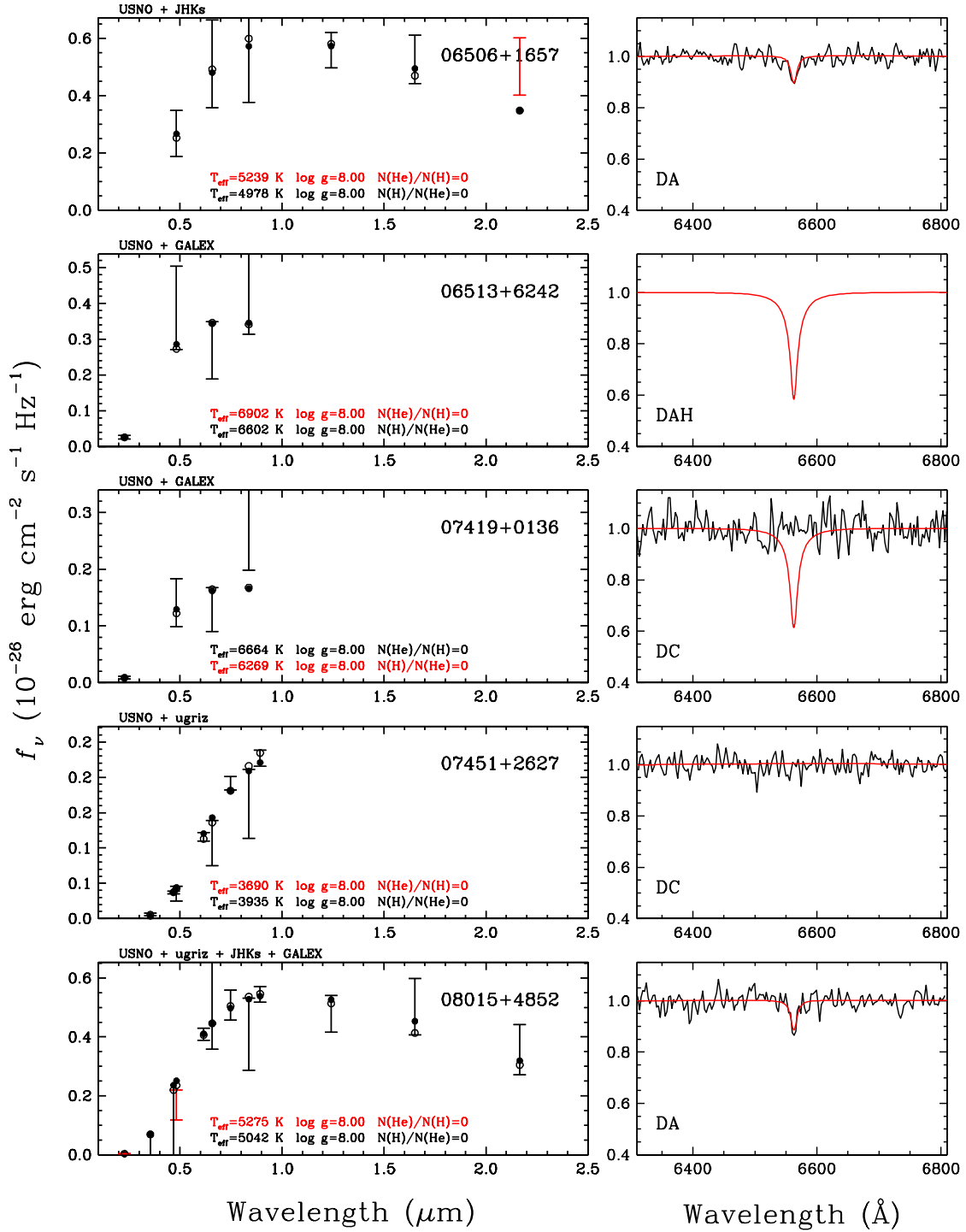


Figure 11i

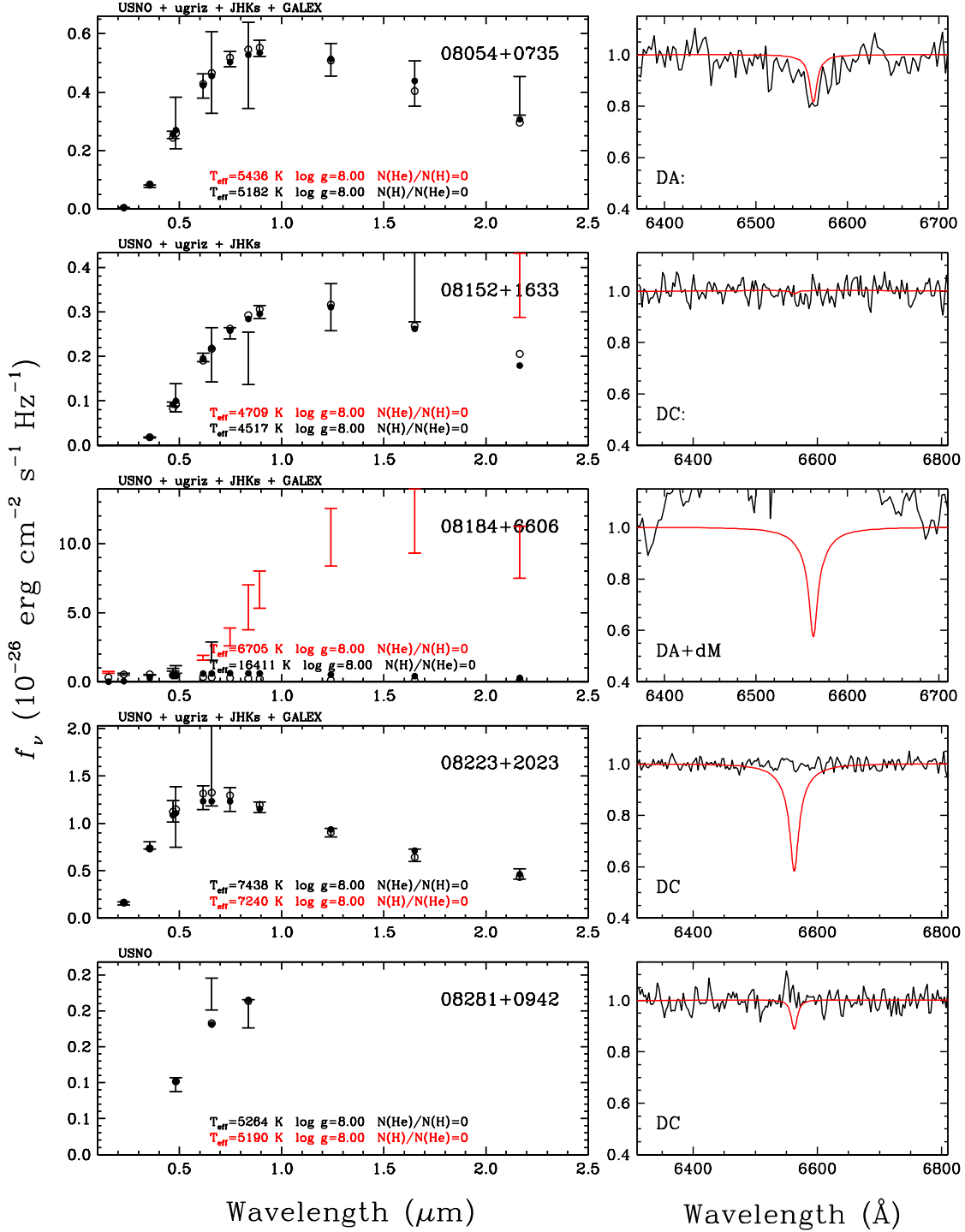


Figure 11j

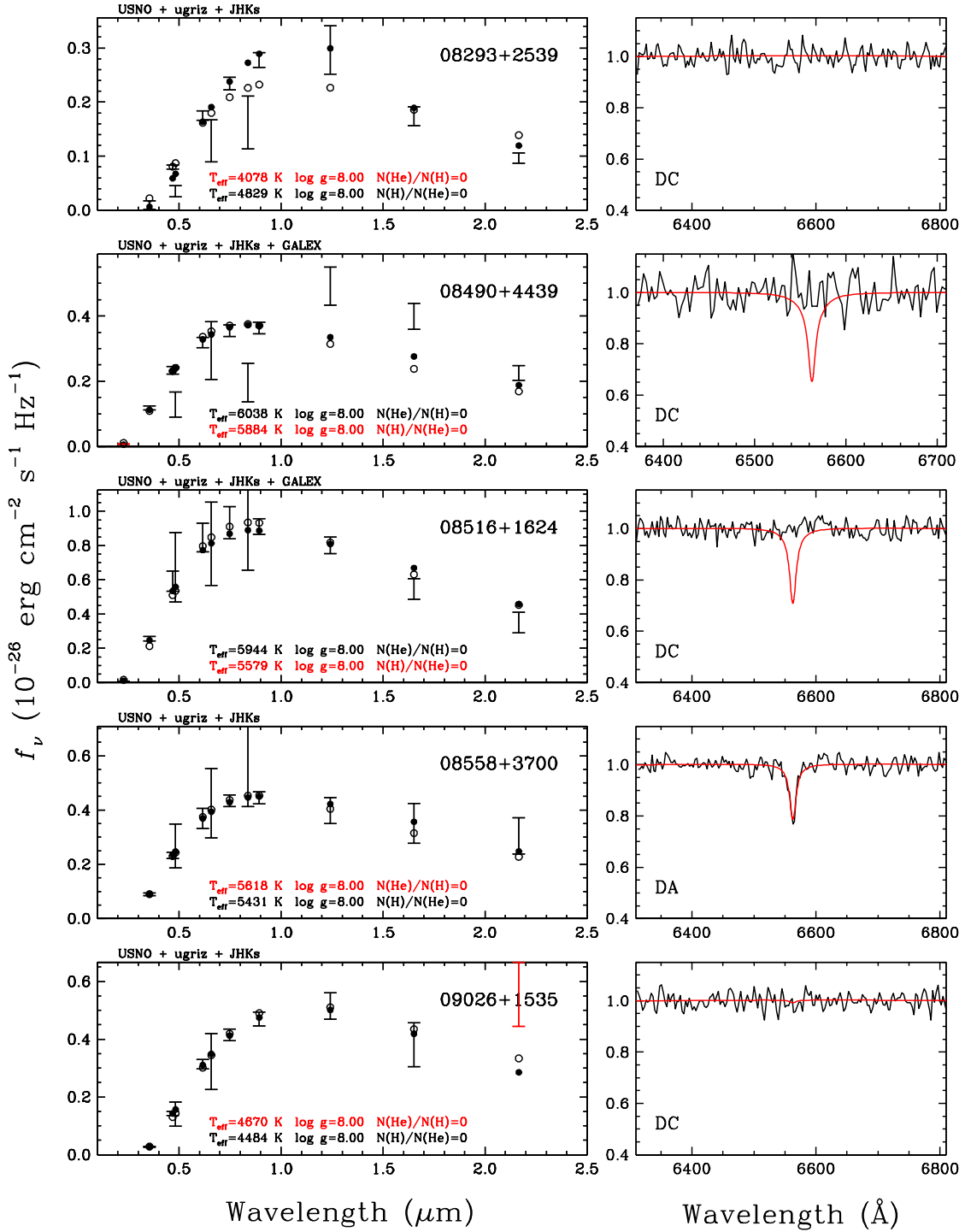


Figure 11k

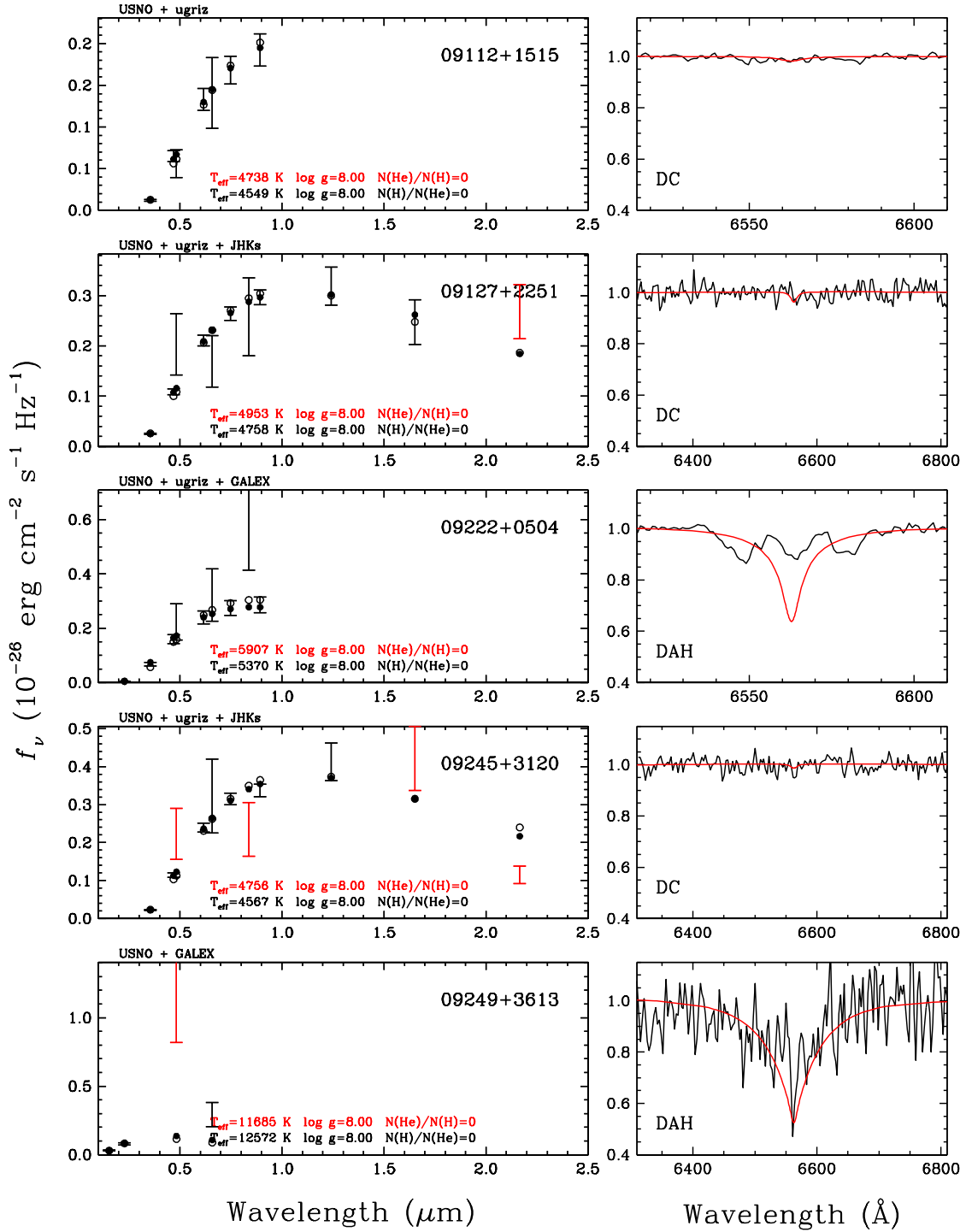


Figure 111

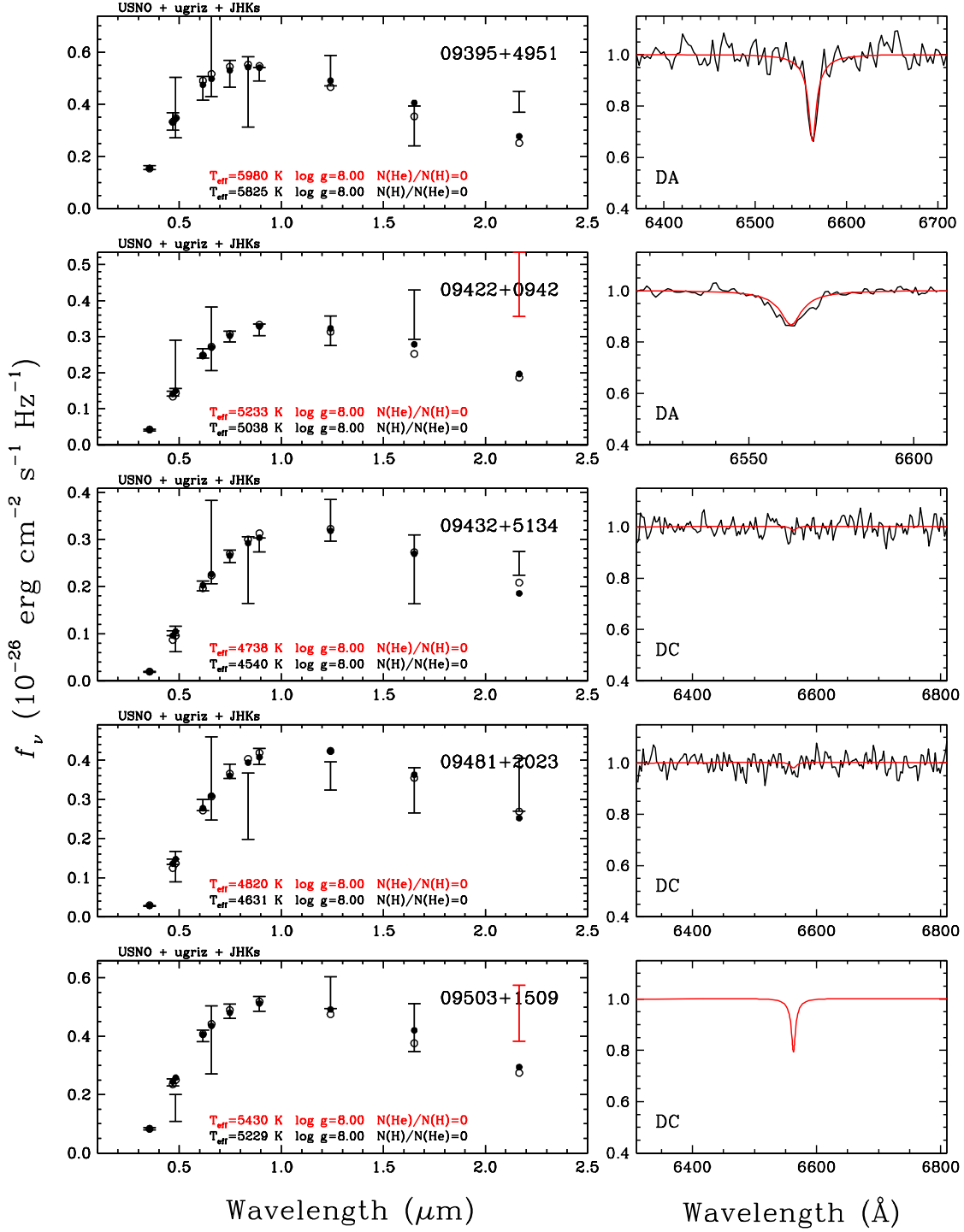


Figure 11m

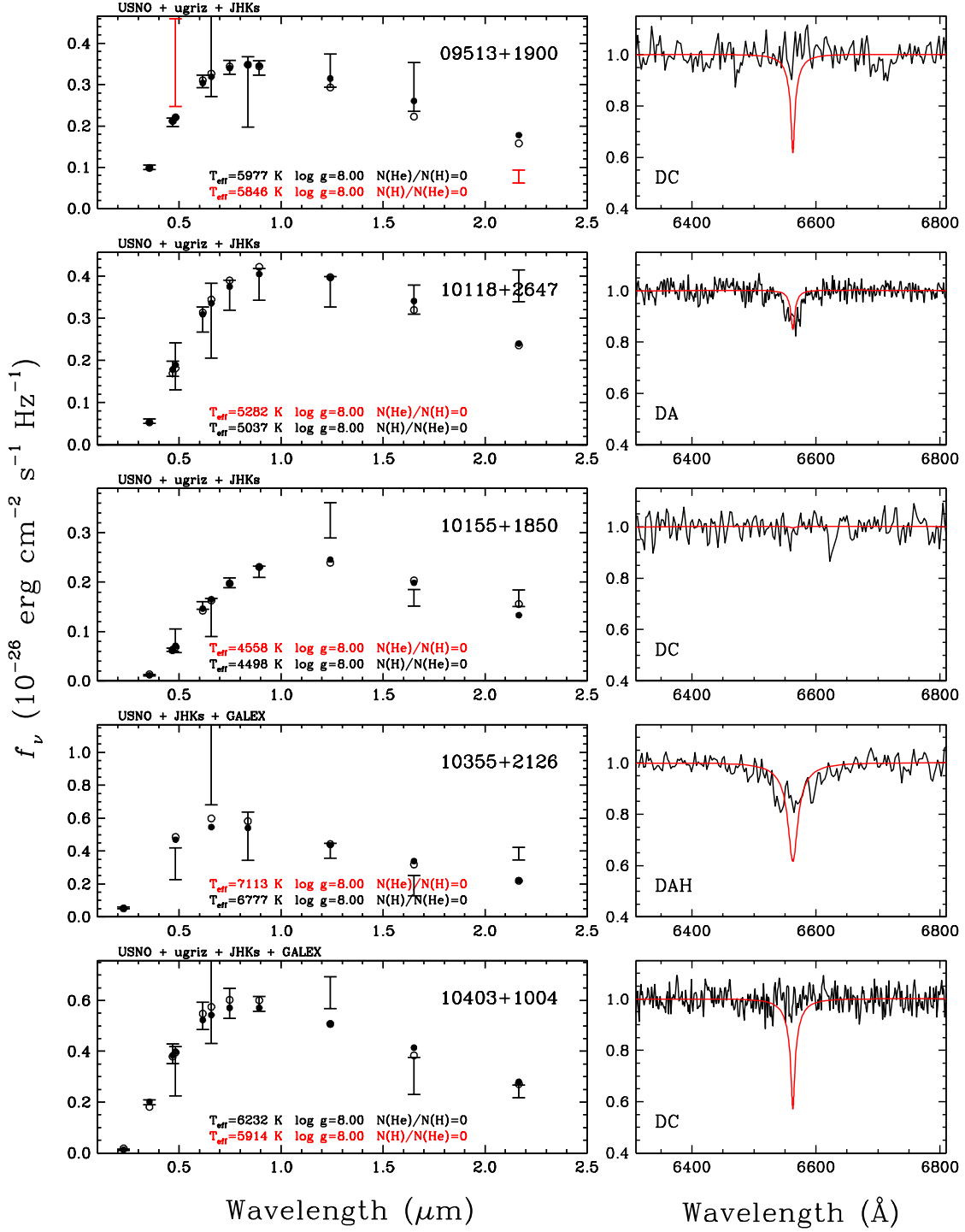


Figure 11n

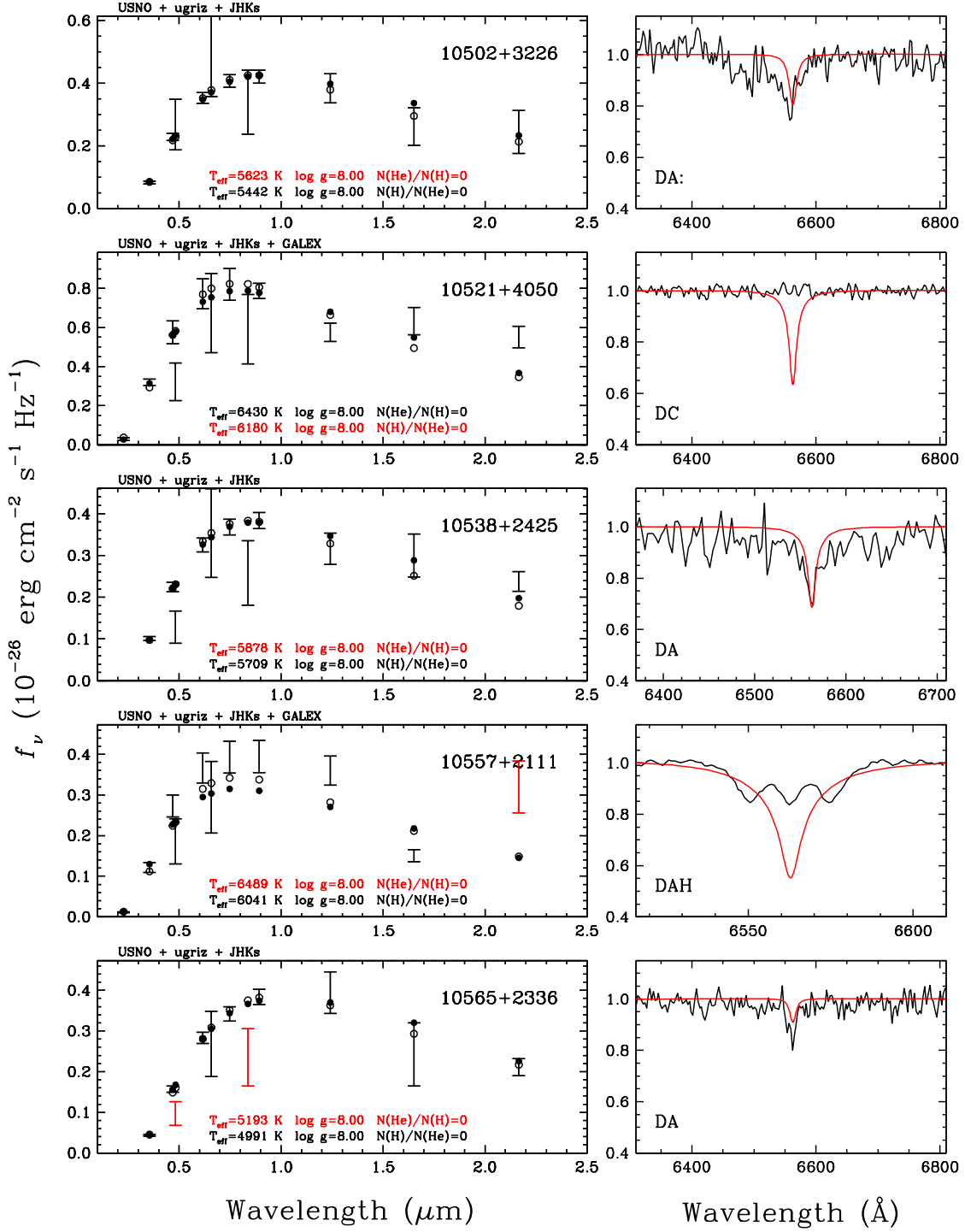


Figure 11o

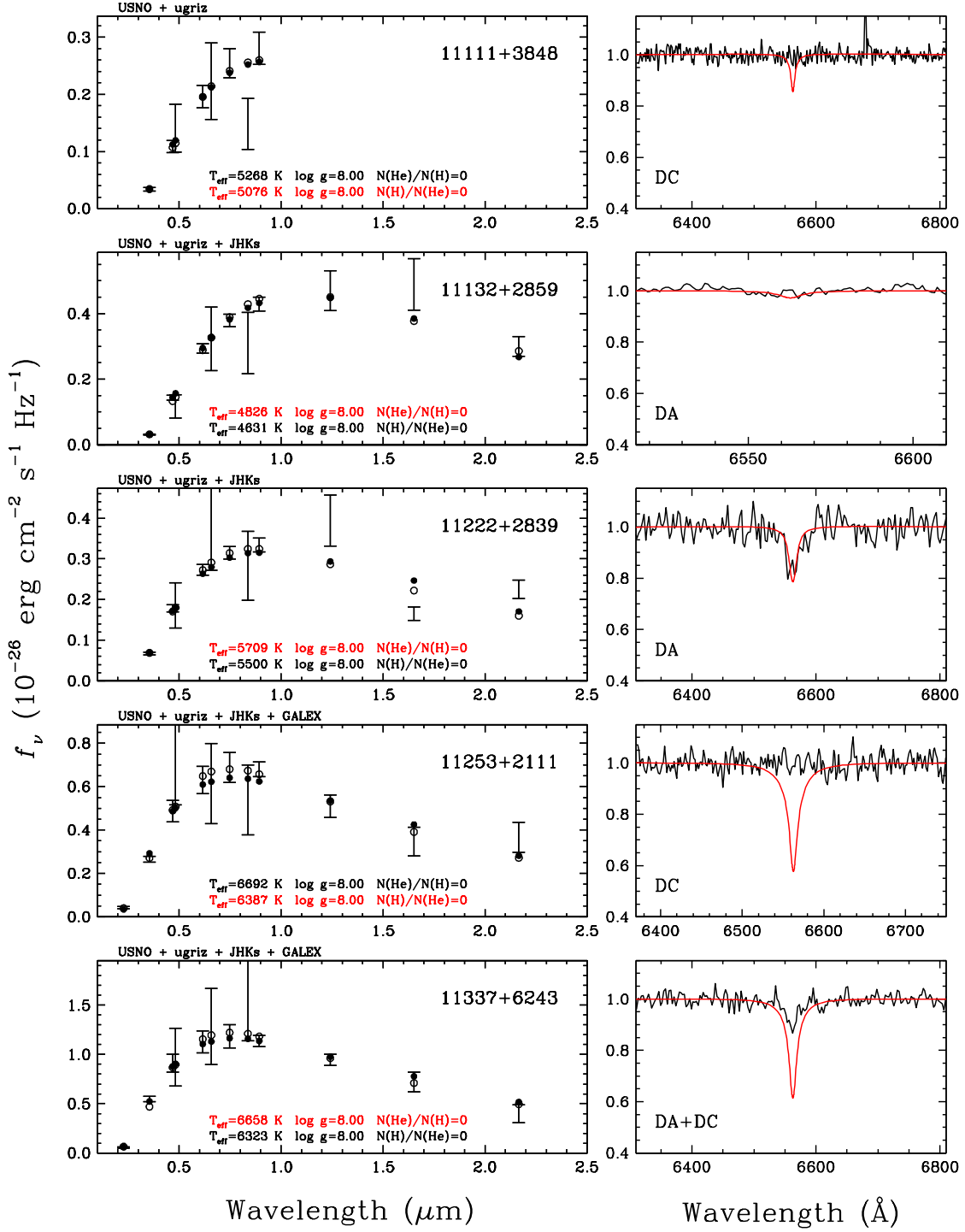


Figure 11p



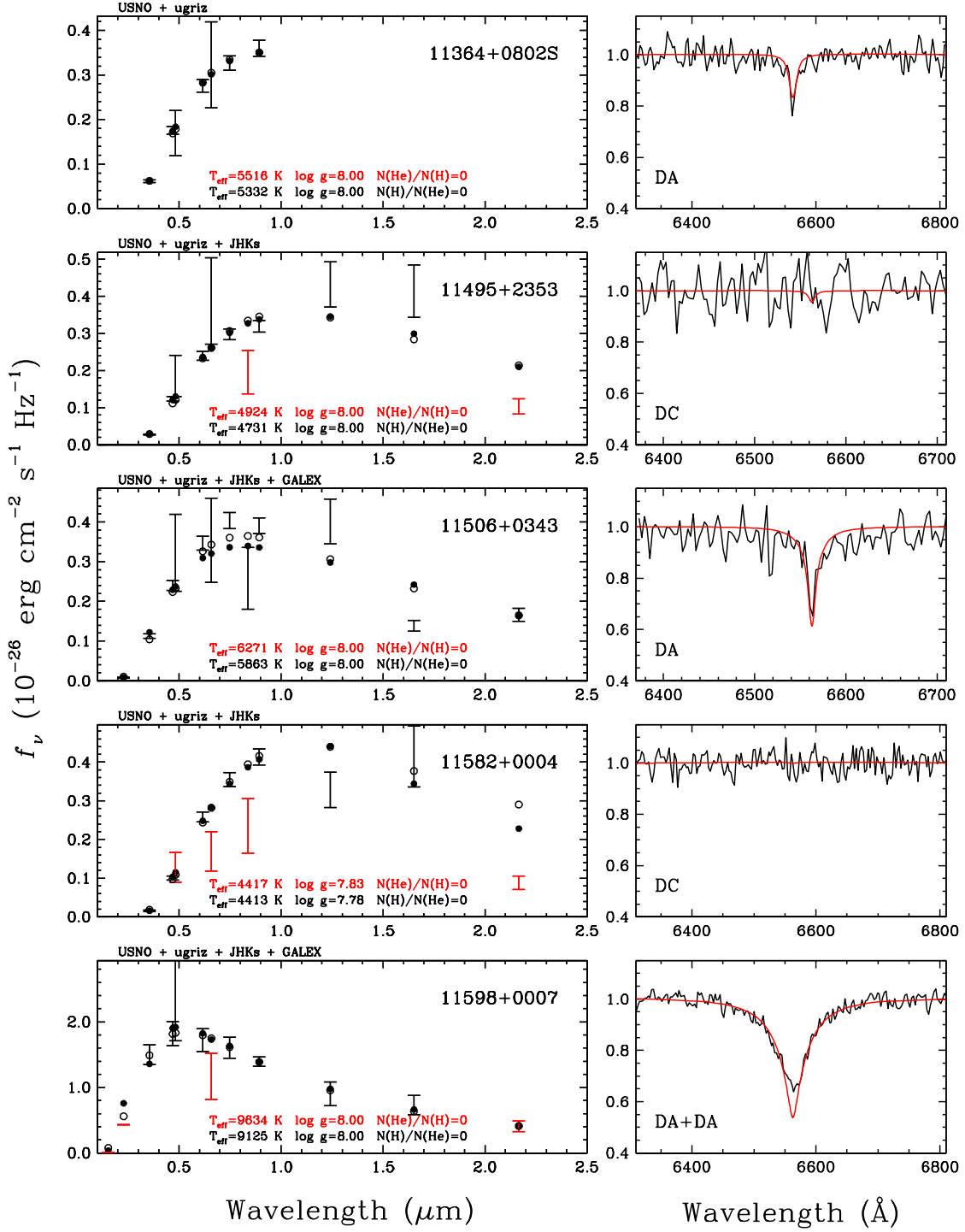


Figure 11q

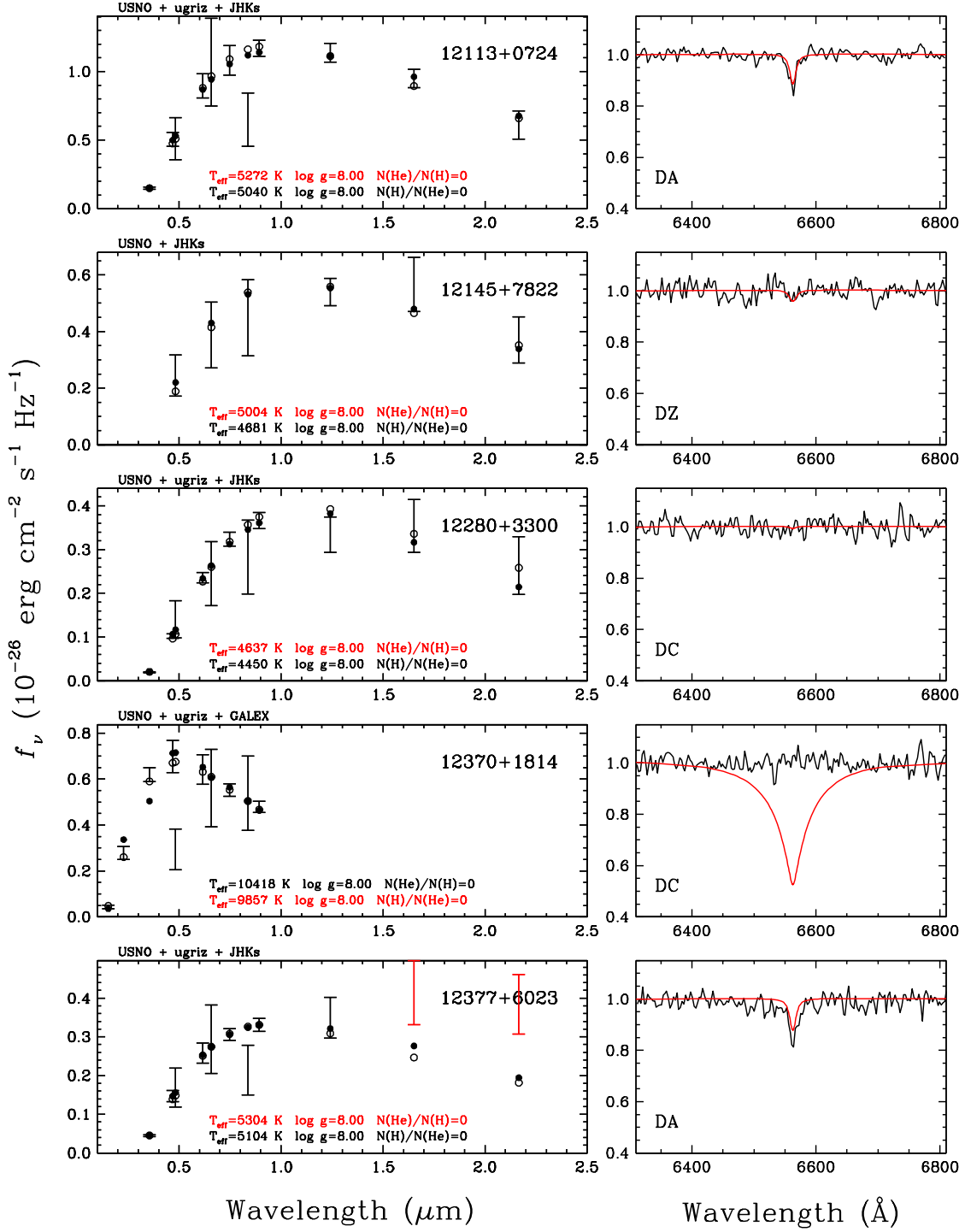


Figure 11r

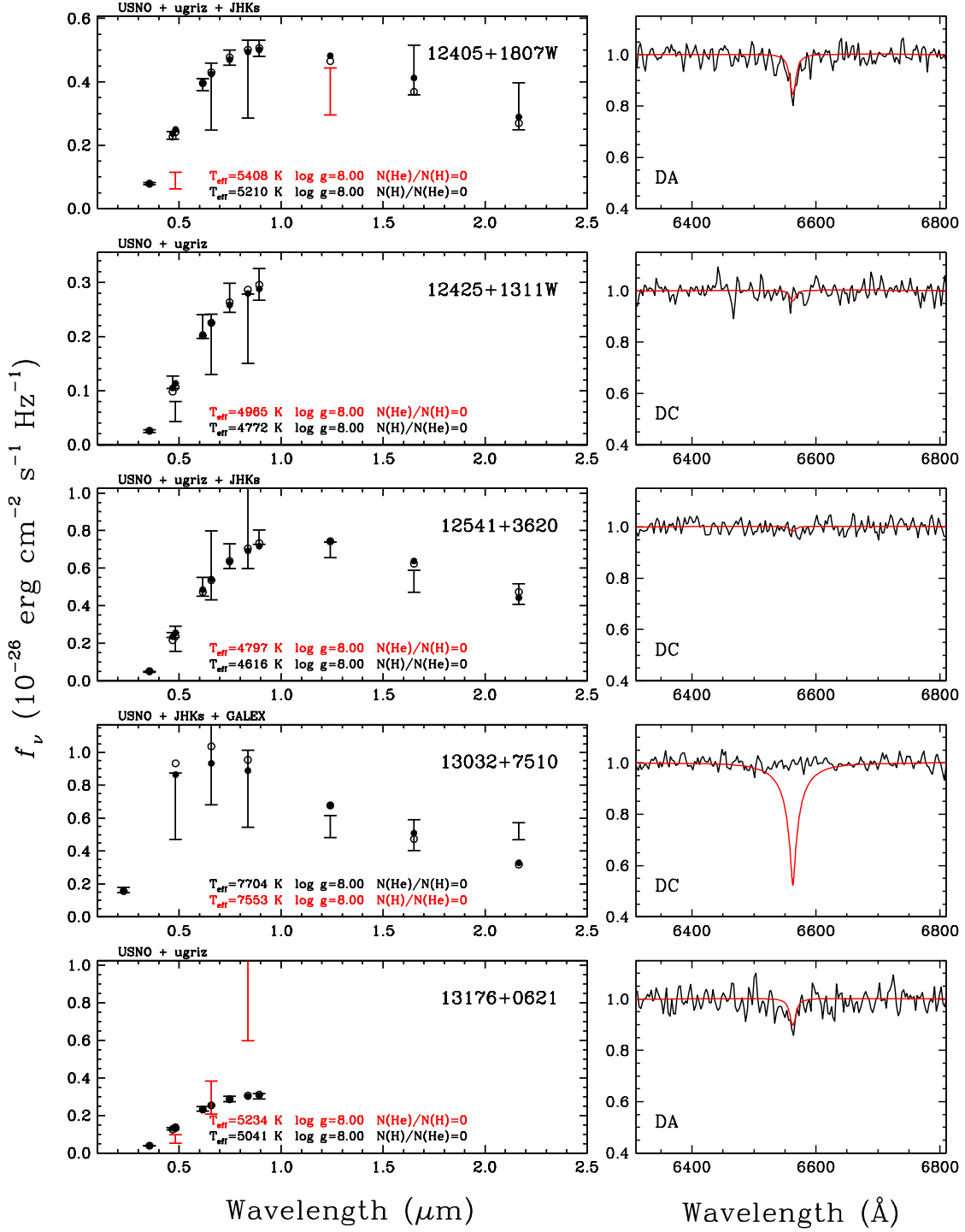


Figure 11s

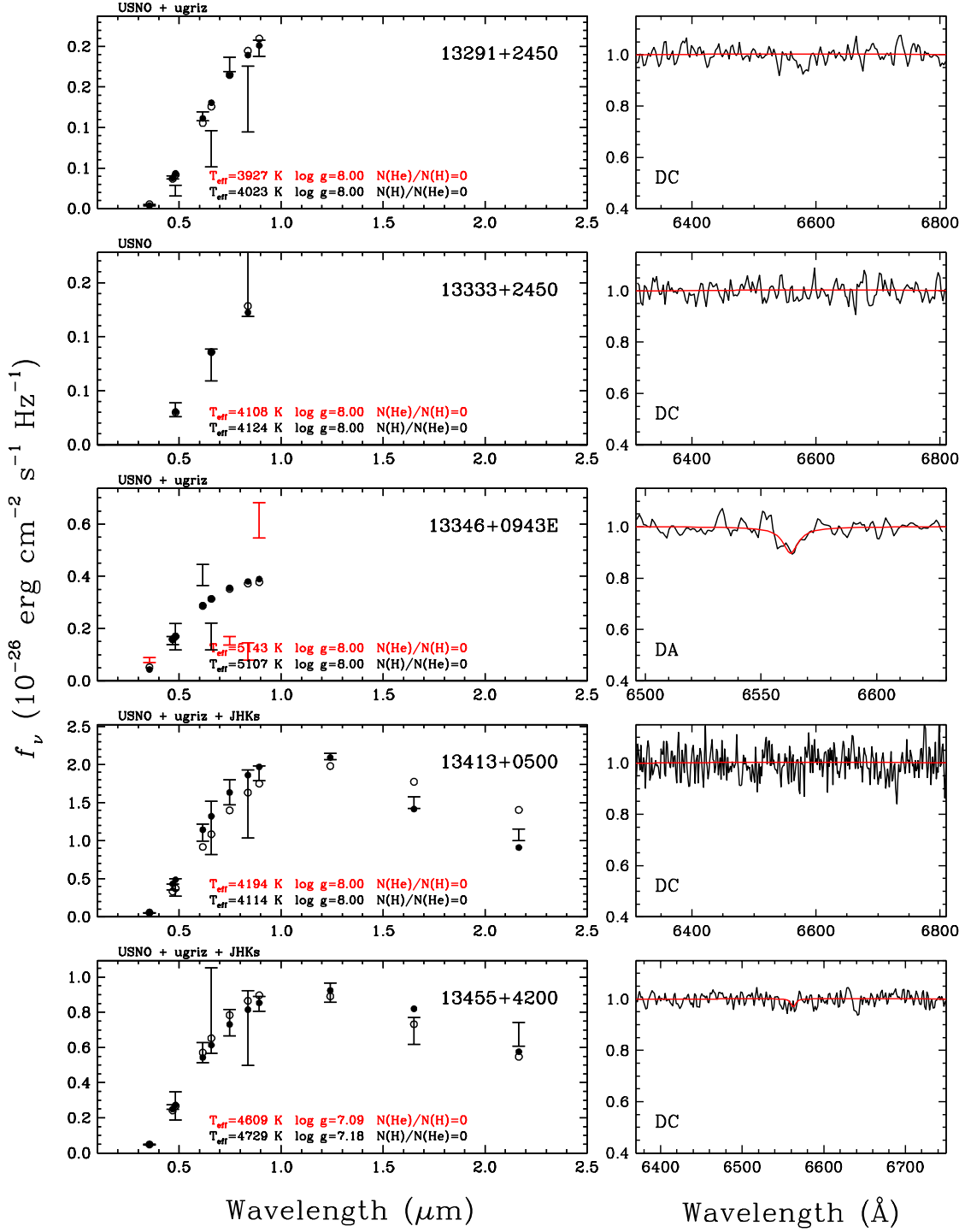


Figure 11t

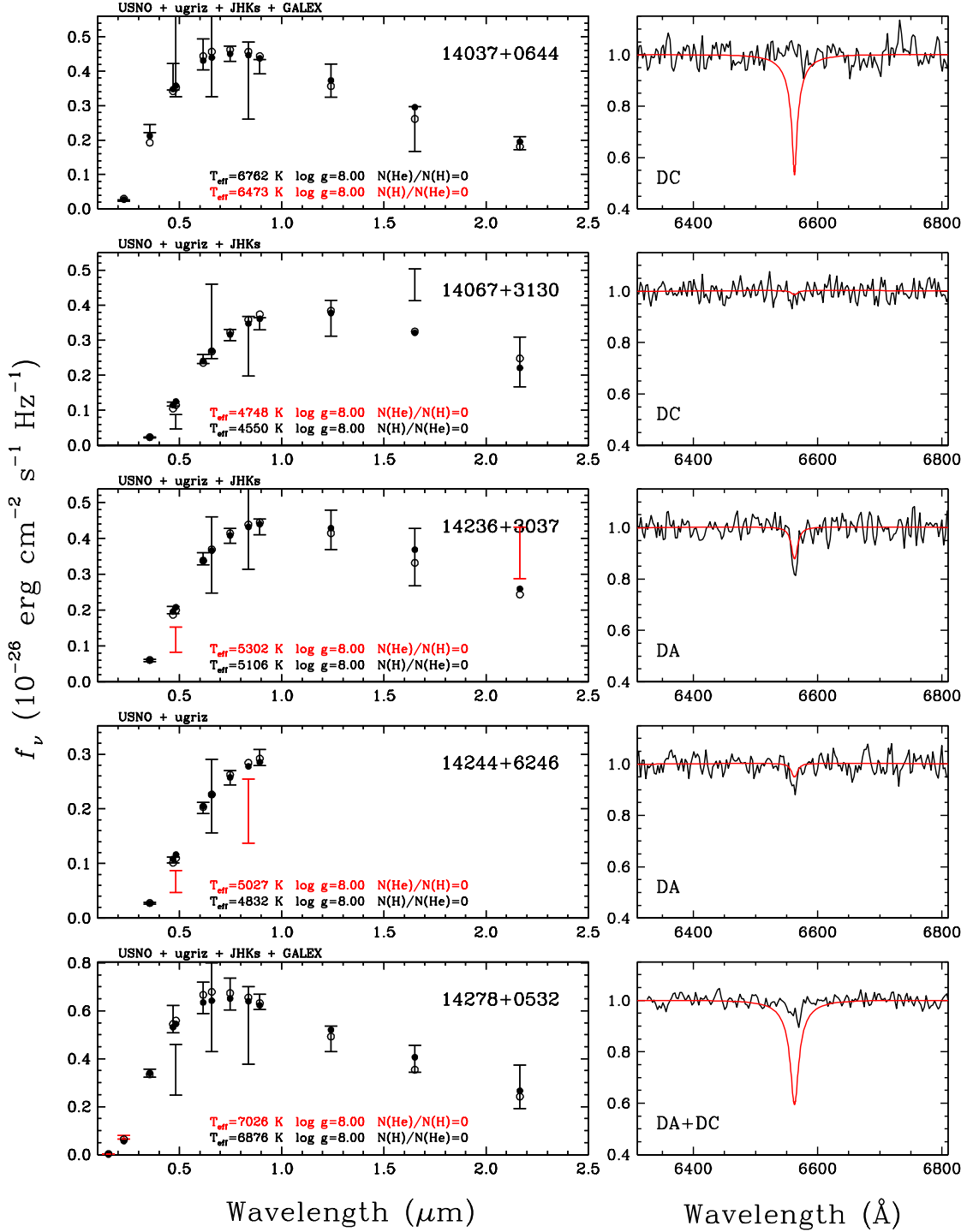


Figure 11u

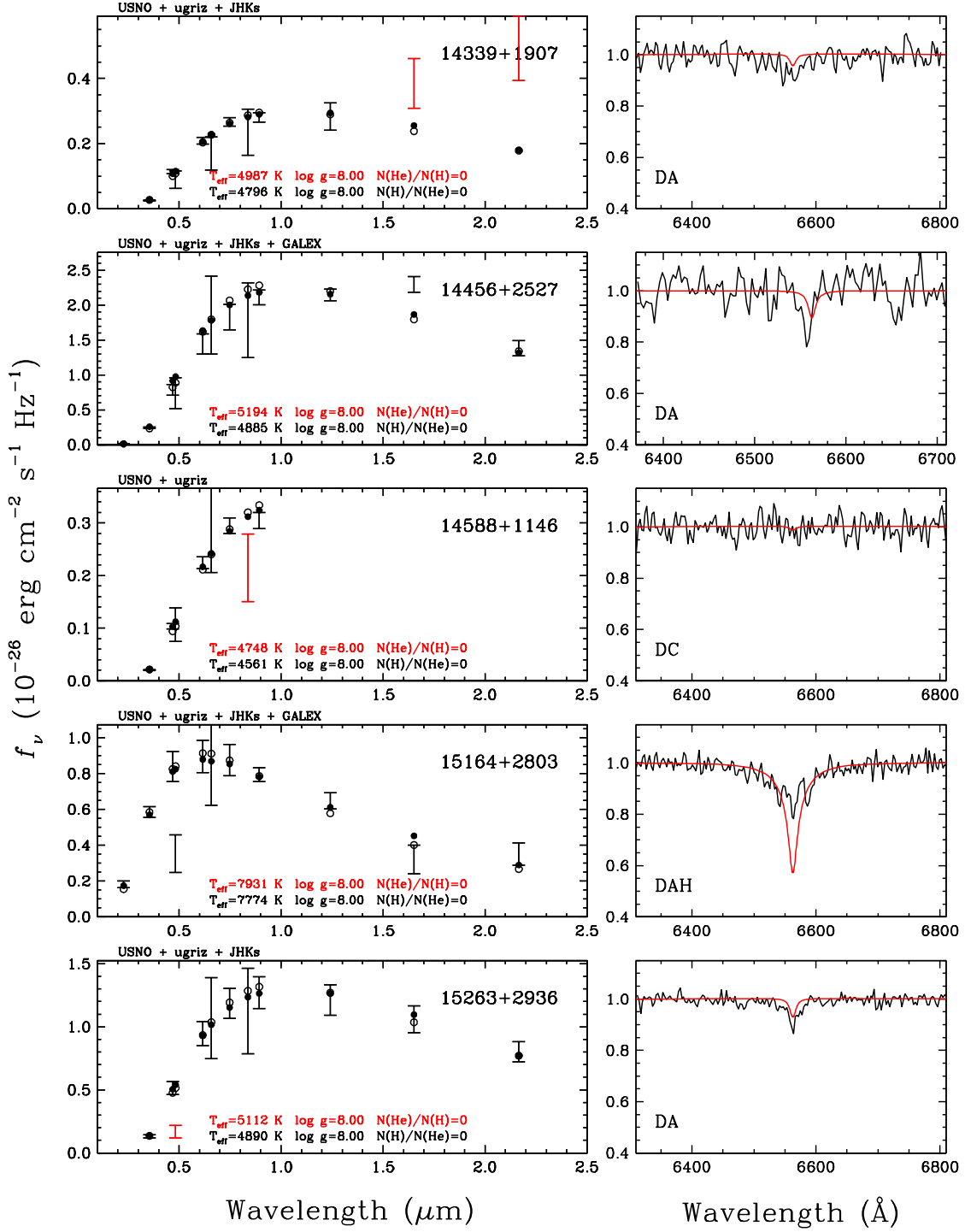


Figure 11v

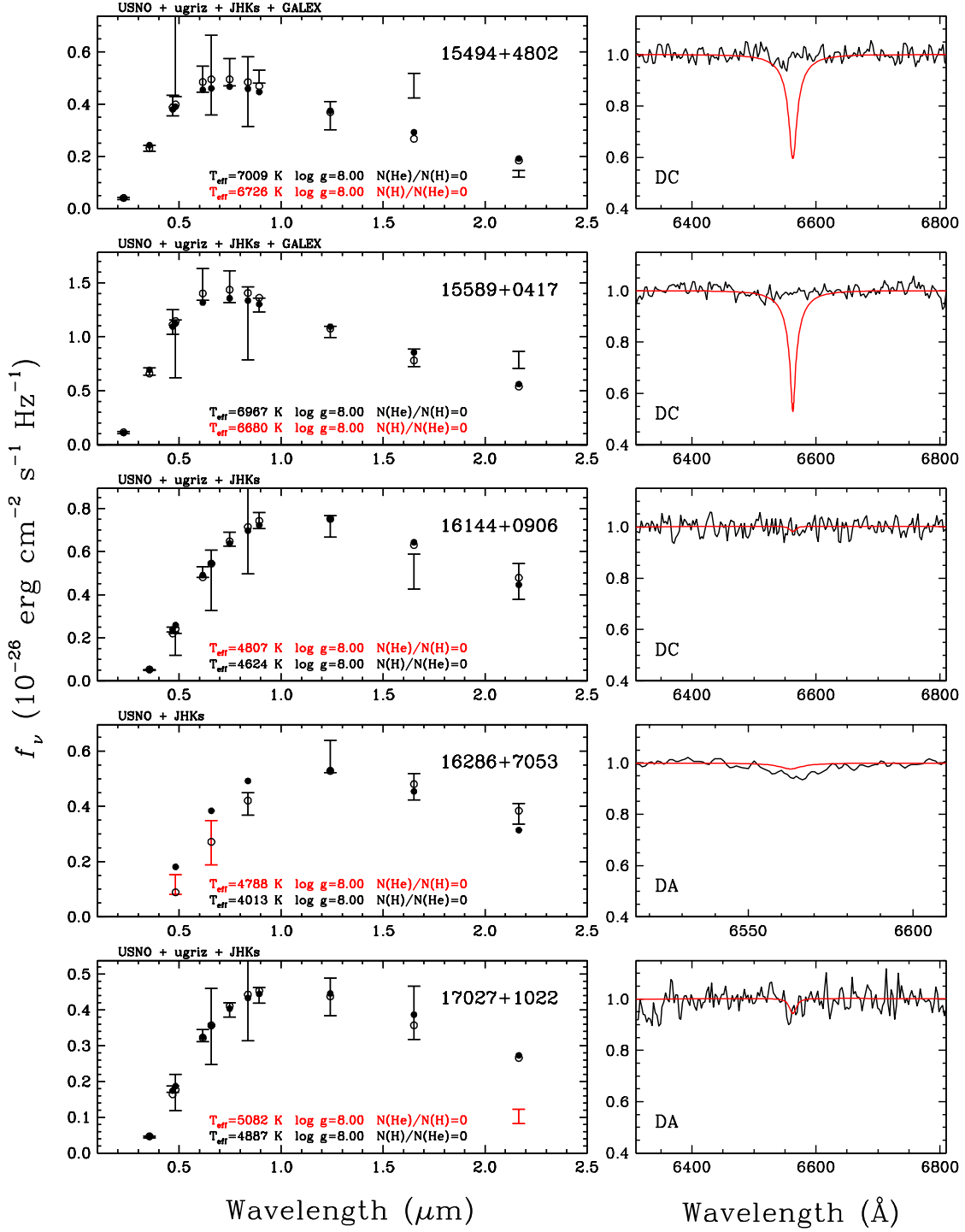


Figure 11w

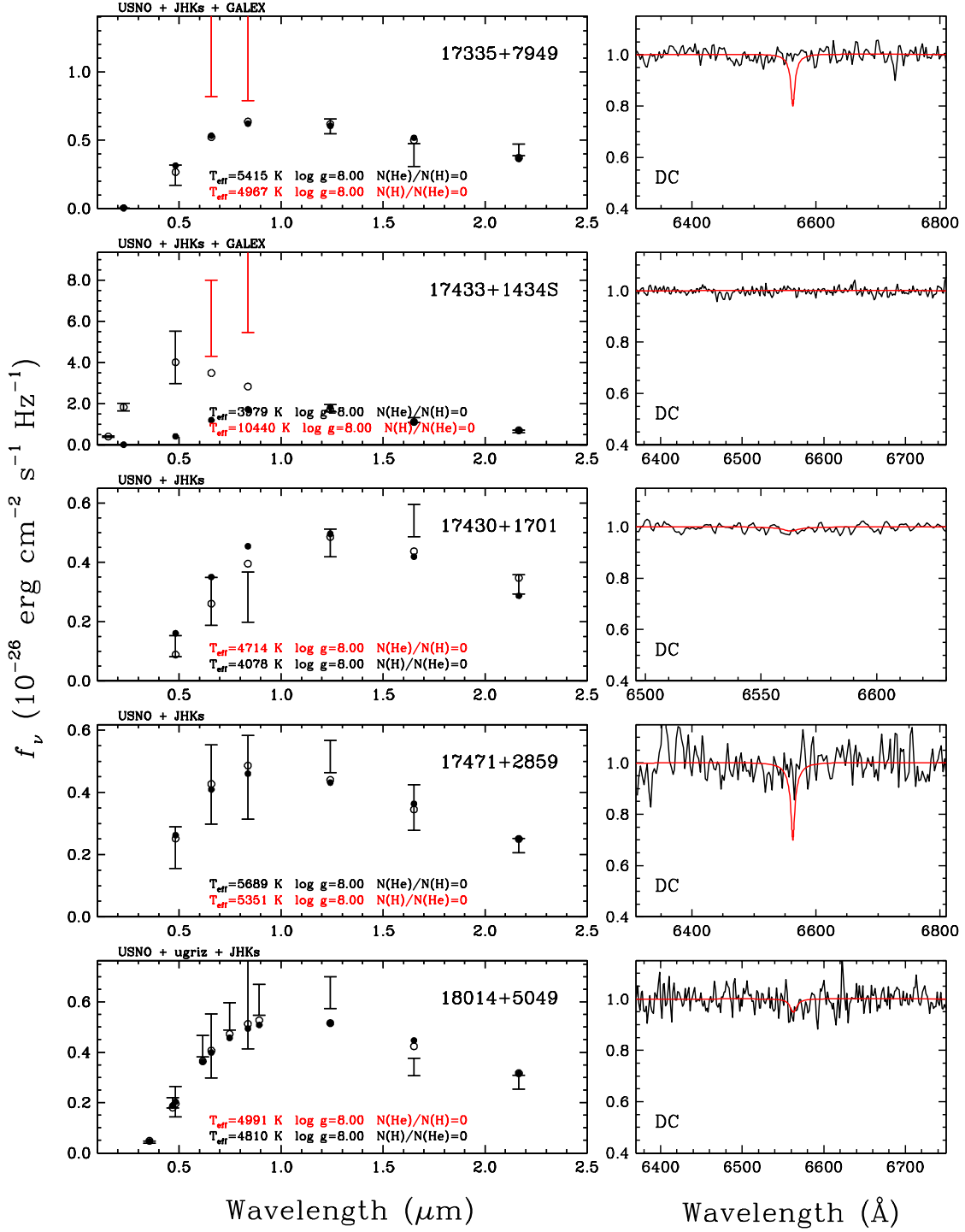


Figure 11x



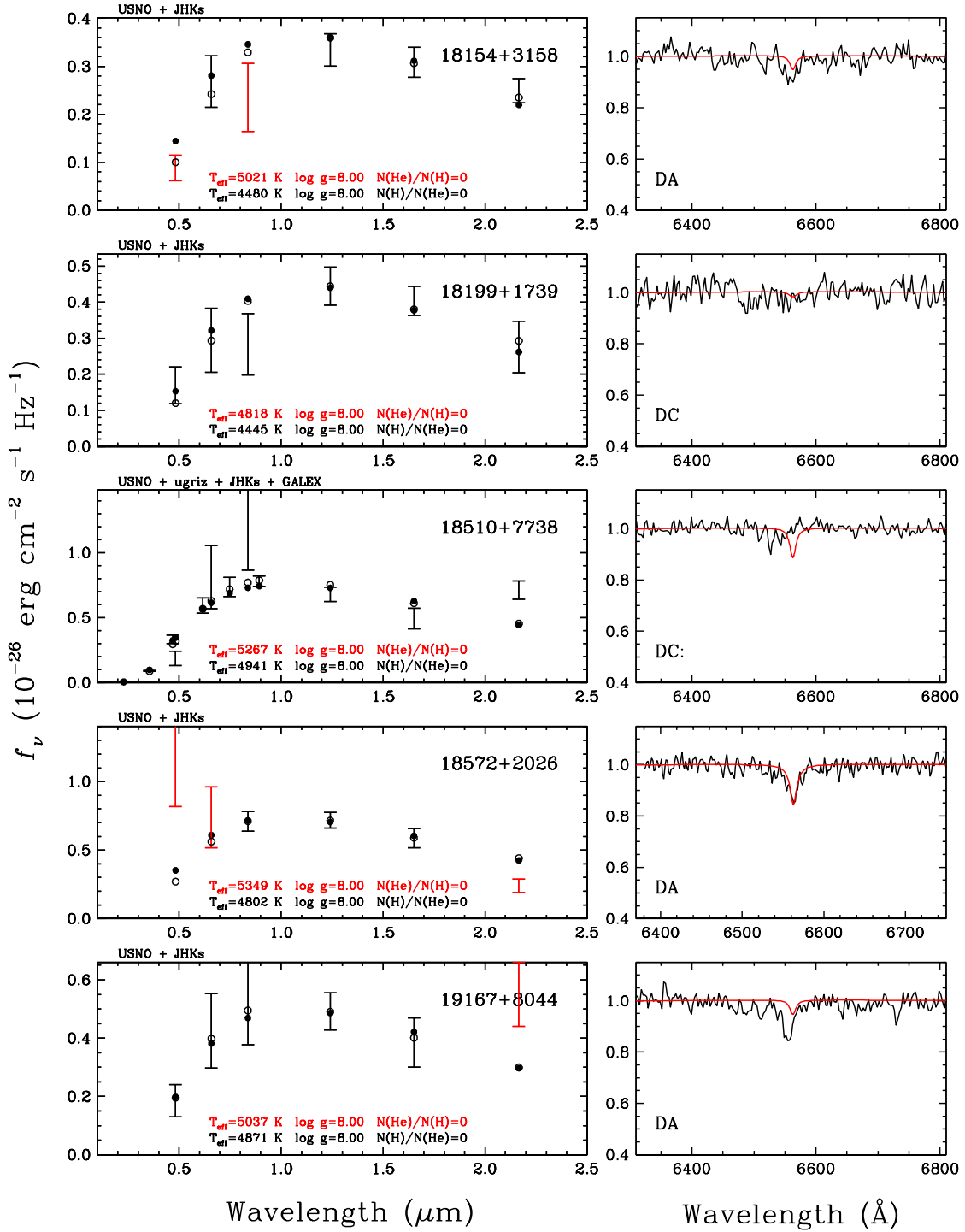


Figure 11y

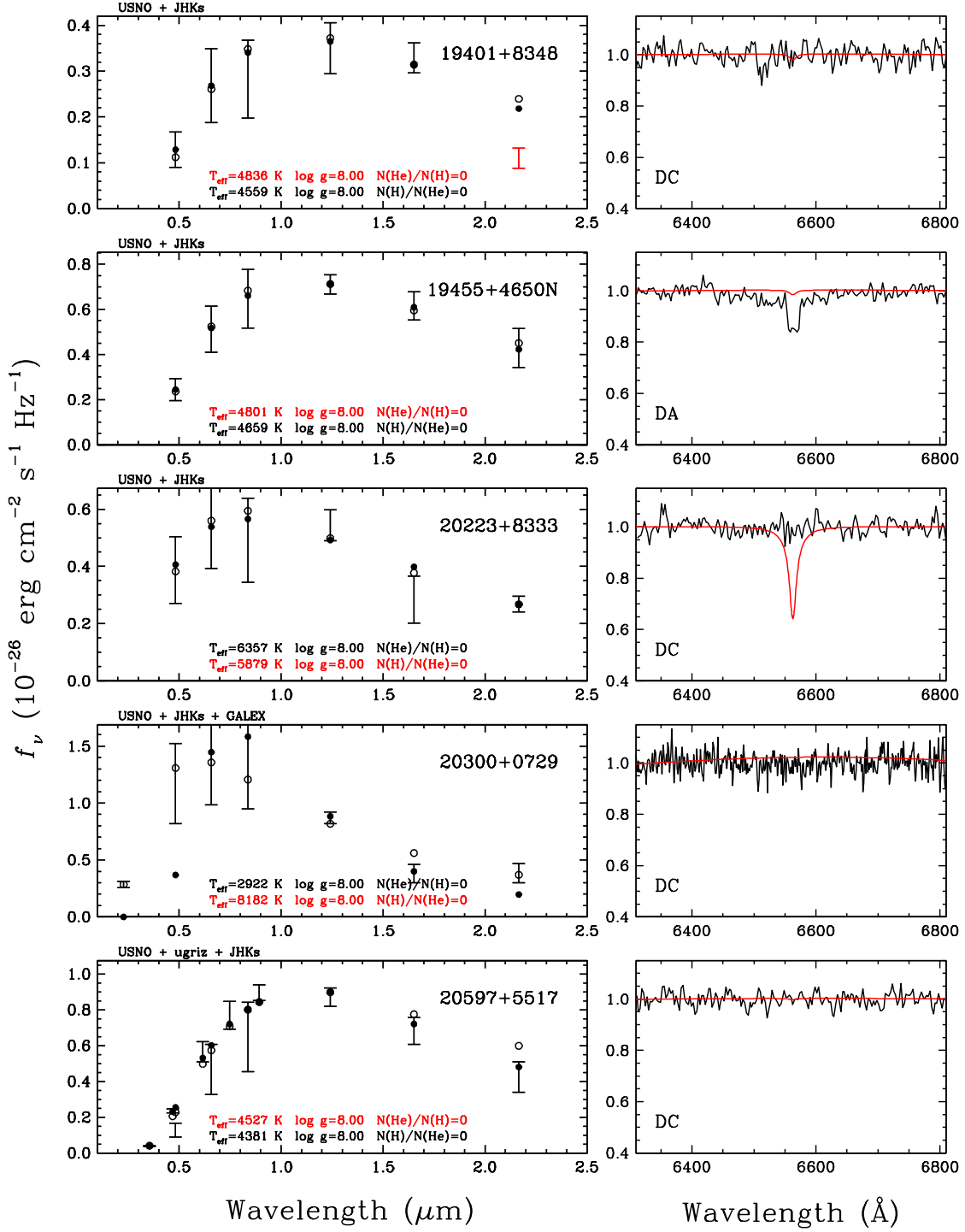


Figure 11z

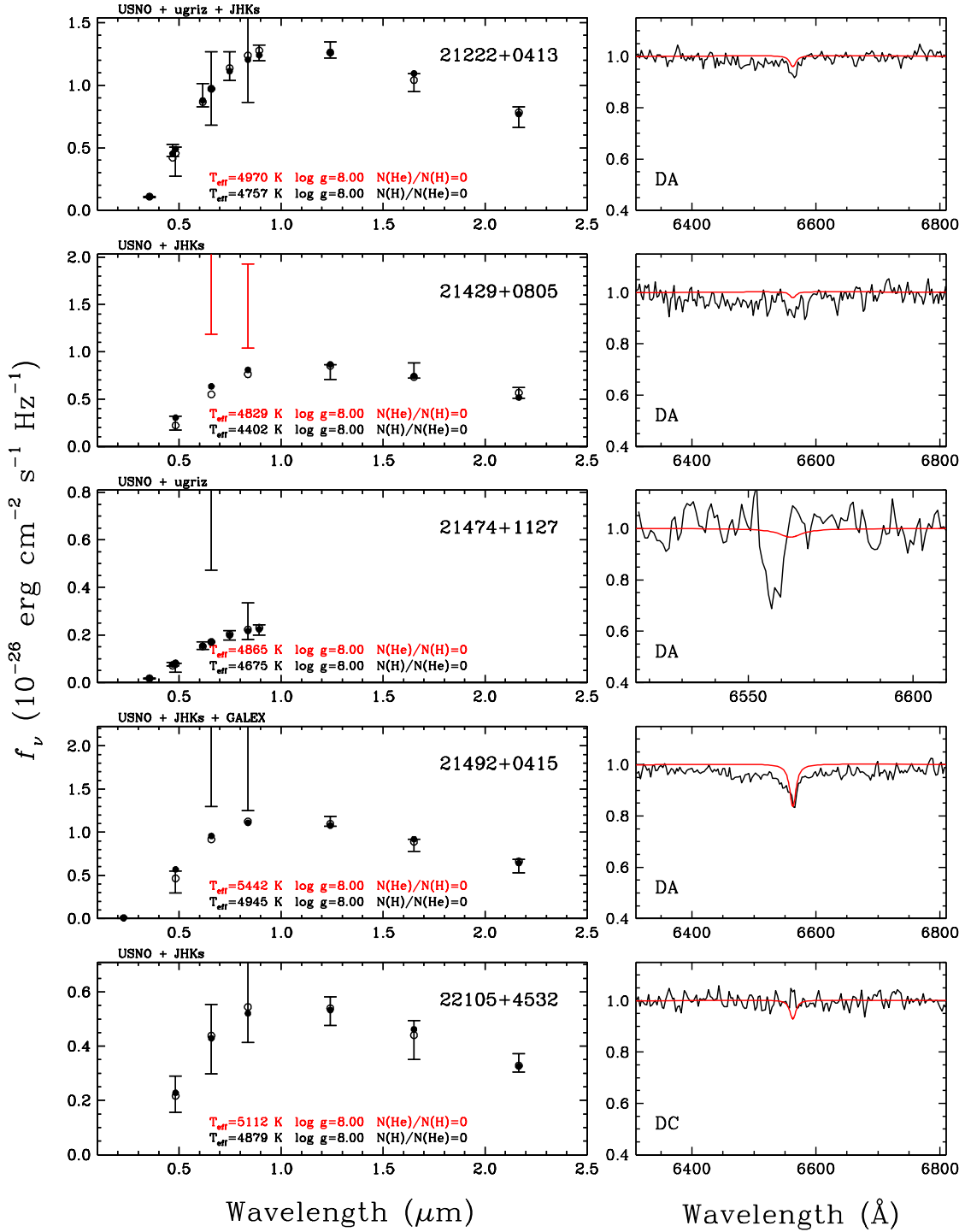


Figure 11A

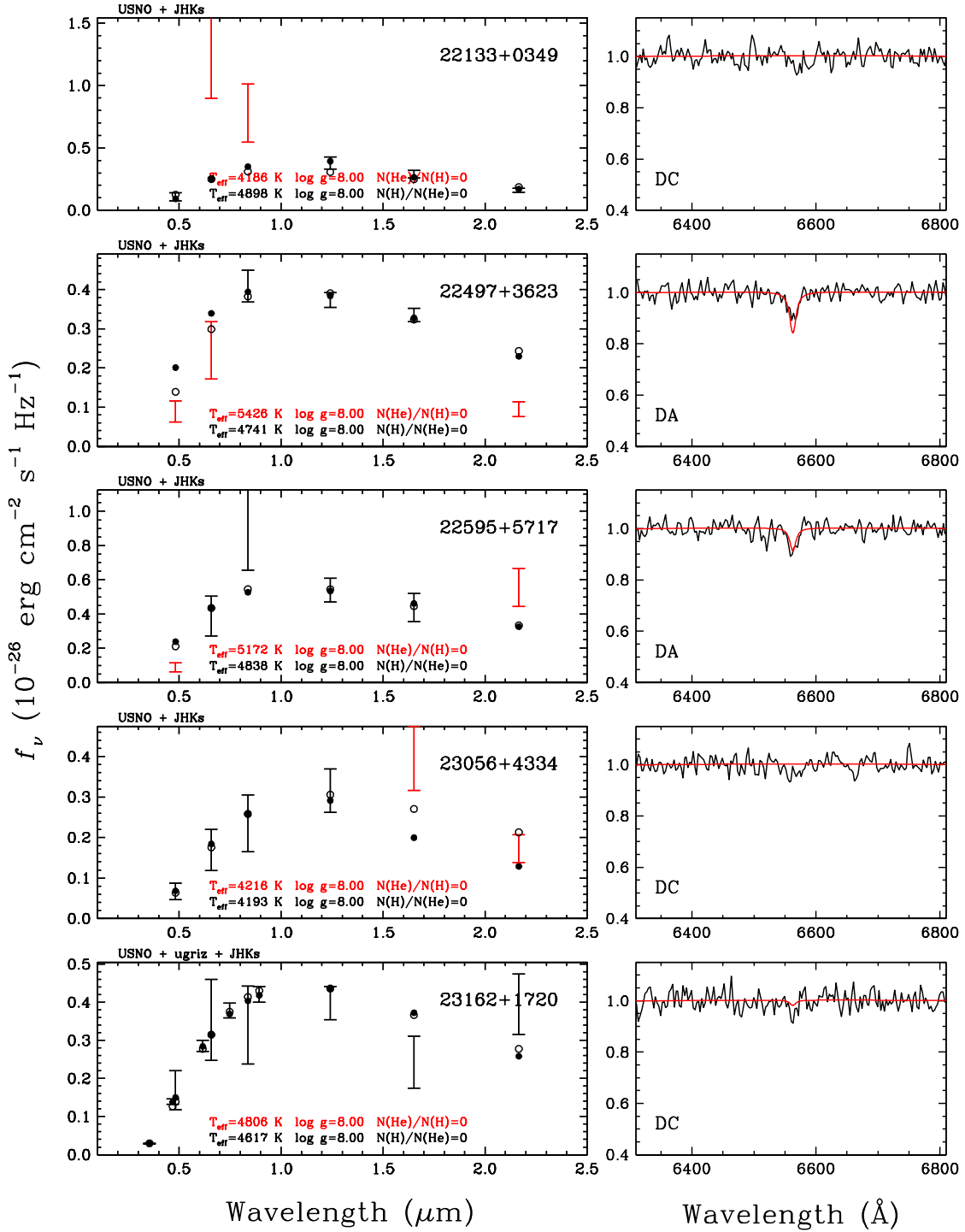


Figure 11B

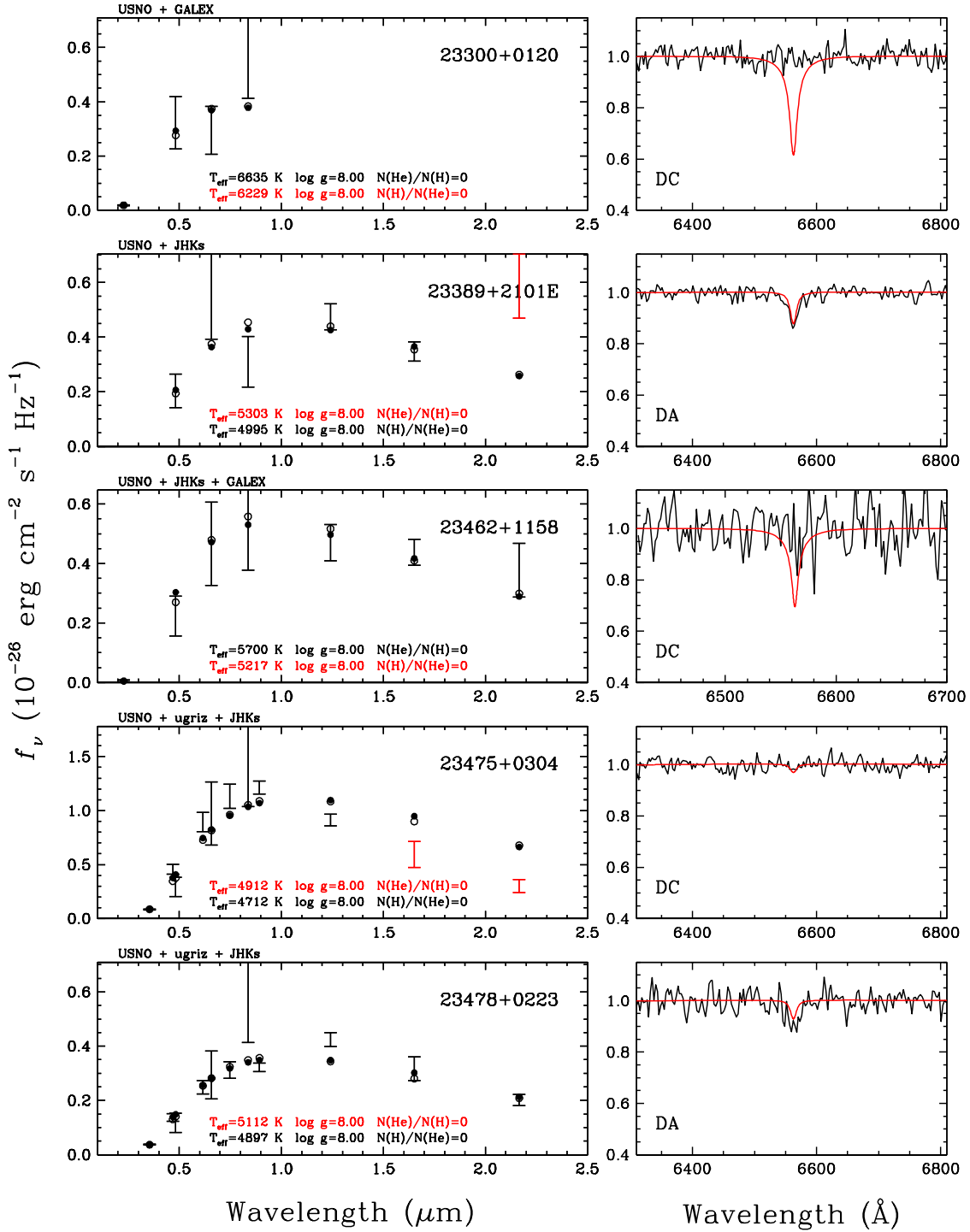


Figure 11C

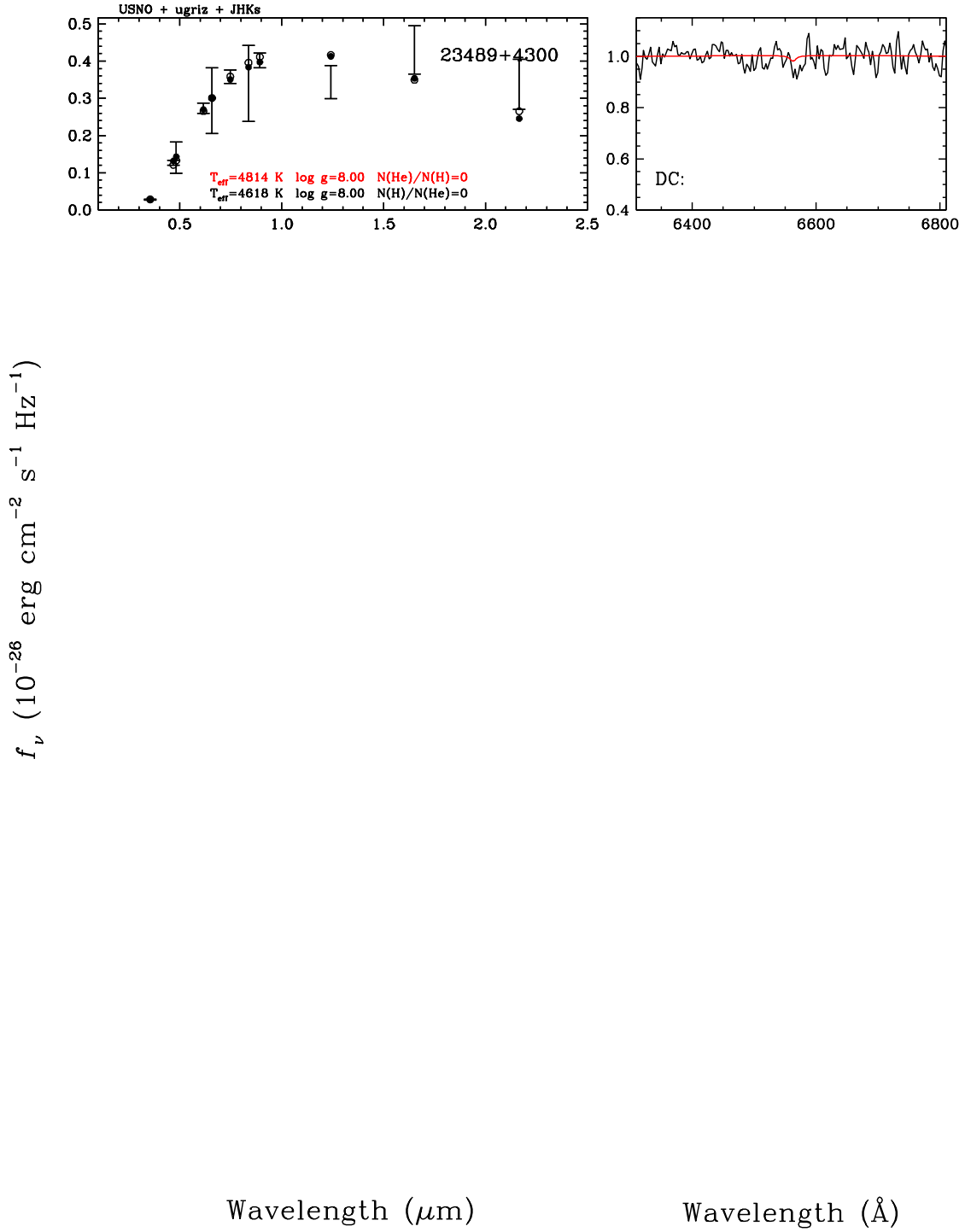


Figure 11D

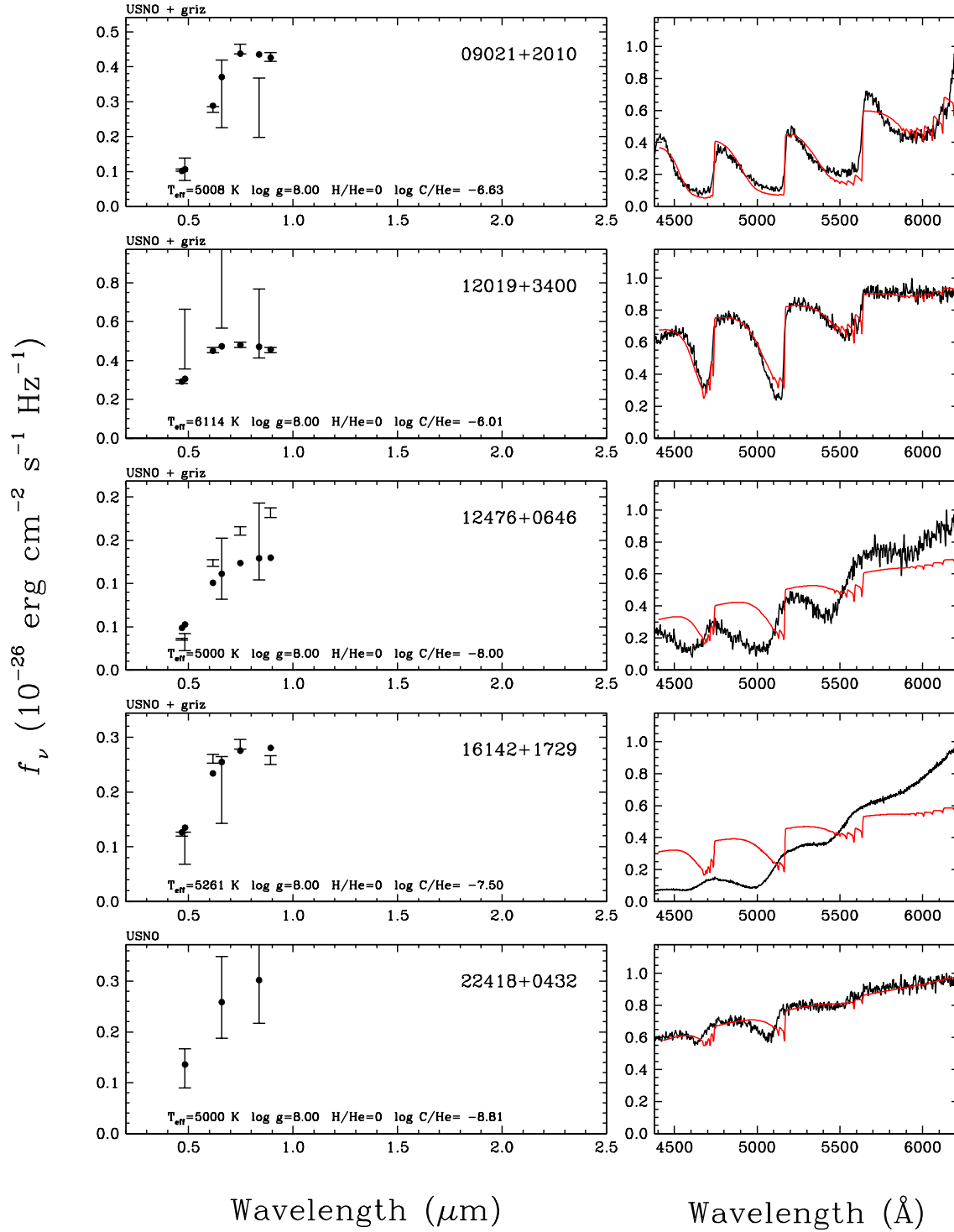


Figure 12

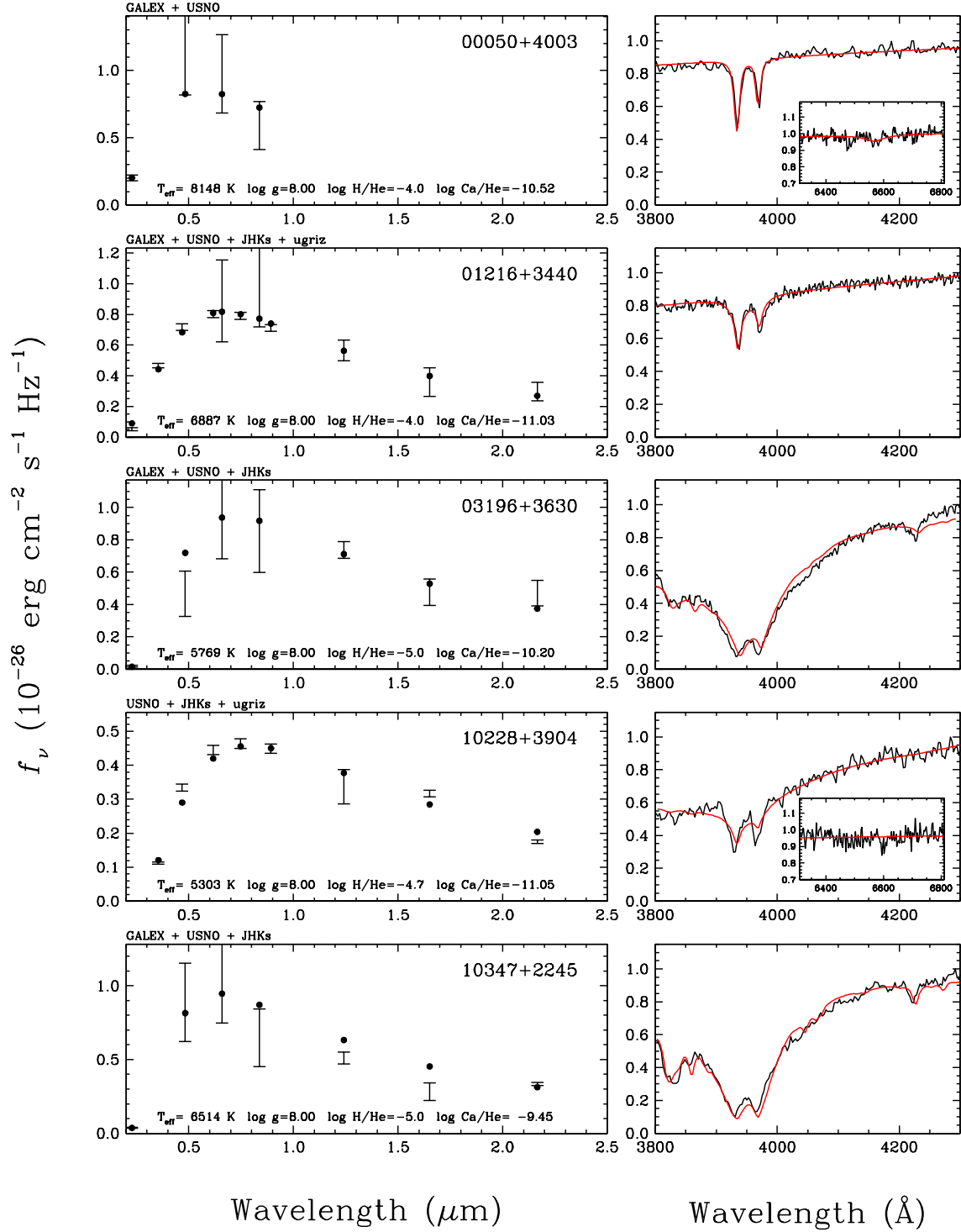


Figure 13a



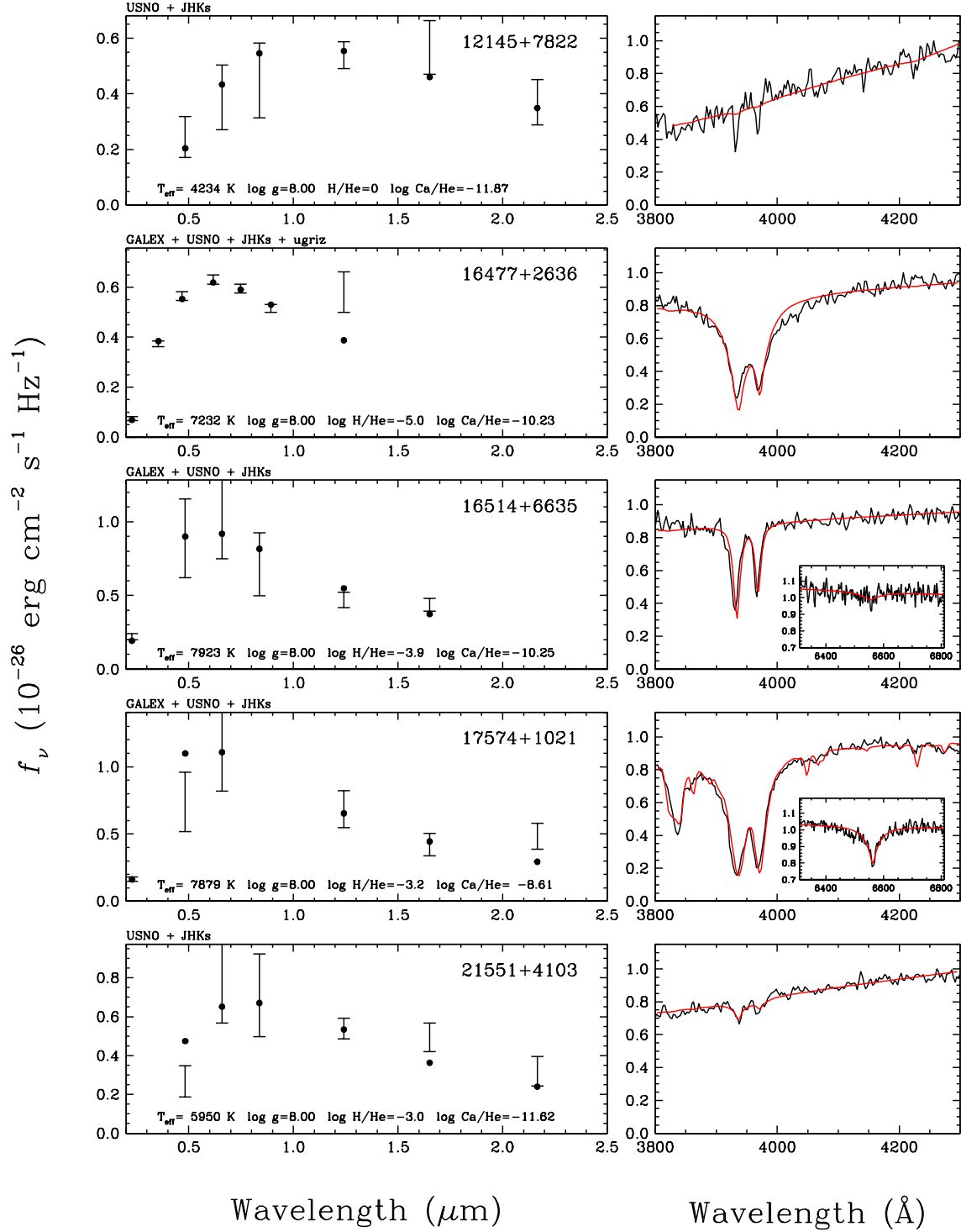


Figure 13b

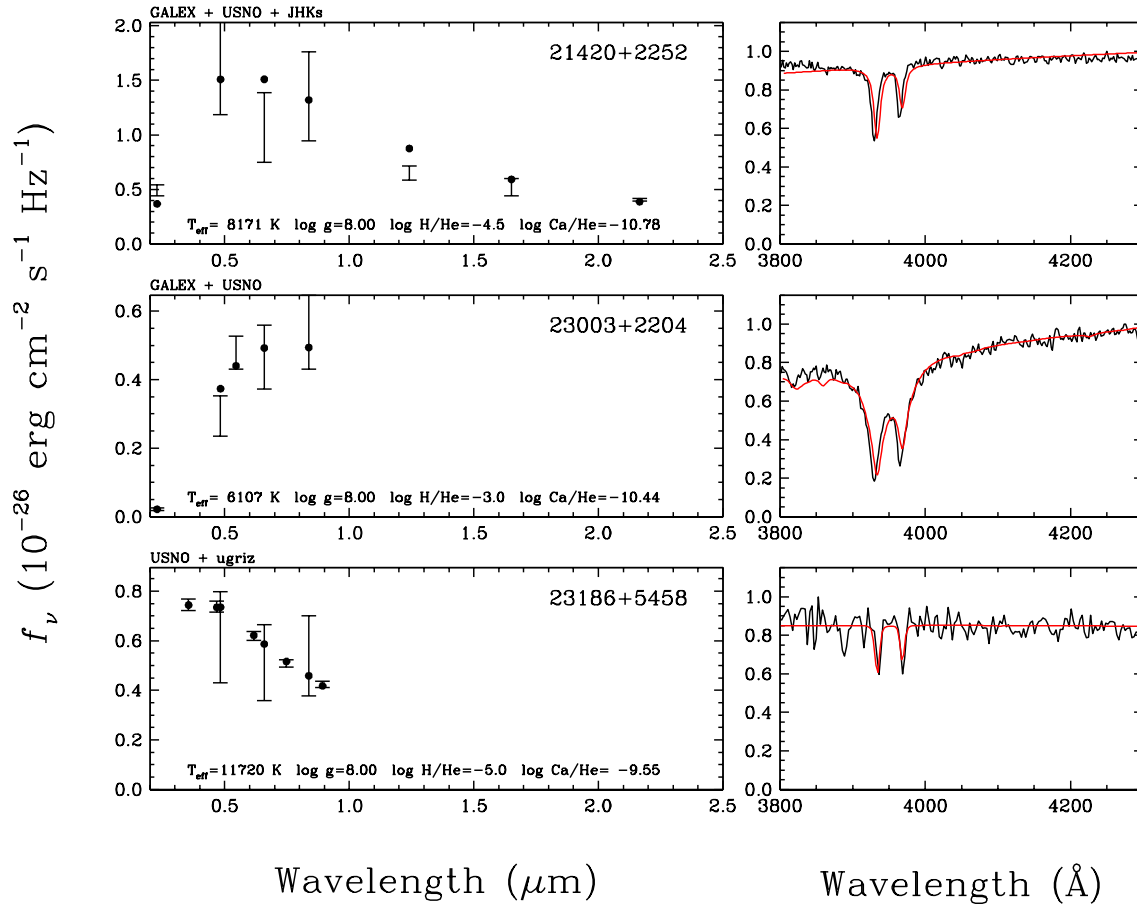


Figure 13c

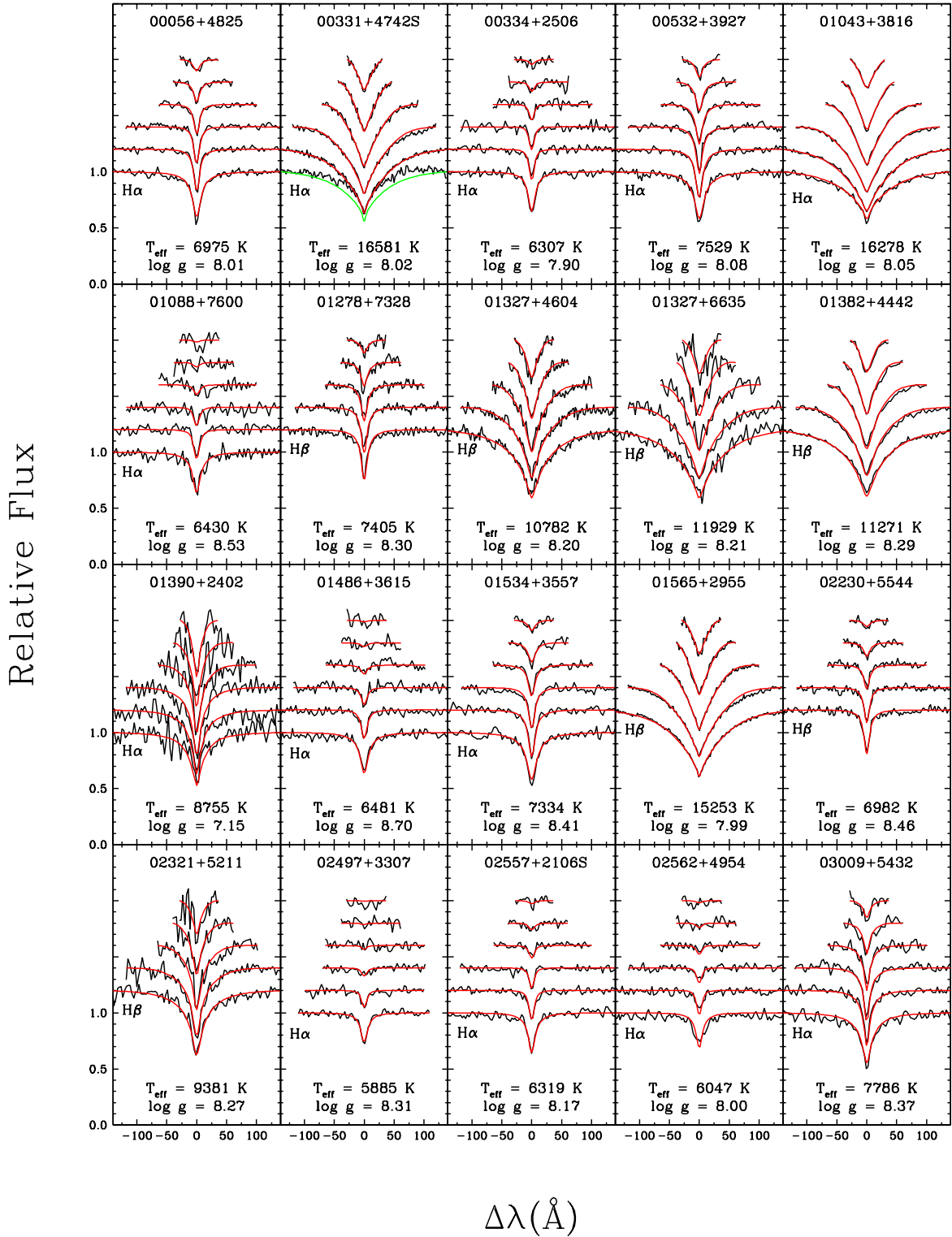


Figure 14a

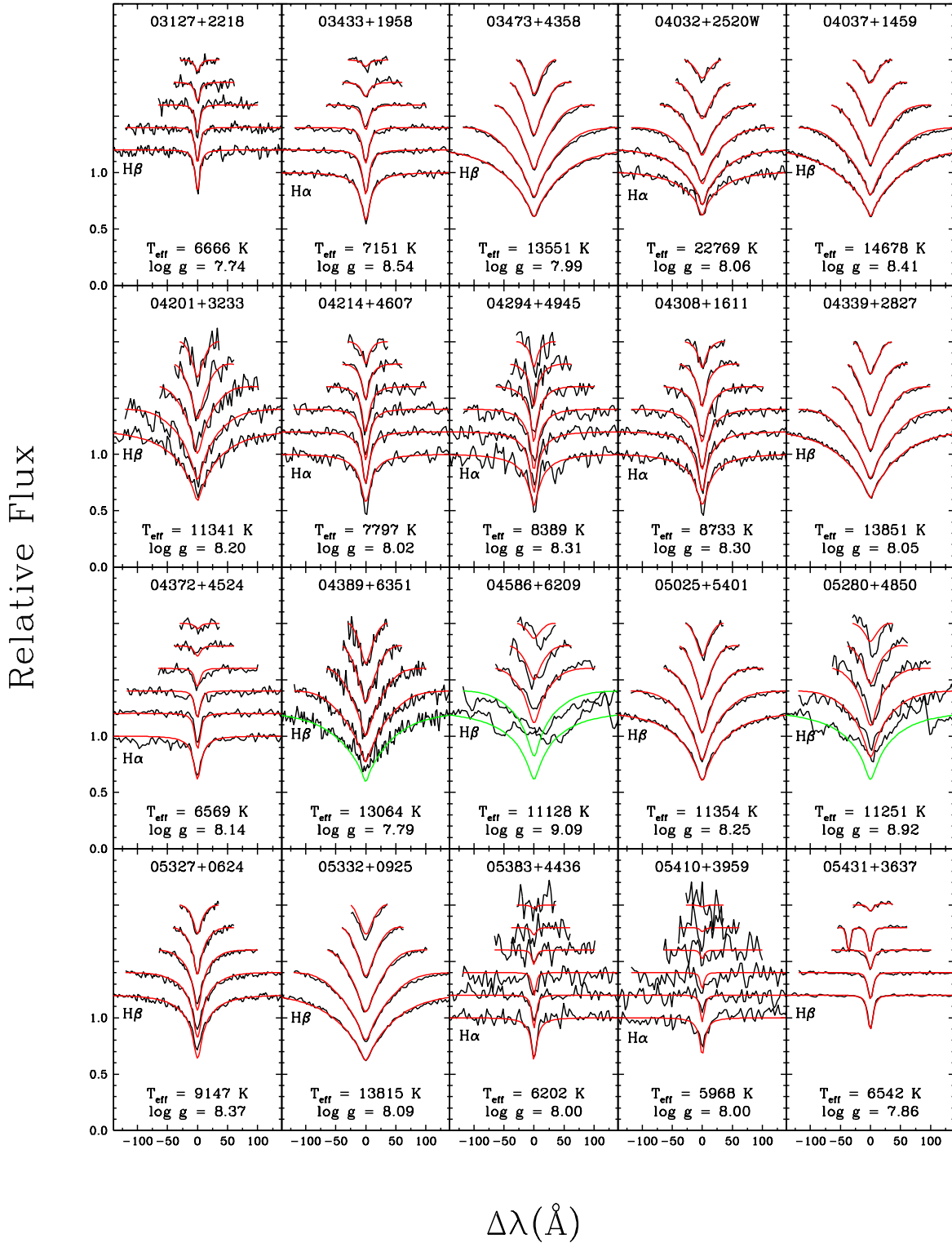


Figure 14b

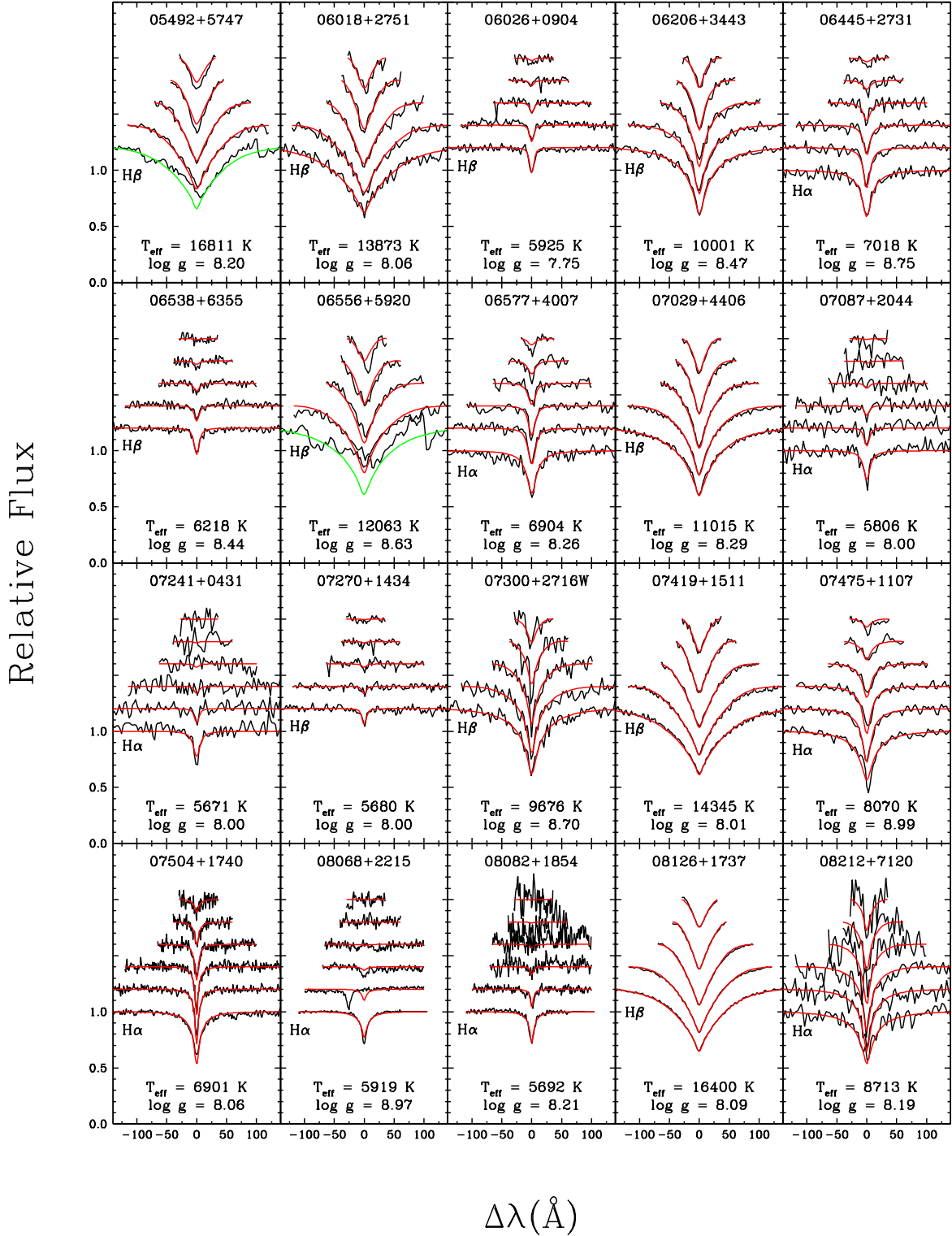


Figure 14c

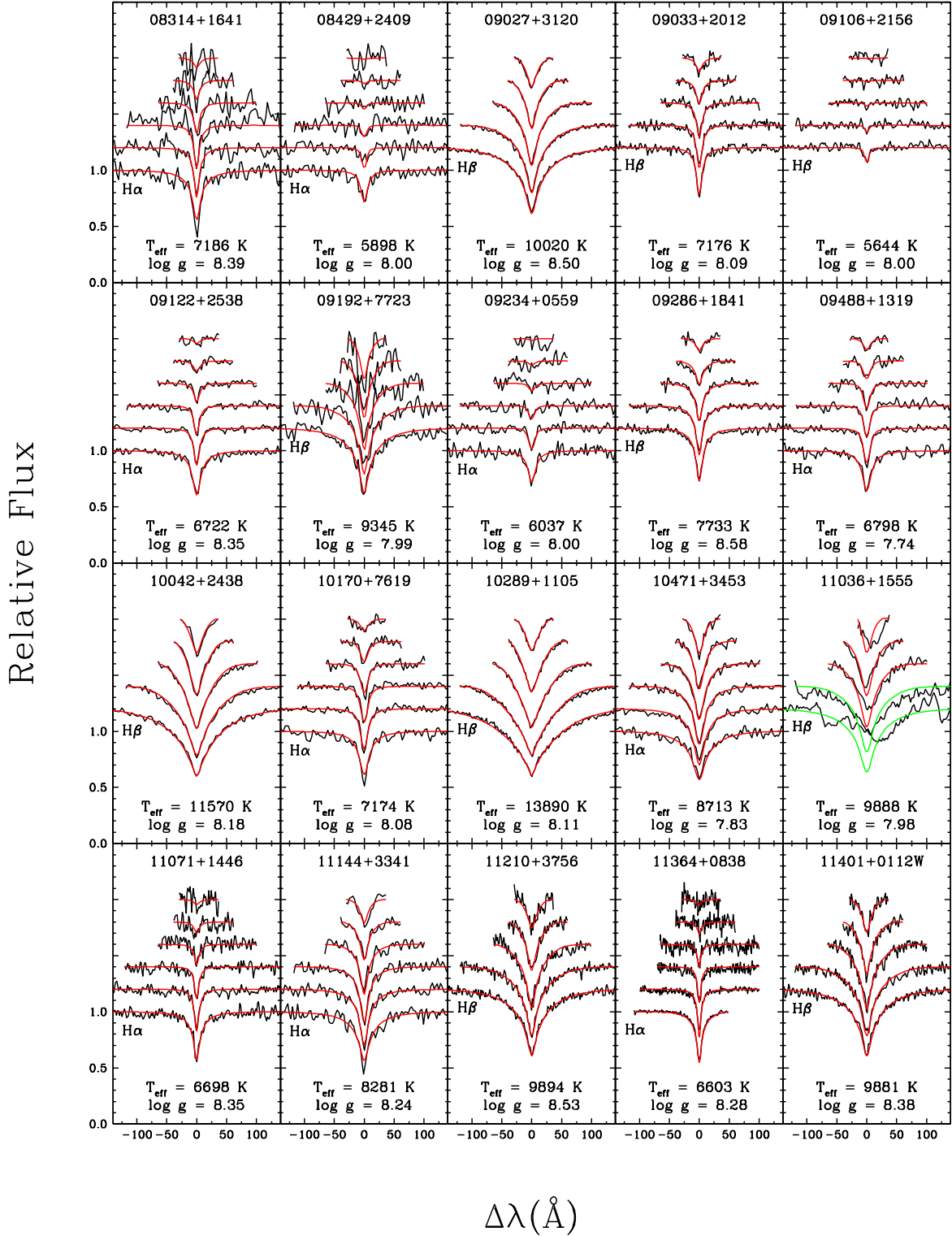


Figure 14d

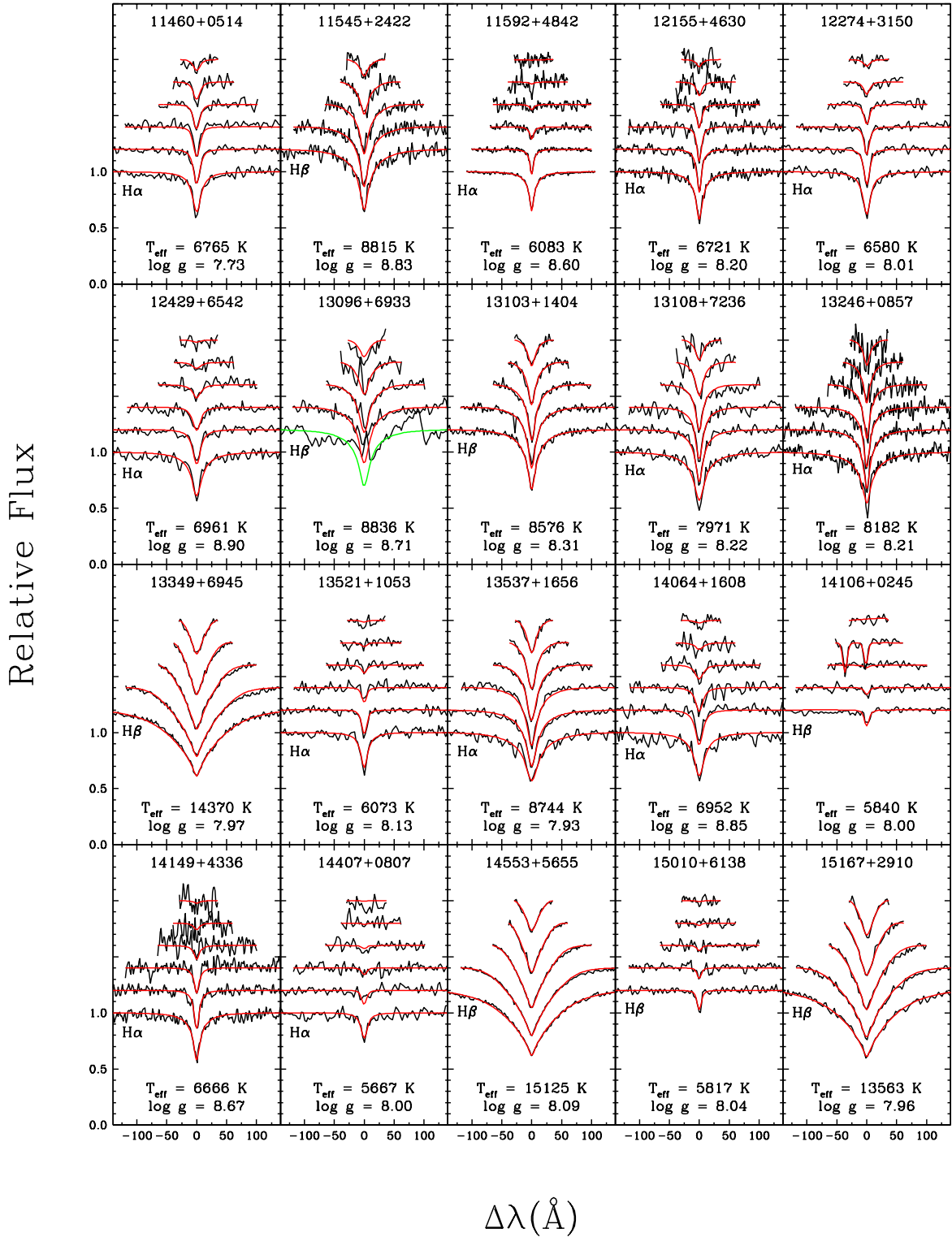


Figure 14e

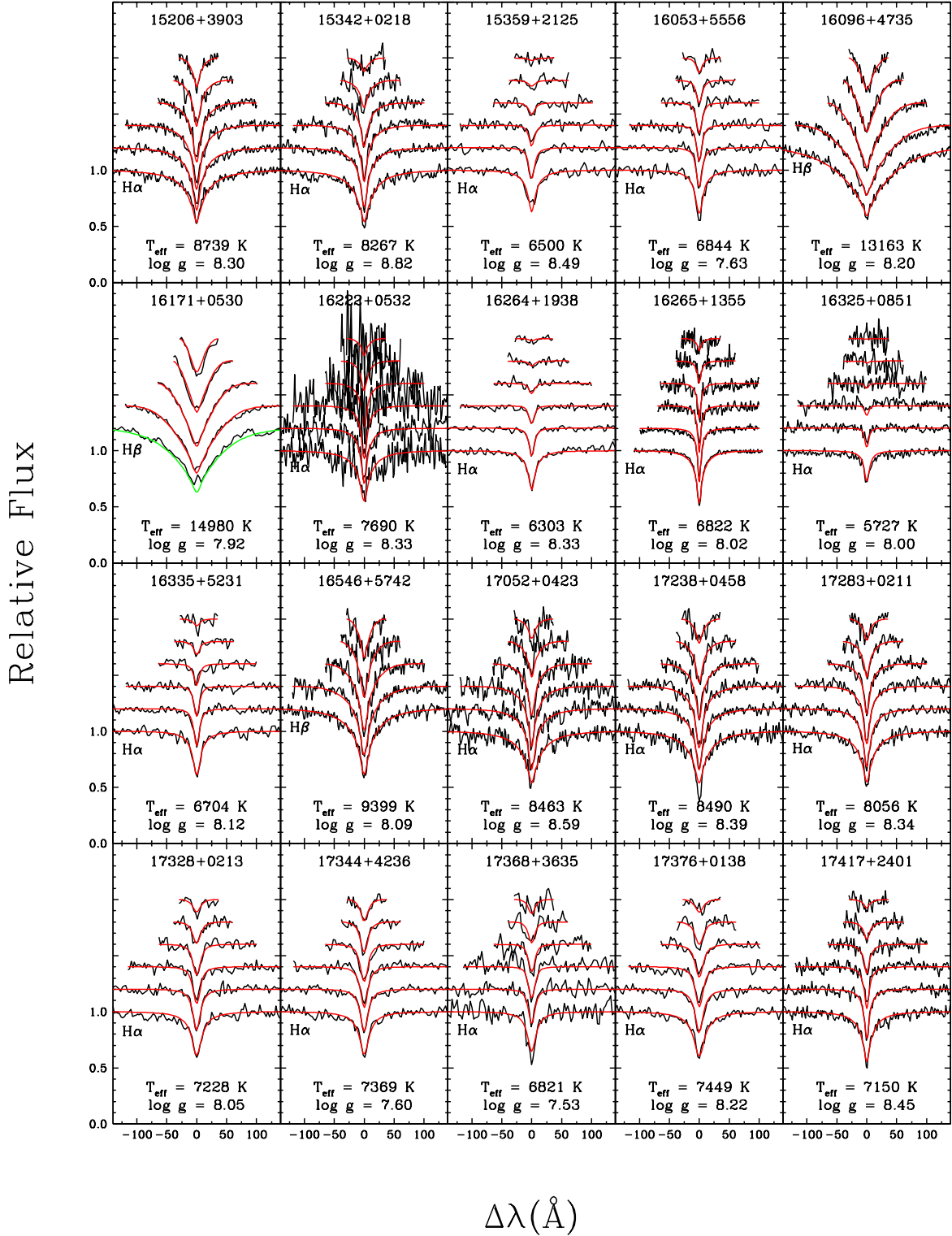


Figure 14f



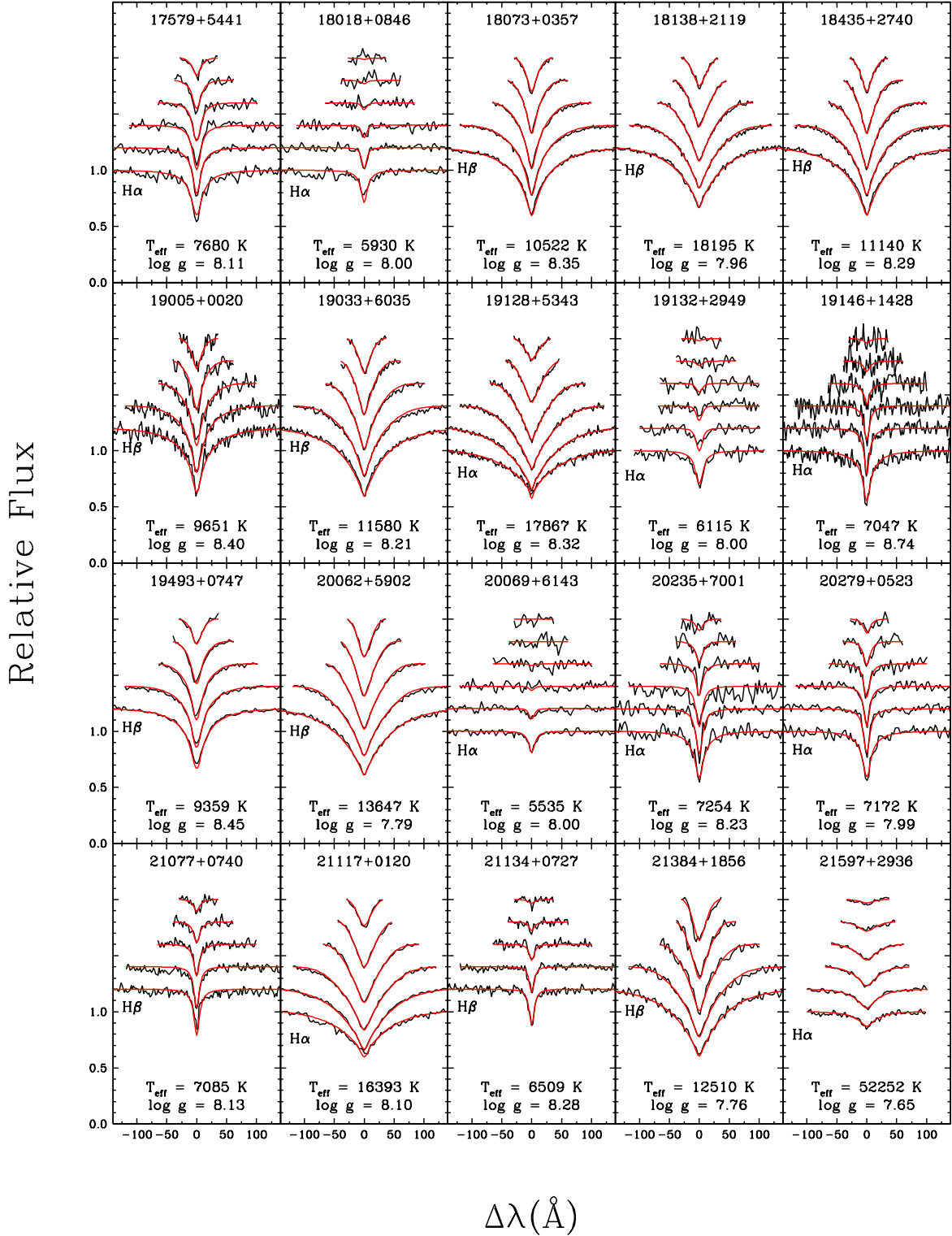


Figure 14g

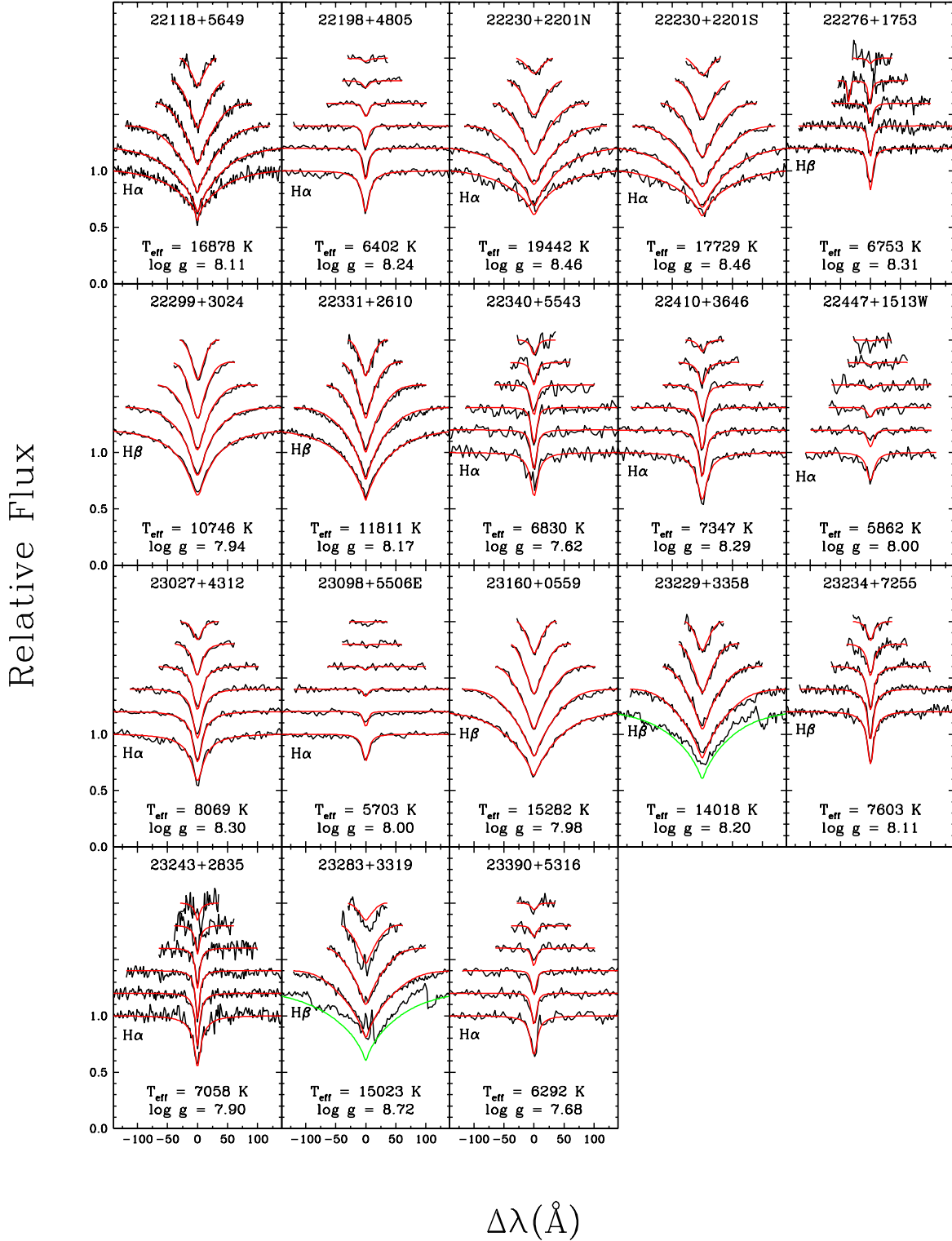


Figure 14h

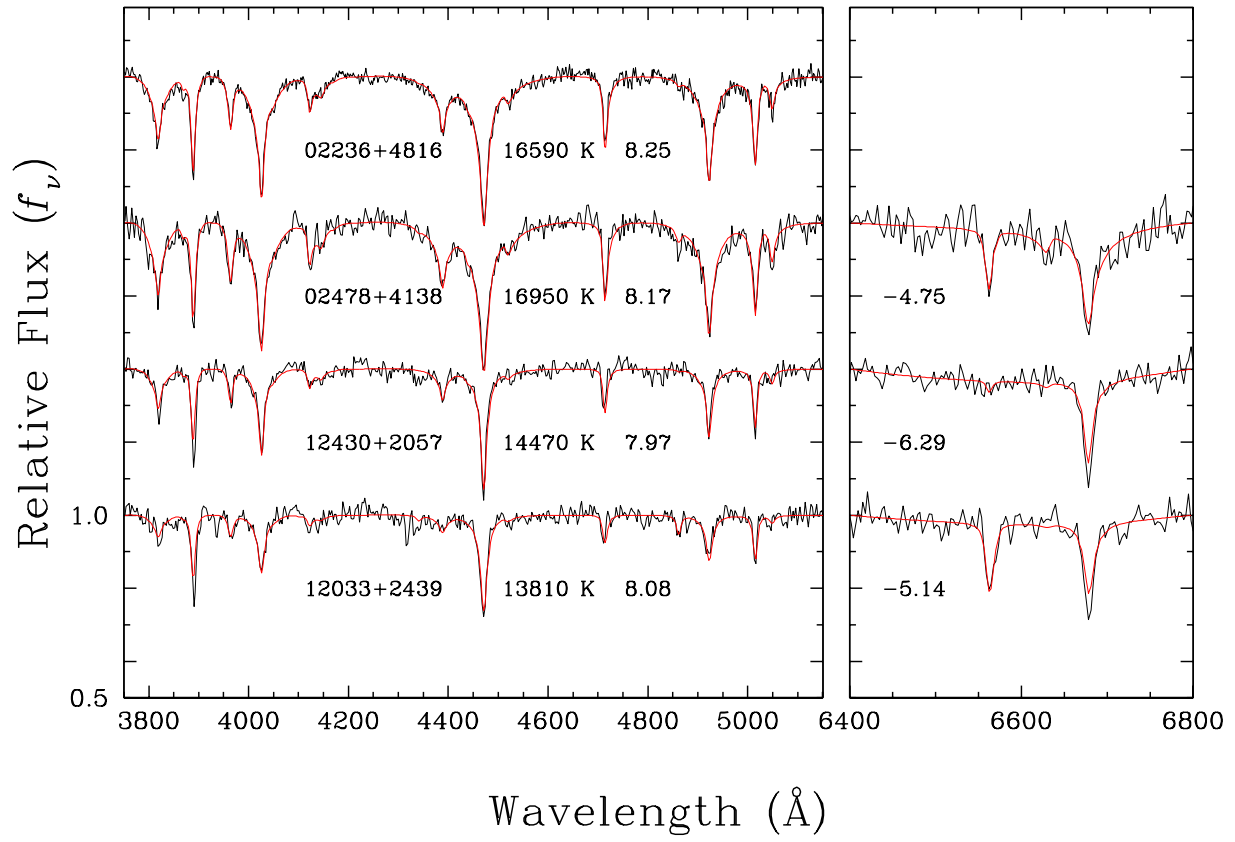


Figure 15

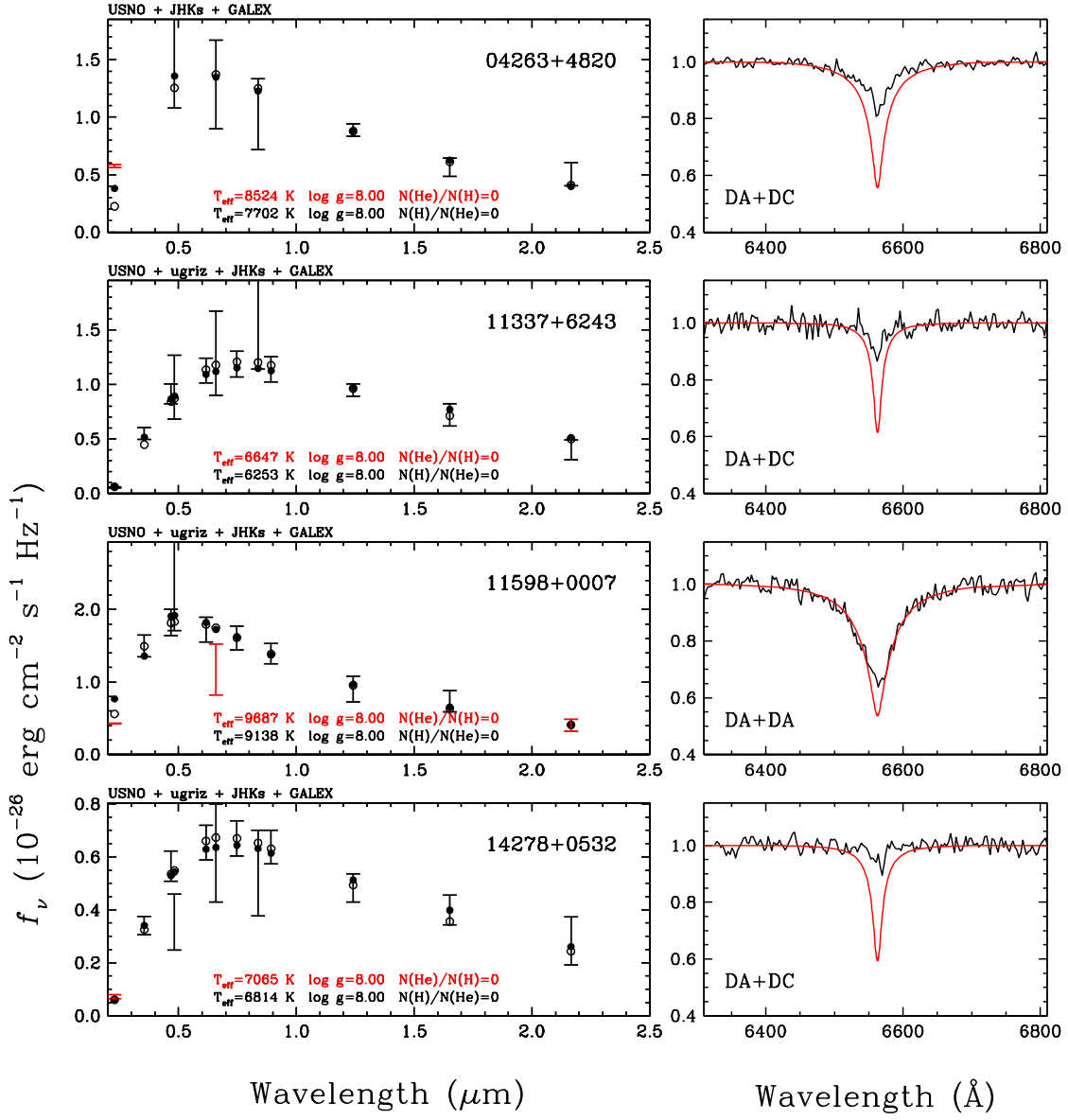


Figure 16

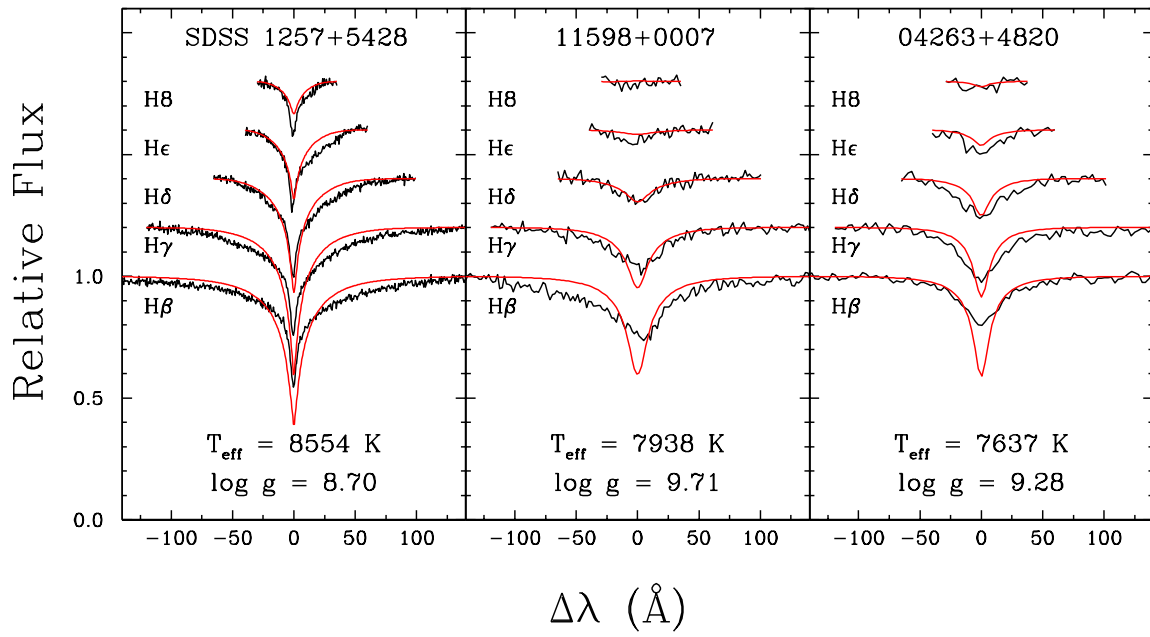


Figure 17

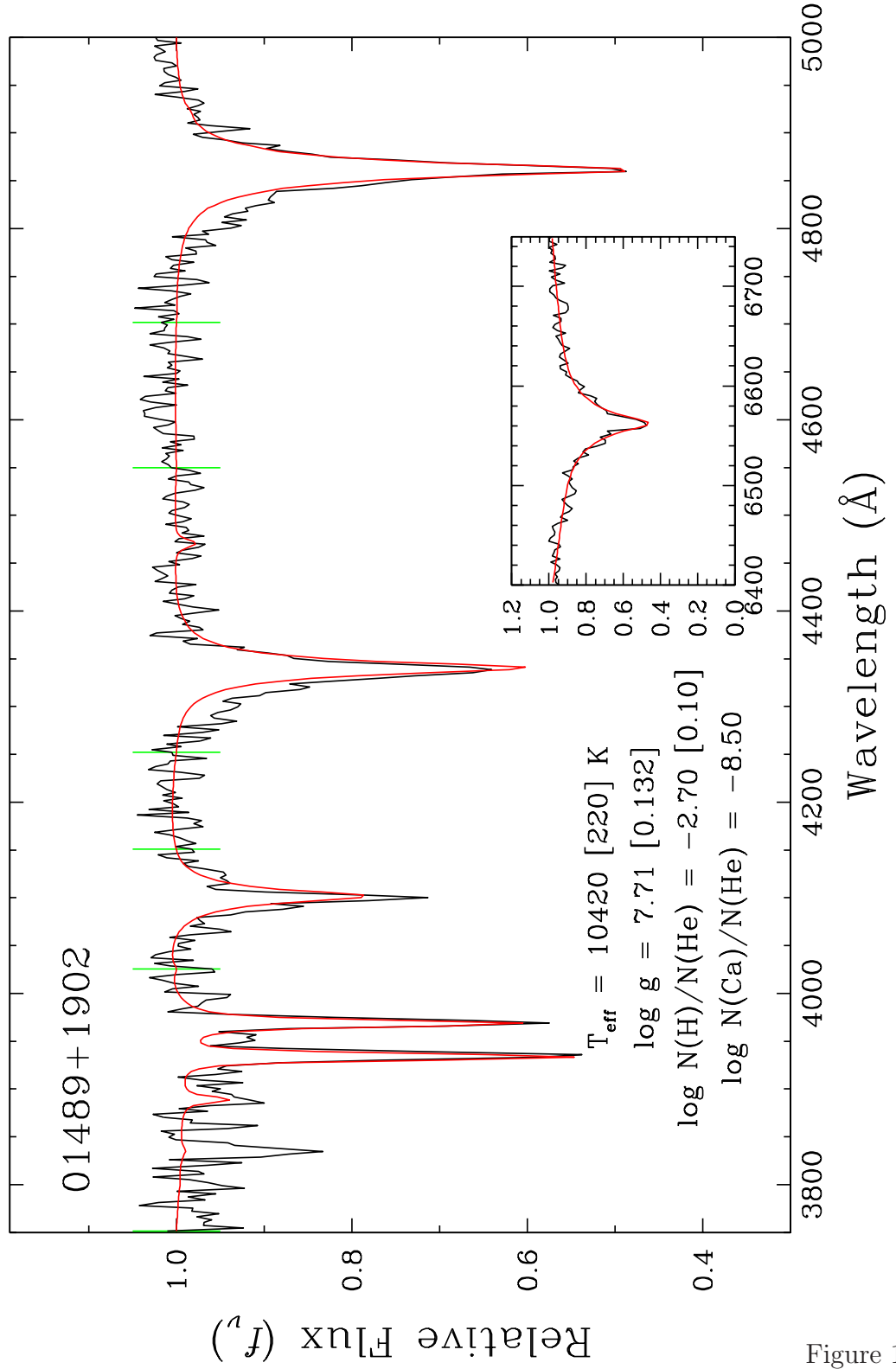


Figure 18

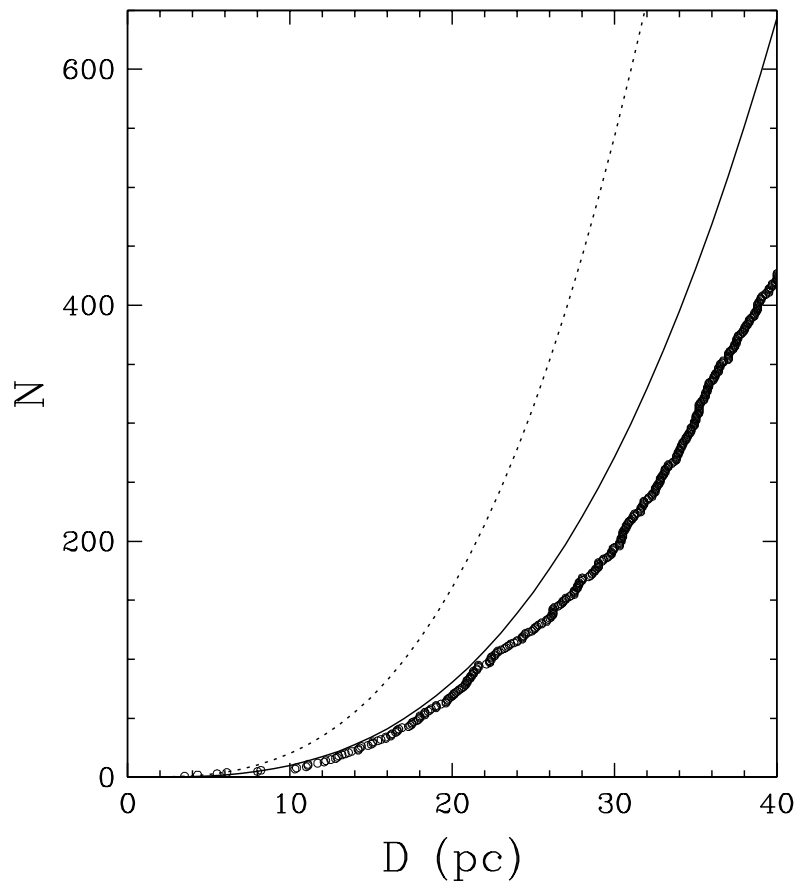


Figure 19

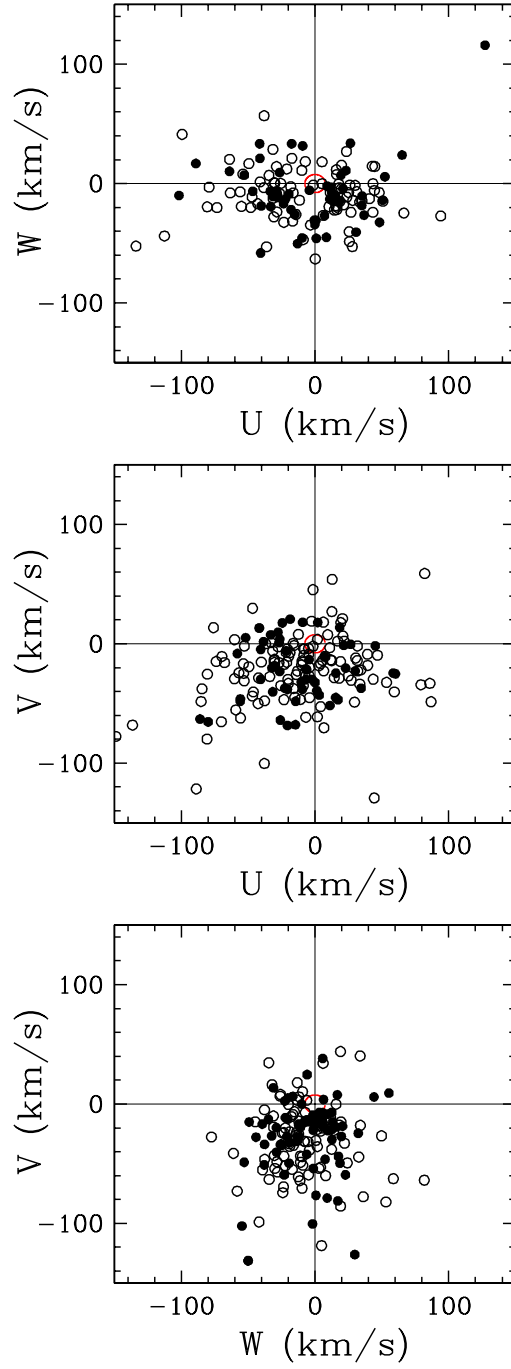


Figure 20



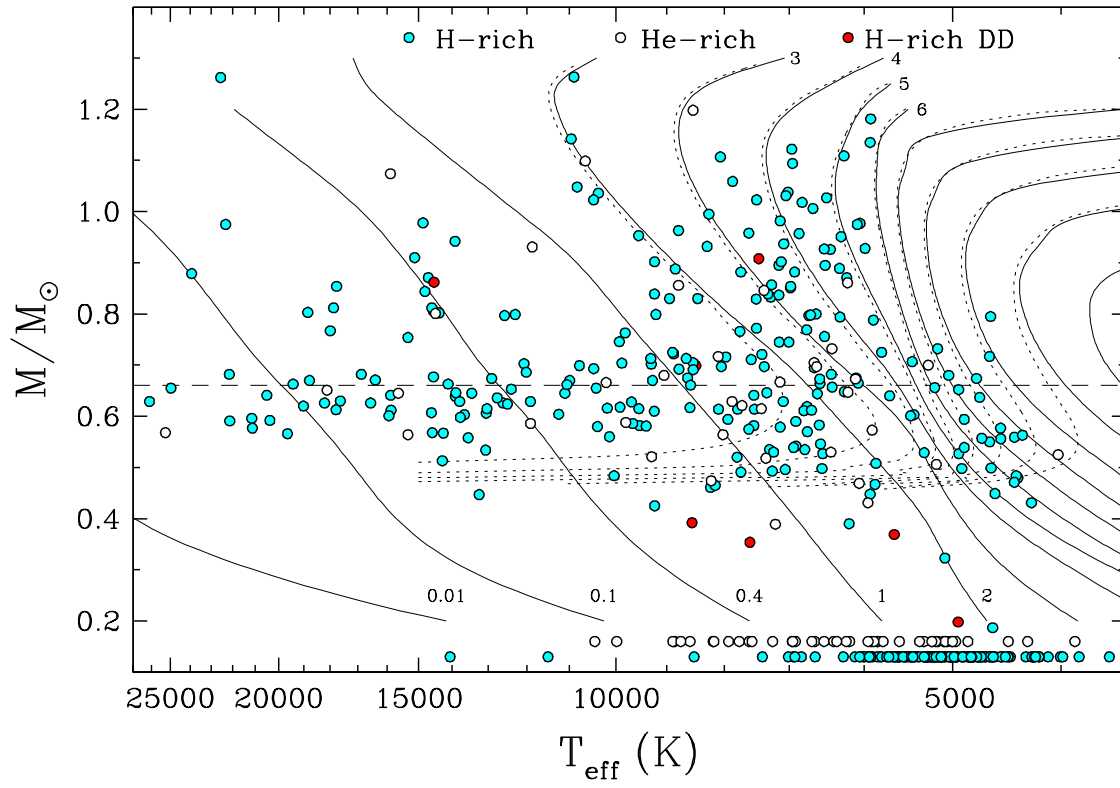


Figure 21

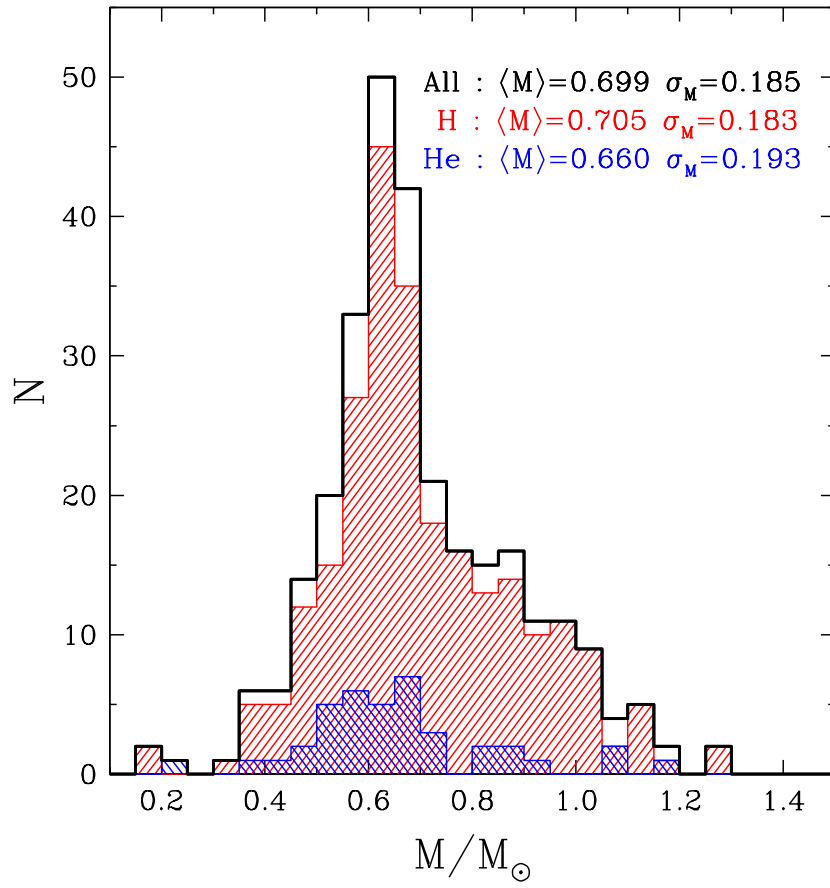


Figure 22

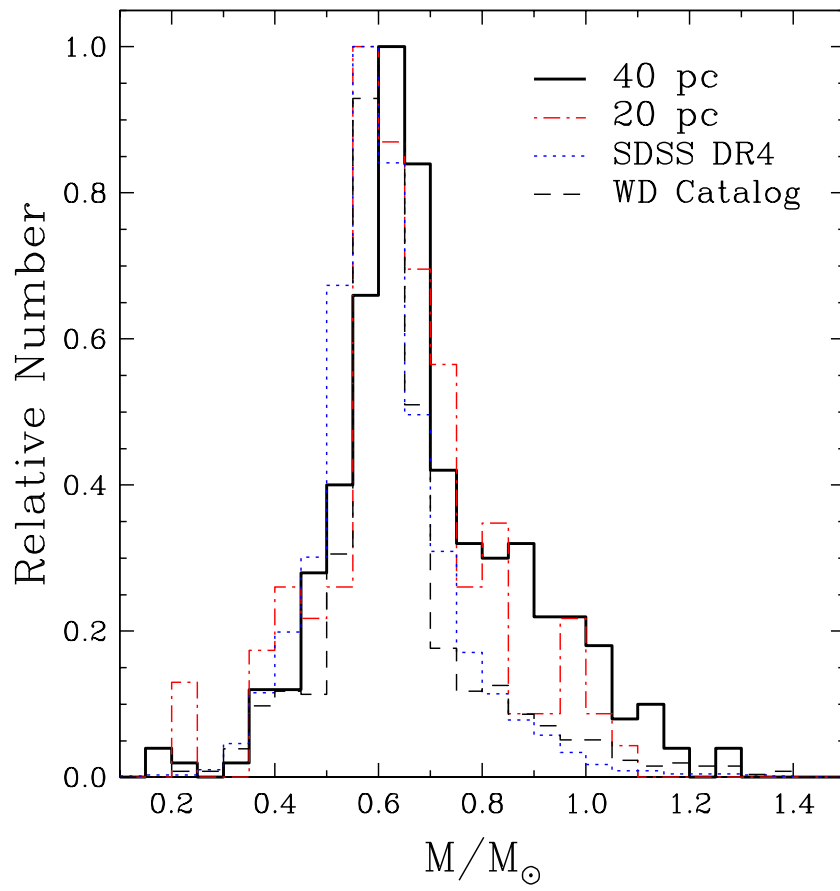


Figure 23

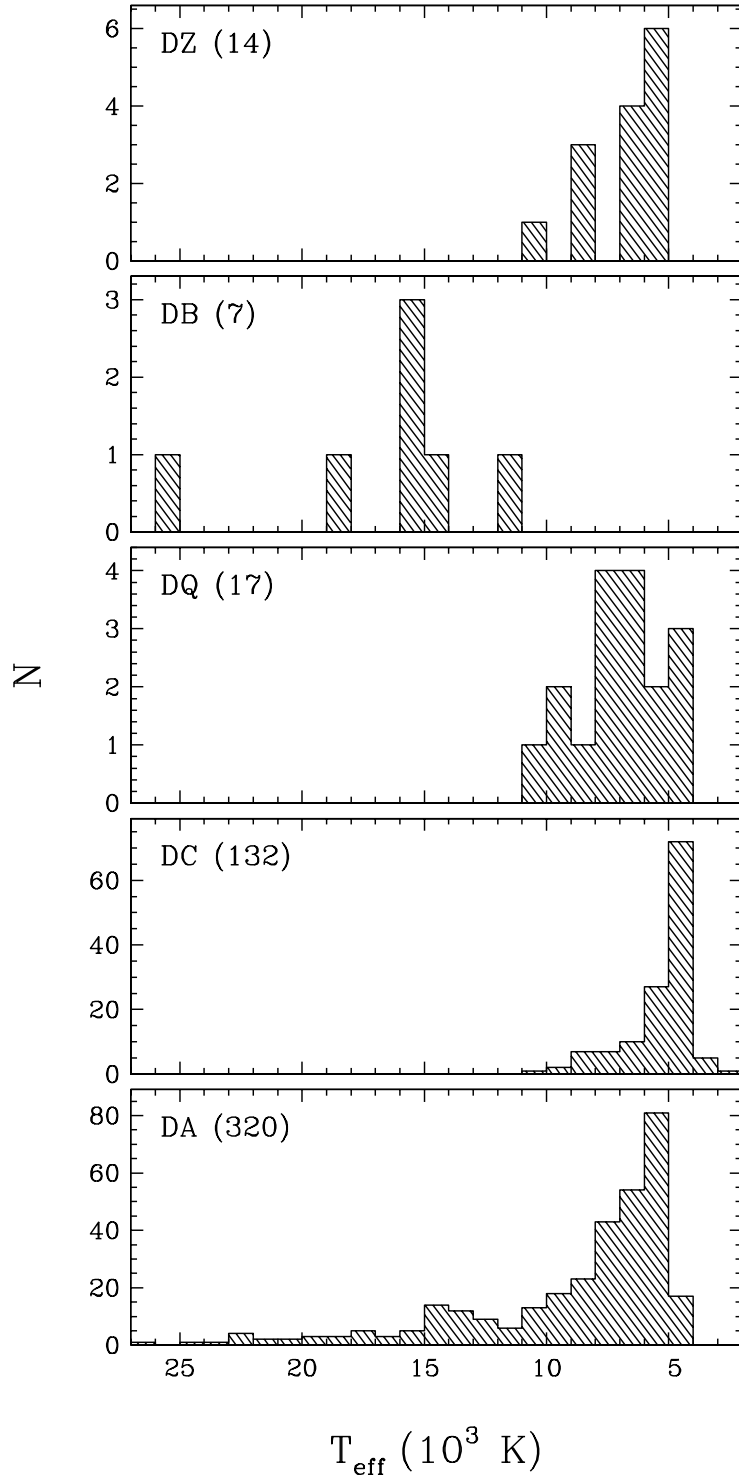


Figure 24

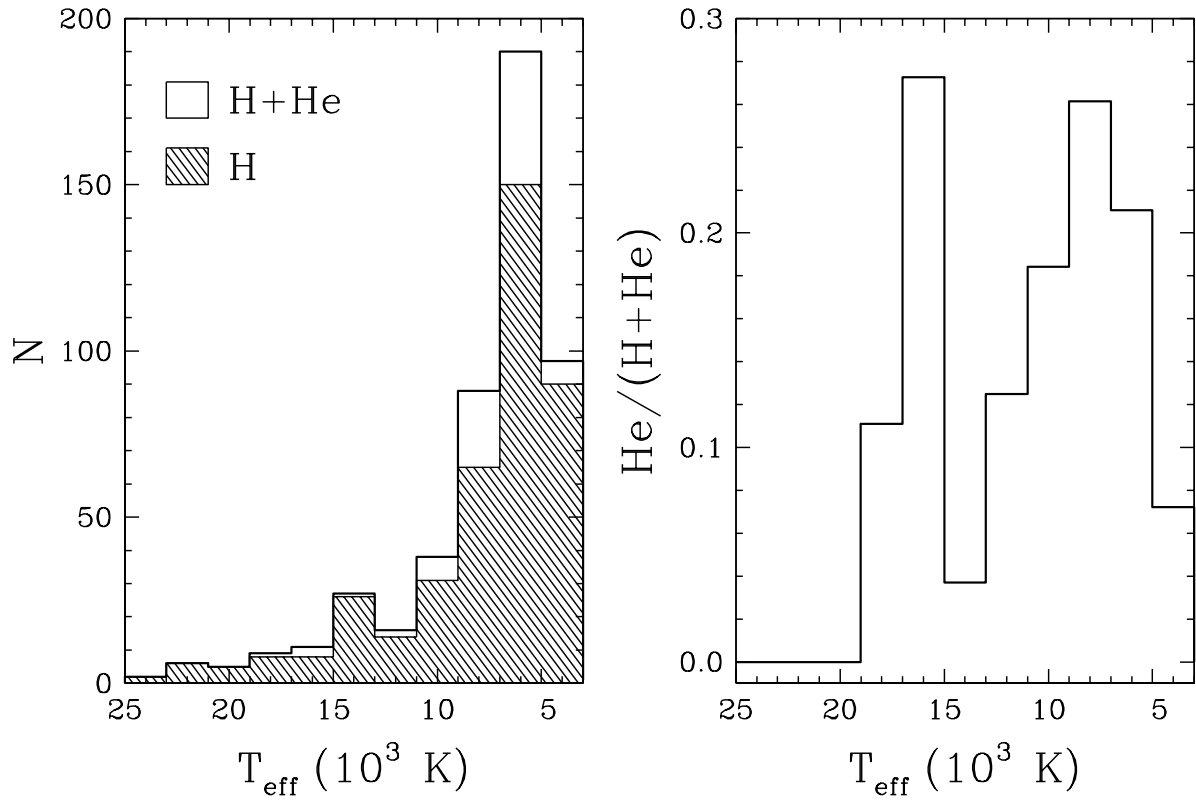


Figure 25

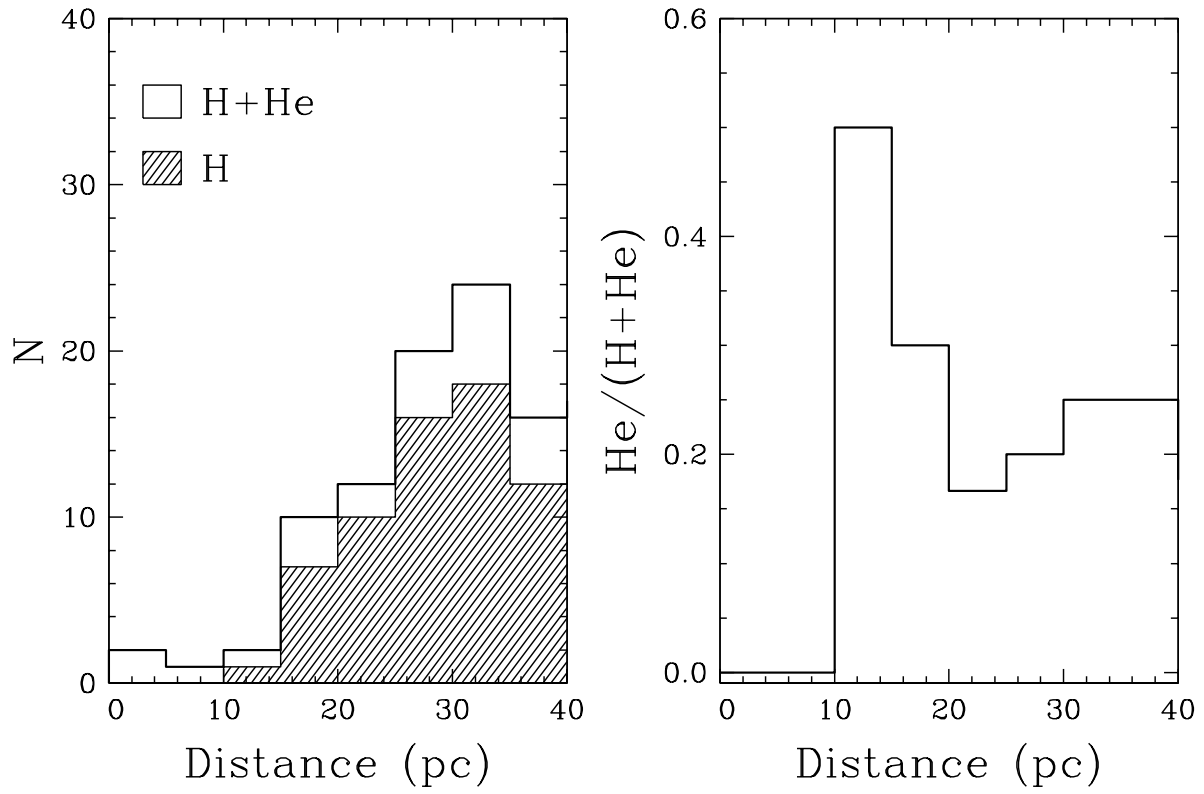


Figure 26

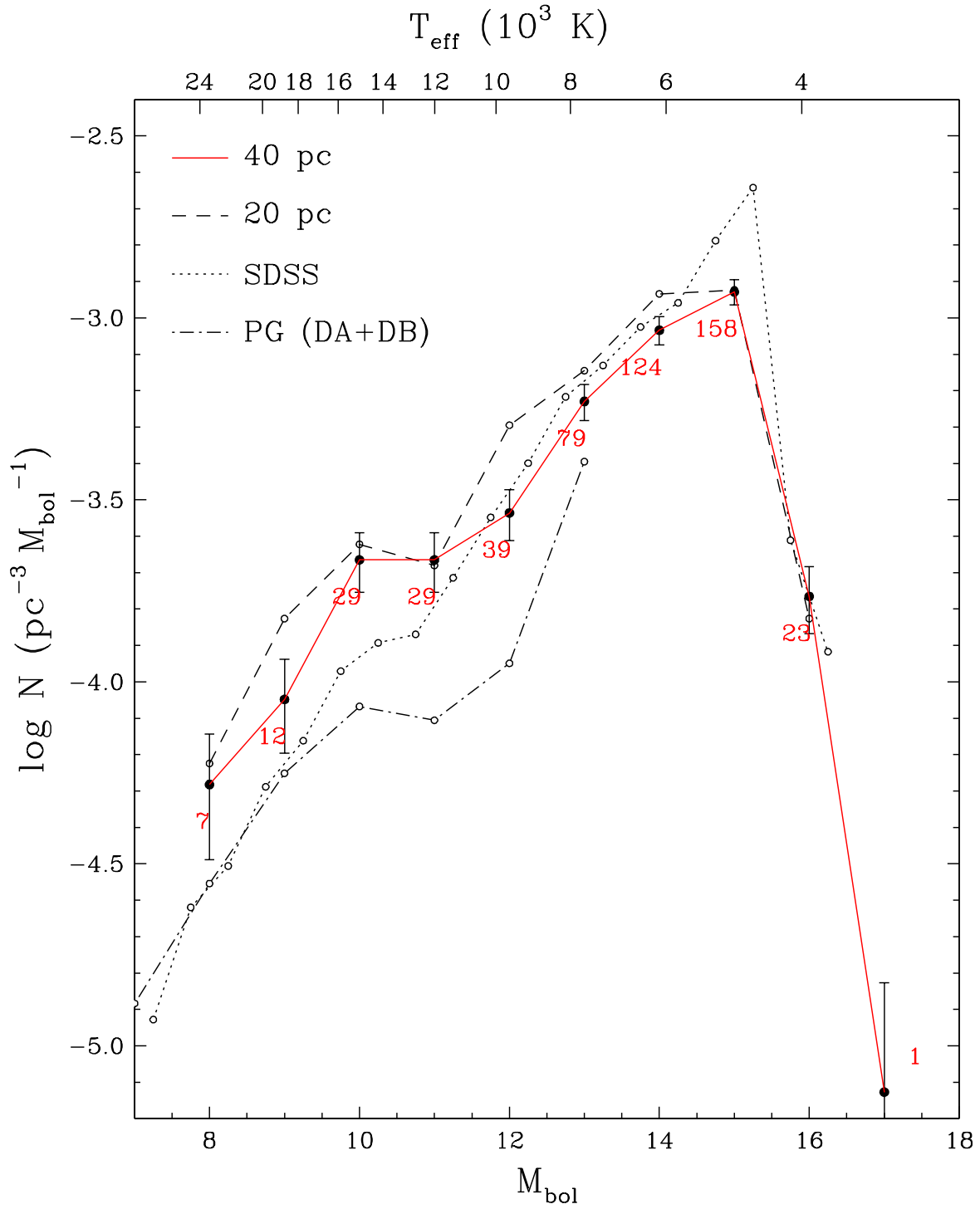


Figure 27

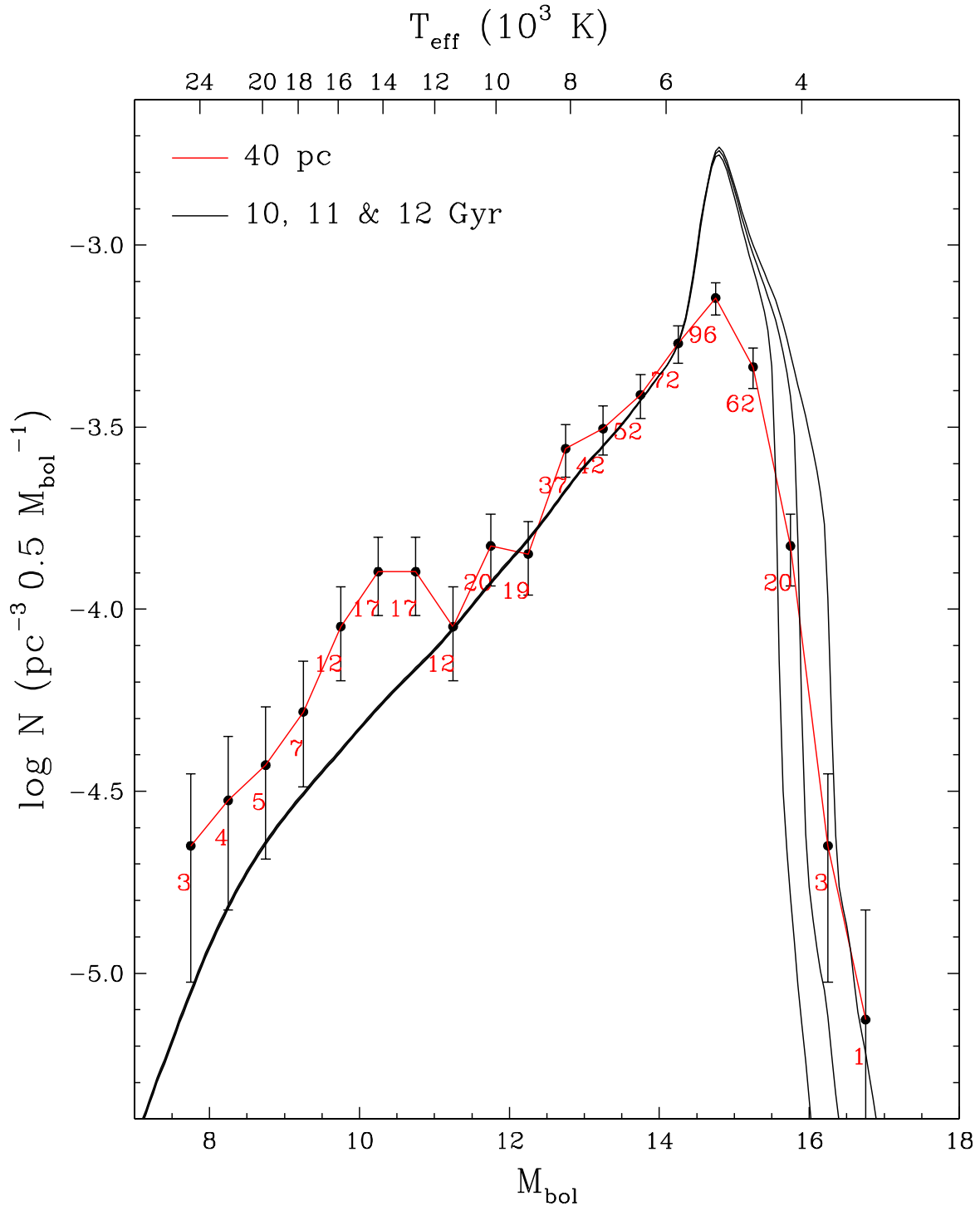


Figure 28